Università degli Studi di Torino

Scuola di Dottorato in
Scienze della Natura e Tecnologie Innovative

Dottorato in
Scienze Farmaceutiche e Biomolecolari
(XXXV ciclo)

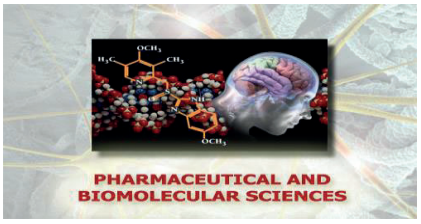

TITOLO

Beta-caryophyllene reduces lipid accumulation in a 3T3-L1 cell model of obesity and in a HepG2 cell model of NAFLD by acting through cannabinoid and PPAR receptors

Candidata: Scandiffio Rosaria **Tutor: Massimo Emilio Maffei**

Università degli Studi di Torino

Dottorato in
Scienze Farmaceutiche e Biomolecolari

Tesi svolta presso il
Dipartimento di Scienze della Vita e Biologia dei Sistemi

TESI PRESENTATA DA: Scandiffio Rosaria

TUTOR: Massimo Emilio Maffei

COORDINATORE DEL DOTTORATO: Roberta Cavalli

ANNI ACCADEMICI: 2019/2022

SETTORE SCIENTIFICO-DISCIPLINARE DI AFFERENZA: BIO/04

Index

Foreword

The scientific interest for natural compounds as novel potential drugs has increased exponentially in the last few years, along with the number of trials and studies on nutraceuticals and herbal extracts, aimed to test their effects on many disorders, including obesity, type II diabetes (T2D) and non-alcoholic fatty liver disease (NAFLD).

(*E*)-β-caryophyllene (BCP) is one of the most promising natural compounds. It is a bicyclic sesquiterpene hydrocarbon widely distributed in the plant kingdom, especially in floral volatiles, occurring in more than 50% of angiosperm families (Maffei et al., 2020).

In plants, BCP acts as chemoattractant for pollinators, defence against bacterial pathogens and has a pivotal role in the survival and evolution of higher plants as well as in contributing to the unique aroma of essential oils extracted from numerous species (Scandiffio et al., 2020). In addition to its role in plants, recent studies have highlighted that BCP plays a role in animal cells as anti-cancer (Mannino et al., 2021), anti-oxidant (Yovas et al., 2022), and anti-inflammatory agent (Picciolo et al., 2020).

Although its mechanism of action is not yet fully understood, studies indicate that BCP could act in animal cells through the specific binding to the CB2 cannabinoid receptors (Gertsch et al., 2008), of which it is a full selective agonist, and possibly through the interaction with members of the family of peroxisome proliferator-activated receptor (PPAR), in particular the isoforms α and γ (Wu et al., 2014; Irrera et al., 2019).

The high selectivity of BCP for CB2 receptors avoids potential psychotropic effects mediated by the neuronal CB1 cannabinoid receptor, being CB2 receptors mainly expressed in peripheral tissues and in central nervous system immune cells (Francomano et al., 2019). This peculiarity makes BCP a safe phytocannabinoid, with countless beneficial and non-psychoactive effects. This class of receptors belongs to the endocannabinoid system (ECS), a complex endogenous system involved in several physiological and pathophysiological functions. The ECS exerts regulatory controls on metabolism and food intake and for this reason it represents a potential target for numerous metabolic disorders such as obesity, diabetes, dyslipidemia and steatosis (Lowe et al., 2021). These diseases very often co-occur during the metabolic syndrome (MetS), a chronic pathological framework that represents a major health hazard in the modern population, being rapidly spread from Western to developing countries (Rochlani et al., 2017).

During my research period, I initially focused on obesity and type 2 diabetes (T2D). Obesity is a chronic metabolic disease characterised by excessive fat accumulation in adipose tissues (Cheng et al., 2019), often associated with insulin resistance, that can be a consequence of a reduction of insulin receptor numbers or a failure in glucose transportation into the cell by the glucose transporter GLUT4 (Cruz et al., 2013). T2D is another chronic metabolic disease associated with impaired insulin secretion and insulin resistance, caused by a combination of genetic and environmental factors.
In the first publication I studied these pathologies and the possible prevention strategies, testing a black pepper extract (PipeNig®-FL), containing a high standardized content of BCP, on 3T3-L1 preadipocytes and on C2C12 myotubes (*in vitro* models for the study of obesity and T2D, respectively), focusing on its potential activity on lipid accumulation and glucose uptake (Geddo, Scandiffio et al., 2019). The first step was the chemical characterization of the extract PipeNig®-FL by gas chromatography–mass spectrometry (GC–MS) and gas chromatography with flame-ionization detection (GC–FID), confirming a high content (814 mg/g) of BCP.
We then tested the effects of PipeNig®-FL on 3T3-L1 pre-adipocytes to assess the possible reduction of lipid content (anti-obesogenic effect) by AdipoRed fluorescence staining quantification. Glucose uptake and GLUT4 membrane translocation were studied in C2C12 myotubes with the fluorescent glucose analogue 2-NBDG and by immunofluorescence analysis.
We demonstrated that PipeNig®-FL reduces 3T3-L1 adipocyte differentiation and lipid accumulation and improves glucose uptake activity and GLUT4 migration, ameliorating the pathological condition (Geddo, Scandiffio et al., 2019).

Given the extensive use of the 3T3-L1 pre-adipocyte model to study obesity and also to test different chemicals, such as Metabolism Disrupting Chemicals (MDCs), I evaluated the reproducibility in 3T3-L1 cell responses and I assessed the variability of efficacy and potency outcomes for triglyceride accumulation and pre-adipocyte proliferation (Kassotis et al., 2021).
The magnitude and range of bioactivities reported varied considerably across laboratories and test conditions, though the presence or absence of activity for each tested chemical was more consistent; as such, working to develop a standardized adipogenic differentiation protocol represents the best strategy for improving consistency of adipogenic responses using the 3T3-L1 model to reproducibly identify MDCs and increase confidence in reported outcomes.

Next I focused on the ECS, a complex biological system involved in metabolic diseases (such as obesity), inflammatory response, as well as neurogenesis. I used the ST14A striatal neural progenitor cell line, a simplified *in vitro* model, to dissect the role and the mechanisms of ECS-regulated neurogenesis and to characterise ECS-targeted pharmacological and functional responses (Cottone et al., 2021). First of all, we assessed the expression of the ECS components necessary to a functional endocannabinoid system. Then, by using CB1/CB2 agonists and antagonists, we evaluated the effects of CB1 and CB2 receptor modulation on neural progenitor proliferation. Finally, we began to characterize the intracellular pathways involved in the CB2-regulated proliferation of striatal projection neuron progenitors.

In the last year I studied non-alcoholic fatty liver disease (NAFLD), the most common chronic liver disorder, characterized by the excessive accumulation of fats, due to overnutrition or unbalanced diet and not to ethanol consumption, with an increase of visceral fats that results in macrophage infiltration and pro-inflammatory conditions (Friedman et al.,2018). Despite being a very common pathological condition, no specific pharmacological therapy has yet been approved. I therefore tested BCP and using a fluorescence-based lipid quantification assay and GC-MS analysis, I showed that it is able to decrease lipid accumulation in steatotic conditions and to change the typical steatotic lipid profile by primarily reducing saturated fatty acids. By employing specific antagonists, I demonstrated that BCP action is mediated by multiple receptors: CB2 cannabinoid receptor, peroxisome proliferator-activated receptor α (PPARα) and γ (PPARγ). Interestingly, BCP was able to counteract the increase in CB2 and the reduction in PPARα receptor expression observed in steatotic conditions. Moreover, through immunofluorescence and confocal microscopy, I demonstrated that CB2 receptors are mainly intracellularly localized and that BCP is internalized in HepG2 cells with a maximum peak at 2 h, suggesting a direct interaction with intracellular receptors (Scandiffio et al., 2023).
These findings suggest that treatment with BCP, which is able to cross the plasma membrane and therefore to act on intracellular localized receptors, induces a reduction in lipid accumulation and a modification in intracellular lipid composition mediated by CB2 and PPAR receptors and that these effects are accompanied by a modulation of their expression.

Part I:

PipeNig®-FL, a fluid extract of black pepper (Piper Nigrum L.) with a high standardized content of Trans-β-Caryophyllene, reduces lipid accumulation in 3T3-L1 preadipocytes and improves glucose uptake in C2C12 myotubes

1. Introduction

Metabolic syndrome is a non-communicable disease characterized by visceral adiposity, insulin resistance, hyperlipidemia, hypertension and a chronic low-grade inflammatory state, often dragging into the onset of type 2 diabetes, coronary disease, stroke, and other disabilities. This chronic illness represents a major health hazard in the modern population, being rapidly spread from Western to developing countries (Reilly et al., 2003). The multiple biological mechanisms included in metabolic syndrome provide a complex interorgan communication, involving adipokines, macrophages, endoplasmic reticulum stress, thyroid hormones, beta adrenergic hormones, gut microbiome and other factors, where epigenetic drivers represent the major component with respect to genetic predisposition (Reilly et al., 2003). The pharmacological treatment of metabolic syndrome commonly involves anti-obesity drugs, thiazolidinediones (TZDs), metformin, statins, fibrates and several other drugs (Ammazzalorso et al., 2019), but its management chiefly lies in the adoption of a healthy lifestyle (Aguilar-Salinas et al., 2019). In this perspective, many studies and clinical trials highlight some quality diets, such as the Mediterranean diet, the Nordic diet, and the Dietary Approaches to Stop Hypertension (DASH) diet, to protect against metabolic syndrome or to improve its phenotype. Moreover, plants and plant-derived molecules have received great attention as complementary supports in managing metabolic dysfunctions (Silva Figuereido et al., 2018). As an example, Piper nigrum, a widely used spice, has been present in traditional medicine of different countries all over the world since ancient times due to the beneficial effects of its biologically active extracts, underlining its possible use in the treatment of metabolic syndrome or other related conditions (Ding et al., 2016). Among active compounds naturally present in Piper nigrum, the dietary cannabinoid trans-β-caryophyllene (BCP) could be considered as a possible key component in the treatment of obesity and type 2 diabetes in the metabolic syndrome scenario (Takooree et al., 2019). BCP is a bicyclic sesquiterpene hydrocarbon, highly present in a consistent number of plant-derived essential oils, such as balsams of Copaiba spp. (up to 53%), black pepper (Piper nigrum, up to 70%), lemon balm (Melissa officinalis, up to 19%), cloves (Syzygium aromaticum, up to 12%) and hops (Humulus lupulus, up to 9%) (Sharma et al., 2016). The Research Institute for Fragrance Materials (RIFM) evaluated BCP safety (Api et al., 2018) and it has been approved by the Food and Drug Administration and by the European Food Safety Authority as a flavouring agent, usable in cosmetic and food additives. In recent years, many studies reported the beneficial properties of BCP against several disorders, in particular cancer, chronic pain and inflammation; among the main ones, recent findings

showed chemosensitizing properties for doxorubicin chemotherapy (Di Giacomo et al., 2017), sorafenib (Di Giacomo et al., 2019), and 5-fluorouracil and oxaliplatin (Ambrož et al., 2019), neuroprotective effects against cerebral ischemia reperfusion injury (Yang et al., 2017) and dopaminergic neuron injury (Viveros-Paredes et al., 2017), cardioprotective features against myocardial infarction (Younis et al., 2019) and doxorubicin toxicity (Meeran et al., 2019) and, especially, a significant impact in the metabolic syndrome context. BCP has indeed been highlighted as a hypocholesterolemic and insulinotropic agent in high-fat diet-fed (Harb et al., 2018; Youssef et al., 2019), or in streptozotocin-induced, diabetic rats (Basha et al., 2014; Basha et al., 2016), where it showed non-clinical toxicity and an absence of adverse effects (da Silva Oliveira et al., 2018). BCP can act as a selective agonist of cannabinoid receptor 2 (CB2) (Gertsch et al., 2008), can directly activate peroxisome proliferator-activated receptor-α (PPAR α) (Wu et al., 2014), involved mainly in liver metabolism, and triggers the activation of PPPAR γ (Youssef et al., 2019), a master regulator of adipogenesis, possibly through an indirect mechanism (Youssef et al., 2019). Therefore, BCP may represent a promising treatment for several metabolic disorders. The effects of BCP on adipose tissue have never been addressed before, and so far, all studies on the BCP effects on glucose metabolism have been reported only *in vivo*. *In vitro* studies are a fundamental step for initial screening of potential cellular targets and characterization of the cellular mechanisms of bioactive molecules. Moreover, in the aim of a dietary approach, natural plant extracts with a high and standardized content of BCP could have a more suitable impact with respect to plain/synthetic BCP. Therefore, the present study was designed to evaluate the chemical characterization of a black pepper extract with a high content of BCP (PipeNig®-FL) produced by Biosfered Srl (Italy), and to study its effects on lipid accumulation and glucose uptake in *in vitro* models. The efficacy of the product was evaluated in two different cellular models, 3T3-L1 and C2C12, by assessing triglycerides accumulation in adipocytes and both glucose uptake and GLUT4 translocation in skeletal muscle myotubes.

2. Materials and Methods

2.1. Reagents

PipeNig®-FL (batch number PNF01-1907001), a *Piper nigrum* L. (black pepper) liquid extract, was kindly provided by Biosfered Srl (Torino, Italy). Certificate of analysis, technical sheets and materials safety data sheet of PipeNig®-FL are available from Biosfered upon request. The method of extraction and production of PipeNig®-FL are covered by the company trade secrets. PipeNig®-

FL contains BCP at a concentration of 3.5 M in rice oil. For experiments, a stock solution of 1 M in DMSO was obtained, then diluted in culture medium for cell treatments. Concentrations reported in this work refer to those of BCP in each dilution. NucBlue™ Live ReadyProbes™ Reagent and 2-(7-Nitrobenz-2-oxa-1,3-diazol-4-yl)Amino)-2- Deoxyglucose) (2-NBDG) were obtained from Invitrogen (Carlsbad, CA, USA); CellTiter-Glo® Luminescent Cell Viability and CellTiter 96® AQueous One Solution Cell Proliferation Assays were from Promega (Madison, WI, USA); anti-GLUT4 primary antibody and anti-rabbit secondary antibody Alexa Fluor 568 were from ThermoFisher Scientific (Waltham, MA, USA). Human insulin was used for cell treatments. Unless otherwise specified, all chemicals were purchased from Sigma Aldrich (St. Louis, MO, USA).

2.2. Gas-Chromatographic Analyses of PipeNig®-FL

PipeNig®-FL was analyzed by gas-chromatography (mod. 6890N, Agilent Technologies, Santa Clara, CA, USA) coupled with mass spectrometry (mod. 5973A, Agilent Technologies) (GC–MS). Compounds were separated on a Zebron ZB-5MS (mod. 7HG-G010-11, Phenomenex, Torrance, CA, USA) capillary column (stationary phase: 95% polydimethyl siloxane—5% diphenyl, 30 m length, 250 µm internal diameter, 0.25 µm film thickness) with the following temperature program: 60 ◦C for 5 min followed by a temperature rise at a 3 ◦C min−1 rate to 270 ◦C (held for 5 min). Carrier gas was He with a constant flow of 1 mL min−1 , transfer line temperature to MSD was 280 ◦C, ionization energy (EI) 70 eV, and full scan range 50–300 m/z. Separated compounds were identified by pure standard comparison, by comparison of their mass spectra with those of reference substances and by comparison with the NIST mass spectral search software v2.0 using the NIST 98 library. Quantitative analyses were confirmed by gas chromatography coupled with flame ionization detector (GC–FID) (mod. 6890N, Agilent Technologies); analyses performed with the same column and GC conditions as above.

2.3. Cell Cultures

3T3-L1 preadipocytes (ATCC® CL-173™; Lot No 70009858, ATCC, Manassas, VA, USA) were cultured in high-glucose (4.5 g/L) Dulbecco's modified Eagle's medium (DMEM) supplemented with 10% calf serum, 2 mM L-glutamine, 50 IU/mL penicillin, and 50 µg/mL streptomycin (Pomatto et al., 2018). For experiments, 5 × 103 cells/well were seeded in 96-black well clear bottom plates (Greiner Bio-One, Frickenhausen, Germany). Two days after reaching confluence (day 0), cells were exposed to the differentiation medium (MDI; which was DMEM containing 10% fetal bovine serum (FBS), 1 µg/mL insulin, 0.25 µM dexamethasone, 0.5 mM isobutylmethylxanthine). Two days later (day

2), MDI was replaced with maintenance medium (MM; which was DMEM 10% FBS, 1 µg/mL insulin). Fresh medium was provided every two days. Experiments ended after 9 days from the beginning of the differentiation (day 9). The mouse myoblast cell line C2C12 (ECACC 91031101, lot 17I044) was purchased from the European Collection of Authenticated Cell Cultures (ECACC, Salisbury, UK) and cultured in high-glucose DMEM supplemented with 10% FBS, 1% penicillin/streptomycin and 2 mM L-glutamine in a humidified atmosphere of 5% CO2 at 37 ◦C. Cultures were plated at a density of 2 × 103 cells per cm2 on tissue plastic dishes (Becton Dickinson, Franklin Lakes, NJ, USA) and sub-cultured before reaching 70% confluence. For experiments, cells were seeded at a density respectively of 2 × 103 cells/cm2 in Nutrients 2019, 11, 2788 4 of 14 96-well plates or 10 × 103 cell/cm2 on coverslips or glass bottom dishes (VWR Int., Radnor, PA, USA), to enhance adhesion. After cells reached confluence, differentiation was induced by changing the medium to DMEM supplemented with 2% horse serum (HS). Cells were allowed to differentiate for additional 5 to 7 days. The day before glucose uptake and GLUT4 translocation experiments, C2C12 cells were starved in DMEM glucose and serum free for 24 h.

2.4. Cell Viability

The viability of 3T3-L1 cells was evaluated at the end of the experiments (day 9) by CellTiter-Glo® Luminescent Cell Viability Assay, based on the quantitation of ATP, which signals the presence of metabolically active cells. After AdipoRed™/NucBlue™ quantification (see below), the dye mixture was removed from the cell cultures and CellTiter-Glo® reagent, diluted 1:1 in phosphate-buffered saline (PBS), was added. Cells were incubated at room temperature in the dark for 10 min, then luminescence was detected and quantified with FilterMax F5™ Multi-Mode microplate reader (Molecular Devices, Sunnyvale, CA, USA). The values of luminescence are directly proportional to the number of viable cells. Data from three independent experiments were expressed as percentage referred to control condition; these values were then summarized to calculate mean ± standard error of the mean (SEM). C2C12 cell viability was evaluated by the CellTiter 96® AQueous One Solution Cell Proliferation Assay, using the tetrazolium compound [3-(4,5-dimethylthiazol-2-yl)-5- (3-carboxymethoxyphenyl)-2-(4-sulfophenyl)-2H-tetrazolium, inner salt (MTS), that is bioreduced by metabolically active cells into a colored formazan product soluble in tissue culture medium. C2C12 cells, grown and differentiated into 96-well plates, were treated in 50 µL DMEM + 2% HS with different concentrations of PipeNig®-FL for one hour; during the last 30 min, 10 µL of MTS were added to each well (six wells for each condition). Formazan product was measured with FilterMax F5 microplate reader at 450

nm; absorbance is directly proportional to the number of viable cells. Data from three independent experiments were expressed as percentage referred to control condition; these values were then summarized to calculate mean ± SEM.

2.5. Quantification of Adipocyte Lipid Accumulation and DNA Staining

The 3T3-L1 cells, grown in 96-black well clear bottom plates, were exposed to PipeNig®-FL from day 0 to day 9 (whole differentiation period treatment), at scalar dilutions ranging from 1 nM to 10 µM (maximum DMSO concentration: 0.1%). Control cells were treated with 0.1% DMSO. Experiments were repeated three times (four wells for each condition), using cells at different passage numbers (p3–p5). At the end of the experiments (day 9 after the induction of differentiation), lipid accumulation was quantified by using AdipoRed™ assay reagent (Lonza, Walkersville, MD, USA), while the DNA content was estimated by NucBlue™ staining. Briefly, medium was removed from 3T3-L1 cultures and cells were rinsed with PBS, subsequently replaced with a dye mixture containing AdipoRed™ and NucBlue™ assay reagents diluted in PBS (25 µL and 1 drop, respectively, per mL of PBS). After 40 min of incubation at room temperature in the dark, fluorescence was measured with Filtermax F5 microplate reader respectively with excitation at 485 nm and emission at 535 nm for AdipoRed™ and excitation at 360 nm and emission at 460 nm for NucBlue™ quantification. Data from three independent experiments were expressed as percentage referred to control condition; these values were then summarized to calculate mean ± SEM.

2.6. Glucose Uptake Measurements

C2C12 cells, plated and differentiated on glass bottom dishes, after 24 h without glucose and serum, were treated with a different concentration of PipeNig®-FL (1–10–100 nM), and simultaneously loaded with 100 µM of 2-NBDG in glucose and serum-free DMEM, for 30 min in the dark. Insulin (25 nM) was used as a positive control. After two washes in PBS, cells were observed in confocal microscopy. Fluorescence images at 488 nm were acquired using an Olympus Fluoview 200 laser scanning confocal system (Olympus America Inc., Melville, NY, USA) mounted on an inverted IX70 Olympus microscope, Nutrients 2019, 11, 2788 5 of 14 equipped with a 60X Uplan FI (NA 1.25) oil-immersion objective. Fluorescence variations were calculated with the definition and measurement of regions of interest (ROIs) using the ImageJ software (Rasband, W.S., U. S. National Institutes of Health, Bethesda, MA, USA; http://rsb.info.nih.gov/ij/, 1997–2008). Data from four independent experiments were evaluated as mean fluorescence/area and expressed as percentage referred to control condition; these values were then summarized to calculate mean ± SEM.

2.7. GLUT4 Translocation Analysis

C2C12 cells were grown and differentiated on glass coverslips. After 24 h without glucose and serum, cells were treated with insulin 25 nM or different concentration of PipeNig®-FL (1–10–100 nM) for 30 min in glucose and serum-free DMEM. Then cells were fixed for 40 min in 4% paraformaldehyde dissolved in 0.1 M phosphate buffer, pH 7.3. After three washes with PBS, cells were incubated for 20 min with 0.3% Triton and 1% bovine serum albumin in PBS and stained for 24 h at 4 ◦C with the primary polyclonal antibody anti-GLUT4, 1:100. Cover slides were washed twice with PBS and incubated for 1 h at room temperature with the secondary antibody, anti-rabbit Alexa Fluor 568, 1:1000. After two washes in PBS, coverslips were mounted on standard slides with DABCO and observed after 24 h under a confocal microscope. GLUT4 staining measurements of both cell periphery and cell interior were performed with the ABSnake plugin of the ImageJ software (Gallo et al., 2019). Briefly, for each myotube the ABSnake plugin was employed to design a ROI band of 1.45 µm around the plasma membrane and the fluorescence intensities of both the band and the cellular inside were collected. Data from three independent experiments were expressed as peripheral/internal fluorescence and summarized to calculate mean ± SEM.

2.8. Statistical Analysis

Data are expressed as mean ± standard error of the mean (SEM); statistical analysis was performed using ANOVA (one-way analysis of variance) followed by Bonferroni's multiple comparison test. Differences with $p < 0.05$ were considered statistically significant.

3. Results

3.1. Chemical Composition of PipeNig®-FL

The chemical composition of PipeNig®-FL was assessed by GC–MS and quantified by GC–FID, as specified in the Materials and Methods section. The extract is characterized by a high content and percentage of the sesquiterpene hydrocarbon BCP, followed by minor mono and sesquiterpenes as depicted in Figure 1 and listed in Table 1. In particular, the total standardized content of PipeNig®-FL was higher than 800 mg g−1 of product, in agreement with what is specified by the producer. Amounts ranging from 0.5 to 7.8 mg g−1 were represented by monoterpenes (with limonene being the most abundant), whereas, among sesquiterpenes, α-caryophyllene showed the highest amount. In terms of relative percentage, BCP reached a level of almost 88%, whereas the total percentage of all other identified compounds was around 8% (Table 1).

Concentrations reported in this work for experiments with cell cultures refer to those of BCP contained in each dilution of PipeNig®-FL.

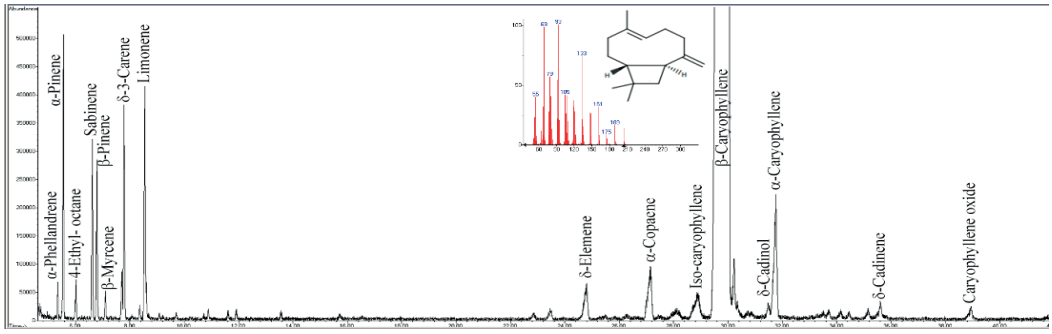

Figure 1. Gas chromatography–mass spectrometry (GC–MS) total ion current gas-chromatogram of PipeNig®-FL. The main compound trans-β-caryophyllene (BCP) is out of scale in order to evidence the other minor monoterpenes and sesquiterpenes that characterize the chemical composition of PipeNig®-FL. The inset shows the chemical formula and the mass spectrum of BCP. The y axis is the total ion current; the x axis represents time (in min).

Table 1. Chemical composition of PipeNig®-FL by gas chromatography coupled to mass spectrometry. Content is calculated based on gas chromatography with GC–FID analysis. R.T., retention time.

Compound	R.T.	Content (mg g^{-1})	Relative %
α-Phellandrene	5.35	0.47	0.11
α-Pinene	5.55	4.06	0.95
4-ethyl-octane	6.02	0.64	0.15
Sabinene	6.62	2.93	0.69
β-Pinene	6.79	2.76	0.65
β-Myrcene	7.11	1.10	0.12
δ-3-Carene	7.79	3.85	0.90
Limonene	8.55	7.84	1.10
δ-Elemene	24.79	2.21	0.52
α-Copaene	27.15	3.37	0.75
Isocaryophyllene	28.86	1.18	0.28
β-Caryophyllene	29.94	814.44	87.61
δ-Cadinol	31.49	0.70	0.16
α-Caryophyllene	31.75	6.13	1.43
δ-Cadinene	35.61	0.74	0.17
Caryophyllene oxide	38.94	0.79	0.18

3.2. Effects of PipeNig®-FL on 3T3-L1 Adipocyte Cell Viability

The long-term viability of 3T3-L1 cells treated with a wide range of PipeNig®-FL concentrations (100 nM, 1 µM, 10 µM, 100 µM, 1 mM, 10 mM) was determined by the CellTiter-Glo® viability assay, a method based on measurement of ATP content, whose amount is directly proportional to the number of metabolically active cells present in culture. As shown in Figure 2, after 9 days from the beginning of adipocyte differentiation (see Materials and Methods section), cell viability was affected only at very high PipeNig®-FL concentrations (1 mM and

10 mM), with only a minor, not statistically significant decrease at 100 µM. Based on these results, concentrations up to 10 µM were chosen for subsequent experiments. Mean values of luminescence signal from three independent experiments were as follow: CTRL (DMSO 0.1%): 100 ± 0.20, PipeNig®-FL 100 nM: 92.31 ± 0.13, PipeNig®-FL 1 µM: 92.65 ± 1.01, PipeNig®-FL 10 µM: 87.86 ± 0.83, PipeNig®-FL 100 µM: 77.55 ± 2.12, PipeNig®-FL 1 mM: 1.46 ± 1.32, PipeNig®-FL 10 mM: 0.93 ± 0.12.

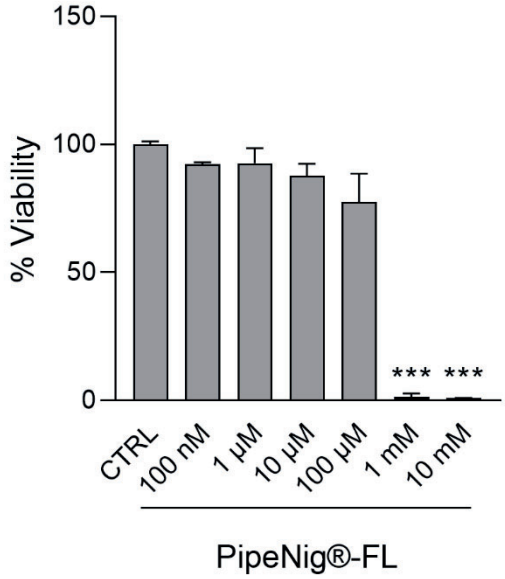

Figure 2. PipeNig®-FL affects 3T3-L1 cell viability only at high (millimolar) concentrations. 3T3-L1 cells were induced to differentiate into adipocytes for 9 days and treated with increasing concentrations of PipeNig®-FL for the entire differentiation period. The bar graph summarizes cell viability based on ATP content. Data in percentage referred to control condition are represented as the mean ± standard error of the mean (SEM) of three independent experiments. *** $p < 0.001$ vs. control.

3.3. PipeNig®-FL Reduces Intracellular Lipid Accumulation in 3T3-L1 Cells without Altering the Cell Number

The potential antiadipogenic activity of PipeNig®-FL was assayed on the murine 3T3-L1 preadipocyte cell line, a commonly used cell model for adipose cell biology research (Kim et al., 2018). Since antiadipogenic effects can be exerted by reducing both intracellular lipid accumulation and/or the number of adipocytes (either by decreasing cell proliferation or inducing cell death), we simultaneously assayed triglyceride accumulation (AdipoRed™ assay) and cell

number (NucBlue™ staining, measuring DNA content). Confluent preadipocytes, cultured in 96-well plates, were induced to start adipogenic differentiation and were treated throughout the differentiation period (9 days) with a vehicle only (0.1% DMSO; differentiated control) or with 1 nM, 10 nM, 1 µM, 10 µM PipeNig®-FL. Higher PipeNig®-FL doses were not used, based on the cell viability data reported above. After 9 days from the beginning of adipocyte differentiation, AdipoRed™/NucBlue™ stainings were performed on 3T3-L1 adipocytes (Figure 3A). Trygliceride accumulation and DNA content were calculated as percentage change from differentiated DMSO-treated controls (Figure 3B,C). The DNA content was used to normalize total triglyceride values to obtain triglyceride content per unit DNA (as a proxy for triglycerides accumulation per cell).

As shown in (Figure 3B), triglyceride accumulation per well was reduced in PipeNig®-FL treated 3T3-L1 cells compared to differentiated control cells; in particular, statistically significant reductions were obtained after treatment with PipeNig®-FL 10 nM, 1 µM and 10 µM. Mean values of fluorescence signal from three independent experiments were as follow: undifferentiated cells: 7.85 ± 2.36, differentiated CTRL: 100 ± 0.20, PipeNig®-FL 1n M: 63.64 ± 2.37, PipeNig®-FL 10 nM: 61.72 ± 1.35, PipeNig®-FL 1 µM: 59.00 ± 2.42, PipeNig®-FL 10 µM: 57.91 ± 3.05.

DNA content was not significantly different in PipeNig®-FL treated cells and control cells, thus indicating that the decrease in lipid accumulation exerted by PipeNig®-FL is not due to a decrease in cell proliferation or to cytotoxic effects (Figure 3C). Mean values of fluorescence signal from three independent experiments were as follows: undifferentiated cells: 81.23 ± 1.36, differentiated control: 100 ± 0.20, PipeNig®-FL 1n M: 91.63 ± 1.39, PipeNig®-FL 10 nM: 86.76 ± 0.96, PipeNig®-FL 1 µM: 90.43 ± 2.03, PipeNig®-FL 10 µM: 90.72 ± 1.92.

On the other hand, a significant reduction in intracellular lipid content per cell was found at all concentrations (Figure 3D); mean values of fluorescence signal from three independent experiments were as follow: undifferentiated cells: 10.63 ± 3.62, differentiated CTRL: 100 ± 0.30, PipeNig®-FL 1 nM: 68.68 ± 1.12, PipeNig®-FL 10 nM: 71 ± 0.88, PipeNig®-FL 1 µM: 64.74 ± 1.01, PipeNig®-FL 10 µM: 62.57 ± 1.31.

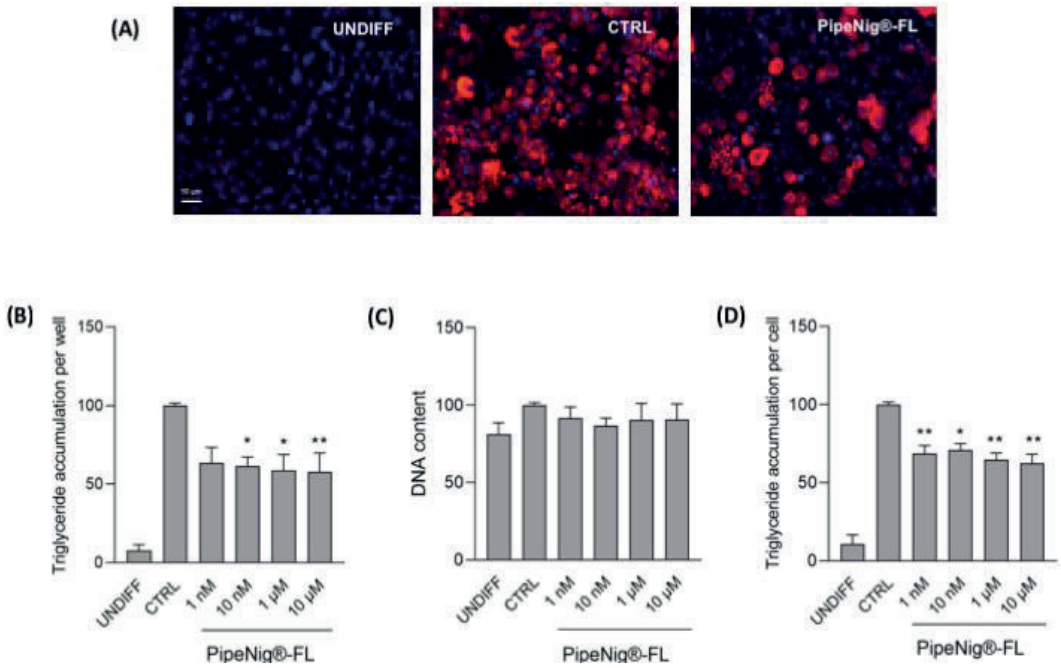

Figure 3. PipeNig®-FL reduces intracellular lipid accumulation in 3T3-L1 cells without altering the cell number. (**A**) Representative images of AdipoRed (red) and NucBlue (blue) staining of undifferentiated preadipocytes (UNDIFF), differentiated control adipocytes (CTRL) and 10 µM PipeNig®-FL-treated 3T3-L1 adipocytes after 9 days of differentiation. Scale bar 50 µm. (**B**) Bar graph summarizing AdipoRed staining experiments to assess lipid accumulation on undifferentiated cells, differentiated control and 3T3-L1 adipocytes treated with various concentrations of PipeNig®-FL for 9 days, showing triglyceride accumulation per well. (**C**) Bar graph summarizing NucBlue staining experiments to assess variations in the number of cells, showing DNA content per well. (**D**) Bar graph showing triglyceride accumulation per cell, calculated as the ratio of AdipoRed and NucBlue staining. Data in percentage referred to differentiated control condition are represented as the mean ± SEM of three independent experiments. * $p < 0.05$; ** $p < 0.01$ vs. control.

3.4. PipeNig®-FL Does Not Affect Cell Viability on C2C12 Muscle Cell

In order to investigate the effect of PipeNig®-FL on C2C12 viability, differentiated cells were treated with increasing concentration of PipeNig®-FL (100 nM, 50 µM, 200 µM, 1 mM, 10 mM) for 1 h. The MTS assay was performed in the last 30 min of treatment. The time considered to evaluate the toxicity of PipeNig®-FL was related to experiments on glucose metabolism that were done in a short time

of treatment. As shown in Figure 4, acute exposure (1 h) to PipeNig®-FL even at the highest doses did not affect significantly ($p < 0.05$) cell viability. Mean values of Abs at 450 nm from three independent experiments were as follows: CTRL: 99.61 ± 1.48, PipeNig®-FL 100 nM: 100.72 ± 1.32, PipeNig®-FL 50 µM: 98.90 ± 1.78, PipeNig®-FL 200 µM: 101.27 ± 2.04, PipeNig®-FL 1 mM: 101.76 ± 1.39, PipeNig®-FL 10 mM: 92.13 ± 2.34.

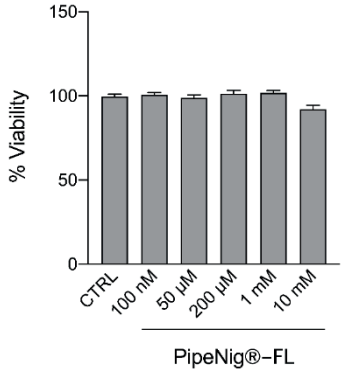

Figure 4. PipeNig®-FL does not have any effects on cell viability in C2C12 muscle cell. C2C12 cells were treated with increasing concentration of PipeNig®-FL for 1h. Data in percentage referred to control condition are represented as the mean ± SEM ($n = 3$).

3.5. PipeNig®-FL Improves Glucose Uptake in C2C12 Myotubes

To verify the potential role of PipeNig®-FL on glucose uptake in skeletal muscle cells, we performed confocal microscopy analyses by using a fluorescent D-glucose analog, 2-NBDG. Cells were incubated simultaneously with either 100 µM 2-NBDG and different concentrations of PipeNig®-FL (1–10–100 nM) without insulin while insulin alone (25 nM) was used as positive control, for 30 min in the dark. Doses of PipeNig®-FL were chosen in the nM range as for insulin, since we have previously verified that stimulation with PipeNig®-FL 100 nM for 1 h did not produce cytotoxic effects. A significant increase of glucose uptake was observed in treated cells with respect to control cells, whereas no differences were observed between insulin and PipeNig®-FL treatments or among PipeNig®-FL concentrations (Figure 5). Values of mean fluorescence/area from four independent experiments were as follows: CTRL: 100.13 ± 4.69, n cells = 68; insulin: 130.10 ± 6.21, n cells = 89; PipeNig®-FL 1 nM: 144.04 ± 7.95, n cells = 45; PipeNig®-FL 10 nM: 133.00 ± 6.73, n cells = 75; PipeNig®-FL 100 nM: 140.72 ± 9.64, n cells = 56.

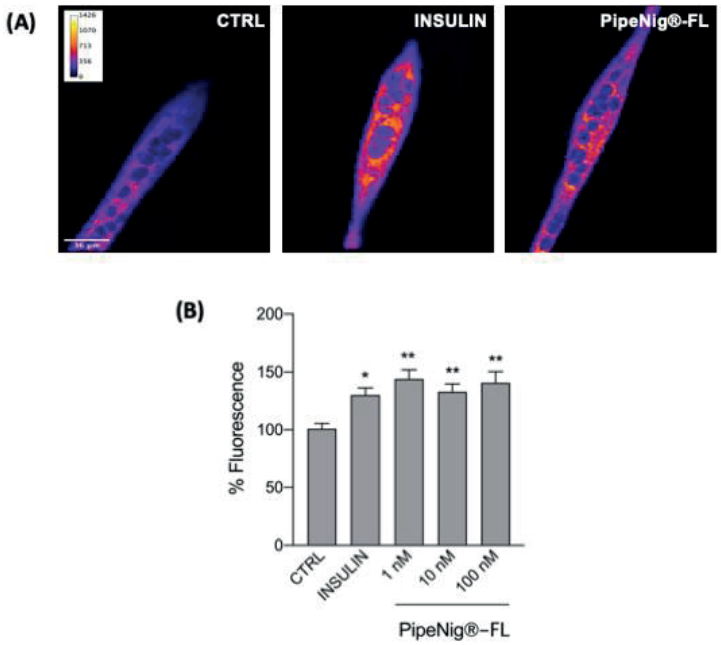

Figure 5. PipeNig®-FL stimulates glucose uptake. (**A**) Representative confocal images of C2C12 myotubes incubated with the fluorescent glucose analog 2-NBDG for 30 min. Images are presented in pseudocolor (LUT = fire) to better show the fluorescence intensity variations. Insulin (25 nm) was used as a positive control. Scale bar 36 µm. (**B**) Bar graph summarizing the experiments of fluorescent glucose uptake. Data in percentage referred to control condition are represented as the mean ± SEM (n = 4). * $p < 0.05$; ** $p < 0.01$ vs. control.

3.6. PipeNig®-FL Induces GLUT4 Translocation in C2C12 Cells

To confirm the involvement of PipeNig®-FL on glucose metabolism, we carried out immunofluorescence experiments using GLUT4 antibody, followed by a detailed image analysis of peripheral vs. internal fluorescence staining. Cells were treated with insulin (25 nM) or different concentrations of PipeNig®-FL (1–10–100 nM) without insulin, for 30 min. An evident translocation of the glucose transporter from the cytosol to the plasma membrane was observed in treated cells with respect to control cells, whereas there were no significant differences in staining among treatments (Figure 6). Values of peripheral vs. internal GLUT4 staining from three independent experiments were as follows: CTRL: 160.36 ± 18.21, n cells = 19; insulin: 282.73 ± 25.00, n cells = 21; PipeNig®-FL 1 nM: 259.26 ± 18.60, n cells = 20; PipeNig®-FL 10 nM: 336.40 ± 14.96, n cells = 18; PipeNig®-FL 100 nM: 270.96 ± 31.36, n cells = 16.

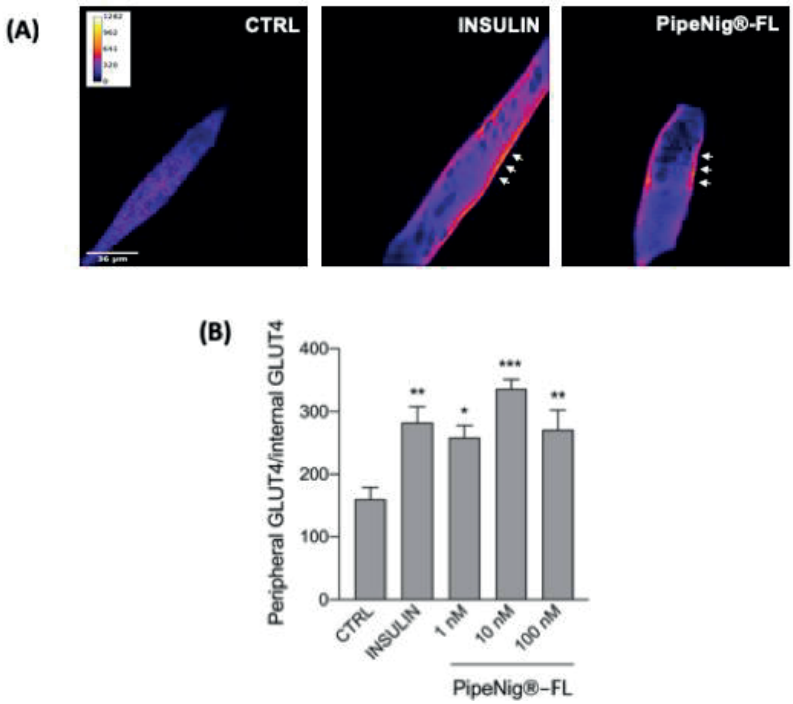

Figure 6. PipeNig®-FL induces GLUT4 translocation to the plasma membrane**.** (**A**) Confocal images of a representative experiment of GLUT4 immunofluorescence staining. After PipeNig®-FL stimulation (1–10–100 nM) the fluorescent signal is clearly localized to the peripheral plasmalemma, thus suggesting the GLUT4 translocation. Images are presented in pseudocolor (LUT = fire) to better show the fluorescence intensity variations. Insulin (25 nM) was used as a positive control. Scale bar 36 µm. (**B**) Bar graph representing the ratio peripheral vs. internal GLUT4 fluorescence intensity. Data are represented as the mean ± SEM of three independent experiments. * $p < 0.05$; ** $p < 0.01$; *** $p <$ 0,001 vs. control.

4. Discussion

This study focuses on two goals: 1. the chemical characterization of a black pepper extract with a high content of BCP (PipeNig®-FL). 2. the *in vitro* investigation of the biological activities of PipeNig®-FL in adipocytes and skeletal myotubes. The present results highlight the high performance of the extract regarding its BCP content (>80%) and underline its beneficial metabolic properties, in terms of reduced lipid accumulation in adipocytes and improved glucose uptake activity in myotubes.

The attractiveness of BCP, a sesquiterpene produced by a consistent number of plant species, arises from its pharmacological feature as a CB2 receptor full agonist, which makes BCP the only phytoendocannabinoid found beyond the Cannabis genus to date (Nuutinen et al., 2018), with the advantage of lacking any psychotropic effect. In addition to CB2 receptors, BCP also activates peroxisome proliferator-activated receptor α and γ (PPARα-γ) (Wu et al., 2014; Youssef et al., 2019), making it suitable to interfere with several metabolic pathways and pathological conditions, including apoptotic, inflammatory, cholesterolemic and behavioral disorders. In line with this, BCP has been demonstrated to possess anticancerogenic, neuroprotective, cardioprotective, hepatoprotective, gastroprotective, nephroprotective, antiinflammatory and immunomodulatary properties (Nuutinen et al., 2018; Fidyt et al., 2016). In particular, several studies recently pointed out potential counteractive functions of BCP against metabolic syndrome (Harb et al., 2018; Youssef et al., 2019; Basha et al., 2014; Basha et al., 2016; Arizuka et al., 2017). Grounding on these premises, the use of a plant-derived extract with a high and standardized BCP content represents a high-impact goal in the cross-sectional fields of plant food-nutrition-human health. In this perspective, the objective of our studies was to evaluate the properties of PipeNig®-FL to reduce lipid accumulation and induce glucose uptake.

The chemical analysis of PipeNig®-FL reveals a high content of BCP, in line with what is declared by the producer. The general GC profile is in line with the chemical composition of a typical black pepper oil (Butt et al., 2013; Bagheri et al., 2014) and confirms the presence of minor monoterpenes and sesquiterpenes as well as the complete absence of piperine.

We verified the suitability of PipeNig®-FL for *in vitro* cellular studies, by performing viability tests on 3T3-L1 preadipocytes and C2C12 myotubes. As shown in Figure 2, long-term 3T3-L1 treatment with PipeNig®-FL (9 days) did not cause any cell damage in the physiologically active range (100 nM–100 µM), only affecting cell viability at much higher concentrations (1–10 mM), while C2C12 viability (Figure 4) was unaffected by acute exposure to PipeNig®-FL (1 h, 100 nM–10 mM). Moreover, a previous study in mice reported the absence of toxicity of both acute (300 and 2000 mg/kg) and repeated doses of BCP (da Silva Oliveira et al., 2018), and BCP has been approved by United States Food and Drug Administration and European agencies as food additive, taste enhancer and flavoring agent (Sharma et al., 2016).

We further tested the properties of PipeNig®-FL as a lipid accumulation-inhibitor during the 3T3-L1 cell differentiation process. The development of

obesity is characterized by an increase in the number of fat cells (hyperplasia) and their lipid content (hypertrophy), as a result of cell proliferation and differentiation. In our experiments PipeNig®-FL led to a significant decrease in the lipid content per cell, without affecting cell proliferation, thus suggesting a role in reducing adipocyte-hypertrophic response typically present in the energy overload conditions that characterizes metabolic syndrome (Hafidi et al., 2019).

Previous *in vitro* studies on bone marrow mesenchymal stem cells showed enhanced osteoblast differentiation and reduced adipogenesis induced by synthetic BCP (Yamaguchi et al.,2016). Moreover, recent *in vivo* studies in rats exposed to fat enriched diet highlighted hypocholesterolemic and protective effects of BCP (Harb et al., 2018; Youssef et al., 2019), proving the involvement of several mechanisms, as the inhibition of endogenous hepatic cholesterol synthesis (Harb et al., 2018), the stimulation of the activity of antioxidant enzymes (Harb et al., 2018) and the engagement of both CB2 and PPARγ receptors (Harb et al., 2018). In this scenario, our results of reduced adipogenesis induced by PipeNig®-FL in 3T3-L1 pre-adipocytes strengthen the message from data obtained with synthetic BCP in bone marrow cells, and support the effectiveness of the extract with respect to its high BCP content.

In addition to its anti-obesogenic properties, our further experiments on skeletal myotubes highlighted PipeNig®-FL capability to be a glucose uptake inducer: as shown in Figure 5, PipeNig®-FL was as efficient as insulin in stimulating cellular glucose uptake. In 2014 Basha and Sankaranarayanan (Basha et al., 2014) reported an insulinomimetic effect of BCP (200 mg/kg) in streptozotocin-induced diabetic rats. In particular they showed a significant decrease in blood glucose levels and a significant increase in the activity of hexokinase, pyruvate kinase and glucose-6-phosphate dehydrogenase in liver, kidney and skeletal muscle. Moreover, other studies in similar animal models (Basha et al., 2016) and in isolated pancreatic beta cells (Suijun et al., 2014) reported antidiabetic properties of BCP through an enhanced insulin release. To gain better understanding of the mechanisms involved in glucose uptake, we performed immunofluorescence GLUT4 staining in insulin and PipeNig®-FL-treated myotubes, showing a significant plasma membrane GLUT4 translocation in both conditions (Figure 6) respect to control. Thus the attractive novelty of these results is to show, for the first time, a direct acute effect of a BCP-enriched extract in promoting glucose uptake in skeletal myotubes, likely through an improvement of GLUT4 trafficking toward the plasma membrane. Translocation of GLUT4 storage vesicles to the plasma membrane, mainly in skeletal muscle and adipose tissue, is directly correlated with the ability to lower elevated blood glucose. Moreover, GLUT4 levels are significantly decreased in the skeletal

muscle of type 2 diabetic patients and in insulin resistant patients (Morgan et al., 2011). The development of therapeutic compounds able to induce GLUT4 expression/translocation can thus improve insulin sensitivity and reduce insulin resistance. Several plant-derived bioactive molecules have been listed as stimulators of GLUT4 translocation and/or expression, among these resveratrol, chlorogenic acid, daidzein (an isoflavone found in soybeans), curcumin and astaxanthin, affecting different key-points in the intracellular cascade involved in vesicle trafficking (Gannon et al., 2015). As a major component of PipeNig®-FL, BCP could now be included in this list.

5. Conclusions

The main limitation of our study resides in the experimental models, since we tested the effects of PipeNig®-FL on cell lines of preadipocytes and skeletal myotubes. On the other hand, *in vitro* approaches account for important advantages, as results reflect direct effects of PipeNig®-FL on specific cellular processes, avoiding complex multi-organ interactions typical of *in vivo* models. At present, we do not provide a detailed analysis on the complex molecular/functional signatures of reduced lipidogenesis activated by PipeNig®-FL in 3T3-L1 cells. Future experiments should be directed to gain further information on the molecular mechanisms initiated by PipeNig®-FL and to confirm its properties as anti-lipidogenic and glucose uptake inducer in animal models.

In conclusion, given its high content in BCP, PipeNig®-FL could represent a promising novel bioactive complex deserving both molecular investigations and *in vivo* studies in order to support its role as a beneficial metabolic modulator.

Part II

Cannabinoid receptor modulation of neurogenesis: ST14A Striatal Neural progenitor cells as a simplified *in Vitro* model

1. Introduction

The endocannabinoid system (ECS) is comprised of several different components: (a) the cannabinoid receptors, the best characterized being CB1 and CB2 receptors; (b) the endogenous cannabinoids, also called endocannabinoids (eCBs), among which anandamide (AEA) and 2-arachidonoylglycerol (2-AG); (c) the enzymes involved in eCB biosynthesis "on demand", e.g., N-acylphosphatidylethanolamine-specific phospholipase D-like hydrolase (NAPE-PLD) and diacylglycerol lipase (DAGL); (d) the enzymes involved in eCB degradation, e.g., fatty acid amide hydrolase (FAAH) and monoacylglycerol lipase (MAGL); (e) the molecules involved in eCB transport across the membrane (Lu et al., 2020; Di Marzo et al., 2018; Shahbazi et al., 2020). Additionally, various natural exogenous cannabinoids do exist, the most potent of which is Δ9-tetrahydrocannabinol (THC), the main psychoactive component of Cannabis sativa (Mechoulam et al., 1965).

Considering that marijuana is one of the most abused substances in the world and it is becoming legal in many countries, a particular concern is on the fact that acute and chronic use of cannabis could lead to cognitive impairments; interestingly, not only chronic treatment with THC, but also the administration of a single ultra-low dose of THC was shown to lead to long-term cognitive impairments, possibly resulting from deficits in attention or motivation (Amal et al., 2010). A noteworthy finding is the fact that THC induces striatal dopamine release in animals and humans (Bossong et al., 2008), thus explaining some of the adverse effects of cannabis consumption on neuropsychiatric disorders, such as schizophrenia, and also suggesting that THC could share addictive properties with other drugs of abuse.

The ECS shares mediators and overlaps with other metabolic processes, thus recently an "expanded endocannabinoid system" or "endocannabinoidome" has been defined (Di Marzo et al., 2015). CB1 and CB2 cannabinoid receptors are seven-transmembrane G protein-coupled receptors (Haspula et al., 2020); they primarily signal through Gi/o proteins, leading to the inhibition of adenylyl cyclase and activation of Mitogen-activated protein kinases (MAPKs). In response to CB1 stimulation, MAPKs such as ERK1/2, c-Jun N-terminal kinase (JNK) and p38 are activated; CB1 was also shown to activate the Phosphoinositide 3-kinases (PI3K) pathway, thus leading to the regulation of neuronal survival. Similar to the CB1 receptor, the stimulation of CB2 has been demonstrated to promote neuronal survival through the activation of the PI3K/AKT/mTORC and JNK pathway; also, a Phospholipase C (PLC)- mediated intracellular calcium increase has been shown to activate MAPKs. Apart from these canonical signaling pathways, cannabinoid receptors are also able to

signal through other non-canonical ways, such as activation of Gs and Gq proteins; also, complex crosstalk among cannabinoid receptors and other receptors, leading to heterodimerization and transactivation, has been shown (Haspula et al., 2020). Interestingly, different ligands can elicit different signaling pathways mediated by cannabinoid receptors (Lu et al., 2020).
CB1 is the most abundant G-protein coupled receptor in the mammalian brain; it is highly expressed by neurons in the cortex, amygdala, hippocampus, basal ganglia, and cerebellum, its activation leading to the modulation of neurotransmitter release (Pertwee et al., 2015). The CB1 cannabinoid receptor has a pivotal role in neuroprotection, control of excitotoxicity, the survival of neural cells, as well as proliferation, differentiation and migration processes of neural progenitors (NPs) (De O liveira et al., 2018; Lutz et al., 2020; Oddi et al., 2020).

Different from CB1, the CB2 receptor is mostly distributed peripherally, especially in cells of the immune system (Galiegue et al., 1995), with a prevalent immunomodulatory role. However, recent studies showed CB2 expression also in the central nervous system (Gong et al., 2016), especially in association with neurodegenerative disorders (Aimerich et al., 2018). In the adult brain, the CB2 receptor is localized in microglia, brain stem neurons, striatal neurons, hippocampal glutamatergic neurons, and dopaminergic neurons of the ventral tegmental area; CB2 mRNA levels are 100–200 times less abundant than CB1 mRNA, being however strongly upregulated in response to chronic pain, neuroinflammation and stroke (Lutz et al., 2020). Interestingly, the CB2 receptor is expressed in oligodendrocyte progenitors and neural progenitors (Palazuelos et al., 2006; Palazuelos et al., 2012; Molina-Holgado et al., 2007) and it has been demonstrated that its activity is important in the control of adult neurogenesis under pathological conditions (Oddi et al., 2020). Indeed, the involvement of the CB2 receptor in neurodegenerative and neuroinflammatory disorders stimulated research toward CB2-targeted pharmacological approaches (Di Marzo et al., 2018). A substantial body of evidence suggests that the ECS modulates the proliferation, migration, specification and survival of neural progenitors in the developing and adult CNS (De Oliveira et al., 2018). During the different phases of neurogenesis in pre- and post-natal brain, all the ECS components are differentially expressed, e.g., 2-AG is prevalent in the prenatal period and dramatically decreases postnatally, while anandamide levels increase postnatally (Anavi-Goffer et al., 2018). Interestingly, NPs commonly co-express CB1 and CB2 receptors; upon commitment to a neuronal fate, CB1 levels become up-regulated at the expense of CB2. CB2 seems more linked to a precursor undifferentiated proliferative state (Palazuelos et al., 2006; Palazuelos et al., 2012; Molina-Holgado et al., 2007; Fernández-Ruiz et al., 2007;

Galve-Roperh et al., 2013) and its involvement in axon guidance along the forming retino-thalamic pathway *in vitro* and *in vivo* has also been demonstrated (Duff et al., 2013). Studies showed that 2-AG can act both on CB1 and CB2 receptors present in NPs derived from the subventricular zone, thus regulating cell proliferation and affecting neuroblast migration towards the olfactory bulbs (Goncalves et al., 2015; Oudin et al., 2011; Jin et al., 2011).
Due to the complexity of the ECS, the full understanding of how its various components may contribute to control neurogenesis in developing and the adult brain is difficult to reach by *in vivo* approaches. A simplified *in vitro* model of neural progenitor cells could therefore be a useful tool to better understand the role of ECS components and to identify the intracellular mechanisms involved, as well as to provide the basis for ECS-targeted pharmacological approaches.
In this paper, we used the ST14A cell line, immortalized neural precursor-derived primary cells, dissociated from the rat striatal primordia at embryonic day 14 and conditionally immortalized by retroviral transduction of the temperature-sensitive variant of the SV40 large T antigen (Cattaneo et al., 1998). At the permissive conditions of 33 ◦C and 10% serum- containing medium, ST14A cells show high proliferative activity, while switching to the non-permissive temperature of 39 ◦C or at low serum concentrations (Cattaneo et al., 1998; Hovakimyan et al., 2008; Ehrlich et al., 2001) the cells stop or slow down their proliferation and start differentiating into striatal medium-sized spiny neurons (Cattaneo et al., 1998; Ehrlich et al., 2001; Rigamonti et al., 2000). Due to their simplicity of *in vitro* culturing, the possibility to be easily transfected and to be transplanted into an adult and developing rodent brain, ST14A has been successfully used by many authors to investigate several processes correlated to neural progenitors development and migration (Cacci et al., 2003; Gambarotta et al., 2004; Pregno et al., 2011; Beyer et al., 2003), as well as a model for studying Huntington's disease (Bari et al., 2013; Saba et al., 2020).

In our research, we tested the suitability of ST14A cells as a simplified *in vitro* model for studying ECS modulation of neurogenesis. First of all, we assessed the expression of the ECS components necessary to a functional endocannabinoid system. Then, by using CB1/CB2 agonists and antagonists, we evaluated the effects of CB1 and CB2 receptor modulation on neural progenitor proliferation. Finally, we began to characterize the intracellular pathways involved in the CB2-regulated proliferation of striatal projection neuron progenitors.

2. Materials and Methods

2.1. Cell Culture

ST14A striatal neural progenitor cell line (kindly provided by Dr. Elena Cattaneo, University of Milan, Milan, Italy) was cultured on 100 mm Petri-dishes (BD Biosciences, San Jose, CA, USA) in Dulbecco's modified Eagle's medium (DMEM) supplemented with 100 units/mL penicillin, 0.1 mg/mL streptomycin, 1 mM sodium pyruvate, 2 mM L- glutamine (all supplied by Sigma-Aldrich, St. Louis, MO, USA), and 10% fetal bovine serum (FBS, GIBCO®, Gaithersburg, MD, USA) decomplemented at 56 ◦C for 30 min. Cells were grown as monolayers at 33 ◦C in a 5% CO2 incubator.

2.2. RNA Extraction and RT-PCR

Cells were seeded and let grow under permissive, proliferating conditions at 33 ◦C for 48 h in DMEM containing 10% FBS. Only for gene expression studies, cells were also grown under non-permissive, differentiating conditions at 33 ◦C for 72 h in DMEM containing 0.5% FBS. Total RNA extraction was performed using TRIZOL® Reagent (Invitrogen, Carlsbad, CA, USA) following the manufacturer's instruction. DNA contaminants were eliminated using TURBO DNA-free kit (Applied Biosystems, San Francisco, CA, USA). cDNA was synthesized from total RNA by using Multiscribe RT (Applied Biosystems,USA) and random nonamers, starting from 2 µg of total RNA for each sample. PCR (30 amplification cycles) was performed using 250 ng cDNAs. Negative controls (C−) were carried out replacing cDNA with an equal amount of total RNA (no RT); as positive controls (C+), cDNAs from rat brain or rat spleen (for CB2 amplification only) were used. The housekeeping gene GAPDH was used as reference gene. Specific primers (Table 1) were designed on the basis of rat sequences, using both Primer3 (http://frodo.wi.mit.edu/ primer3/, accessed on 15 December 2020) and AnnHyb (http://www.bioinformatics.org/ annhyb/, accessed on 15 December 2020) programs, paying attention to choose primers on different exons to avoid amplification of genomic DNA.

Table 1. List of the primers used for PCR analysis.

	PCR Primers	Annealing T (°C)
GAPDH	Fw: 5′-TGGCATTGTGGAAGGGCTCATGAC-3 Rev: 5′-ATGCCAGTGAGCTTCCCGTTCAGC-3′	60
CB1	Fw: 5′-GGGTTACAGCCTCCTTCACA-3′ Rev: 5′-CAGATTGCAGCTTCTTGCAG-3′	55
CB2	Fw: 5′-GGAGTACATGATCTTGAGTGAT-3′ Rev: 5′-AGAACAGGGACTAGGACAAC-3′	50
DAGLα	Fw: 5′-GGCAAGACCCTGTAGAGCTG-3′ Rev: 5′-TAAAACAGGTGGCCCTCATC-3′	60

PCR reaction products were separated by 2% agarose gel electrophoresis in 1X TAE buffer. The correct length of the amplicons was confirmed by analysis with Gel Doc system and the software Quantity One (BioRad, Hercules, CA, USA), using Low DNA Mass Ladder (Invitrogen, USA) as molecular weight standards.

2.3. Western Blot

Cells were seeded and let grow under proliferating conditions at 33 ◦C for 48 h in DMEM containing 10% FBS, then total proteins were extracted by lysing cells in boiling Laemmli buffer (2.5% SDS, 0.125 M Tris-HCl, pH 6.8), followed by 3 min denaturation at 100 ◦C. Protein concentration was determined by BCA kit (Sigma-Aldrich, USA). As positive controls, rat brain or rat spleen (for CB2) total proteins were used. Protein extracts (20 µg/lane) were subjected to 10% SDS polyacrylamide gel electrophoresis (SDS-PAGE) and then blotted onto nitrocellulose membranes (BioRad, Hercules, CA, USA) according to the manufacturer's instructions. After blocking with 5% powder milk in TBS-T buffer (20 mM Tris, 150 mM NaCl, 0.1% Tween20, pH 7.4), filters were probed with anti-CB1 C-terminus (last 15 aa of CB1 rat receptor) or anti-CB2 N-terminus (first 39 aa of CB2 rat receptor) primary polyclonal antibodies (diluted 1:800 in TBS-T containing 1% no-fat milk); both the antibodies were produced in Ken Mackie's lab (Indiana University, Blooming- ton, IN, USA). Membranes were then washed in TBS-T and incubated with an anti-rabbit IgG HRP-conjugated secondary antibody (1:5000 dilution; Amersham Biosciences, Little Chalfont, UK). In order to check protein integrity, the expression of the housekeeping protein β-actin was revealed by means of anti-β-actin monoclonal primary antibody (diluted 1:10,000; Sigma-Aldrich, USA) and anti-mouse IgG HRP-conjugated secondary antibody (1:5000 dilution; Amersham Biosciences, USA). Specific bands were visualized by using enhanced chemiluminescence (ECL) detection system (Amersham Biosciences, USA). The apparent molecular weights of the stained proteins were determined by analysis with Gel Doc system and the software Quantity One, using prestained protein ladders (PageRuler Plus, Fermentas,

Waltham, MA, USA) as reference.

2.4. Immunofluorescence

ST14A cells were seeded on poly-L-lysine-coated coverslips (3500 cells/cm2). After 48 h of growth in DMEM containing 10% FBS, at 33 ◦C (proliferating conditions), cell were first rinsed in PBS containing Ca2+ and Mg2+, and then in 0.05% sucrose-PBS. Cells were subsequently fixed with 4% PAF in 0.1 M phosphate buffer (PB), pH 7.4 for 10 min. After 4 washings in PBS, cells were incubated in blocking serum (PBS containing 5% BSA, 10% normal serum, 0.1% TritonX-100) at RT for 1 h. Cells were then incubated O/N at 4 ◦C with the anti-CB1 or anti-CB2 primary antibody, diluted 1:400 or 1:200, respectively, in 0.01 M PBS plus 10% normal goat serum. Controls were set up by incubating cells with primary antibodies pre-adsorbed O/N with the specific immunogens. Cells were washed in PBS and incubated for 1 h with anti-rabbit IgG AlexaFluor 488-conjugated secondary antibody (1:250 dilution; Invitrogen, USA), washed again and mounted with 1,4- diazabicyclo [2.2.2]-octane (DABCO; Sigma-Aldrich, USA). Image analysis was performed with a Nikon fluorescent microscope coupled with a computer-assisted image analysis system (Neurolucida software, MicroBrightField, Williston, VT, USA).

2.5. Cell Count Assays

Cells were seeded at a density of 1500 cells/well in 96-well plates, in 200 µL DMEM containing 10% FBS and incubated at 33 ◦C. The following day, the medium was replaced with DMEM plus 10% FBS, containing alternatively or in combination (depending on the experiment) 5 µM 2-AG, 300 nM JWH133, 250 nM AM251, 50 nM PF514273, 300 nM AM630 (all purchased from Tocris Bioscience, Bristol, UK); for controls, medium plus 0.05% DMSO was used. Then, 24 h later, 20 µL of MTS Cell Titer 96 solution (Promega, Madison, WI, USA) was added and plates were incubated at 37 ◦C for 4 h. The absorbance was measured in a Microplate Reader (Bio-Rad, USA) at a wavelength (λ) of 490 nm. At least 5 replicates for each condition were set up and the experiment was repeated three times.

For PLC- and PI3K-blockade experiments, cells were seeded as before, then the medium was replaced with DMEM plus 2% FBS, containing 2 µM U73122 (PLC inhibitor, Sigma-Aldrich, USA), 150 nM wortmannin (PI3K inhibitor, Sigma-Aldrich, USA) or 0.05% DMSO (vehicle only) for 30 min. Then, all the wells were washed with PBS and the medium was replaced with DMEM plus 2% FBS, containing alternatively 5 µM 2-AG or 300 nM JWH133. Then, 24 h later, MTS

assay was performed and cell density was measured following the protocol reported above.

2.6. Cell Proliferation Assay

Cells were seeded on poly-L-lysine coated coverslips in 10% FBS-DMEM at a density of 3500 cells/cm2. The following day, the medium was replaced with 10% FBS-DMEM with or without 5 µM 2-AG, 300 nM JWH133, 300 nM AM630 and cells were cultured for another 24 h. Six hours before cell fixation, BrdU (10 µM) was added to the culture medium, then cells were fixed with 4% PAF in 0.1 M PB, pH 7.4, for 10 min and processed for BrdU-immunocytochemistry and DAPI staining. Briefly, cells were washed in PBS, then incubated at 37 ◦C with 2N HCl for 30 min and washed for 10 min with boric acid (0.1 M, pH = 8.5). Cells were washed and incubated in blocking serum (0.01 M PBS plus 10% normal serum) at RT for 1 h. Cells were incubated O/N at 4 ◦C with anti-BrdU mouse monoclonal antibody (Sigma-Aldrich, USA; dilution 1:3000 in 0.01 M PBS and 10% normal serum). Cells were washed and incubated for 1 h with anti-mouse IgG Cy3-conjugated secondary antibody (dilution 1:400; Jackson ImmunoResearch, West Grove, PA, USA). For nuclear staining, cells were labelled with 4',6-diamidino-2-phenylindole (DAPI) for 10 min and mounted with DABCO. Cell counts and image analysis were performed with a Nikon fluorescent microscope coupled with a computer-assisted image analysis system (Neurolucida Software, MicroBrightField, USA). Five random fields were counted in each well and each treatment was done at least in triplicate; the experiment was repeated three times. The cell proliferation was determined for each sample as the ratio of the number of BrdU+ cells over the total cell number (cells stained with DAPI).

2.7. Statistical Analysis

All the data were analyzed using commercially available software (SPSS version 26 for Windows; SPSS Inc., Chicago, IL, USA). Statistical analysis was performed using one-way ANOVA followed by Tukey's and Bonferroni's post hoc tests. The level of significance was set at $p < 0.05$.

3. Results

3.1 The Endocannabinoid System Is Expressed in ST14A Striatal Neural Progenitor Cells

The expression of ECS components was evaluated in the ST14A striatal neural progenitor cell line. Cells were cultured for 48 h under permissive, proliferating conditions (P; 10% serum-containing medium, incubation at 33 ◦C). By means of qualitative RT-PCR, ST14A cells were shown to express mRNAs encoding for CB1 and CB2 receptors; moreover, diacylglycerol lipase α (DAGLα) and monoacylglycerol lipase (MAGL), mainly involved respectively in the biosynthesis and degradation of 2-AG, were also expressed (Figure 1A). Focusing on cannabinoid receptors, CB1 and CB2 expression was also investigated at the protein level by Western blot analysis (Figure 1B). In the case of CB1, two bands with apparent molecular weights around 60 and 55 kDa, possibly corresponding to differently glycosylated forms, were observed. The Western blot for CB2 receptor revealed instead a major band of 45 kDa and a weaker band of about 40 kDa. CB receptor cellular localization was then assessed by means of immunofluorescence (Figure 1C); CB1 and CB2 immunoreactivities were abundantly found in the cytoplasm, especially around the nucleus.

The expression of the ECS was also evaluated in ST14A cells cultured for 72 h in differentiating conditions (D; 0.5% serum-containing medium, incubation at 33 ◦C), which favors a reduction of cell proliferation and allows the progenitors to start the differentiation toward striatal medium-sized spiny neurons. Differentiating ST14A cells were found to express the mRNAs encoding for both CB1 and CB2 receptors, as well as for DAGLα and MAGL (Figure 1A).

The detection of cannabinoid receptors mRNAs and proteins, as well as the expression of the mRNAs encoding endocannabinoid synthetic and degradative enzymes, strongly support the presence of an active ECS in ST14A neural progenitor cells.

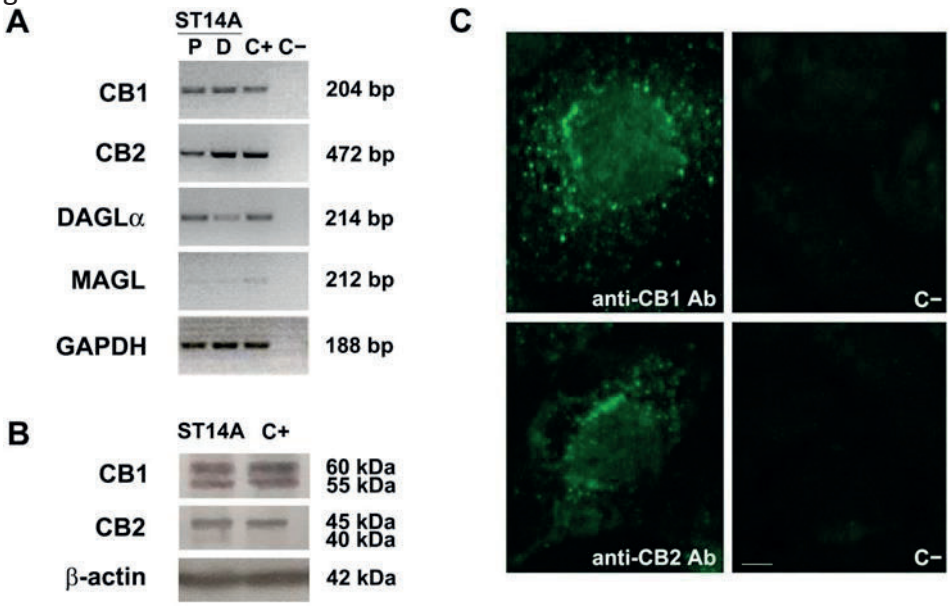

Figure 1. Endocannabinoid system expression in ST14A neural progenitor cells. (A) RT-PCR revealed specific bands corresponding to CB1 and CB2 receptors and to the enzymes DAGLα and MAGL in ST14A cells cultured 48 h under proliferating conditions (P). The same genes were also expressed in ST14A cells induced to differentiate toward a neuronal phenotype for 72 h (D, differentiating conditions). The housekeeping gene GAPDH was used as reference gene. The base pair (bp) length of the different amplicons is indicated. C+: positive controls, i.e., cDNA from rat brain or from rat spleen (for CB2 only); C−: negative control (no RT). (B) Western blot showing the expression of CB1 and CB2 receptors in ST14A neural progenitors (cells cultured 48 h under proliferating conditions); β-actin protein expression was used as a quality control of the protein extract. The apparent molecular weights of the bands are indicated (kDa). C+: positive controls, i.e., protein extracts from rat brain or spleen (for CB2 only). (C) Immunofluorescence for CB1 and CB2 receptors in ST14A cells neural progenitors (cells cultured 48 h under proliferating conditions). Single-cell magnification. Specific immunoreactivities are mainly distributed in the cytoplasm and in proximity to the nucleus. C−: negative controls, i.e., anti-CB1 or anti-CB2 pre-adsorbed antibodies. Calibration bar: 5 μm.

3.2. The Pharmacological Blockade of Cannabinoid Receptors Does Not Affect ST14A Cell Number

In order to determine if ST14A progenitor proliferation is under constitutive endocannabinoid regulation, we tested the effects of CB1 and CB2 pharmacological blockade.

Cells were cultured in proliferating conditions (at 33 ◦C, in 10% serum-containing medium) and treated for 24 h with alternatively one of the two selective CB1 antagonists AM251 and PF514273, and the CB2 antagonist AM630. A dose–response experiment (Figure S1) was conducted in order to verify different antagonist concentration effects on cell number, as well as to exclude cytotoxic effects and to select the best antagonist concentration to be used in subsequent experiments; based on previously unpublished experiments performed in our lab, a 24 h treatment was chosen. As shown in Figure 2 and Figure S1, neither CB1 nor CB2 blockade, at any antagonist concentration used, led to a change in ST14A cell number compared to untreated control cells, suggesting that constitutive cannabinoid signaling is not involved in ST14A cell proliferation/survival.

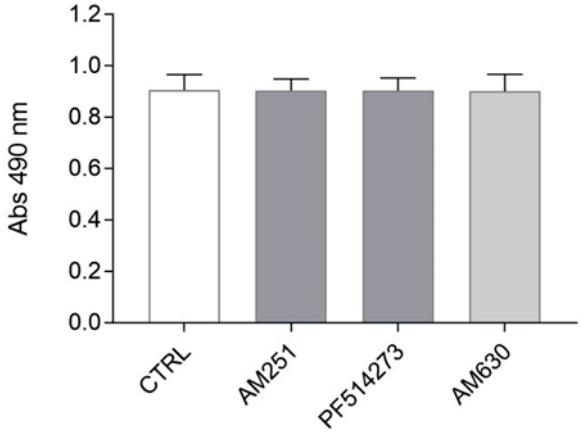

Figure 2. Evaluation of CB1/CB2 blockade effects on ST14A cell number. ST14A were treated for 24 h with 250 nM AM251 or 50 nM PF514273 (CB1 antagonists), or 300 nM AM630 (CB2 antagonist), then an MTS assay was performed. No effect on ST14A cell number was observed in treated cells, in respect to control (CTRL, medium plus 0.05% DMSO). Data from the MTS assay are expressed as mean ± standard deviation (SD) of the absorbance (λ = 490 nm); n = 8 replicates, 3 independent experiments.

3.3. Exogenous Administration of the Endocannabinoid 2-AG and the CB2 Agonist JWH133 Induces ST14A Cell Proliferation through CB2 Receptor Activation

We subsequently tested whether exogenous activation of CB1 and CB2 receptors by the administration of the CB1/CB2 agonist 2-AG could affect ST14A cell proliferation. Cells were stimulated for 24 h under proliferating conditions with 2-AG, then an MTS assay was performed. A preliminary dose–response experiment (Figure S2, panel A) allowed us to select the optimal agonist concentration to be used in this and subsequent experiments; based on previously unpublished experiments performed in our lab, a 24 h treatment was chosen.

As shown in Figure 3, 2-AG (5 µM) was able to induce a statistically significant increase in ST14A cell number, compared to control levels. To clarify the receptor subtype involved, CB1 and CB2 selective antagonists, used at the previously selected concentrations, were co-administered with 2-AG. 2-AG (5 µM) effects were not modified by co-treatment with the CB1 antagonists (250 nM AM251 or 50 nM PF514273), thus excluding a CB1- mediated effect. On the other hand, the 2-AG-mediated increase in ST14A cell number was specifically reverted by the coadministration of the CB2 selective antagonists AM630 (300 nM), indicating the involvement of CB2 receptor. This result was further

confirmed by treatment for 24 h with a selective CB2 receptor agonist; indeed, JWH133 (300 nM; see Figure S2, panel B for preliminary dose–response experiment) induced an increase in cell number, in respect to control, and the effect was specifically reverted by coadministration of AM630 (300 nM) (Figure 3).

To confirm that the increase in ST14A cell number observed after 2-AG and JWH133 treatment was the result of an increase in cell proliferation and not in the survival rate, a BrdU-based proliferation assay was performed. Both the endocannabinoid 2-AG (5 µM) and the synthetic CB2 agonist JWH133 (300 nM) significantly increased BrdU incorporation in ST14A cells, thus indicating a proliferative effect (Figure 4). AM630 (300 nM) administration alone did not influence ST14A proliferation rate, while its coadministration with 2-AG and JWH133 specifically blocked the proliferative effect induced by the agonists (Figure 4).

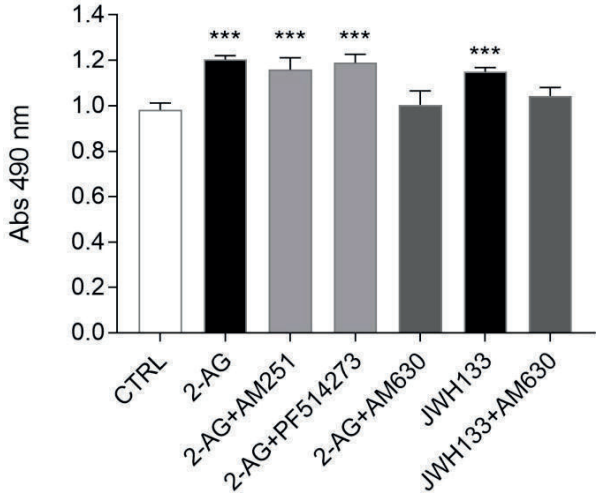

Figure 3. Evaluation of the effects of 2-AG and JWH133 alone or in the presence of specific CB1/CB2 antagonists on ST14A cell number. 2-AG (5 µM) induces an increase of ST14A cell number after 24 h, with respect to control cells (CTRL). The effect was not reverted by the coadministration of 2-AG with the CB1 selective antagonists AM251 (250 nM) and PF514273 (50 nM); on the other hand, cell number was comparable to control when 2-AG was co-administered with the selective CB2 antagonist AM630 (300 nM). Similarly, the selective CB2 receptor agonist JWH133 (300 nM) induced ST14A cell number increase, which was specifically reverted by the coadministration of AM630 (300 nM). Data from the MTS assay are expressed as means ± SD of the absorbance (λ = 490 nm); n = 5 replicates, 3 independent experiments. *** = $p \leq 0.001$ vs. control.

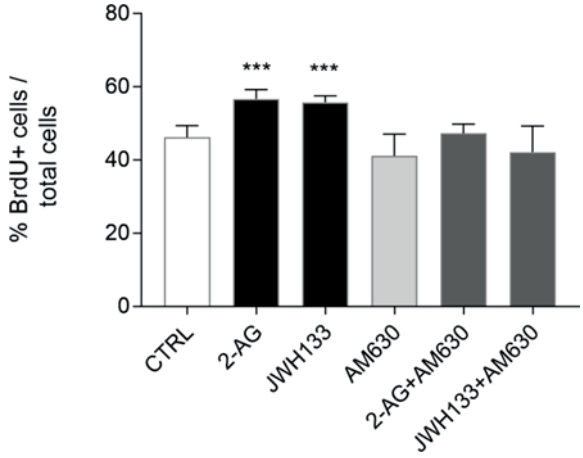

Figure 4. Evaluation of the effects of 2-AG and JWH133 alone or in the presence of the specific CB2 antagonist AM630 on ST14A cell proliferation rate. Results are shown as ratio (%) of the number of BrdU+ cells over the number of total cells, stained with DAPI fluorophore. After 24 h treatment with 2-AG (5 µM) and JWH133 (300 nM) an increase in BrdU incorporation was observed, with respect to untreated cells (CTRL); the effect was specifically reverted in both the cases by 300 nM AM630 coadministration. Data are expressed as mean ± standard deviation (SD); n = 3 replicates (5 random fields counted in each well), 3 independent experiments. *** = $p \leq 0.001$ vs. control.

BrdU-based experiments demonstrated therefore that exogenously administered endocannabinoid 2-AG induces ST14A neural progenitor proliferation via a CB2- mediated mechanism.

3.4. PLC Pharmacological Blockade Impairs CB2-Mediated ST14A Cell Proliferation

In order to identify the possible intracellular effectors involved in CB2-mediated ST14A cell proliferation, we evaluated the effects of pharmacological blockade of the signalling cascades involving PLC and PI3K activation.
The day after seeding, ST14A cells were pre-incubated for 30 min with the PLC inhibitor U73122 (2 µM) or the PI3K inhibitor wortmannin (150 nM), then inhibitors were removed and cells were cultured for 24 h in the presence of the agonists 2-AG or JWH133; cell counting was then performed with an MTS assay. The experiments were conducted in a medium containing 2% serum (instead of 10%) in order to reduce possible interference of serum components on the effects of PLC and PI3K inhibitors on cell proliferation.
As shown in Figure 5, at the concentrations used, the pre-treatment with the two inhibitors did not have any effect per se on ST14A viability/cell number,

allowing further investigations. Interestingly, wortmannin pretreatment did not counteract the 2-AG- and JWH133-driven increase in cell number. On the opposite, the presence of the PLC inhibitor U73122 was able to revert the cell number increase induced by 2-AG- and JWH133 to control conditions.

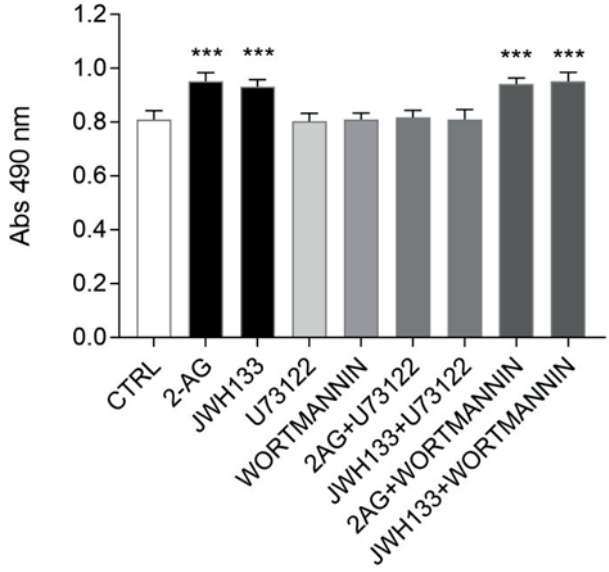

Figure 5. Evaluation of Phospholipase C (PLC) and PI3K pharmacological blockade on 2-AG- and JWH133-induced ST14A cell number increase. *Cells were pretreated 30 min with U73122 (2 µM) or wortmannin (150 nM) prior to 2-AG (5 µM) or JWH133 (300 nM) incubation for 24 h in 2% serum- containing medium. U73122, but not wortmannin pretreatment, reverted 2-AG- and JWH133-driven ST14A cell number increase. Data from MTS assay are expressed as means ± standard deviation (SD) of the absorbance (λ = 490 nm); n = 8 replicates, 3 independent experiments. *** = p ≤ 0.001 vs. control.*

Overall, our findings indicate that exogenously administered 2-AG promote ST14A neural progenitor proliferation through CB2 receptor engagement and PLC pathway activation.

4. Discussion

The endocannabinoid system modulates several biological processes, including the generation and survival of neurons in the developing and adult CNS, also under pathological conditions (De Oliveira et al., 2018). Indeed, the involvement of CB2 receptor in neurogenesis, as well as neurodegenerative and neuroinflammatory disorders, open to new possible pharmacological strategies based on the use of CB2-specific therapeutic drugs, possibly overcoming the

neuropsychiatric adverse effects of CB1-targeted therapies (Di Marzo et al., 2018 ; Haspula et al., 2020).

In this work, we propose ST14A striatal neural progenitor cells as a simplified *in vitro* model suitable for studying the role of the ECS in neurogenesis, as well as for ECS-targeted pharmacological approaches.

The ST14A cell line was established by immortalization of neural precursor-derived primary cells dissociated from the rat striatal primordia at embryonic day 14 (Cattaneo et al., 1998). Compared to neuroblast primary cultures, this experimental model is easier to handle and to maintain in culture, so it is more suitable when approaching initial studies on molecular interactions. Furthermore, ST14A cells have also been used extensively for genetic manipulation experiments and transplantation into an adult and developing rodent brain, making these cells an *in vitro* system with great potential for biochemical, molecular, and biological studies correlated to neural progenitors development and migration (Ehrlich et al., 2001; Rigamonti et al., 2000; Cacci et al., 2003; Beyer et al., 2007), as well as a model for studying neurological diseases (Bari et al., 2013; Saba et al.,2020).

In this paper we showed that ST14A neural progenitor cells display an active ECS, in agreement with the findings obtained by Bari and colleagues (Bari et al., 2013) on ST TetOn 12.7, a ST14A subclone able to express reverse tetracycline-controlled transactivator under the control of doxycycline; also, previous studies on primary cultures of neural progenitors demonstrated functional CB1 and CB2 receptor expression (Palazuelos et al., 2012; Oudin et al., 2011; Aguado et al., 2005; Avraham et al., 2014).

In particular, we found that several components of the system, such as the cannabinoid receptors CB1 and CB2, as well as the endocannabinoid synthetic and degradative enzymes DAGLα and MAGL, are expressed in ST14A neural progenitors (cultured under permissive, proliferating conditions). Consistent with previous results (Bari et al., 2013), Western blot analysis confirmed the expression of both CB1 and CB2 receptors; CB1 receptor appeared as two bands with an apparent molecular weight around 60 and 55 kDa, possibly corresponding to differently glycosylated forms, while in the case of CB2 receptor a major band of 45 kDa and a weaker band of about 40 kDa were seen. In ST TetOn 12.7, instead, CB1 and CB2 receptors were detected as single bands of 60 kDa and 45 kDa, respectively (Bari et al., 2013); the discrepancy with our results could be either due to the different ST14A clone and/or the different primary antibodies used. Immunofluorescence analysis for CB1 and CB2 revealed, accordingly with (Bari et al., 2013), cytoplasmic localizations of both the receptors, rather than a membrane localization, probably due to their intense trafficking and internalization; a marked perinuclear localization was

found for CB2, according to the observations reported by Atwood and colleagues (Atwood et al., 2011). Actually, CB2 binding sites were demonstrated to be predominantly located intracellularly in prefrontal cortical pyramidal neurons (Boon et al., 2012) and functional CB2 receptors were demonstrated at the endo-lysosome level (Brailoiu et al., 2014); also, CB1 receptor localization is not exclusively on the plasma membrane, since active CB1 were localized also in the outer membrane of mitochondria (Bénard et al., 2012) and a predominant intracellular localization have been observed in diverse cell types and also undifferentiated neuronal cells (Rozenfeld et al., 2010). In our study, we also widened our analysis to ECS expression in ST14A cells induced to differentiate toward a medium-size spiny neuron phenotype; mRNAs encoding for CB1 and CB2 receptors, as well as for DAGLα and MAGL were detected, consistent with studies showing the presence of a functional ECS in the striatum (Gong et al., 2006;Augustin et al., 2018).

We subsequently focused our attention on the possible modulation played by the ECS on ST14A neural progenitor proliferation (Soldati et al., 2008; Lange et al., 2006).

First, we assessed the effects of a perturbation of the endogenous ECS by pharmacological blockade of the cannabinoid receptors. Under these conditions, neither CB1 nor CB2 blockade had significant effects on ST14A neural progenitor cell number. On the other hand, the stimulation of cannabinoid receptors with a non-selective CB1/CB2 ligand, the endocannabinoid 2-AG, induced ST14A cell number increase through the activation of the CB2 receptor, as indicated by the fact that the effect was reverted by the co-administration of 2-AG with the CB2 specific antagonist AM630, but not with the CB1 antagonists AM251 and PF514273. CB2 involvement was further supported by the finding that the CB2 specific synthetic agonist JWH133 increased ST14A cell number, an effect reversed by the coadministration of the CB2 antagonist. Interestingly, a BrdU assay allowed us to demonstrate that the increase in ST14A cell number was related to an enhancement of neural precursor proliferation rate, rather than an increase in cell survival. In our study, we chose to use the endogenous ligand 2-AG to better mimic the ECS in an embryonic environment, since until birth 2-AG is much more abundant than AEA (Anavi-Goffer et al., 2009). Our results about CB2-mediated proliferation are in agreement with the findings of (Plazuelos et al., 2006; Palazuelos et al., 2012; Goncalves et al., 2008; Oudin et al., 2011), showing that endocannabinoids and synthetic cannabinoids can act on CB2 receptors present in NPs, regulating cell proliferation. The fact that we did not observe any effect on neural progenitor cell number following CB2 blockade, while CB2 agonist administration induced cell proliferation, could possibly be explained by the fact

that only a few receptors might be activated in basal conditions; conversely, following exposure to exogenous ligands, CB2 receptors are massively activated and the effect of inhibition could be readily visible.

We aimed also to identify some of the possible intracellular effectors involved in CB2-mediated ST14A cell proliferation. CB1 and CB2 share several downstream signaling mechanisms in neural progenitors (Galve-Roperh et al., 2013); in particular, they are coupled to the activation of the ERK and the PI3K/Akt pathways. In cerebellar progenitor cells, CB1-induced cell proliferation was shown to be mediated by the PI3K/Akt/GSK3β and in cortical progenitors, CB1 drives mTORC1 signaling and cell proliferation. CB2 was shown to promote hippocampal neural progenitor proliferation through activation of the PI3K/Akt/mTORC axis (Palazuelos et al., 2012; Shoemaker et al., 2005). In addition, previous studies demonstrated that 2-AG-mediated activation of CB2 leads to a PLC-IP3R dependent intracellular calcium increase and subsequent massive activation of MAPK/ERK cascade (Shoemaker et al., 2005). By preincubation with the PI3K inhibitor wortmannin or the PLC inhibitor U73122, we observed that the inhibition of PI3K had no consequence on CB2 ligand-mediated proliferation, while the PLC inhibitor U73122 significantly impaired the process. The dissimilarity between our data and Palazuelos and colleagues' observations (Palazuelos et al., 2012) could be possibly due to the different brain areas of cell origin (hippocampus vs. striatum). Furthermore, cells belonging to different brain areas and ages (embryonic and adult) could display diverse intracellular cascades related to their stage-specific enzymatic equipment. Interestingly, intracellularly located CB2 receptors were demonstrated to open IP_3R-dependent Ca^{2+}-activated Cl^- channels in prefrontal cortex pyramidal neurons (Shoemaker et al., 2005).

In conclusion, our study indicates that ST14A cells express a functional endocannabinoid system that is actively involved in the regulation of neural progenitor proliferation. ST14A cells could therefore represent a useful, simplified *in vitro* model for studying ECS modulation of neurogenesis. Moreover, the model could be used to test new therapeutic drugs acting on the cannabinoid system, thus providing the basis for *in vivo* pharmacological studies.

Part III

Beta-Caryophyllene Modifies Intracellular Lipid Composition in a Cell Model of Hepatic Steatosis by Acting through CB2 and PPAR Receptors

1. Introduction

Non-alcoholic fatty liver disease (NAFLD) is the most common chronic liver disorder, with an average prevalence of 25%, ranging from 13% (adult African population) to 32% (Middle East population) (Powell et al., 2021). This disease is characterized by the excessive accumulation of fats, due to overnutrition or an unbalanced diet and not to ethanol consumption, with an increase of visceral fats that results in macrophage infiltration and pro-inflammatory conditions (Friedman et al., 2018). In this context, insulin resistance occurs, causing dysregulated lipolysis of triglyceride in the adipose tissue and delivery of fats to the liver. This is accompanied by increased *de novo* lipogenesis, the process through which hepatocytes convert excess carbohydrates to free fatty acids (FFA). The disposal of FFA occurs through beta-oxidation or re-esterification, and when this process is overloaded the formation of lipotoxic lipids may occur. This causes oxidative stress, endoplasmic reticulum stress and hepatocellular damages. The exacerbation of this condition leads to nonalcoholic steatohepatitis (NASH) that can progress to cirrhosis and liver cancer (Powell et al., 2021; Friedman et al., 2018). No specific pharmacological treatments are currently approved for NAFLD and NASH. The therapeutic strategies are based on lifestyle improvement (i.e., physical activity and healthy diet) associated with periodical checking of cardiometabolic risk factors to avoid advanced forms of NAFLD and the prevention of complications (Mantovani et al., 2021). Nevertheless, numerous anti-hypertensive, lipid-lowering (statins) and glucose-lowering drugs (metformin) have been investigated because of NAFLD association with type 2 diabetes (T2DM), hypertension, obesity and dyslipidemia (Mantovani et al., 2021). Other investigated drugs are those belonging to peroxisome proliferator-activated receptor (PPAR)γ agonists (e.g., pioglitazone, rosiglitazone). However, because of the side effects, the incomplete efficacy of these drugs and the variability of the conditions that exist among different patients, the suggested strategies remain those mentioned above (Mantovani et al.,2021).

In recent years, natural molecules have been demonstrated to ameliorate typical conditions of NAFLD, from steatosis to inflammation. Among them, the methyl brevifolincarboxylate, a polyphenolic compound, can reduce inflammation and oxidative stress in an hepatocarcinoma cell line (Geethangili et al., 2021) and berberine, a benzylisoquinoline alkaloid, can reduce triglyceride synthesis-related genes in *in vitro* and *in vivo* models (Zhu et al., 2019); nevertheless these molecules have not yet been approved by the FDA. Instead, (E)-β-caryophyllene (BCP) has been recognized by the FDA as a safe food or cosmetic additive. BCP is a bicyclic sesquiterpene hydrocarbon widely

distributed in the plant kingdom, especially in floral volatiles, occurring in more than 50% of angiosperm families (Maffei et al., 2020). In plants, BCP acts as a chemoattractant for pollinators, defence against bacterial pathogens and has a pivotal role in the survival and evolution of higher plants as well as in contributing to the unique aroma of essential oils extracted from numerous species (Scandiffio et al., 2020). In addition to its role in plants, recent studies have highlighted that BCP plays a role in animal cells as anti-cancer (Mannino et al., 2021), anti-oxidant (Yovas et al., 2022), anti-inflammatory agent (Picciolo et al., 2020). Although its mechanism of action is not yet fully understood, studies indicate that BCP could act in animal cells through the specific binding to the CB2 cannabinoid receptors (Gertsch et al., 2008; Geddo et al., 2021), of which it is a full selective agonist, and possibly through the interaction with members of the family of peroxisome proliferator-activated receptor (PPAR), in particular the isoforms α and γ (Wu et al., 2014; Irrera et al., 2019).

CB2 receptors belong to the endocannabinoid system (ECS), a complex endogenous system involved in several physiological and pathophysiological functions. The ECS exerts regulatory control on metabolism and food intake and for this reason it represents a potential target for numerous metabolic disorders such as obesity, eating disorders, dyslipidemia and steatosis (Charytoniuk et al., 2022; Lowe et al., 2021). The ECS is also involved in the regulation of inflammation and in the modulation of depression, schizophrenia and chronic pain (Machado et al., 2018; Mlost et al.,2019). The selectivity of BCP for CB2 receptors avoids potential psychotropic effects mediated by the neuronal CB1 cannabinoid receptor, being CB2 receptors mainly expressed in peripheral tissues and in central nervous system (CNS) immune cells (Francomano et al., 2019). This peculiarity makes BCP a safe phytocannabinoid, with countless beneficial and non-psychoactive effects.

PPAR nuclear receptors are transcriptional modulators, with each isoform having a specific location and role regarding energy homeostasis, lipid and glucose metabolism and inflammatory response (Berthier et al., 2021). PPARα is mainly expressed in the liver (but also in brown adipose tissue, heart, muscles and kidney) and acts as the master regulator of hepatic lipid metabolism, being involved especially in fatty acid (FA) beta-oxidation. PPARγ is characterized by three isoforms: PPARγ1, PPARγ2 and PPARγ3. PPARγ1 is ubiquitously expressed, PPARγ2 is mainly expressed in adipose tissue and in the liver, whereas PPARγ3 is expressed in the colon and adipose tissue (Berthier et al., 2021). The role of the three isoforms slightly changes based on cell type, but in the liver they are essentially involved in the regulation of glucose and lipid metabolism, protection against inflammation, oxidation and liver fibrosis (Wu et al., 2020).

The interaction between BCP and PPARα and PPARγ is not as well documented as it is for CB2 receptors; however, some studies have shown that there is a direct interaction between BCP and PPARα (Wu et al., 2014) and probably an indirect interaction with PPARγ. In fact, the triggering of PPARγ via BCP-mediated CB2 receptor activation has been hypothesized (Youssef et al., 2019).

This study aimed to investigate the anti-steatotic effects of BCP in the immortalized human hepatoma cell line HepG2, one of the cell models mostly used to induce NAFLD and to test the therapeutic effects of pharmacological and natural compounds (Gómez-Lechón et al., 2007). To mimic the key NAFLD risk factor, increased fat intake, we added palmitic and oleic acid to cell culture media obtaining significant intracellular lipid accumulation in the absence of overt cytotoxicity. We first investigated the effect of BCP on the intracellular lipid accumulation and lipid profile, then we examined the involvement of different receptors in these processes. Our findings suggest that treatment with BCP induces a reduction in lipid accumulation and a modification in intracellular lipid composition mediated by CB2 and PPAR receptors and that these effects are accompanied by a modulation of their expression. We also observed that BCP is able to cross the plasma membrane and therefore to act on intracellular localized receptors.

2. Materials and Methods

2.1. Reagents

Chemicals used were: (E)-β-caryophyllene (BCP) purchased from Sigma-Aldrich (St. Louis, MO, USA), AdipoRed™ assay reagent from Lonza (Walkersville, MD, USA), NucBlue Live ReadyProbes Reagent from Invitrogen (Carlsbad, CA, USA), CellTiter-Glo® Luminescent Cell Viability from Promega (Madison, WI, USA), anti-CB2 primary antibody from Cayman chemical (Ann Arbor, MI, USA), anti-Rabbit IgG AlexaFluor647 secondary antibody from Jackson Immunoresearch (Ely, UK), AM630, GW9662 and GW6741 antagonists from Cayman chemical and sodium oleate, sodium palmitate and bovine serum albumin from Sigma-Aldrich. Unless otherwise specified, all other chemicals were purchased from Sigma-Aldrich.

2.2. Cell Cultures

HepG2 human hepatoma cell line (European Collection of Authenticated Cell Cultures ECACC catalogue number 85011430) was purchased from Sigma-Aldrich. Cells were cultured in Minimum Essential Medium Eagle (MEM) supplemented with 10% fetal bovine serum, 2 mM L-glutamine, 50 IU/mL penicillin, 50 µg/mL streptomycin and 1% non-essential amino acids (NEAA). For every experiment, cells were grown at sub-confluence.

2.3. Cell Viability

The viability of HepG2 cells was evaluated at the end of the steatosis induction experiments and treated with different concentrations of BCP, by CellTiter-Glo® Luminescent Cell Viability Assay, based on the quantitation of ATP, which signals the presence of metabolically active cells. Cells were washed in phosphate-buffered saline (PBS), then CellTiter-Glo® reagent, diluted 1:1 in PBS, was added. Cells were incubated at room temperature in the dark for 10 min, then luminescence was detected and quantified with the FilterMax F5 Multi-Mode microplate reader (Molecular Devices, Sunnyvale, CA, USA). The values of luminescence are directly proportional to the number of viable cells.

2.4. In Vitro Steatosis Induction and Lipid Quantification

For steatosis induction experiments, 2×10^4 cells/well were seeded in 96-well black clear bottom plates (Greiner Bio-One, Frickenhausen, Germany). Prior to the experiments, cells were starved overnight with serum-free MEM, then cells were incubated for 12 h or 24 h in serum-free MEM containing 0.25 mM, 0.5 mM or 1 mM free fatty acid mixture (FFAm). The mixture was prepared by coupling sodium palmitate (Na^+-hexadecanoate) and sodium oleate (Na^+-(Z)-octadec-9-enoate) (1:2 ratio) with 1% *w*/*v* FFA-free BSA in serum free MEM, at 38 °C in agitation overnight, to allow FFA coupling with BSA; the mixture was then filtered and used immediately in subsequent experiments or frozen at 20 °C. Based on the preliminary results we obtained, for subsequent experiments, HepG2 cells were treated for 24 h with 0.5 mM FFAm alone or in the presence of scalar dilutions of BCP (50 nM−50 µM); control cells were grown with serum-free MEM containing 1% *w*/*v* BSA. At the end of the experiments, cells were washed in PBS, then a dye mixture containing AdipoRed and NucBlue reagents (25 µL and 1 drop, respectively, for each mL of PBS) was added. AdipoRed assay reagent quantifies intracellular triglycerides, while the DNA content was estimated by NucBlue staining. After 40 min of incubation at room temperature in the dark, fluorescence was measured with Filtermax F5 microplate reader; for AdipoRed, quantification excitation was performed at 485 nm and emission read at 535 nm, while for NucBlue, excitation was at 360 nm and emission read at 460 nm.

2.5. Antagonists Treatment

For antagonists experiments, 2×10^4 cells/well were seeded in 96-well black clear bottom plates, starved and treated as above mentioned with FFA mixture, 5 µM BCP and the following antagonists: 5 µM AM630 (CB2 receptor

antagonist), 100 nM GW6471 (PPARα receptor antagonist) or 10 µM GW9662 (PPARγ receptor antagonist).

2.6. Lipid Extraction, Identification and Quantification by Gas Chromatography

For lipid extraction and quantification experiments, 2×10^6 cells were grown on T-25 flasks. After cell starvation, HepG2 cells were treated with FFAm alone or FFAm and 5 µM BCP for 24 h. One ml of culture medium was then taken for gas chromatography–mass spectrometry (GC-MS) analysis of free fatty acids. The intracellular fatty acid content was also analyzed; cells were washed with PBS, detached with trypsin and centrifuged at 800 g, 5 min. Lipids were extracted from cell pellets using cyclohexane (1:10, *w*/*v* ratio) and then esterified with boron tri-fluoride (10% *w*/*v* in methanol). Fifty µg heptadecanoic acid (C17:0) was added as the internal standard. Fatty acid methyl esters (FAME) identification was performed by gas chromatography coupled with mass spectrometry (GC-MS) (5975T, Agilent Technologies, Santa Clara, CA, USA). FAME quantitative analyses were performed through GC coupled with a flame ionization detector (GC-FID) (GC-2010 Plus, SHIMADZU, Kyoto, Japan). The GC carrier gas was helium with a constant flux of 1 mL min^{-1}, and separation was obtained with a non-polar capillary column ZB5-MS (30 m length, 250 µm diameter and stationary phase thickness of 0.25 µm, 5% phenyl-arylene and 95% poly-dimethyl siloxane stationary phase) (Phenomenex, Torrance, CA, USA). GC-FID FAME separation was performed in the same conditions, by using a similar column. Mass spectrometer parameters were: ionization energy of the ion source set to 70 eV and the acquisition mode set to 50–350 *m/z*. Separated molecules were identified through the comparison of mass fragmentation spectra with reference spectra of the software NIST v2.0 and libraries NIST 98, by comparison of Kovats indexes and the internal standard injection (C17,C20:4, C20:5—Sigma Aldrich, St Louis, MO, USA). The results are expressed as mg g^{-1} fresh weight (f.wt).

2.7. Intracellular Quantification of BCP in Time-Course Experiments

For BCP time-course uptake experiments, 1×10^6 cells were grown on 6-well plates and treated with 5 µM BCP. Starting from time zero and after 30 min, 1 h, 1.5 h, 2 h, 3 h, 4 h, 5 h, 6 h, 10 h and 24 h cells were washed in PBS, detached with trypsin, centrifuged and the pellets were transferred in glass vials where 1 mL of hexane was added. The identification of BCP amounts in cells at different times was performed with the Single Ion Monitoring (SIM) method by GC-MS. The following chromatographic conditions were used: column ZB5-MS (30 m length, 250 µm diameter and stationary phase thickness of 0.25 µm, 5 % phenyl-arylene and 95% of poly-dimethyl siloxane stationary phase); splitless mode,

oven program: 40° for 1 min, then a 5 °C min^{-1} ramp to 200 °C, a 10 °C min^{-1} ramp to 220 °C, and a 30 °C min^{-1} ramp to 260 °C, final temperature held for 3.6 min. Mass spectra were acquired within the 29–350 m/z interval operating the spectrometer at 70 eV and at scan speed mode. The identification of BCP was performed on the basis of both matches of the peak spectra with a library spectral database, and comparison with pure standards.

2.8. Immunofluorescence

For immunofluorescence experiments, 6 x 10^4 cell/cm^2 were seeded on glass coverslips and incubated for at least 3 h to allow adhesion. Then, cells were fixed for 30 min in 4% paraformaldehyde dissolved in 0.1 M phosphate buffer, pH 7.3. After three washes with PBS, cells were incubated for 15 min with PBS containing 0.01% Triton-X100 and then for 45 min with PBS containing 1% BSA and 10% normal donkey serum. Triton-X100, normal donkey serum and BSA concentrations were selected after several trials to avoid autofluorescence of HepG2. Cells were then incubated overnight at 4 °C with anti-CB2 (1:100 in PBS) primary polyclonal antibody. Coverslips were washed twice with PBS and incubated for 1 h at room temperature with the secondary antibody, anti-rabbit IgG Alexa Fluor 647 (1:600 in PBS containing 1% normal donkey serum). After two washes in PBS, cells were incubated for 20 min in DAPI (1:200 in PBS), washed again twice in PBS and then coverslips were mounted on standard slides with DABCO. Pictures of HepG2 cells immunolabeled for CB2 were taken with a TCS SP5 confocal microscope (Leica Microsystems, Wetzlar, Germany). Confocal image z-stacks were captured throughout the thickness of the cells and were performed with 0.7 µm optical step size using an objective 63X/1.4 NA oil immersion lens with a resolution of 8-bit, 1024/1024 pixels and 100-Hertz scan-speed (without additional zoom: 1 voxel, xyz = 240 × 240 × 692 nm; with 2.5× additional zoom: 1 voxel, xyz= 96 × 96 × 692 nm). Images are shown as maximum intensity projection or single plane with reslice.

2.9. RNA Extraction and qRT-PCR

For qRT-PCR experiments, 1 × 10^6 cells were grown on 6-well plates and treated to induce steatosis in the presence/absence of 5 µM BCP (see above). Total RNA extraction was performed using TRIZOL® Reagent (Invitrogen) following manufacturer's instructions. Chloroform was added and, after 5 min of centrifugation at 14,000 rpm, RNA was precipitated in isopropanol for 3 h at −20 °C. Samples were then centrifuged at 14,000 rpm for 15 min, the RNA was washed with 70% ethanol and centrifuged at 14,000 rpm for 5 min. The RNA pellet was briefly air-dried and resuspended in 30 µL sterile water. Samples were quantified using NanoDrop 8000 Spectrophotometer (Thermo Fisher

Scientific, Waltham, USA). qReal-time PCR was performed using SensiFast SYBR No-ROX One-Step Real-Time qPCR kit (Bioline, London, UK) in the thermal cycler Rotor Gene Q (Qiagen, Hilden, Germany). qRT-PCR conditions were: retrotranscription (55 °C, 15 min), initial denaturation (95 °C, 2 min), 50 cycles of denaturation (94 °C, 15 s), annealing (55 °C, 10 s), extension (68 °C, 24 s) and final melting (ramp from 56 °C to 99 °C). Each RNA sample was analyzed in three technical replicates containing 50 ng of total RNA. Relative quantification of mRNA abundance in each sample was performed using a standard curve, built with several dilutions of the samples. The widely used housekeeping gene β-actin was used as an internal control to normalize target gene expression. The reliability of the housekeeping gene was confirmed by its consistency of expression across treatments. qRT-PCR starting from constant amounts (50 ng) of different RNA samples, accurately quantified by NanoDrop Spectrophotometer analysis, resulted in fact in comparable levels of amplification (Ct, cycle threshold values). Specific primers were designed with PrimerBlast software on the basis of human sequences (Table 1). The qPCR primer efficiencies were first assessed by the amplification of serial dilutions of RNA pools (three replicates for each dilution); the efficiency values were directly calculated by Rotor Gene Q software and were as follows: β-actin 98%, *CNR2* 103%, *PPARα* 95%, *PPARγ* 105%.

Primers sequences and amplicon size are reported in Table 1

Table 1. Specific primers used in qRT-PCR

Gene	Forward Sequence	Reverse Sequence	Amplicon Size
β-actin	5′ CCAACCGCGAGAAGATGA 3′	5′ CCAGAGGCGTACAGGGATAG 3′	97 bp
CNR2	5′ TGGCATAGAAGACGGAGCTG 3′	5′ CCCGGAGAGCCCCAAATG 3′	177 bp
PPARα	5′ ACACCGAGGACTCTTGCGA 3′	5′ GGAAAGGGCAAGTCCCGATG 3′	207 bp
PPARγ	5′ TACTGTCGGTTTCAGAAATGCC 3′	5′ GTCAGCGGACTCTGGATTCAG 3′	141 bp

2.10. Statistical Analysis

All experimental data are presented as means ± standard error of the mean (SEM) from at least three technical replicates of 3–5 independent biological experiments (the exact number of independent experiments is indicated in the figure legends). Statistical analysis was performed using the SPSS package version 28. Statistically significant differences between treatment and control groups were assessed by a one-way analysis of variance (ANOVA) followed by Bonferroni's multiple-comparison *post hoc* test. Differences were considered statistically significant at $p < 0.05$.

3. Results

3.1. HepG2 Cell Viability Is Not Affected by Steatosis Induction and BCP Treatment

HepG2 hepatoma cells were induced to become steatotic by 24 h treatment with 0.5 mM FFA mixture, made of sodium palmitate and sodium oleate (1:2, w/w, referred hereafter as FFAm) along with BSA (1%, *w*/*v*).

To analyze BCP effect on cell viability, HepG2 cells were treated for 24 h with 0.5 mM FFAm alone or in the presence of different concentrations of BCP (50 nM, 500 nM, 1 µM, 5 µM, 10 µM and 50 µM). Untreated cells and cells treated with 1% BSA only were used as controls. The CellTiter-Glo® viability assay shows that neither FFAm nor FFAm + BCP affect HepG2 steatotic cell viability (Figure 1).

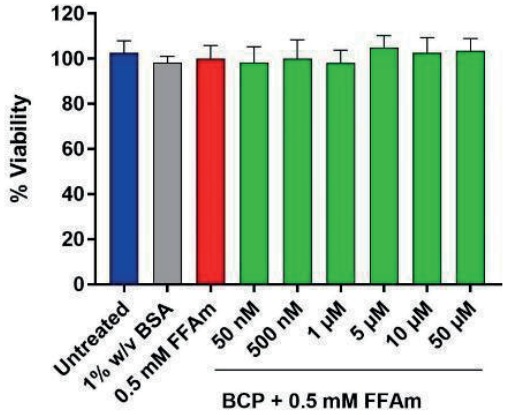

Figure 1. Cell viability assay of HepG2 cells based on ATP content. HepG2 cells were treated for 24 h with 0.5 mM FFAm and with increasing concentrations of BCP. Either BCP plus 0.5 mM FFAm, FFAm alone or 1% *w/v* BSA did not affect HepG2 cell viability. Control conditions (untreated) and treatments are represented as the mean ± SEM of three independent experiments.

3.2. BCP Reduces Intracellular Triglyceride Content in HepG2 Steatotic Cells

To study the effect of BCP on the induction of steatosis, HepG2 cells were co-treated with 0.5 mM FFAm and increasing concentrations of BCP (ranging from 50 nM to 50 µM). After 24 h treatment, lipid droplets and nuclei were visualized by AdipoRed™/NucBlue™ fluorescent staining (Figure 2A). Triglyceride accumulation and DNA content were quantified and expressed as a percentage change with respect to 0.5 mM FFAm-treated cells (positive control) (Figure 2B–D).

Triglyceride accumulation was highly increased by the treatment with FFAm, compared to untreated control cells, while the co-treatment with 500 nM, 1 µM, 5 µM and 10 µM BCP significantly ($p < 0.01$) reduced the amount of intracellular triglycerides (Figure 2B). This result was not due to cytotoxic effects or to a reduction in HepG2 cell proliferation, since the treatment with FFAm and BCP did not induce any significant change in the DNA content (Figure 2C), nor in the cell viability (Figure 1), in respect to untreated and FFAm-treated cells. No changes in triglyceride accumulation or the DNA content were observed in cells cultured in the presence of 1% *w/v* BSA alone.

The DNA content was used to normalize the total triglyceride values to obtain the triglyceride content per unit DNA (as a proxy for triglycerides accumulation per cell). Figure 2D shows that 500 nM, 1 µM, 5 µM and 10 µM BCP were able to induce a significant ($p < 0.01$) decrease in triglyceride accumulation/cell, with

the maximum reduction at 5 µM (corresponding to a 22% reduction of the levels of the FFAm positive control).

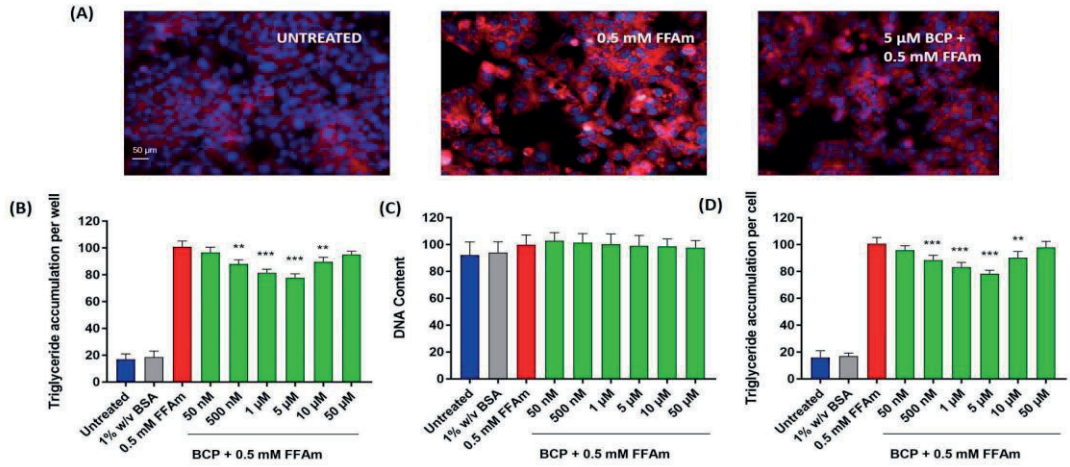

Figure 2. Lipid accumulation in HepG2 cells. BCP attenuates intracellular lipid accumulation in steatotic HepG2 cells without altering the cell number (DNA content). (A) Representative images of AdipoRed (red, triglycerides) and NucBlue (blue, nuclei) stainings; UNTREATED = untreated hepatocytes (control); 0.5 mM FFAm = palmitate and oleate-treated hepatocytes; 5 µM BCP + 0.5 mM FFAm = HepG2 cells co-treated for 24 h with BCP and FFAm. Scale bar: 50 µm. (B) Bar graph summarizing AdipoRed staining experiments to assess triglyceride accumulation per well in untreated cells, BSA-treated cells, 0.5 mM FFAm-treated positive control cells and HepG2 cells treated with 0.5 mM FFAm and various concentrations of BCP for 24 h. (C) Bar graph summarizing the DNA content per well (NucBlue staining). (D) Bar graph showing the triglyceride accumulation per cell, calculated as the ratio of AdipoRed and NucBlue stainings. Data are expressed as percentage change with respect to 0.5 mM FFA control condition (set equal to 100) and represent the mean ± SEM of five independent experiments. ** $p < 0.01$; *** $p < 0.001$ vs. positive control (0.5 mM FFAm-treated cells).

3.3. BCP Modifies the Intracellular Lipid Profile of HepG2 Steatotic Cells

To evaluate whether the effect of BCP on total lipid content could be linked to changes in the intracellular lipid profile, GC-MS was employed to identify specific intracellular FFA, whereas GC-FID was used for the quantitative analysis. The FFA composition of steatotic HepG2 cells (0.5 mM FFAm-treated cells) was consistent with that of typical NAFLD models, including myristic acid (C14:0), palmitic acid (C16:0), palmitoleic acid (*cis*-Δ^9-C16:1), stearic acid (C18:0), oleic acid (*cis*Δ^9-C18:1) and arachidonic acid (C20:4). Compared to untreated

controls, steatotic HepG2 cells (Figure 3, red bars) showed a statistically significant ($p < 0.01$) increase of *cis*-Δ^9-C18:1 and C16:0 (Figure 3A), as well as C14:0, C18:0 and *cis*-Δ^9-C16:1 (Figure 3B); no significant ($p > 0.05$) changes were found for C20:4 (Figure 3B). Treatment of steatotic cells with BCP (Figure 3, green bars) caused a significant ($p < 0.01$) reduction (−22%) in the amount of *cis*-Δ^9-C18:1 and C16:0 (Figure 3A), compared to 0.5 mM FFAm-treated cells; the same reduction was found for C14:0, whereas a 19% reduction occurred for C18:0 (Figure 3B). Interestingly, a significant 37% increase was found for *cis*-Δ^9-C16:1. No changes were found for C20:4 ($p > 0.05$) (Figure 3B). These results indicate that BCP was able to reduce the amount of all the identified saturated FFA, while the unsaturated C20:4 was unaffected and the levels of the unsaturated *cis*-Δ^9-C16:1 were increased by BCP treatment.

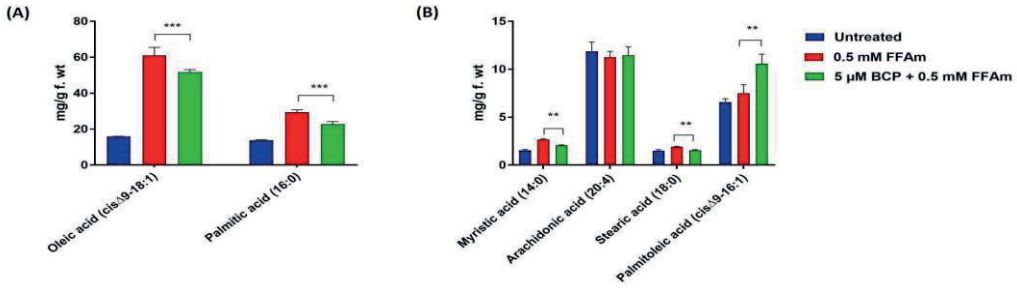

Figure 3. FFA composition of HepG2 cells after incubation for 24 h with 0.5 mM FFAm with or without BCP. Six fatty acids were identified and quantified. (A) BCP reduces the amount of oleic acid (cis-Δ9-C18:1) and palmitic acid (C:16) of steatotic cells. (B) BCP treatment significantly reduces the content of myristic acid (C14:0) and stearic acid (C18:0), while it increases palmitoleic acid (cis-Δ9-C16:1), in comparison to steatotic control cells. Data are represented as the mean ± SEM of three independent experiments and the values are expressed as mg g−1 fresh weight (f.wt). ** $p < 0.01$; *** $p < 0.001$ vs. positive control (0.5 mM FFAm-treated cells).

3.4. BCP Inhibits Lipid Accumulation through Interaction with Different Receptors: Effects of CB2 and PPAR Receptor Antagonists

In order to characterize the mechanism of action of BCP in the reduction of lipid accumulation in steatotic HepG2 cells, a receptor antagonist approach was employed. In particular, we focused on cannabinoid CB2 receptors and receptors involved in lipid metabolism, i.e., PPARα and PPARγ. The specific CB2 receptor antagonist AM630, the PPARα receptor antagonist GW6471 and the PPARγ antagonist GW9662 were used at concentrations obtained from literature data (Gertsch et al., 2008; Kamikubo et al., 2016; Ma et al., 2017). No

effects on lipid accumulation (Figure 4A–C) nor on cell viability were observed when treating HepG2 cells with each of the different antagonists alone, AM630, GW6471 and GW9662.

At the concentration range between 500 nM and 10 µM BCP (identified as the most effective doses in previous experiments), the co-treatment of HepG2 cells with the CB2 receptor antagonist AM630 (5 µM) completely reversed BCP-driven reduction of lipid accumulation, restoring values of intracellular triglycerides comparable to that of steatotic cells (Figure 4A). Similarly, treatment with the PPARα antagonist GW6471 (100 nM) completely reversed the anti-steatotic effect of BCP at all concentrations (Figure 4B). The treatment with the PPARγ-specific antagonist GW9662 (10 µM) partially reversed the lipid reduction induced by 1, 5 and 10 µM BCP (Figure 4C).

These results indicate that BCP is able to reduce lipid accumulation in steatotic HepG2 cells by interacting with CB2 and PPAR receptors.

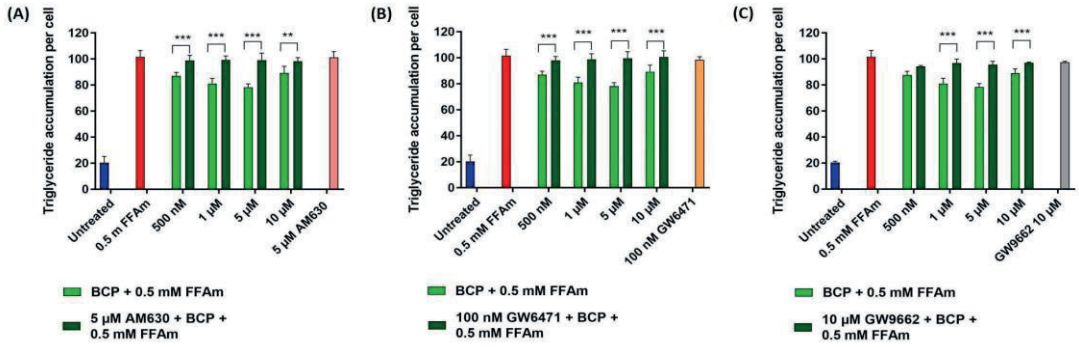

Figure 4. Effect of CB2, PPARα and PPARγ receptor antagonists on triglyceride accumulation per cell. Cells were incubated with different concentrations of BCP and 0.5 mM FFAm, in the presence or absence of specific receptor antagonists for 24 h. (A) Treatment of HepG2 cells with 5 µM CB2 antagonist AM630. (B) Treatment with 100 nM PPARα antagonist GW6471. (C) Treatment with 10 µM PPARγ antagonist GW9662. Data are expressed as a percentage change with respect to 0.5 mM FFA control condition (set equal to 100) and represent the mean ± SEM of five independent experiments. ** $p < 0.01$; *** $p < 0.001$ vs. BCP + 0.5 mM FFAm treated cells.

3.5. CB2, PPARα and PPARγ mRNA Expression Is Affected by Steatosis and BCP Treatment

To investigate whether CB2, PPARα and PPARγ mRNA expression levels are modified by steatosis and the ability of BCP to revert these changes, qRT-PCR experiments were conducted. The expression level of the *CNR2* gene resulted in

significantly upregulated steatotic cells, when compared to untreated cells. Interestingly, co-treatment with BCP significantly reduced ($p < 0.001$) CB2 mRNA levels in steatotic cells, bringing CB2 expression levels closer to those of the non-pathological condition (Figure 5A).

The expression of PPARs was significantly reduced in steatotic conditions compared to untreated cells (Figure 5B, C). Co-treatment of steatotic cells with BCP resulted in a significant ($p < 0.001$) increase in PPARα expression (Figure 5B), while no statistically significant change was observed in the expression of PPARγ (Figure 5C).

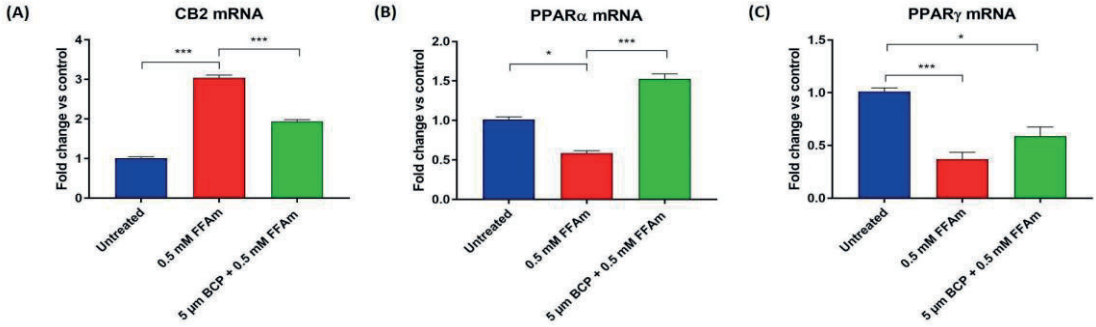

Figure 5. qRT-PCR analysis of CB2 (A), PPARα (B) and PPARγ (C) mRNAs normalized for the housekeeping gene β-actin. Data are represented as the mean ± SEM of three independent experiments. * $p < 0.05$, *** $p < 0.001$ vs. control (untreated cells, set equal to 1) or vs. 0.5 mM FFAm-treated cells.

3.6. CB2 Receptors Are Localized Intracellularly in HepG2 Cells

Since data on CB2 receptor localization are lacking in hepatocytes, we performed CB2 immunofluorescence experiments on HepG2 cells. Figure 6 shows a confocal image with punctate staining mainly located at intracellular sites. The staining level for CB2 in HepG2 cells appears quite heterogeneous, as evidenced by the presence of CB2high+ cells (arrows) and CB2low + (arrowheads) cells in the same clusters of cells (Figure 6, left panel). Single confocal planes show a prevalent perinuclear distribution of CB2 immunopositive puncta (Figure 6, right panels).

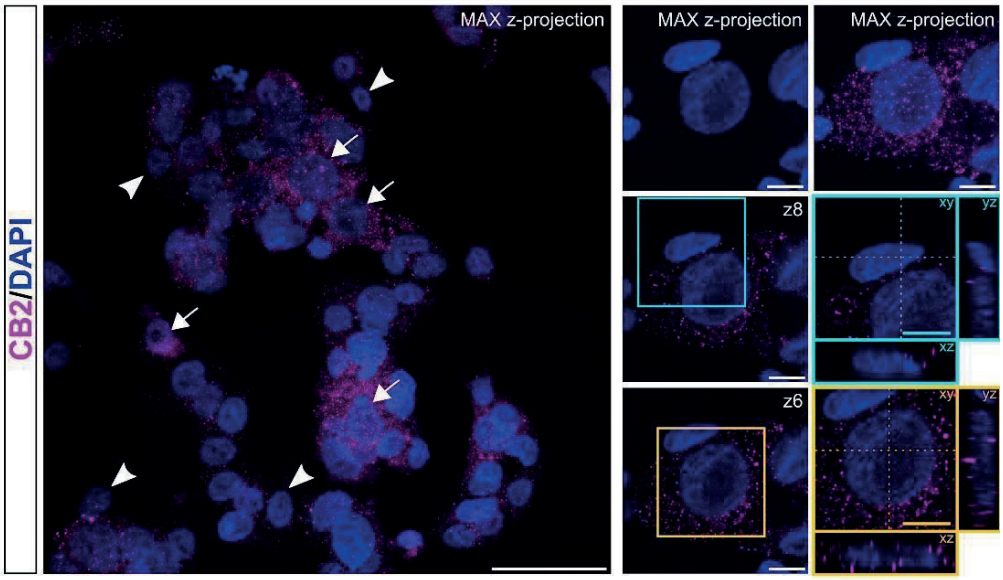

Figure 6. Localization of CB2 receptors. Representative confocal images showing CB2 immunostaining (magenta) in HepG2 cell line. Nuclei are stained with DAPI (blue). Pictures are shown as max z-projections (low magnification; left) with white arrows and arrowheads to highlight CB2high+ cells and CB2low+ cells, respectively, and a single confocal plane with reslicing (right) to better appreciate the intracellular distribution of CB2+ puncta in two of the cells present in the image. The cyan contoured image shows a cell positive for CB2 at low levels; the yellow contoured image identifies a cell with extensive immunolabelling for CB2. Scale bars: 50 µm (low magnification) and 10 µm (high magnification).

3.7. BCP Enters HepG2 Cells with a Maximum Uptake at 2 h from the Beginning of Treatment

Since we demonstrated that CB2 receptors are mostly intracellularly localized and PPAR receptors are well-known nuclear receptors, we decided to assess whether BCP is indeed able to enter HepG2 cells. The quantification of BCP intracellular uptake was evaluated by a time-course analysis in living cells by GC-MS. HepG2 cells were treated with 5 µM BCP for 24 h and samples were taken from time 0 to 24 h after treatment. By using GC-MS in the single ion monitoring (SIM) for BCP ions, we found that BCP was able to cross the cell membrane and enter HepG2 cells as soon as 1 h from the beginning of the treatment, with a maximum uptake measured at 2 h. After this period, the BCP intracellular concentration decreased linearly up to 24 h after treatment (Figure 7).

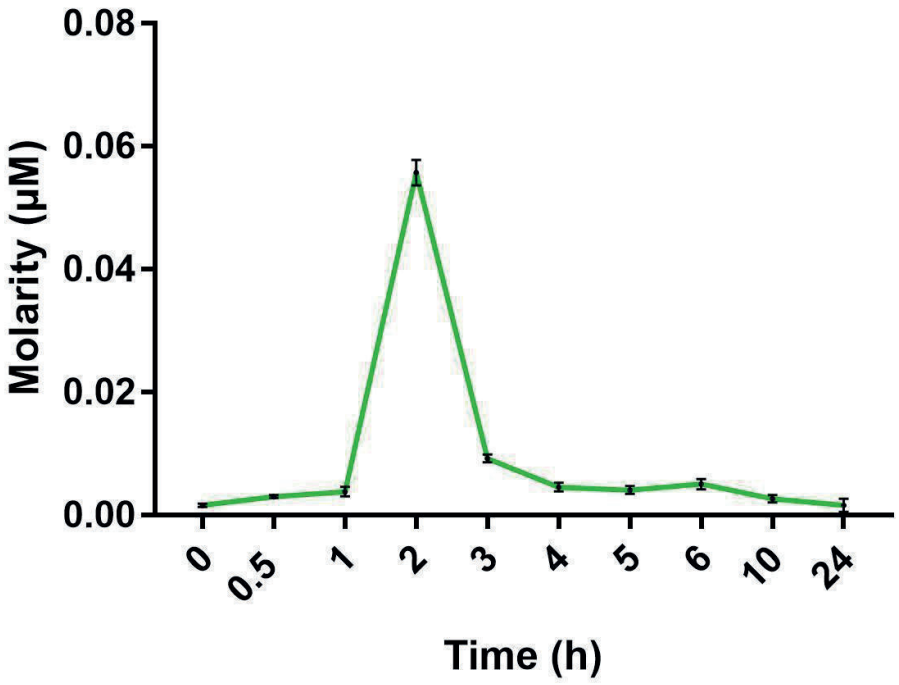

Figure 7. Time-course of BCP uptake by HepG2 cells measured with GC-MS. Maximum concentration of BCP was found 2 h after the beginning of the treatment. Data are represented as the mean ± SEM of three independent experiments.

4. Discussion

Despite recent progress in understanding the various steps involved in the development and progression of NAFLD, no approved pharmacological treatments for this very common chronic disease are yet available (Mantovani et al., 2021). Therefore, additional efforts are needed to find molecules able to interact with the molecular targets identified in NAFLD pathogenesis. Plant-derived molecules can be an important source for the development of new drugs (Atanasov et al., 2021); in this work, we focused our attention on the anti-steatotic activity of BCP, a phytocannabinoid with promising therapeutic effects in metabolic disorders and inflammation.

In order to mimic NAFLD *in vitro*, we incubated HepG2 hepatocytes for 24 h with a mixture of oleate and palmitate, which are the most abundant monounsaturated and saturated FFA in human diet (Gómez-Lechón et al., 2007). Our steatosis protocol differed from the one used by Kamikubo and

colleagues (Kamikubo et al., 2016), who incubated HepG2 cells with palmitic acid only, a treatment that generally induces higher toxicity and the release of pro-inflammatory chemokines, which are typical of NASH more than the NAFLD condition (Gómez-Lechón et al., 2007). In line with the results obtained by Kamikubo et al. (Kamikubo et al., 2016), we found that BCP co-incubation can reduce the total lipid accumulation in a dose-dependent manner, with maximal activity at 5 µM. BCP was able to reduce both oleic and palmitic acid, here used to induce steatosis in HepG2 cells and also significantly reduced stearic and myristic acid, both saturated fatty acids associated with cellular damage (Saraswathi et al., 2022; Lu et al., 2021). Noticeably, BCP was able to induce a 37% increase in palmitoleic acid, a monounsaturated fatty acid that has been widely studied in *in vivo* models of obesity because of its anti-inflammatory properties (Simão et al., 2022). We argue that the increase in palmitoleic acid might represent a protective detoxifying strategy converting palmitic acid into an unsaturated FFA. There is a general agreement that NAFLD progression occurs when mechanisms aimed at counteracting FFA-induced lipotoxicity are ineffective, leading to oxidative stress, ER stress, mitochondrial damage, immune-mediated cellular damage and apoptotic death (Powell et al., 2021). Our data strongly suggest that BCP is able to reduce the amount of possibly toxic saturated fatty acids and increase selected monounsaturated fatty acids, thus representing a valuable agent in preventing cellular injuries associated with NASH.

Besides emphasizing BCP ability to modify intracellular lipid composition, our data suggest that BCP effects involve the activation of CB2 as well as PPAR receptors.

PPARα and PPARγ are ligand-activated transcription factors with pleiotropic actions in several tissues. They are critical regulators not only of fatty acid metabolism, but also of glucose metabolism, inflammation and fibrosis [20]. The role of PPARα in the liver has been widely investigated both in physiological and steatotic conditions. The activation of PPARα induces the transcription of a range of genes involved in mitochondrial and peroxisomal FA oxidation, ketogenesis and lipid transport, thereby reducing hepatic lipid levels (Berthier et al., 2021). A recent study demonstrated that the deletion of hepatic *Pparα* in mice results in enhanced liver steatosis because of the impaired oxidation of FFA (Montagner et al., 2016), underscoring the relevance and potential of hepatocyte PPARα as a drug target for NAFLD.

PPARγ is involved in FFA uptake and lipogenesis and has significant anti-inflammatory properties. Early results demonstrated that its activation is

steatogenic in the liver (Yu et al., 2003) while recent works showed that PPARγ ligands (such as thiazolidinediones) ameliorate fat accumulation by decreasing saturated fatty acids in a zebrafish model of NAFLD (Singh et al., 2023). This last effect possibly depends on the enhanced release of adiponectin by the adipose tissue and a concomitant increase in FFA oxidation in hepatocytes by AMPK activation as demonstrated in *in vivo* studies (Wang et al., 2020). There are also *in vitro* studies demonstrating the role of PPARγ agonists in ameliorating lipid accumulation and inflammation associated with NASH. This is the case of GVS-12, a synthetic PPARγ agonist that can reduce triglycerides, inflammatory interleukins and other biomarkers associated with NASH in HepG2 cells (Wang et al., 2019). An interesting synthetic ligand is saroglitazar, a dual PPARα/γ agonist with prevalent PPARα agonist activity. The efficacy of saroglitazar in counteracting NAFLD/NASH has been compared to that of fenofibrate, a PPARα agonist, and pioglitazone, a PPARγ agonist, showing that the combined action of saroglitazar improves lipid-mediated oxidative stress, inflammation and impaired mitochondrial biogenesis more effectively than single agonists, both *in vitro* and *in vivo* (Jain et al., 2018). Many PPAR agonists, such as saroglitazar, are currently tested in clinical trials or have already been approved for the treatment of other metabolic diseases, such as pioglitazone used for the treatment of T2DM (Mantovani et al., 2021; Berthier et al., 2021). Ongoing clinical trials indicate that dual PPAR agonists can have ameliorating effects on NASH by acting on interrelated mechanisms. Thus, combining PPARα and PPARγ activation may be a successful strategy in the therapy of NAFLD (Francque et al., 2021).

According to our data, BCP effects are mediated both through PPARα and PPARγ. The activation of PPARα likely occurs through a direct mechanism; in support of this view, an interesting study demonstrated through a surface plasmon resonance (SPR)-BIA core system that BCP directly binds the PPARα ligand binding domain (LBD) even if it is a hydrophobic molecule and has a relatively small molecular weight compared with conventional PPAR ligands (Wu et al., 2014). For PPARγ, there are no studies demonstrating a direct interaction with BCP; however, there is evidence of an indirect activation, possibly through CB2 receptors (Youssef et al., 2019; Cheng et al., 2014). BCP dual activation of PPARα and PPARγ, observed in our *in vitro* experiments and previously shown in cocaine addiction studies performed *in vivo* (Galaj et al., 2020), highlights the possibility that BCP might behave as a dual PPARα/γ agonist like saroglitazar. It should also be noted that GW9662, the PPARγ antagonist used in our experiments, has an IC50 value of 3.3 nM for PPARγ and 32 nM for PPARα (Indrayanto et al., 2021). Therefore, it cannot be excluded that GW9662 partially blocks PPARα, contributing to the reversion of the anti-

steatotic effect of BCP observed in our experiments. In accordance with recently published results (Songtrai et al., 2022), we found that both PPARα and γ are downregulated during the pathological condition of steatosis. Intriguingly, co-treatment with BCP induced a marked upregulation of PPARα, bringing it back to even higher expression levels than in the untreated control. This latter result suggests that BCP might be able to enhance FA oxidation, therefore reducing hepatic steatosis.

The binding of BCP to the CB2 receptor has been well characterized (Gertsch et al., 2008), and the role of the endocannabinoid system (ECS) in the liver has been widely studied since it may be a therapeutic target for chronic liver disease (Basu et al., 2014), characterized by dysregulation of hepatic lipid metabolism and also perturbation of the hepatic endocannabinoid system (Bouassa et al., 2022). Although CB2 expression in the liver is moderate, its role has been demonstrated in both physiological (regulating liver development in zebrafish embryos (Liu et al., 2016)) and pathological conditions. For example, recent studies showed that CB2, in contrast to CB1 (Jorgačević et al., 2021), elicits anti-fibrogenic and anti-inflammatory effects (Julien et al., 2005). However, the role of CB2 in the progression of NAFLD has been debated: on the one hand, studies on the activation of both CB1 and CB2 receptors have shown increased lipid accumulation (De Gottardi et al., 2010) and potentiation of hepatic steatosis (Deveaux et al., 2009); on the other hand, our results with a CB2 antagonist show that CB2 activation can counteract steatosis, in line with other works (Kamikubo et al., 2016; Bazwinsky-Wutschke et al., 2019; Baldassarre et al., 2013). In agreement with *in vivo* data (Rivera et al., 2020; Mendez-Sanchez et al., 2007), we show that steatotic conditions upregulate CB2 expression in hepatocytes, and that concomitant exposure to BCP is able to revert the level of CB2 expression almost to control levels, thus facilitating return-to-normal conditions.

While PPARs are well known intracellular receptors, CB2 are seven-domain transmembrane receptors, whose localization is assumed to be on the plasma membrane. To verify this assumption, we performed immunolocalization studies. Unexpectedly, we found that CB2 receptors are located mainly intracellularly in HepG2 cells, often in a perinuclear position, most likely on the ER membrane or other intracellular organelles. Recent studies have suggested possible intracellular CB2 localization in specific cell types; for instance, Castaneda and colleagues (Castaneda et al., 2017) demonstrated that in peripheral blood B cells, CB2 receptor expression is regulated by different factors and these receptors are localized both on the cell membrane and on intracellular membranes. In line with this result, by kinetics studies, we showed

for the first time that BCP can cross the hepatocyte plasma membrane and enter the cells with a maximum peak at 2 h, followed by a decrease, possibly due to BCP metabolism. Further studies are needed to determine the exact localization of intracellular CB2 receptors in hepatocytes and their involvement in the regulation of lipid metabolism.

5. Conclusions

Taken together, our results suggest that BCP is a promising molecule for the treatment of NAFLD. This conclusion is based on several key aspects of this molecule. BCP may act on multiple targets, many of which are included in NAFLD and metabolic syndrome, since it is able to reduce lipid accumulation in hepatocytes but also in adipocytes (Geddo et al., 2019), may improve muscle insulin resistance (Geddo et al., 2021) and systemic inflammation, therefore resulting in a greater overall improvement compared with compounds with a more liver-restricted mode of action. It should also be considered that BCP is an approved dietary additive with a good safety profile and a safe phytocannabinoid, since it binds specifically to CB2 receptors, thus avoiding the psychotropic effects mediated by CB1 receptors (Hempel et al., 2022). There are, however, issues related to BCP bioavailability; in fact some studies have already focused on alternative formulations and vectorization techniques to allow better absorption, overcoming the limitations of BCP and making the most of all the properties of this phytocannabinoid (Santos et al., 2018; Mödinger et al., 2022).

Concluding remarks

In conclusion, the present PhD thesis shows that BCP is a very promising phytocannabinoid for the treatment of obesity, NAFLD and diabetes, either as a pure molecule or as present in extracts such as PipeNig®-FL, a black pepper extract containing 88% of BCP.

Its main and most useful feature is to act on multiple targets, as summarized in Figure 1, many of which are included in metabolic syndrome, since it is able to reduce lipid accumulation in 3T3-L1 adipocytes, decreasing the lipid content per cell and in HepG2 hepatocytes, reducing it in a dose-dependent manner without altering cell number. In addition, I demonstrated that BCP is an efficient glucose uptake inducer (as efficient as insulin) and it is able to determine plasma membrane GLUT4 translocation in C2C12 skeletal myotubes.

Translocation and fusion of GLUT4 storage vesicles with the plasma membrane, mainly in skeletal muscle and adipose tissue, is directly correlated with the ability to lower elevated blood glucose. Moreover, GLUT4 levels are significantly decreased in the skeletal muscle of type 2 diabetic patients and in insulin resistant patients (Morgan et al., 2011). The development of therapeutic compounds able to induce GLUT4 expression/translocation can thus improve insulin sensitivity and reduce insulin resistance.

In HepG2 hepatocytes, BCP is able not only to reduce intracellular lipid content but also to modify the lipid profile by reducing oleic, palmitic, stearic and myristic acid and increasing palmitoleic acid, a monounsaturated fatty acid that has been widely studied in *in vivo* models of obesity because of its anti-inflammatory properties (Simao et al., 2022). We argue that the increase in palmitoleic acid might represent a protective detoxifying strategy converting palmitic acid into an unsaturated FFA, suggesting that BCP is able to reduce the amount of possibly toxic saturated fatty acids and increase selected monounsaturated fatty acids, thus representing a valuable agent in preventing cellular injuries associated with NASH.

It was already demonstrated (Kamikubo et al., 2019) that BCP exerts its activity by binding to CB2 endocannabinoid receptors, involved not only in metabolism and food intake, but also in neurogenesis, as well as neurodegenerative and neuroinflammatory disorders, opening to new possible pharmacological strategies based on the use of CB2-specific therapeutic drugs, overcoming the neuropsychiatric adverse effects of CB1-targeted therapies.

In our study on ST14A striatal neural progenitors, we indicate that these cells express a functional endocannabinoid system that is actively involved in the regulation of neural progenitor proliferation, in fact we demonstrated a cell number increase following CB2 receptors activation, as indicated also in Figure 1. Thus, ST14A cells could therefore represent a useful, simplified *in vitro* model for studying ECS modulation of neurogenesis and to test new therapeutic molecules acting on the cannabinoid system, such as BCP, thus providing the basis for *in vivo* pharmacological studies of neurodegenerative pathologies, as for example Huntington's disease, characterized by striatal neurodegeneration (Behl et al., 2022).

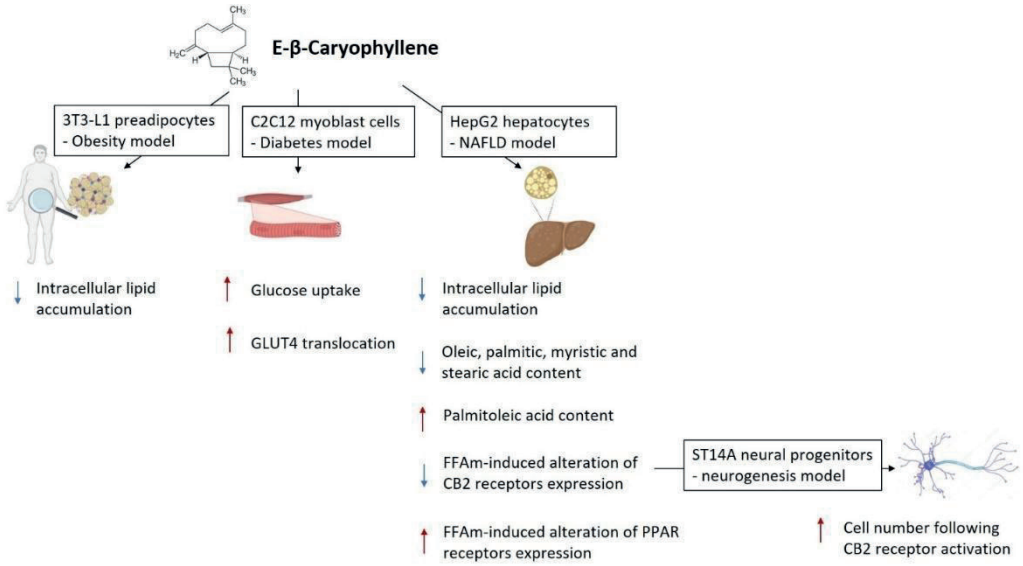

Figure 1. Summary figure of the results. BCP is able to act on multiple targets such as: 3T3-L1 preadipocytes, in which it reduces the intracellular lipid accumulation; C2C12 myoblast cells, in which it increases the glucose uptake and GLUT4 translocation; HepG2 hepatocytes, in which it reduces the total intracellular lipid accumulation by reducing the oleic, palmitic, myristic and stearic acid content, while increasing the protective palmitoleic acid content. BCP action takes place through PPAR receptors, by increasing their expression, altered by the pathological steatosis condition; it acts also by activating CB2 receptors and it is able to reduce the FFAm-induced alteration of its expression. CB2 receptors are expressed also in ST14 neural progenitors in which we demonstrated a cell number increase as a result of CB2 receptors activation.

We focused on CB2 receptors also in our work on HepG2 cells showing that steatotic conditions upregulate CB2 expression in hepatocytes, and that concomitant exposure to BCP is able to revert the level of CB2 expression almost to control levels, thus facilitating return-to-normal conditions. Moreover, to check the localization of seven-domain transmembrane CB2 receptors we performed immunolocalization studies, founding that CB2 receptors are located mainly intracellularly in HepG2 cells, often in a perinuclear position, most likely on the ER membrane or other intra-cellular organelles. In line with this result, by kinetics studies, we showed for the first time that BCP can cross the hepatocyte plasma membrane and enter the cells with a maximum peak at 2 h, followed by a decrease, possibly due to BCP metabolism.

In addition, our pharmacological data suggest that BCP effects involve the activation of CB2 as well as PPAR receptors since the co-treatment of BCP and CB2, PPARα or PPARγ antagonists completely blocked BCP activity on lipid accumulation.

PPARα and PPARγ are ligand-activated transcription factors with pleiotropic actions in several tissues. They are critical regulators not only of fatty acid metabolism, but also of glucose metabolism, inflammation and fibrosis (Berthier et al., 2021).

The activation of PPARα likely occurs through a direct mechanism; in support of this view, an interesting study demonstrated through a surface plasmon resonance (SPR)-BIA core system that BCP directly binds the PPARα ligand binding domain (LBD) even if it is a hydrophobic molecule and has a relatively small molecular weight compared with conventional PPAR ligands (Wu et al., 2014). For PPARγ, there are no studies demonstrating a direct interaction with BCP; however, there is evidence of an indirect activation, possibly through CB2 receptors (Youssef et al., 2019). BCP dual activation of PPARα and PPARγ, observed in our in vitro experiments and previously shown in cocaine addiction studies performed in vivo (Galaj et al., 2021), highlights the possibility that BCP might behave as a dual PPARα/γ agonist. It should also be noted that GW9662, the PPARγ antagonist used in our experiments, has an IC50 value of 3.3 nM for PPARγ and 32 nM for PPARα (Galaj et al., 2021). Therefore, it cannot be excluded that GW9662 partially blocks PPARα, contributing to the reversion of the anti-steatotic effect of BCP observed in our experiments. We also found that both PPARα and γ are downregulated during the pathological condition of steatosis. Intriguingly, co-treatment with BCP induced a marked upregulation of PPARα, bringing it back to even higher expression levels than in the untreated

control. This latter result suggests that BCP might be able to enhance FA oxidation, therefore reducing hepatic steatosis.

Thus, BCP determines a greater overall improvement compared with compounds with a more restricted mode of action. It should also be considered that BCP is an approved dietary additive with a good safety profile and a safe phytocannabinoid, since it binds specifically to CB2 receptors, thus avoiding the psychotropic effects mediated by CB1 receptors. All these features make BCP a promising bioactive molecule useful to improve steatosis, obesity and T2D, deserving more *in vivo* studies in order to support its role as a beneficial metabolic modulator.

Appendix

Reproducibility of adipogenic responses to metabolism disrupting chemicals in the 3T3-L1 pre-adipocyte model system: An interlaboratory study

1. Introduction

The 3T3-L1 murine pre-adipocyte cell line is an established model for *in vitro* screening of metabolism disrupting chemicals (MDCs) (Heindel et al., 2015, 2017). When exposed to adipogenic stimuli, pre-adipocytes will differentiate into mature adipocytes, undergo morphological changes, accumulate triglycerides, and eventually develop into a rounded white fat cell with a number of large lipid droplets often displacing the nucleus (Green and Meuth, 1974; Green and Kehinde, 1975).

Adipocyte differentiation requires eventual activation of the peroxisome proliferator-activated receptor-gamma (PPARγ), often considered the "master regulator" of adipocyte differentiation (Rosen et al., 1999).

Molecular pathways upstream that contribute to this activation are diverse and include modulation of thyroid receptor-beta (TRβ), glucocorticoid receptor (GR), estrogen receptor (ER), androgen receptor (AR), liver X receptor (LXR), retinoid X receptor (RXR), and others (Niemela et al., 2008), including non-receptor mediated mechanisms (Bournat and Brown, 2010; Kassotis and Stapleton, 2019; Luz et al., 2018). These receptor pathways are highly conserved across vertebrate species (Fu et al., 2005; Zhao et al., 2015), suggesting that mechanisms of adipogenesis are highly translatable. Indeed, active MDCs identified using 3T3-L1 cells and other *in vitro* models (increased triglyceride accumuation/differentiation, pre-adipocyte proliferation, etc.) have been routinely shown to be active *in vivo*, such as bisphenol A and tributyltin chloride, among others (Angle et al., 2013; Chamorro-Garcia et al., 2013; Li et al., 2011; Masuno et al., 2005). Compounds that modulate these receptors belong to diverse chemical classes (Fang et al., 2015; Hamers et al., 2006; Orton et al., 2011), and many are frequently detected in indoor environments and in human tissues (Hoffman et al., 2015; Kitamura et al., 2005; Meerts et al., 2000; Shen et al., 2009; Stapleton et al., 2009, 2011; Takeuchi et al., 2005). A number of these chemicals have been associated with adiposity, obesity, type 2 diabetes, and other chronic metabolic health conditions in humans (Gore et al., 2015; Heindel et al., 2015, 2017; Ruiz et al., 2018). As such, there is a critical need to ensure robust and validated models that promote highly reproducible toxicological outcomes across laboratories. Despite a need to accurately identify MDCs, relatively little research has been performed to comprehensively evaluate reproducibility across laboratories, and comprehensively assess factors that might contribute to varying degrees of differentiation among laboratories. Previous research has described diverse differentiation success and declining performance over time with various cell bank stocks of 3T3-L1 cells (Zebisch et

al., 2012). Cell culture vessel size and proprietary tissue culture coatings have also been demonstrated to influence differentiation success of 3T3-L1 cells (Mehra et al., 2007), and various cell line suppliers provide disparate protocols and techniques for eliciting maximal differentiation success (American Type Culture Collection (ATCC) ATTC, 2011; Zenbio Inc, 2015). Other providers suggest an inability to differentiate their 3T3-L1 cell stocks, with timelines of 2–5 weeks and very limited differentiation (European Collection of Authenticated Cell Cultures (ECACC), 2020). Despite these notable gaps, reproducibility studies across toxicological studies are limited, and often conducted only within the establishment of guideline assays such as Organisation for Economic Cooperation and Development (OECD) test guidelines. Chemists, in contrast, have demonstrated robust success in improving methodology and laboratory-specific measurement reliability through participation in interlaboratory reproducibility programs (Boyer et al., 1985; Ikonomou et al., 2012; M.Weiss et al., 2013; Voet et al., 1999; Wong et al., 2010). For example, recent initiatives to improve measurements for novel brominated and organophosphate flame retardants have demonstrated high precision between technical replicates within laboratories but not as strong accuracy for measuring the provided values across laboratories (Melymuk et al., 2015, 2018).

Importantly, analytical reproducibility studies benefit from the concrete nature of the outcome: chemicals can be included at specific, known concentrations, making the determination of the "correct" result more straightforward than possible in toxicological studies. A limited number of studies have attempted this with endocrine outcomes such as measurement of nuclear receptor activation (Hettwer et al., 2018; Mehinto et al., 2015; Zava et al., 1982), reporting variable consistency across trials and pathways, with variances often seemingly resulting from non-harmonized protocols.

We previously published an assessment of some disparities in adipogenic cell culture systems under various conditions (Kassotis et al., 2017b). Specifically, both cell line (3T3-L1 vs. OP9) and source (ATCC vs. Zenbio 3T3-L1) had a significant impact on the responses to various chemicals. Ligands for LXR, RXR, GR, and TR promoted disparate responses between cell sources (Kassotis et al., 2017b), in some cases apparently mediated through gene expression differences. We also noted significant differences based on the cell culture plastic utilized, with different 96-well plates contributing to <50 % reduction in maximal fold induction differences and appreciably altering chemical potencies (Kassotis et al., 2017b). Cytotoxicity and proliferative response differences were also observed among plates, in some cases negatively impacting the ability to even detect chemicals acting via pre-adipocyte proliferation (Kassotis et al.,

2017b). Significant differences were also noted in both triglyceride accumulation and DNA content among different differentiation induction times (7, 10, 14 days) (Kassotis et al., 2017b), and it is still unclear what differences might stem from the wide degree of heterogeneity in media additives across varying differentiation protocols. For example, while many researchers do not include dexamethasone in the differentiation cocktail (Boucher et al., 2015; Kassotis et al., 2017a, 2018; Kassotis et al., 2019; Sargis et al., 2010), others use a 1000-fold range of concentrations (Li et al., 2011; Masuno et al., 2002; Temkin et al., 2016; Zebisch et al., 2012). Differing protocols and cell culture supplies utilized may contribute to a lack of reproducibility and bias in measuring adipogenic potency and efficacy of chemicals between laboratories. Importantly, while reported previously, these factors have never been assessed in a systematic manner across laboratories.

As such, the objectives of this study were to evaluate the interlaboratory variability in the response of 3T3-L1 cells to the exposures of several chemical compounds. Given previous reports of inconsistencies in responses using this model, we sought to comprehensively evaluate the underlying factors and how they might influence differences in efficacy (magnitude of effects) and/or potency (concentration of effects) for both triglyceride accumulation (marker of differentiation success) and pre-adipocyte proliferation (marker of cell number). To accomplish this, we assessed three blinded test chemicals (bisphenol A, BPA; tributyltin chloride, TBT; pyraclostrobin) between ten laboratories in the United States, Canada, Italy, Norway, and the United Kingdom. These data should provide comprehensive insight into the most important factors that influence the assay's responses and to inform strategies to increase interlaboratory reproducibility.

2. Materials and methods

2.1. Chemicals

Chemicals for use in bioassays were purchased as follows: rosiglitazone (Sigma cat # R2408, > 98 %), pyraclostrobin (Sigma cat # 33696, 99.9 %), tributyltin chloride (TBT; Aldrich cat # T50202, 96 %), and bisphenol A (BPA; Sigma cat # 239658, >99 %). Stock solutions were prepared in 100 % cell-culture grade DMSO (Sigma cat # D2650) and stored at -20 °C between uses. Laboratories were recruited via a scientific conference discussion and coordination via a metabolism disruption research listserv. Rosiglitazone (1 mM) was provided as a labeled amber glass vial, and laboratories were instructed to dilute the solution 1000-fold and then perform four 10-fold dilutions (0.1 nM – 1 µM in contact with cells). Pyraclostrobin, TBT, and BPA (10 mM) were provided as blinded chemicals (Chemicals A, B, and C, respectively) in amber glass vials, and laboratories were instructed to perform the same 1000-fold dilution and four 10-fold dilution scheme (1 nM – 10 µM).

2.2. Samples shipment

Packages were shipped to participating laboratories in insulated Styrofoam shipping boxes with between one and five kilograms of dry ice, depending on distance of shipment. All packages were shipped priority overnight, generally resulting in next day domestic delivery; however, international shipments often took as long as ten days to clear customs and be delivered by local couriers. Additional dry ice was added by Fedex as necessary to ensure packages arrived frozen, and this was confirmed by receiving laboratories upon receipt. Given the long length of delivery for certain participating international laboratories, a cryo- shipper was utilized (Chart MVE BL-7) to allow for improved assurance on the frozen cell stock.

2.3. Testing, differentiation, and evaluation protocol

The following materials were provided to each laboratory (Fig. 1). One vial of murine 3T3-L1 cells (Zenbio cat# SP-L1-F, lot# 3T3062104; Research Triangle Park, NC), one vial NucBlue® Live ReadyProbes® Reagent (Thermo cat # R37605), one vial of laboratory prepared Nile Red reagent (40 µg/mL Nile Red in acetone; Sigma 72485 - 100MG), one sleeve containing six black clear-bottom 96-well tissue culture plates (Greiner cat # 655090; four for assays and two replacements), one vial of DMSO for use as a solvent control, one vial of

rosiglitazone for use as a positive control, and three vials containing the blinded test chemicals. A shared differentiation protocol, differentiation data sheet, and test instructions were emailed to each participating laboratory. Differentiation data sheets included spaces to include raw fluorescence values from Nile Red and NucBlue outputs, a plate map to denote placement of all test chemicals and replicates, and spaces to specify differentiation details, media constituents, and other assay details. The shared differentiation protocol was adapted based on a previously published protocol (Zebisch et al., 2012) and has been described in detail previously (Kassotis et al., 2017a, b). A short protocol was provided to detail the desired test conditions. Laboratories were requested to prepare media according to the shared differentiation protocol and according to their own protocols and then test blinded test chemicals under four sets of conditions: 1) using their laboratory-specific differentiation protocol, media, and supplies along with laboratory-specific stock of 3T3-L1 cells (LC/LP), 2) using their laboratory-specific differentiation protocol, media, and supplies along with the provided stock of 3T3-L1 cells (SC/LP), 3) using the provided differential protocol, media prepared according to the shared protocol, and using the included cell culture plates along with laboratory-specific stock of 3T3-L1 cells (LC/SP, and 4) using the provided differential protocol, media prepared according to the shared protocol, and using the included cell culture plates along with the provided stock of 3T3-L1 cells (SC/SP, Fig. 1).

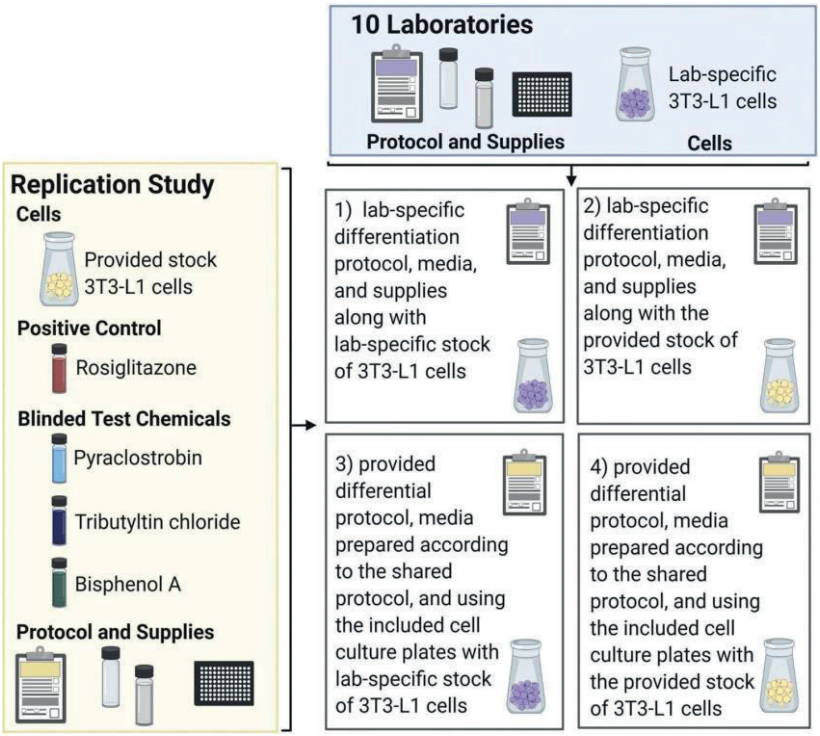

Fig. 1. Study Design and Test Conditions.

Schematic of the study design and test conditions. Ten laboratories were recruited from the United States and other countries. The following materials were provided to each laboratory: one vial of 3T3-L1 cells, one vial NucBlue® Live ReadyProbes® Reagent, one vial of laboratory prepared Nile Red reagent, black clear-bottom 96-well tissue culture plates, DMSO, rosiglitazone, and three vials containing the blinded test chemicals. A shared differentiation protocol, differentiation data sheet, and test instructions were emailed to each participating laboratory. A short protocol was provided to detail the desired test conditions. Laboratories were requested to prepare media according to the shared differentiation protocol and according to their own protocols and then test blinded test chemicals under four sets of conditions: 1) using their laboratory-specific differentiation protocol, media, and supplies along with laboratory-specific stock of 3T3-L1 cells, 2) using their laboratory-specific differentiation protocol, media, and supplies along with the provided stock of 3T3-L1 cells, 3) using the provided differential protocol, media prepared according to the shared protocol, and using the included cell culture plates along with laboratory-specific stock of 3T3-L1 cells, and 4) using the provided differential protocol, media prepared according to the shared protocol, and using the included cell culture plates along with the provided stock of 3T3-L1 cells.

2.4. 3T3-L1 cell care and differentiation assays

Zenbio 3T3-L1 cells were provided to all laboratories and were used for SC test conditions. Laboratory-specific cell sources of 3T3-L1 cells (LC) varied depending on the laboratory and are detailed within Table 1.

The shared protocol called for cells to be maintained in pre-adipocyte media (Dulbecco's Modified Eagle Medium – High Glucose; DMEM- HG; Gibco cat# 11995, supplemented with 10 % bovine calf serum and 1% penicillin and streptomycin; Gibco cat# 15140). These cells were seeded in pre-adipocyte media into 96-well tissue culture plates (Greiner cat # 655090) at approximately 30,000 cells/well and grown to confluency; after confluency, cells were allowed 48 h to undergo growth arrest and initiate clonal expansion. Media was then replaced with controls, and/or blinded test chemicals using a DMSO vehicle (at 0.1 %) in differentiation media (DMEM-HG with 10 % fetal bovine serum, 1% penicillin/streptomycin, 1.0 μg/mL human insulin, and 0.5 mM 3-isobutyl-1-methylXanthine, IBMX). After 48 h of differentiation induction, media was

replaced with fresh dilutions of test chemicals in adipocyte maintenance media (differentiation media without IBMX), and this media was refreshed every 2–3 days until assay, ten days after induction.

Laboratory-specific protocols varied among laboratories, with variations to this general protocol specified within Table 1. 3T3-L1 cells were utilized between passages 8 (at shipment) and 12 (provided Zenbio cells) or as noted in Table 1 for laboratory-specific cells, and were maintained in a sub-confluent state until differentiation.

2.5. 3T3-L1 triglyceride accumulation, cell proliferation, and cell viability measurements

Fluorescence endpoint measurements were measured using a plate reader for the shared protocol tests and using standard laboratory practice for laboratory-specific protocol tests. For shared protocol experiments, media was removed from plates, and cells were rinsed with Dulbecco's phosphate-buffered saline (DPBS; Gibco cat # 14040) before replacing with 200 µL of a live-cell dye mixture (19 mL DPBS, 1 drop/mL NucBlue® Live ReadyProbes® Reagent (cell proliferation/cytotoXicity measure of DNA content; Thermo cat # R37605) and 500 µL Nile Red (intracellular lipid measure of triglyceride accumulation; 40 µg/mL in acetone; Sigma 72485 - 100MG) per plate). Plates were protected from light and incubated at room temperature for approximately forty minutes; fluorescence was then measured on plate readers with excitation 485 nm/emission 572 nm (previously demonstrated to be ideal wave- lengths for intracellular neutral lipids (Greenspan et al., 1985)) and/or 485/535 (more accessible, generally used) for Nile Red and 360/460 for NucBlue®. Measurement wavelengths varied for laboratory-specific protocols, with most laboratories also providing their data from plate readers using these wavelengths.

All laboratories provided raw data, and as such, normalizations and activity calculations and determinations were made in a uniform manner for all data. For triglyceride accumulation data, percent activities were calculated relative to the maximal rosiglitazone-induced fold induction over intra-assay differentiated vehicle control (0.1 % dimethylsulfoxide, DMSO) responses, after correcting for background fluorescence. Rosiglitazone was utilized as the positive control herein (provided as an unblinded chemical stock to all laboratories) due to selective, robust, and potent activation of PPARγ (Lehmann et al., 1995; Seimandi et al., 2005; Spiegelman, 1998) and in order to provide ease of

comparisons across laboratories and experiments. DNA content was calculated as percent change from differentiated vehicle control (0.1 % DMSO) responses for each chemical at each concentration and was then used to normalize total triglyceride values to obtain triglyceride content per unit DNA (proxy for triglyceride accumulation per cell). Four technical (replicates within each assay plate) and two biological replicates (separate cell passages/assays) were requested for every test chemical and concentration herein.

2.6. Statistical analysis

Data for adipogenic activities (triglyceride accumulation and pre- adipocyte proliferation) are presented as means ± standard error of the mean (SEM) from replicates. First, the median of four technical replicates (within plates) was determined and then medians of two or three (depending on laboratory) biological replicates (separate experimental plates) were averaged to provide a final value for each chemical for each laboratory under each test condition. Efficacy values were defined as the percent maximal activity relative to the rosiglitazone- induced maximal response for each laboratory and test condition. Relative potency values (effective concentration, EC20; concentration of each chemical that exhibits 20 % of assay maximal activity, respectively) values were estimated from raw fluorescence data, setting the axis to 20 % of response and estimating the concentration at which the response curve passes this activation value. Values were extrapolated as necessary for efficacy and potency values for samples approaching the cut-off; potency values were not extrapolated when there was no apparent activity (samples not approaching 20 % activity), as potencies cannot be calculated for inactive chemicals/samples. Sensitivity was defined as the lowest concentration that exhibited a significant effect for each chemical above its own solvent control under each set of test conditions for each laboratory. To ease comparisons among laboratories, a uniform limit of quantification was set between laboratories as follows: a biological activation threshold approach was utilized, where the variation in the differentiated solvent (0.1 % DMSO) control was calculated as the average differentiated solvent value plus three times the standard deviation of the differentiated solvent control response. All reproducibility metrics were based on the raw, unadjusted data to assess variance within experimental groups and across laboratories; they were calculated by subtracting the average experimental group response from each individual laboratory response and dividing by the standard deviation. Values further from zero in either direction represent greater variation from the average experimental group response. Responses

were analyzed using a one-way ANOVA and Dunnett's post-hoc test. Differences between treatment and control groups were considered statistically significant at $p < 0.05$.

3. Results

Ten participating laboratories were asked to test three blinded test chemicals and one standard positive control chemical (rosiglitazone) under a defined concentration range and four defined sets of conditions (Fig. 1). Laboratories were asked to test using a shared differentiation protocol to assess the potential differences contributed by differentiation protocol variations and using a shared source of 3T3-L1 cells to assess potential differences contributed by variations in cell sources. Activity determinations were assessed as presence of significant activity above the biological activation threshold as described in the methods, and were based on triglyceride accumulation (standard marker for extent of differentiation) and pre-adipocyte proliferation (increase in DNA content relative to differentiated solvent controls).

3.1. Rosiglitazone responses across laboratories and test conditions

Rosiglitazone was tested under four sets of conditions within each laboratory (Fig. 2). Given that triglyceride accumulation efficacies for rosiglitazone were normalized to the maximal intra-assay rosiglitazone- induced response, maximal efficacies (percent activation) could not be compared and fold induction responses relative to the differentiated solvent control were used instead. Maximal triglyceride accumulation fold inductions for rosiglitazone did not vary considerably across the four test conditions (2.5–3.2-fold), with the highest fold induction responses observed in the shared protocol groups (Table S1, Fig. 2). More variation was observed among laboratories relative to among test conditions, with fold inductions ranging from 1.3–6.0 (agnostic of test conditions; Table S2) and Z-scores exceeding ±1.0. Lower variances were again observed in the shared protocol groups. With some exceptions, most laboratories reported the highest fold induction responses using the shared cell/shared protocol (SC/SP) test conditions. Dose responses were varied when laboratories utilized laboratory-specific cells and laboratory-specific protocols (LC/LP), with more than two orders of magnitude difference in potencies, three orders of magnitude difference in lowest observed effect level (LOEL; lowest tested concentration with significant increase above baseline), two orders of magnitude in maximal effective concentration, and a wide range of fold inductions relative to differentiated solvent controls (0.1 % DMSO; Fig. 2, Table

S2). Similar variances were observed when all laboratories used the SC, with no apparent improvement in responses across laboratories, though variances improved slightly in the SP conditions (e.g. maximal concentrations demonstrated much greater consistency). Mean potencies (EC20) for triglyceride accumulation were very similar, with values ranging from 0.009 µM for SC/SP, 0.004 for LC/SP, 0.006 for SC/ LP, and 0.008 for LC/LP, though these trends were not evidence for pre-adipocyte proliferation (mean potencies of 18.45 µM for SC/SP, 146.72 for LC/SP, 0.17 for SC/LP, and 6.00 for LC/LP). For most laboratories, fold induction increased when using the shared protocol (with or without shared cells). Mean SC/SP metrics for rosiglitazone performance (triglyceride accumulation) were 0.04 ± 0.01 µM for LOEL, 0.72 ± 0.14 µM for maximal response concentration, 3.2 ± 0.4 for fold induction of response, and 0.02±0.01 µM for potency (Table S2).

Pre-adipocyte proliferation means/deviations did not appreciably change across the test groups, though a greater proportion of laboratories reported significant adipogenic activity when using SC (with the most consistency using SC/SP; Fig. 1, Table S1, Table S2). Only one laboratory reported inactivity for pre-adipocyte proliferation using the SC/SP, while 30–60 % of laboratories reported inactivity when assessed under the other test conditions. Efficacy ranged from < limit of detection (LOD) to ~ 80 % increased DNA content relative to the differentiated solvent control, and the magnitude of proliferation seemed to be highest in the SC/SP group (Table S1, Table S2). Average reproducibility metrics for the SC/SP conditions included LOEL (mean: 0.26 ± 0.13 µM), maximal efficacy (mean: 32.1 % ± 6.7 %), concentration at which maximal response was induced (mean: 0.9 ± 0.1 µM), and potency (18.45 15.63 µM; Table S2). Maximal response concentration was nearly unanimous using the SC/SP, but large variances and potency shifts were observed in the other test groups (Fig. 1, Table S2). Some low-level cytotoxicity was observed for certain laboratories under certain test conditions, only at 10 mM, and all using the LC test conditions.

	Laboratory cells/laboratory protocol														
Participating Laboratory	Cell Source	Cell Lot #	Passage	Test Chem Length (d)	Diff. Length (d)	Cocktail Length (d)	TC Plate	TC plate #	Base Media	IBMX	Insulin	Dexamethasone	Biotin	Ca Pantothenate	FBS
Lab 1	ATCC	Batch 6	u + 3	10	10	2	Falcon	353219	DMEM-LG	0.5 mM	0.6 mg/mL	250 nM	–	–	Wisent #090150, Lot#115680
Lab 2	ATCC	700009858	u + 3, 9	10	10	2	Greiner BioOne	82050–748	DMEM-HG	0.5 mM	1 mg/mL	250 nM	–	–	Euroclone, ECS0180 L, lot # EUS0040912
Lab 3	ATCC	63343749	u + 3	10	10	2	Corning	07–200-565	DMEM-HG	0.5 mM	1 mg/mL	250 nM	–	–	Sigma F6178, Lot #013K8411
Lab 4	ATCC	MBX clone[1]	u + 5	10	10	2	Greiner BioOne	82050–748	DMEM/F12	0.5 mM	1 mg/mL	–	33 mM	17 mM	Fisher Scientific (Gibco) 10437–028
Lab 5	ATCC	2268173	u + 9	14	14	2	Greiner BioOne	82050–748	DMEM-HG	0.5 mM	1 mg/mL	20 nM	–	–	Sigma #F2442, lot 1982183
Lab 6	ATCC	–	u + 3, 8	10	10	2	Greiner BioOne	82050–748	DMEM-HG	0.5 mM	10 mg/mL	1 mM	–	–	GE Healthcare life sciences, SH30910.03HI
Lab 7	ATCC	63891946	u + 3	10	10	2	Greiner CellStar	655090	DMEM-HG	0.5 mM	10 mg/mL	–	–	–	GIBCO; Ref: 10270–106; Lot: 41G1780K
Lab 8	Green[2]	–	11	8	8	2	Falcon	353219	DMEM-HG	125 mM	2.5 ug/mL	1.25 mM	2 mg/L	1 mg/L	Gemini #100–106
Lab 9	Zenbio	3T3L1062104	10	10	10	2	Greiner CellStar	M0562–32EA	DMEM-HG	0.5 mM	1 mg/mL	–	–	–	Sigma F9665
Lab 10	ATCC	–	u + 4	11	11	2	USA Scientific	5665–5087	DMEM-HG	0.5 mM	10 mg/mL	1 mM	–	–	Hyclone SH30541.03
Shared	Zenbio	3T3L1062104	8	10	10	2	Greiner BioOne	82050–748	DMEM-HG	0.5 mM	1 mg/mL	–	–	–	

Table 1. Descriptive statistics for laboratory-specific differentiation protocols provided by each participating laboratory. These cells and differentiation details were utilized for the LC and LP conditions only. The "Shared" cell source was utilized for all SC conditions, and the shared protocol (Supplemental information) for all SP conditions. All laboratories completed tests using each of the four defined test conditions. u = unknown passage number. Differentiation length specifies the total duration of adipocyte differentiation and adipocyte maintenance media treatment, whereas cocktail length specifies just the duration of the differentiation induction media treatment.

[1] 3T3-L1 MBX clone utilized for these experiments: designed to ensure more complete adipocyte differentiation and insulin sensitivity; unknown lot #.

[2] Green H (isolating laboratory) source as gift from Philip Pekala (same apparent source as commercial Zenbio cells); no reported lot #.

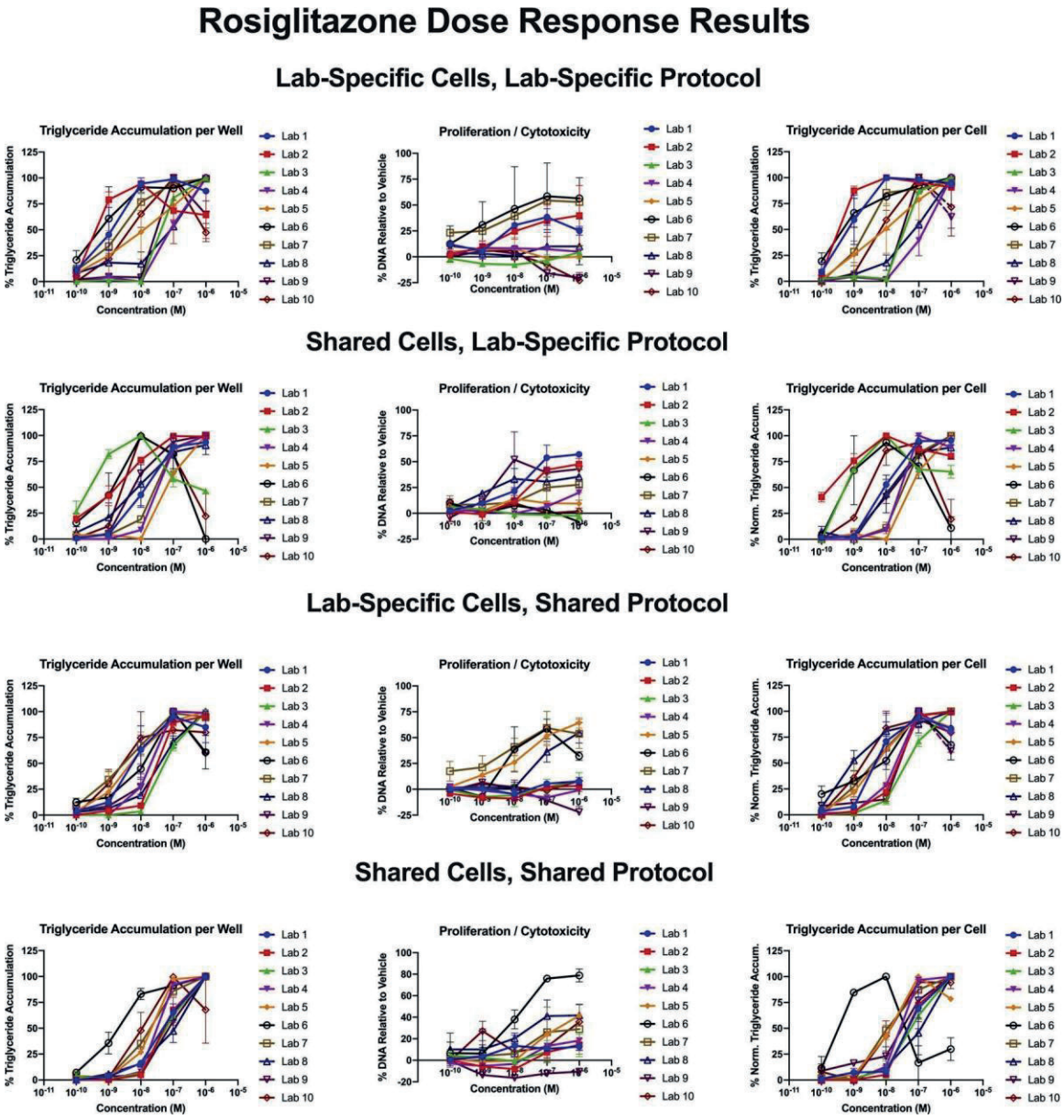

Fig. 2. Rosiglitazone Responses Across Laboratories and Conditions. Comparison of dose responses for rosiglitazone (provided, not blinded) across the ten participating laboratories. Responses are provided as raw triglyceride accumulation per well of tissue culture plate, normalized to maximal rosiglitazone-induced response using those test conditions (left column); cell proliferation and/or cytotoxicity as per Hoechst DNA dye (middle column); and normalized triglyceride accumulation per cell, normalized to DNA content of that treatment (right column). Laboratories were asked to test equivalent

concentrations using their laboratory stock of 3T3-L1 cells and their laboratory differentiation protocol (top row), using the provided stock of 3T3-L1 cells and their laboratory protocol (second row), using their laboratory stock of 3T3-L1 cells and the provided protocol (third row), and using the provided 3T3-L1 cells and provided protocol (bottom row).

3.*2.* *Pyraclostrobin responses across laboratories and conditions*

Pyraclostrobin is a fungicide that has been reported previously to exhibit adipogenic effects (Kassotis et al., 2017a; Luz et al., 2018), though reportedly not through PPARγ activation (Luz et al., 2018). Maximal triglyceride accumulation efficacies for pyraclostrobin varied considerably across test conditions (<LOD – 400 %), with generally lower variances observed in the SP groups (Table S3, Table S4, Figure S1). Under each set of test conditions, there was at least one laboratory below or near the LOD for triglyceride accumulation. There appeared to be two groupings among laboratories for maximal efficacy results (low/no activity responders and high activity responders; Fig. 3). Three laboratories were consistently low responders, one was consistently a high responder, four laboratories were high responders in three of the four test conditions (test condition varied by laboratory), and two laboratories were split in responses across test conditions. The LOEL and maximal response concentrations appeared to be more consistent when using the SP, albeit with slightly lower potencies (particularly for the SC/SP condition; Fig. 3, Table S4). Almost all laboratories identified this chemical as active for inducing triglyceride accumulation with the exception of one each using LC/SP and SC/SP (blue boxes denote active determinations, whereas red denote inactive; Fig. 3, Table S3, Table S4).

For pre-adipocyte proliferation, maximal efficacies also varied widely (<LOD – 201 %; Fig. S1, Fig. 3, Table S4). A greater proportion of laboratories reported significant proliferative activity using the SC: 30 % using LC/LP, 40 % using LC/SP, 70 % using SC/LP, and 60 % using SC/ SP. In most cases, greater efficacies for proliferation were observed when in SP groups. Greater consistency but lower sensitivity/potency were observed for the SC/SP group. At the level of activity determination, there was an almost even split in responses (Fig. 3D). Only five laboratories reported pyraclostrobin as active for proliferation in three or more four conditions (generally reported as inactive using LC/LP). Significant toxicity was observed for some laboratories under certain test conditions. No toxicity was observed for any laboratory in the SC/SP condition, but 40 % of laboratories reported significant toxicity in both the SC/LP (one at 1 and 10 mM and three at 10 mM only) and LC/SP (three at 1 and 10 mM and one at 10 mM only)

conditions, and 50 % reported significant toXicity using LC/LP (two at 0.1, 1, and 10 mM; two at 1 and 10 mM; and one at 10 mM only).

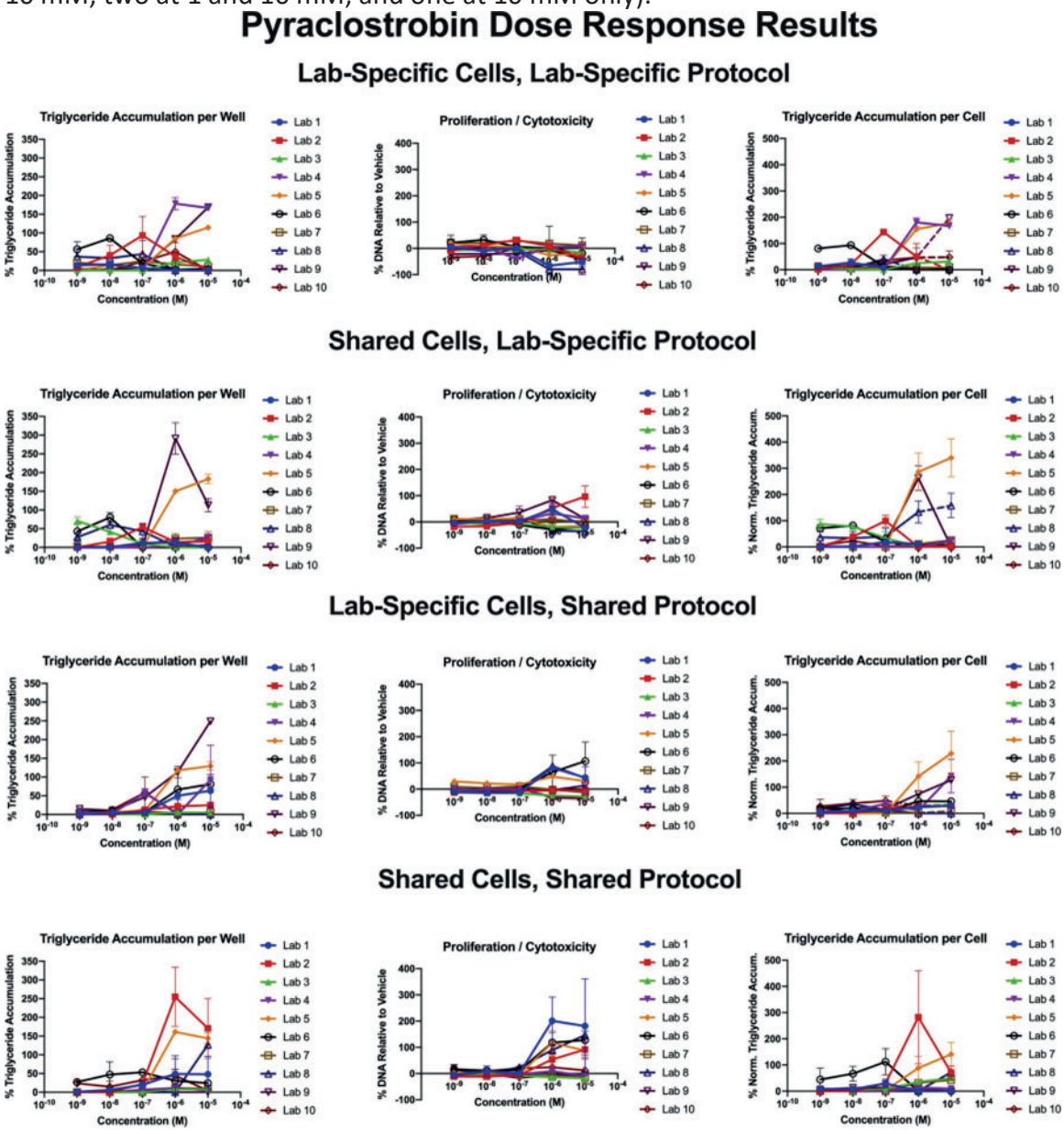

Fig. 3. Pyraclostrobin Responses Across Labs and Conditions. Comparison of dose responses for pyraclostrobin across the ten participating laboratories. Mean responses ± standard error of the mean (SEM) are provided as raw triglyceride accumulation per well of tissue culture plate, normalized to maximal rosiglitazone- induced response using those test conditions (left column); cell proliferation and/or cytotoxicity as per Hoechst DNA dye (middle column); and

normalized triglyceride accumulation per cell, normalized to DNA content of that treatment (right column). Laboratories were asked to test equivalent concentrations using their lab stock of 3T3-L1 cells and their laboratory differentiation protocol (top row), using the provided stock of 3T3-L1 cells and their laboratory protocol (second row), using their lab stock of 3T3-L1 cells and the provided protocol (third row), and using the provided 3T3-L1 cells and provided protocol (bottom row). Dashed lines represent concentrations at which cytotoxicity was observed (significant decreased DNA content at that concentration).

3.3. Tributyltin chloride (TBT) responses across laboratories and conditions

TBT is a biocide that has been reported previously to exhibit robust adipogenic effects *in vitro* (Grun et al., 2006; Li et al., 2011; Pereira-Fernandes et al., 2013) and *in vivo* (Chamorro-Garcia et al., 2013; Penza et al., 2011). Maximal triglyceride accumulation efficacies for TBT varied considerably across test conditions (<LOD – 429 %), with lower variances in the LC/LP and SC/SP groups (Fig. 4, Fig. S2, Table S5, Table S6). Relative to pyraclostrobin, wide variances were observed even within laboratories, and two response groupings (high and low consistency) were observed. Five laboratories ranged widely in triglyceride accumulation responses across test conditions, and five laboratories were more consistent (moderate to high triglyceride accumulation). No differences were observed in LOELs, though maximum response concentrations and potencies appeared more consistent in the SC/SP group, albeit with slightly lower potencies (Fig. 4, Table S6). Almost all laboratories identified this chemical as active for inducing triglyceride accumulation, with the exception of two laboratories using the LC and one using the SC/SP (Fig. 4D).

For pre-adipocyte proliferation, maximal efficacies had low consistency (<LOD – 84 %; Fig. S2, Fig. 4, Table S6), but the highest consistencies for efficacy, LOEL, and potencies were observed in the SC/SP group. At the level of activity determination, 50–70 % of laboratories reported TBT as inactive for proliferation across all test conditions (Fig. 4D), with no laboratory reporting consistent activity across test conditions. Two laboratories identified TBT as inactive for proliferation for all conditions and two as inactive in three of four conditions. Clear cytotoxicity was observed for TBT at 1 and 10 mM, with high consistency across laboratories and conditions (Fig. S2).

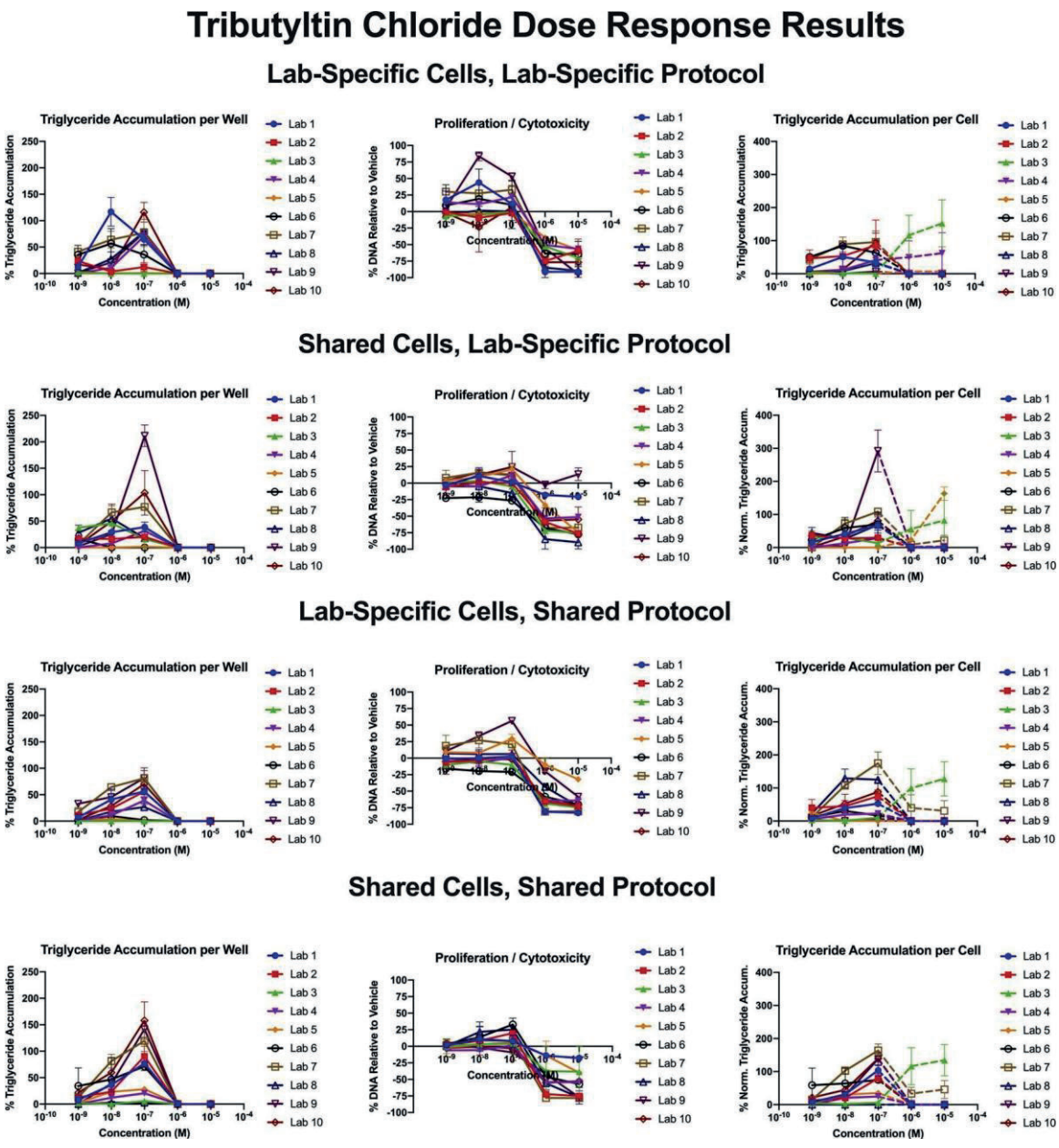

Fig. 4. Tributyltin Chloride Responses Across Labs and Conditions. Comparison of dose responses for tributyltin chloride across the ten participating laboratories. Mean responses ± standard error of the mean (SEM) are provided as raw triglyceride accumulation per well of tissue culture plate, normalized to maximal rosiglitazone-induced response using those test conditions (left column); cell proliferation and/or cytotoxicity as per Hoechst DNA dye (middle column); and normalized triglyceride accumulation per cell, normalized to DNA content of that treatment (right column). Laboratories were asked to test

equivalent concentrations using their lab stock of 3T3-L1 cells and their laboratory differentiation protocol (top row), using the provided stock of 3T3-L1 cells and their laboratory protocol (second row), using their lab stock of 3T3-L1 cells and the provided protocol (third row), and using the provided 3T3-L1 cells and provided protocol (bottom row). Dashed lines represent concentrations at which cytotoxicity was observed (significant decreased DNA content at that concentration).

3.4. Bisphenol A responses across laboratories and conditions

BPA is a synthetic chemical used often as a cross-linker in the synthesis of some plastics and can be found in some consumer products. (vom Saal et al., 2007; Welshons et al., 2006) BPA has been extensively described to disrupt metabolic health *in vitro* (Masuno et al., 2002; Sargis et al., 2010; Taxvig et al., 2012), *in vivo* (Angle et al., 2013; Somm et al., 2009; Vom Saal et al., 2012), and in epidemiological studies (Carwile and Michels, 2011; Rochester, 2013; Trasande et al., 2012). Maximal triglyceride accumulation efficacies for BPA varied across test conditions (<LOD – 93 %), with apparent lower variances in the SP groups (Table S7, Table S8, Fig. S3, Fig. 5). Relatively wide variances were observed even within laboratories, and three response groupings (inactive, low/moderate and moderate/high activity) were observed. Given lower reported activity, potency and LOEL comparisons were difficult to ascertain (Fig. 5, Table S8). Nearly all laboratories identified this chemical as active for triglyceride accumulation, though with considerable variation across test conditions and no apparent difference between groups (Fig. 5).

For pre-adipocyte proliferation, maximal efficacies were again less consistent but with a smaller dynamic range (<LOD – 42 %; Fig. S3, Fig. 5, Table S8) that hindered evaluation of several reproducibility metrics. Greater agreement was observed for inactivity of BPA on the proliferation metric (Fig. 5D). Three laboratories reported BPA as inactive for proliferation across test conditions, three laboratories as inactive in three of four test conditions, and the remaining laboratories reported higher rates of activity. Within test conditions, the greatest consistency was observed using the SC/LP and SC/SP conditions, with 80 % of laboratories reporting BPA as inactive for proliferation. No significant toxicity was reported for BPA at any test concentration by any laboratory and in any test condition.

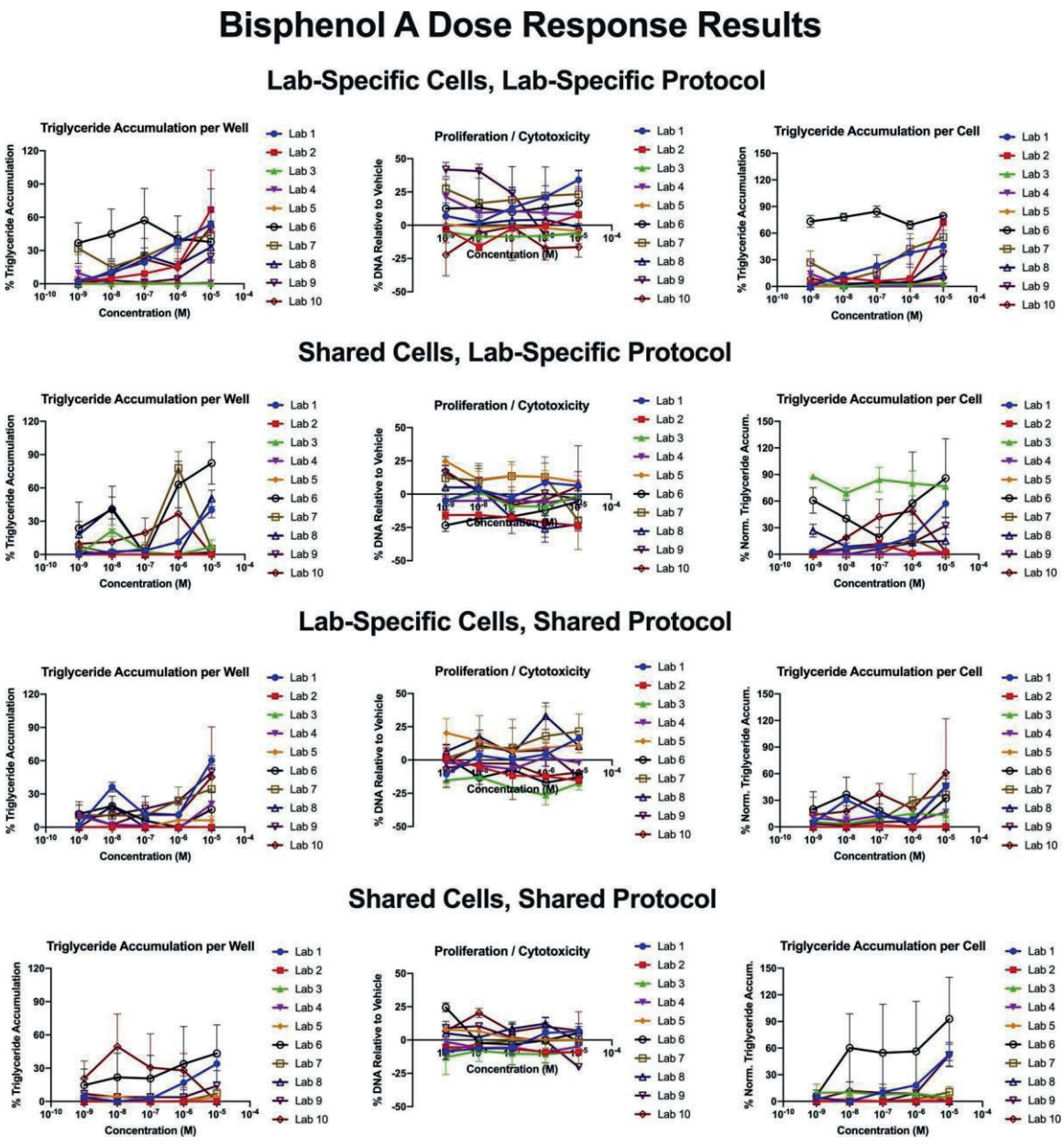

Fig. 5. Bisphenol A Responses Across Labs and Conditions. Comparison of dose responses for bisphenol A across the ten participating laboratories. Mean responses ± standard error of the mean (SEM) are provided as raw triglyceride accumulation per well of tissue culture plate, normalized to maximal rosiglitazone- induced response using those test conditions (left column); cell proliferation and/or cytotoxicity as per Hoechst DNA dye (middle column); and normalized triglyceride accumulation per cell, normalized to DNA content of that treatment (right column). Laboratories were asked to test equivalent

concentrations using their lab stock of 3T3-L1 cells and their laboratory differentiation protocol (top row), using the provided stock of 3T3-L1 cells and their laboratory protocol (second row), using their lab stock of 3T3-L1 cells and the provided protocol (third row), and using the provided 3T3-L1 cells and provided protocol (bottom row).

4. Discussion

These results confirm that repeatability of adipogenic (pre-adipocyte proliferation) and lipogenic (triglyceride accumulation) responses utilizing 3T3-L1 cells are highly variable across laboratories, which can be problematic for reproducibility and data comparability. There have been previous reports of inconsistencies in adipogenic determinations for specific chemicals (Kassotis et al., 2017b), but this has not previously been evaluated in a blinded, systematic manner. While standard in most areas, reproducibility studies are relatively uncommon for toxicological outcomes, and as a consequence, reproducibility across laboratories is not well-appreciated. While bioactivities (efficacies/potencies) varied considerably across laboratories and test conditions, activity determinations (active/inactive) were more consistent, which suggests that most laboratories can accurately identify MDCs. Though importantly, even these determinations were less consistent when using LC/LP, suggesting that standardization may greatly improve reproducibility between laboratories (at least for triglyceride accumulation) and thus confidence in reported outcomes. The most consistent results across test conditions and chemicals tested were generally observed in the LC/SP and SC/SP groups. While potencies were lower for rosiglitazone-induced triglyceride accumulation in the SC/SP group, this pattern did not carry over to other test chemicals or the pre-adipocyte proliferation metric, and this group had the most potent responses for other test chemicals.

Pyraclostrobin was selected for screening given the previously reported non-traditional mechanism(s) of action (antagonism of TRb and/ or mitochondrial dysfunction) and robust adipogenic response (Kassotis et al., 2017a; Luz et al., 2018). A high degree of consistency was observed for triglyceride accumulation activity determination between laboratories and test conditions for this chemical, though magnitude and potency of responses were much more variable. Efficacy did not seem to vary based on test conditions, but instead was more laboratory-specific, with laboratories reporting more consistent responses regardless of test condition. These responses appeared independent of cell source and protocol, which could suggest more overarching variables such as fetal bovine serum source/consistency that may impact results across

these conditions. Maximal response concentrations and LOELs were more consistent when using the SP, albeit with slightly lower potencies. Pre-adipocyte proliferation was much more variable (50 % of laboratories and test conditions reported active), though twice the laboratories reported significant proliferative activity using the SP. In most cases, greater proliferative responses were observed when using the SP, for which laboratories were provided tissue culture plates; it has been previously reported that the tissue culture plates used could drastically impact the proliferative response (Kassotis et al., 2017b; Mehra et al., 2007). Overall, greater consistency but lower sensitivity/potency were observed for the SC/SP group. It is worth noting that pyraclostrobin exhibited much greater activity TBT was selected due to well-reported adipogenic effects via activation of PPAR and RXR (Chamorro-Garcia et al., 2013; Grun et al., 2006; le Maire et al., 2009; Li et al., 2011; Penza et al., 2011; Pereira-Fernandes et al., 2013). We previously demonstrated consistent expression for PPAR isoforms and RXRα in ATCC and Zenbio-sourced 3T3-L1 cells (Kassotis et al., 2017b), suggesting this chemical might have greater consistency across laboratories and test conditions. However, while nearly all laboratories and test conditions successfully identified TBT as active for promoting significant triglyceride accumulation, the broad range of efficacies, potencies, and sensitivities reported here would suggest that these methods may not be sensitive enough to accurately characterize less active chemicals. This could be due to small differences in cytotoxicity impacting our broad concentration response curves. Pre-adipocyte proliferation is a less frequently examined and/or reported endpoint in 3T3-L1 cells, with explicit reporting only becoming more standard in the last several years. Accounting for varying cell densities across wells and replicates can be achieved by normalizing the triglyceride content with the DNA content. Indeed, when examining the total triglyceride content per well only (Table S5), the number of laboratories and conditions reporting TBT inactive would increase from five to nine. Thus, the normalization to DNA content is important to accurately defining adipogenic activity, particularly given that varying cell densities across plates are common and since mature adipocytes detach easily from the plate bottom during media changes and rinses. Pre-adipocyte proliferation as its own metric, however, was considerably less consistent. Approximately half of the laboratories and test conditions reported TBT as inactive for proliferation (17/40) and half as active, demonstrating no clear correct determination for this endpoint. Greater consistency was observed when using SC/SP, however, demonstrating that greater concordance in testing may be possible if protocols were standardized.

BPA was selected due to the non-canonical mechanism of action and the less reproducible outcomes reported previously *in vitro* (Kassotis et al., 2017b). BPA

has been reported to increase adipogenic gene expression (aP2) through an estrogen receptor-mediated mechanism (Boucher et al., 2014), which we reported to have differential expression between 3T3-L1 cell sources (Kassotis et al., 2017b). As expected, lower consistency was observed for BPA-induced triglyceride accumulation (65 % of laboratories/conditions reported as active). Lower variance was observed for DNA content measurements, with only 30 % of labs and test conditions reporting BPA as active for this metric. While test condition did not appreciably influence activity determinations for triglyceride accumulation, improved consistency was observed for the pre-adipocyte proliferation metric using the LC/SP and SC/SP conditions, suggesting that protocol and not cell differences were the primary factors in these disparities.

Overall, cell source appeared to be a significant factor in variation observed between laboratories and test conditions. Zenbio-sourced cells often had lower variation than ATCC-sourced cells for chemicals, which we reported previously (Kassotis et al., 2017b). It is perhaps unsurprising that 3T3-L1 cells sourced from different companies had high variation in responses between them, though it is notable that considerable variation was observed even when comparing cells obtained from the same provider (Table 1, Figs. 2–5); cells sourced from the Green Lab were unsurprisingly more similar to the Zenbio-sourced cells. It has been previously established that ATCC maintains a variety of 3T3-L1 cell lots, which are described in ATCC protocols to differentiate to different extents (Kassotis et al., 2017b). This appears to be a common problem, as noted above, as the European Collection of Authenticated Cell Culture (ECACC) currently reports that their 3T3-L1 cells will not differentiate. It is likely, based on the varied responses reported herein and the differentiation issues noted by the providers, that continuity of this cell line has not been properly controlled across sources. This may be contributing to a portion of the divergent responses observed across laboratories. As observed here, this contributes to considerable variance even for laboratories ordering presumably the same cell line from the same supplier. This has been reported previously for MCF-7 cells obtained by two laboratories that ordered the same lot of MCF-7 cells from ATCC (Kleensang et al., 2016). Phenotypic, gene expression, metabolomic, and hormone-responsiveness were all demonstrated to clearly vary between these sub-clones even of the same lot of cells and were eventually linked to genetic variability in a single frozen lot of ATCC MCF-7 cells (Kleensang et al., 2016). As these authors recommended, future research should investigate these 3T3-L1 cell sources and lots through Direct Compararative Genome Hybridization and/or deep sequencing approaches to determine shifts in frozen cell line stocks that may be contributing to disparate responses. This should be pursued to improve response consistency and to increase confidence and transparency of results.

For a number of chemicals and laboratories, the most reproducible and least variable outcomes (lower Z-score ranges; Supplemental Tables) based on the performance metrics examined here were observed in the SC/SP group. Often, we observed reduced variance in the LC/SP group as well, suggesting that while cell source should be considered as a contributory factor in improving reproducibility, improvements can be made more readily through taking steps to harmonize differentiation protocols across laboratories. Numerous factors varied widely across laboratories (Table 1). While the differentiation timeline was often consistent, a variety of cell culture plastics were used, concentrations and presence of media additives varied considerably. The source of additives such as fetal bovine serum have been reported to vary substantially and may have contributed to varying degrees of differentiation. While isobutylmethylxanthine (IBMX) concentrations were quite consistent, insulin concentrations varied >1000-fold, and seven laboratories used dexamethasone (10-fold variation in concentrations). Even 10-fold variations in insulin concentration have been described to promote robust impacts on adipogenesis via both triglyceride accumulation and pre-adipocyte proliferation (Green and Kehinde, 1975). Additionally, dexamethasone has been demonstrated to promote potent and efficacious effects on triglyceride accumulation (Kassotis et al., 2017b). Taken together, the concentrations of these additives are likely contributory factors, though no clear trends in media additive use could be associated with specific patterns of activity (Fig. S4). While the SP groups utilized consistent detection and staining protocols, these were not consistent in the LP groups and may have contributed to some of the protocol-specific variances. Despite these factors, particularly variation likely contributed by fetal bovine serum sourcing, we need to utilize models such as this to evaluate the tens of thousands of chemicals requiring toxicological characterization. Appreciating these factors, and understanding the inherent variability, is key to making proper determinations based on studies utilizing these and similar models

In summary, we report poor reproducibility (efficacies, potencies, and sensitivities) for several blinded test chemicals across laboratories, though this largely did not impact determination of chemical activity classification (e.g. categorized as “active” or “inactive”). While activity determinations for triglyceride accumulation were quite consistent, even this gross level of bioactivity measurement was not consistent for pre-adipocyte proliferation. These results suggest that toxicologic reproducibility assessments are warranted for other endpoints (for other assays and other metrics of differentiation success such as percent of differentiated cells, etc.) and suggests some avenues for improvements through harmonization of cell sourcing and differentiation protocols. It is also important to note that analytical

reproducibility efforts have also reported high variance across laboratories (Melymuk et al., 2015, 2018); we do not believe this should reduce confidence in bioassay findings, but should be acknowledged to support accurate determinations of activity for unknown test chemicals when considering regulatory next steps. We report that the differentiation protocol and the source of the 3T3-L1 cells both contributed to variance in responses and even some dissimilar determinations of activity, suggesting that these factors may provide opportunity for reducing inter-laboratory variability. While we did not detect specific differences that we could associate with individual media additives, further research should evaluate this more explicitly. It should be noted that pyraclostrobin exhibited much greater activities than BPA, though has received as of yet very limited relative research attention.

While human mesenchymal stem cell and human pre-adipocyte cell lines are increasingly available commercially, there are wide reported variations based on sex, race and ethnicity, as well as physiological status of the donor. These models should see increased use, and direct comparisons to 3T3-L1 results, in future research; however, the decades of research on 3T3-L1 cells support continued use of this model at least until there are clearly superior models and/or clear translation of prior findings to human models.

Given the increasing need for accurate and reliable metabolic health assays and the difficulty of policing cell line providers, we suggest that future efforts focus on establishing best practices and consistency in differentiation protocols to improve translation across laboratories. There are also notable efforts ongoing through the Horizon 2020 program in the European Union to develop and validate new and diverse metabolism disrupting chemical assays *in silico*, *in vitro*, and *in vivo* (Audouze et al., 2020; Legler et al., 2020). Towards that end, we have provided the detailed shared differentiation protocol used in this study (Supplemental File 1), though further efforts towards harmonization should be undertaken with experts to weigh inclusion or exclusion of specific factors in the protocol and to consider the issues inherent with specific sources of 3T3-L1 cells.

References

- Aguado, T.; Monory, K.; Palazuelos, J.; Stella‡, N.; Cravatt, B.; Lutz, B.; Marsicano, G.; Kokaia, Z.; Guzmán, M.; Galve-Roperh, I. The endocannabinoid system drives neural progenitor proliferation. FASEB J. 2005, 19, 1704–1706.
- Aguilar-Salinas, C.A.; Viveros-Ruiz, T. Recent Advances in Managing/Understanding the Metabolic Syndrome. F1000Res 2019, 8, doi:10.12688/f1000research.17122.1.
- Amal, H.; Fridman-Rozevich, L.; Senn, R.; Strelnikov, A.; Gafni, M.; Keren, O.; Sarne, Y. Long-term consequences of a single treatment of mice with an ultra-low dose of Δ9-tetrahydrocannabinol (THC). Behav. Brain Res. 2010, 206, 245–253.
- Ambrož, M.; Šmatová, M.; Šadibolová, M.; Pospíšilová, E.; Hadravská, P.; Kašparová, M.; Skarková, V.H.; Králová, V.; Skálová, L. Sesquiterpenes α-Humulene and β-Caryophyllene Oxide Enhance the Efficacy of 5-Fluorouracil and Oxaliplatin in Colon Cancer Cells. Acta Pharm. 2019, 69, 121–128, doi:10.2478/acph-2019-0003.
- American Type Culture Collection (ATCC) ATTC, 2011. Chemically-induced Differentiation of ATCC CL-173 (3T3-L1) Using Single-component Commercially- available Reagents. Available: http://www.atcc.org//media/ 6124AF1E4C2A47CF904435117909AC25.ashX [accessed 17 May 2016.
- Ammazzalorso, A.; Maccallini, C.; Amoia, P.; Amoroso, R. Multitarget PPARγ Agonists as Innovative Modulators of the Metabolic Syndrome. Eur. J. Med. Chem. 2019, 173, 261–273, doi:10.1016/j.ejmech.2019.04.030.
- Anavi-Goffer, S.; Mulder, J. The Polarised Life of the Endocannabinoid System in CNS Development. ChemBioChem 2009, 10, 1591–1598.
- Angle, B.M., Do RP, Ponzi D., Stahlhut, R.W., Drury, B.E., Nagel, S.C., et al., 2013. Metabolic disruption in male mice due to fetal exposure to low but not high doses of bisphenol A (BPA): evidence for effects on body weight, food intake, adipocytes, leptin, adiponectin, insulin and glucose regulation. Reprod. Toxicol. 42, 13.
- Api, A.M.; Belsito, D.; Botelho, D.; Bruze, M.; Burton, G.A.; Buschmann, J.; Dagli, M.L.; Date, M.; Dekant, W.; Deodhar, C.; et al. RIFM Fragrance Ingredient Safety Assessment, β-Caryophyllene Alcohol, CAS Registry Number 472-97-9. Food Chem. Toxicol. 2018, 122, S566–S572, doi:10.1016/j.fct.2018.10.020.

- Arizuka, N.; Murakami, T.; Suzuki, K. The Effect of β-Caryophyllene on Nonalcoholic Steatohepatitis. J. Toxicol. Pathol. 2017, 30, 263–273, doi:10.1293/tox.2017-0018.
- Atanasov, A.G.; Zotchev, S.B.; Dirsch, V.M.; Supuran, C.T. Natural Products in Drug Discovery: Advances and Opportunities. Nat. Rev. Drug Discov. 2021, 20, 200–216. https://doi.org/10.1038/s41573-020-00114-z.
- Atwood, B.K.; Lee, D.; Straiker, A.; Widlanski, T.S.; Mackie, K. CP47,497-C8 and JWH073, commonly found in 'Spice' herbal blends, are potent and efficacious CB1 cannabinoid receptor agonists. Eur. J. Pharmacol. 2011, 659, 139–145.
- Audouze, K., Sarigiannis, D., Alonso-Magdalena, P., Brochot, C., Casas, M., Vrijheid, M., et al., 2020. Integrative strategy of testing systems for identification of endocrine disruptors inducing metabolic disorders-an introduction to the Oberon project. Int. J. Mol. Sci. 21.
- Augustin, S.M.; Lovinger, D.M. Functional Relevance of Endocannabinoid-Dependent Synaptic Plasticity in the Central Nervous System. ACS Chem. Neurosci. 2018, 9, 2146–2161.
- Avraham, H.K.; Jiang, S.; Fu, Y.; Rockenstein, E.; Makriyannis, A.; Zvonok, A.; Masliah, E.; Avraham, S. The cannabinoid CB2receptor agonist AM1241 enhances neurogenesis in GFAP/Gp120 transgenic mice displaying deficits in neurogenesis. Br. J. Pharmacol. 2014, 171, 468–479.
- Aymerich, M.S.; Aso, E.; Abellanas, M.A.; Tolon, R.M.; Ramos, J.A.; Ferrer, I.; Romero, J.; Fernández-Ruiz, J. Cannabinoid pharmacology/therapeutics in chronic degenerative disorders affecting the central nervous system. Biochem. Pharmacol. 2018, 157, 67–84.
- Bagheri, H.; Abdul Manap, M.Y.B.; Solati, Z. Response Surface Methodology Applied to Supercritical Carbon Dioxide Extraction of Piper Nigrum L. Essential Oil. LWT-Food Sci.Technol. 2014, 57, 149–155.
- Baldassarre, M.; Giannone, F.A.; Napoli, L.; Tovoli, A.; Ricci, C.S.; Tufoni, M.; Caraceni, P. The Endocannabinoid System in Advanced Liver Cirrhosis: Pathophysiological Implication and Future Perspectives. Liver Int. 2013, 33, 1298–1308. https://doi.org/10.1111/liv.12263.
- Bari, M.; Battista, N.; Valenza, M.; Mastrangelo, N.; Malaponti, M.; Catanzaro, G.; Centonze, D.; Finazzi-Agrò, A.; Cattaneo, E.;
- Basha, R.H.; Sankaranarayanan, C. β-Caryophyllene, a Natural Sesquiterpene, Modulates Carbohydrate Metabolism in Streptozotocin-Induced Diabetic Rats. Acta Histochem. 2014, 116, 1469–1479, doi:10.1016/j.acthis.2014.10.001.

- Basha, R.H.; Sankaranarayanan, C. β-Caryophyllene, a Natural Sesquiterpene Lactone Attenuates Hyperglycemia Mediated Oxidative and Inflammatory Stress in Experimental Diabetic Rats. Chem. Biol. Interact. 2016, 245, 50–58, doi:10.1016/j.cbi.2015.12.019.
- Basu, P.P.; Aloysius, M.M.; Shah, N.J.; Brown, R.S., Jr.; Review Article: The Endocannabinoid System in Liver Disease, a Potential Therapeutic Target. Aliment. Pharmacol. Ther. 2014, 39, 790–801. https://doi.org/10.1111/apt.12673.
- Bazwinsky-Wutschke, I.; Zipprich, A.; Dehghani, F. Endocannabinoid System in Hepatic Glucose Metabolism, Fatty Liver Disease, and Cirrhosis. Int. J. Mol. Sci. 2019, 20, 2516. https://doi.org/10.3390/ijms20102516.
- Behl T, Makkar R, Sehgal A, Sharma N, Singh S, Albratty M, Najmi A, Meraya AM, Bungau SG. Insights into the Explicit Protective Activity of Herbals in Management of Neurodegenerative and Cerebrovascular Disorders. Molecules. 2022 Aug 4;27(15):4970. doi: 10.3390/molecules27154970. PMID: 35956919; PMCID: PMC9370592.
- Bénard, G.; Massa, F.; Puente, N.; Lourenço, J.; Bellocchio, L.; Soria-Gómez, E.; Matias, I.; Delamarre, A.; Metna-Laurent, M.; Cannich, A.; et al. Mitochondrial CB1 receptors regulate neuronal energy metabolism. Nat. Neurosci. 2012, 15, 558–564.
- Berthier, A.; Johanns, M.; Zummo, F.P.; Lefebvre, P.; Staels, B. PPARs in Liver Physiology. Biochim. Biophys. Acta Mol. Basis Dis. 2021, 1867, 166097. https://doi.org/10.1016/j.bbadis.2021.166097.
- Beyer, S.; Mix, E.; Hoffrogge, R.; Lünser, K.; Völker, U.; Rolfs, A. Neuroproteomics in stem cell differentiation. Proteom. Clin. Appl. 2007, 1, 1513–1523.
- Boon, F.S.D.; Chameau, P.; Schaafsma-Zhao, Q.; Van Aken, W.; Bari, M.; Oddi, S.; Kruse, C.G.; Maccarrone, M.; Wadman, W.J.; Werkman, T.R. Excitability of prefrontal cortical pyramidal neurons is modulated by activation of intracellular type-2 cannabinoid receptors. Proc. Natl. Acad. Sci. USA 2012, 109, 3534–3539. Molecules 2021, 26, 1448 14 of 14
- Bossong, M.G.; Van Berckel, B.N.M.; Boellaard, R.; Zuurman, L.; Schuit, R.C.; Windhorst, A.D.; Van Gerven, J.M.A.; Ramsey, N.F.; Lammertsma, A.A.; Kahn, R.S. Δ9-Tetrahydrocannabinol Induces Dopamine Release in the Human Striatum. Neuropsychopharmacology 2008, 34, 759–766.
- Boucher, J.G., Boudreau, A., Ahmed, S., Atlas, E., 2015. In vitro effects of bisphenol A beta-d-glucuronide (BPA-G) on adipogenesis in human and murine preadipocytes. Environ. Health Perspect. 123, 1287–1293.

- Boucher, J.G., Boudreau, A., Atlas, E., 2014. Bisphenol A induces differentiation of human preadipocytes in the absence of glucocorticoid and is inhibited by an estrogen-receptor antagonist. Nutr. Diabetes 4, e102.
- Bournat, J.C., Brown, C.W., 2010. Mitochondrial dysfunction in obesity. Curr. Opin. Endocrinol. Diabetes Obes. 17, 446–452.
- Boyer, K.W., Horwitz, W., Albert, R., 1985. Interlaboratory variability in trace element analysis. Anal. Chem. 57, 454–459.
- Brailoiu, G.C.; Deliu, E.; Marcu, J.; Hoffman, N.E.; Console-Bram, L.; Zhao, P.; Madesh, M.; Abood, M.E.; Brailoiu, E. Differential Activation of Intracellular versus Plasmalemmal CB2Cannabinoid Receptors. Biochem. 2014, 53, 4990–4999.
- Butt, M.S.; Pasha, I.; Sultan, M.T.; Randhawa, M.A.; Saeed, F.; Ahmed, W. Black Pepper and Health Claims: A Comprehensive Treatise. Crit. Rev. Food Sci. Nutr. 2013, 53, 875–886, doi:10.1080/10408398.2011.571799.
- Cacci, E.; Salani, M.; Anastasi, S.; Perroteau, I.; Poiana, G.; Biagioni, S.; Augusti-Tocco, G. Hepatocyte growth factor stimulates cell motility in cultures of the striatal progenitor cells ST14A. J. Neurosci. Res. 2003, 74, 760–768.
- Carwile, J.L., Michels, K.B., 2011. Urinary bisphenol A and obesity: nhanes 2003-2006. Environ. Res. 111, 825–830.
- Castaneda, J.T.; Harui, A.; Roth, M.D. Regulation of Cell Surface CB2 Receptor during Human B Cell Activation and Differentiation. J. Neuroimmune Pharm. 2017, 12, 544–554. https://doi.org/10.1007/s11481-017-9744-7.
- Cattaneo, E.; Conti, L. Generation and characterization of embryonic striatal conditionally immortalized ST14A cells. J. Neurosci. Res. 1998, 53, 223–234.
- Chamorro-Garcia, R., Sahu, M., Abbey, R.J., Laude, J., Pham, N., Blumberg, B., 2013. Transgenerational inheritance of increased fat depot size, stem cell reprogramming, and hepatic steatosis elicited by prenatal exposure to the obesogen tributyltin in mice. Environ. Health Perspect. 121, 359–366.
- Charytoniuk, T.; Zywno, H.; Berk, K.; Bzdega, W.; Kolakowski, A.; Chabowski, A.; Konstantynowicz-Nowicka, K. The Endocannabinoid System and Physical Activity—A Robust Duo in the Novel Therapeutic Approach against Metabolic Disorders. Int. J. Mol. Sci. 2022, 23, 3083. https://doi.org/10.3390/ijms23063083.
- Cheng, C.; Zhuo, S.; Zhang, B.; Zhao, X.; Liu, Y.; Liao, C.; Quan, J.; Li, Z.; Bode, A.M.; Cao, Y.; et al. Treatment implications of natural compounds

targeting lipid metabolism in nonalcoholic fatty liver disease, obesity and cancer. Int. J. Biol. Sci. 2019, 15, 1654–1663.
- Cheng, Y.; Dong, Z.; Liu, S. β-Caryophyllene Ameliorates the Alzheimer-like Phenotype in APP/PS1 Mice through CB2 Receptor Activation and the PPARγ Pathway. Pharmacology 2014, 94, 1–12. https://doi.org/10.1159/000362689.
- Cruz, N.G.; Sousa, L.P.; Sousa, M.O.; Pietrani, N.T.; Fernandes, A.P.; Gomes, K.B. The linkage between
- da Silva Oliveira, G.L.; Machado, K.C.; Machado, K.C.; da Silva, A.P.D.S.C.L.; Feitosa, C.M.; de Castro Almeida, F.R. Non-Clinical Toxicity of β-Caryophyllene, a Dietary Cannabinoid: Absence of Adverse Effects in Female Swiss Mice. Regul. Toxicol. Pharmacol. 2018, 92, 338–346, doi:10.1016/j.yrtph.2017.12.013.
- De Gottardi, A.; Spahr, L.; Ravier-Dall'Antonia, F.; Hadengue, A. Cannabinoid Receptor 1 and 2 Agonists Increase Lipid Accumulation in Hepatocytes. Liver Int. 2010, 30, 1482–1489. https://doi.org/10.1111/j.1478-3231.2010.02298.x.
- De Oliveira, R.W.; Oliveira, C.L.; Guimarães, F.S.; Campos, A.C. Cannabinoid signalling in embryonic and adult neurogenesis: Possible implications for psychiatric and neurological disorders. Acta Neuropsychiatr. 2018, 31, 1–16.
- Deveaux, V.; Cadoudal, T.; Ichigotani, Y.; Teixeira-Clerc, F.; Louvet, A.; Manin, S.; Nhieu, J.T.-V.; Belot, M.P.; Zimmer, A.; Even, P.; et al. Cannabinoid CB2 Receptor Potentiates Obesity-Associated Inflammation, Insulin Resistance and Hepatic Steatosis. PLoS ONE 2009, 4, e5844. https://doi.org/10.1371/journal.pone.0005844.
- Di Giacomo, S.; Briz, O.; Monte, M.J.; Sanchez-Vicente, L.; Abete, L.; Lozano, E.; Mazzanti, G.; Di Sotto, A.; Marin, J.J.G. Chemosensitization of Hepatocellular Carcinoma Cells to Sorafenib by β-Caryophyllene Oxide-Induced Inhibition of ABC Export Pumps. Arch. Toxicol. 2019, 93, 623–634, doi:10.1007/s00204-019-02395-9.
- Di Giacomo, S.; DI Sotto, A.; Mazzanti, G.; Wink, M. Chemosensitizing Properties of β-Caryophyllene and β-Caryophyllene Oxide in Combination with Doxorubicin in Human Cancer Cells. Anticancer Res. 2017, 37, 1191–1196, doi:10.21873/anticanres.11433.
- Di Marzo, V. New approaches and challenges to targeting the endocannabinoid system. Nat. Rev. Drug Discov. 2018, 17, 623–639.
- Di Marzo, V.; Piscitelli, F. The Endocannabinoid System and its Modulation by Phytocannabinoids. Neurotherapeutics 2015, 12, 692–698.

- Ding, Y.; Gu, Z.; Wang Y.; Wang, S.; Chen, H.; Zhang, H.; Chen, W.; Chen, Y.Q. Beyond Cannabis: Plants and the Endocannabinoid System. Trends Pharmacol. Sci. 2016, 37, 594–605, doi:10.1016/j.tips.2016.04.005.
- Duff, G.; Argaw, A.; Cecyre, B.; Cherif, H.; Tea, N.; Zabouri, N.; Casanova, C.; Ptito, M.; Bouchard, J.-F. Cannabinoid Receptor CB2 Modulates Axon Guidance. PLoS ONE 2013, 8, e70849.
- Ehrlich, M.E.; Conti, L.; Tosellic, M.; Tagliettic, L.; Fiorilloc, E.; Tagliettic, V.; Ivkovica, S.; Guineaa, B.; Tranberga, A.; Sipioneb, S.; et al. ST14A Cells Have Properties of a Medium-Size Spiny Neuron. Exp. Neurol. 2001, 167, 215–226.
- European Collection of Authenticated Cell Cultures (ECACC), 2020. ECACC General Cell Collection: 3T3-L1. Available: https://www.phe-culturecollections.org.uk/products/ celllines/generalcell/detail.jsp?refId 86052701&collection ecacc_gc#medDoc [accessed 4 February 2021].
- Fang, M., Webster, T.F., Stapleton, H.M., 2015. Activation of human peroxisome proliferator-activated nuclear receptors (PPARgamma1) by semi-volatile compounds (SVOCs) and chemical mixtures in indoor dust. Environ. Sci. Technol. 49, 10057–10064.
- Fernández-Ruiz, J.; Romero, J.; Velasco, G.; Tolón, R.M.; Ramos, J.A.; Guzmán, M. Cannabinoid CB2 receptor: A new target for controlling neural cell survival? Trends Pharmacol. Sci. 2007, 28, 39–45.
- Fidyt, K.; Fiedorowicz, A.; Strządała, L.; Szumny, A. β-Caryophyllene and β-Caryophyllene Oxide—Natural Compounds of Anticancer and Analgesic Properties. Cancer Med. 2016, 5, 3007–3017, doi:10.1002/cam4.816.
- Francomano, F.; Caruso, A.; Barbarossa, A.; Fazio, A.; La Torre, C.; Ceramella, J.; Mallamaci, R.; Saturnino, C.; Iacopetta, D.; Sinicropi, M.S. β-Caryophyllene: A Sesquiterpene with Countless Biological Properties. Appl. Sci. 2019, 9, 5420. https://doi.org/10.3390/app9245420.
- Francomano, F.; Caruso, A.; Barbarossa, A.; Fazio, A.; La Torre, C.; Ceramella, J.; Mallamaci, R.; Saturnino, C.; Iacopetta, D.; Sinicropi, M.S. β-Caryophyllene: A Sesquiterpene with Countless Biological Properties. Appl. Sci. 2019, 9, 5420. https://doi.org/10.3390/app9245420.
- Francque, S.; Szabo, G.; Abdelmalek, M.F.; Byrne, C.D.; Cusi, K.; Dufour, J.-F.; Roden, M.; Sacks, F.; Tacke, F. Nonalcoholic Steatohepatitis: The Role of Peroxisome Proliferator-Activated Receptors. Nat. Rev. Gastroenterol. Hepatol. 2021, 18, 24–39. https://doi.org/10.1038/s41575-020-00366-5.

- Friedman, S.L.; Neuschwander-Tetri, B.A.; Rinella, M.; Sanyal, A.J. Mechanisms of NAFLD Development and Therapeutic Strategies. Nat. Med. 2018, 24, 908–922. https://doi.org/10.1038/s41591-018-0104-9.
- Friedman, S.L.; Neuschwander-Tetri, B.A.; Rinella, M.; Sanyal, A.J. Mechanisms of NAFLD Development and Therapeutic Strategies. Nat. Med. 2018, 24, 908–922. https://doi.org/10.1038/s41591-018-0104-9.
- Fu, M., Sun, T., Bookout, A.L., Downes, M., Yu, R.T., Evans, R.M., et al., 2005. A nuclear receptor atlas: 3T3-L1 adipogenesis. Mol. Endocrinol. 19, 2437–2450.
- Galaj, E.; Bi, G.-H.; Moore, A.; Chen, K.; He, Y.; Gardner, E.; Xi, Z.-X. Beta-Caryophyllene Inhibits Cocaine Addiction-Related Behavior by Activation of PPARα and PPARγ: Repurposing a FDA-Approved Food Additive for Cocaine Use Disorder. Neuropsychopharmacology 2021, 46, 860–870. https://doi.org/10.1038/s41386-020-00885-4.
- Galiegue, S.; Mary, S.; Marchand, J.; Dussossoy, D.; Carriere, D.; Carayon, P.; Bouaboula, M.; Shire, D.; Fur, G.; Casellas, P. Expression of Central and Peripheral Cannabinoid Receptors in Human Immune Tissues and Leukocyte Subpopulations. JBIC J. Biol. Inorg. Chem. 1995, 232, 54–61.
- Gallo, M.P.; Femminò, S.; Antoniotti, S.; Querio, G.; Alloatti, G.; Levi, R. Catestatin Induces Glucose Uptake and GLUT4 Trafficking in Adult Rat Cardiomyocytes; doi:10.1155/2018/2086109.
- Galve-Roperh, I.; Chiurchiù, V.; Díaz-Alonso, J.; Bari, M.; Guzmán, M.; Maccarrone, M. Cannabinoid receptor signaling in progenitor/stem cell proliferation and differentiation. Prog. Lipid Res. 2013, 52, 633–650.
- Gambarotta, G.; Garzotto, D.; Destro, E.; Mautino, B.; Giampietro, C.; Cutrupi, S.; Dati, C.; Cattaneo, E.; Fasolo, A.; Perroteau, I. ErbB4 Expression in Neural Progenitor Cells (ST14A) Is Necessary to Mediate Neuregulin-1β1-induced Migration. J. Biol. Chem. 2004, 279, 48808–48816.
- Gannon, N.P.; Conn, C.A.; Vaughan, R.A. Dietary Stimulators of GLUT4 Expression and Translocation in Skeletal Muscle: A Mini-Review. Mol. Nutr. Food Res. 2015, 59, 48–64, doi:10.1002/mnfr.201400414.
- Geddo, F.; Antoniotti, S.; Querio, G.; Salaroglio, I.C.; Costamagna, C.; Riganti, C.; Gallo, M.P. Plant-Derived Trans-β-Caryophyllene Boosts Glucose Metabolism and ATP Synthesis in Skeletal Muscle Cells through Cannabinoid Type 2 Receptor Stimulation. Nutrients 2021, 13, 916. https://doi.org/10.3390/nu13030916.
- Geddo, F.; Scandiffio, R.; Antoniotti, S.; Cottone, E.; Querio, G.; Maffei, M.E.; Bovolin, P.; Gallo, M.P. Pipenig®-FL, a Fluid Extract of Black Pepper (Piper Nigrum L.) with a High Standardized Content of Trans-β-

Caryophyllene, Reduces Lipid Accumulation in 3T3-L1 Preadipocytes and Improves Glucose Uptake in C2C12 Myotubes. Nutrients 2019, 11, 2788. https://doi.org/10.3390/nu11112788.
- Geethangili, M.; Lin, C.-W.; Mersmann, H.J.; Ding, S.-T. Methyl Brevifolincarboxylate Attenuates Free Fatty Acid-Induced Lipid Metabolism and Inflammation in Hepatocytes through AMPK/NF-KB Signaling Pathway. Int. J. Mol. Sci. 2021, 22, 10062. https://doi.org/10.3390/ijms221810062.
- Gertsch, J.; Leonti, M.; Raduner, S.; Racz, I.; Chen, J.Z.; Xie, X.Q.; Altmann, K.H.; Karsak, M.; Zimmer, A. Beta-Caryophyllene Is a Dietary Cannabinoid. Proc. Natl. Acad. Sci. USA 2008, 105, 9099–9104. https://doi.org/10.1073/pnas.0803601105.
- Gertsch, J.; Leonti, M.; Raduner, S.; Racz, I.; Chen, J.-Z.; Xie, X.-Q.; Altmann, K.-H.; Karsak, M.; Zimmer, A. Beta-Caryophyllene Is a Dietary Cannabinoid. Proc. Natl. Acad. Sci. USA 2008, 105, 9099–9104, doi:10.1073/pnas.0803601105.
- Gómez-Lechón, M.J.; Donato, M.T.; Martínez-Romero, A.; Jiménez, N.; Castell, J.V.; O'Connor, J.-E. A Human Hepatocellular in Vitro Model to Investigate Steatosis. Chem. -Biol. Interact. 2007, 165, 106–116. https://doi.org/10.1016/j.cbi.2006.11.004.
- Goncalves, M.B.; Suetterlin, P.; Yip, P.; Molina-Holgado, F.; Walker, D.J.; Oudin, M.J.; Zentar, M.P.; Pollard, S.; Yáñez-Muñoz, R.J.; Williams, G.; et al. A diacylglycerol lipase-CB2 cannabinoid pathway regulates adult subventricular zone neurogenesis in an age-dependent manner. Mol. Cell. Neurosci. 2008, 38, 526–536.
- Gong, J.-P.; Onaivi, E.S.; Ishiguro, H.; Liu, Q.-R.; Tagliaferro, P.A.; Brusco, A.; Uhl, G.R. Cannabinoid CB2 receptors: Immunohistochemical localization in rat brain. Brain Res. 2006, 1071, 10–23. Molecules 2021, 26, 1448 13 of 14
- Gore, A.C., Chappell, V.A., Fenton, S.E., Flaws, J.A., Nadal, A., Prins, G.S., et al., 2015. Edc-2: the Endocrine Society's second scientific statement on endocrine-disrupting chemicals. Endocr. Rev. 36, E1–E150.
- Green, H., Kehinde, O., 1975. An established preadipose cell line and its differentiation in culture. II. Factors affecting the adipose conversion. Cell 5, 19–27.
- Green, H., Meuth, M., 1974. An established pre-adipose cell line and its differentiation in culture. Cell 3, 127–133.
- Greenspan, P., Mayer, E.P., Fowler, S.D., 1985. Nile red: a selective fluorescent stain for intracellular lipid droplets. J. Cell Biol. 100, 965–973.

- Grun, F., Watanabe, H., Zamanian, Z., Maeda, L., Arima, K., Cubacha, R., et al., 2006. Endocrine-disrupting organotin compounds are potent inducers of adipogenesis in vertebrates. Mol. Endocrinol. 20, 2141–2155.
- Hafidi, M.E.; Buelna-Chontal, M.; Sánchez-Muñoz, F.; Carbó, R. Adipogenesis: A Necessary but Harmful Strategy. Int. J. Mol. Sci. 2019, 20, 3657, doi:10.3390/ijms20153657.
- Hamers, T., Kamstra, J.H., Sonneveld, E., Murk, A.J., Kester, M.H., Andersson, P.L., et al., 2006. In vitro profiling of the endocrine-disrupting potency of brominated flame retardants. Toxicol. Sci. 92, 157–173.
- Harb, A.A.; Bustanji, Y.K.; Abdalla, S.S. Hypocholesterolemic Effect of β-Caryophyllene in Rats Fed Cholesterol and Fat Enriched Diet. J. Clin. Biochem. Nutr. 2018, 62, 230–237, doi:10.3164/jcbn.17-3.
- Haspula, D.; Clark, M.A. Cannabinoid Receptors: An Update on Cell Signaling, Pathophysiological Roles and Therapeutic Opportunities in Neurological, Cardiovascular, and Inflammatory Diseases. Int. J. Mol. Sci. 2020, 21, 7693.
- Heindel, J.J., Blumberg, B., Cave, M., Machtinger, R., Mantovani, A., Mendez, M.A., et al., 2017. Metabolism disrupting chemicals and metabolic disorders. Reprod. Toxicol. 68, 3–33.
- Heindel, J.J., vom Saal, F.S., Blumberg, B., Bovolin, P., Calamandrei, G., Ceresini, G., et al., 2015. Parma consensus statement on metabolic disruptors. Environ. Health 14, 54.
- Hempel, B.; Xi, Z.-X. Receptor Mechanisms Underlying the CNS Effects of Cannabinoids: CB1 Receptor and Beyond. Adv. Pharm. 2022, 93, 275–333. https://doi.org/10.1016/bs.apha.2021.10.006.
- Hettwer, K., Jahne, M., Frost, K., Giersberg, M., Kunze, G., Trimborn, M., et al., 2018. Validation of arxula yeast estrogen screen assay for detection of estrogenic activity in water samples: results of an international interlaboratory study. Sci. Total Environ. 621, 612–625.
- Hoffman, K., Butt, C.M., Chen, A., Limkakeng, A.T., Stapleton, H.M., 2015. High exposure to organophosphate flame retardants in infants: associations with baby products. Environ. Sci. Technol. 49, 14554–14559.
- Hovakimyan, M.; Weinreich, K.; Haas, S.J.-P.; Cattaneo, E.; Rolfs, A.; Wree, A. In Vitro Characterization of Embryionic ST14A-Cells. Int. J. Neurosci. 2008, 118, 1489–1501.
- Ikonomou, M.G., Kelly, B.C., Blair, J.D., Gobas, F.A., 2012. An interlaboratory comparison study for the determination of dialkyl

phthalate esters in environmental and biological samples. Environ. ToXicol. Chem. 31, 1948–1956.
- Indrayanto, G.; Putra, G.S.; Suhud, F. Chapter Six—Validation of in-Vitro Bioassay Methods: Application in Herbal Drug Research. In Profiles of Drug Substances, Excipients and Related Methodology; Al-Majed, A.A., Ed.; Academic Press: Cambridge, MA, USA, 2021; Volume 46, pp. 273–307.
  inflammation and Type 2 diabetes mellitus. Diabetes Res. Clin. Pract. 2013, 99, 85–92.
- Irrera, N.; D'ascola, A.; Pallio, G.; Bitto, A.; Mazzon, E.; Mannino, F.; Squadrito, V.; Arcoraci, V.; Minutoli, L.; Campo, G.M.; et al. β-Caryophyllene Mitigates Collagen Antibody Induced Arthritis (CAIA) in Mice Through a Cross-Talk between CB2 and PPAR-γ Receptors. Biomolecules 2019, 9, 326. https://doi.org/10.3390/biom9080326.
- Irrera, N.; D'ascola, A.; Pallio, G.; Bitto, A.; Mazzon, E.; Mannino, F.; Squadrito, V.; Arcoraci, V.; Minutoli, L.; Campo, G.M.; et al. β-Caryophyllene Mitigates Collagen Antibody Induced Arthritis (CAIA) in Mice Through a Cross-Talk between CB2 and PPAR-γ Receptors. Biomolecules 2019, 9, 326. https://doi.org/10.3390/biom9080326.
- Jain, M.R.; Giri, S.R.; Bhoi, B.; Trivedi, C.; Rath, A.; Rathod, R.; Ranvir, R.; Kadam, S.; Patel, H.; Swain, P.; et al. Dual PPARα/γ Agonist Saroglitazar Improves Liver Histopathology and Biochemistry in Experimental NASH Models. Liver Int. 2018, 38, 1084–1094. https://doi.org/10.1111/liv.13634.
- Jin, K.; Xie, L.; Kim, S.H.; Parmentier-Batteur, S.; Sun, Y.; Mao, X.O.; Childs, J.; Greenberg, D.A. Defective Adult Neurogenesis in CB1 Cannabinoid Receptor Knockout Mice. Mol. Pharmacol. 2004, 66, 204–208.
- Jorgačević, B.; Vučević, D.; Samardžić, J.; Mladenović, D.; Vesković, M.; Vukićević, D.; Ješić, R.; Radosavljević, T. The Effect of CB1 Antagonism on Hepatic Oxidative/Nitrosative Stress and Inflammation in Nonalcoholic Fatty Liver Disease. Curr. Med. Chem. 2021, 28, 169–180. https://doi.org/10.2174/0929867327666200303122734.
- Julien, B.; Grenard, P.; Teixeira-Clerc, F.; Van Nhieu, J.T.; Li, L.; Karsak, M.; Zimmer, A.; Mallat, A.; Lotersztajn, S. Antifibrogenic Role of the Cannabinoid Receptor CB2 in the Liver. Gastroenterology 2005, 128, 742–755. https://doi.org/10.1053/j.gastro.2004.12.050.
- Kamikubo, R.; Kai, K.; Tsuji-Naito, K.; Akagawa, M. β-Caryophyllene Attenuates Palmitate-Induced Lipid Accumulation through AMPK Signaling by Activating CB2 Receptor in Human HepG2 Hepatocytes.

Mol. Nutr. Food Res. 2016, 60, 2228–2242. https://doi.org/10.1002/mnfr.201600197.
- Kassotis, C.D., Hoffman, K., Stapleton, H.M., 2017a. Characterization of adipogenic activity of semi-volatile indoor contaminants and house dust. Environ Sci Technol In 51, 8735–8745.
- Kassotis, C.D., Kollitz, E.M., Ferguson, P.L., Stapleton, H.M., 2018. Nonionic ethoxylated surfactants induce adipogenesis in 3T3-L1 cells. Toxicol. Sci. 162, 124–136.
- Kassotis, C.D., Kollitz, E.M., Hoffman, K., Sosa, J.A., Stapleton, H.M., 2019. Thyroid receptor antagonism as a contributory mechanism for adipogenesis induced by environmental mixtures in 3T3-L1 cells. Sci. Total Environ. 666, 431–444.
- Kassotis, C.D., Masse, L., Kim, S., Schlezinger, J.J., Webster, T.F., Stapleton, H.M., 2017b. Characterization of adipogenic chemicals in three different cell culture systems: implications for reproducibility based on cell source and handling. Sci. Rep. 7, 42104.
- Kassotis, C.D., Stapleton, H.M., 2019. Endocrine-mediated mechanisms of metabolic disruption and new approaches to examine the public health threat. Front. Endocrinol. (Lausanne) 10, 39.
- Kim, N.-H.; Jegal, J.; Kim, Y.N.; Heo, J.-D.; Rho, J.-R.; Yang, M.H.; Jeong, E.J. Chokeberry Extract and Its Active Polyphenols Suppress Adipogenesis in 3T3-L1 Adipocytes and Modulates Fat Accumulation and Insulin Resistance in Diet-Induced Obese Mice. Nutrients 2018, 10, doi:10.3390/nu10111734.
- Kitamura, S., Kato, T., Iida, M., Jinno, N., Suzuki, T., Ohta, S., et al., 2005. Anti-thyroid hormonal activity of tetrabromobisphenol A, a flame retardant, and related compounds: affinity to the mammalian thyroid hormone receptor, and effect on tadpole metamorphosis. Life Sci. 76, 1589–1601.
- Kleensang, A., Vantangoli, M.M., Odwin-DaCosta, S., Andersen, M.E., Boekelheide, K., Bouhifd, M., et al., 2016. Genetic variability in a frozen batch of MCF-7 cells invisible in routine authentication affecting cell function. Sci. Rep. 6, 28994.
- Lange, C.; Mix, E.; Rateitschak, K.; Rolfs, A. Wnt Signal Pathways and Neural Stem Cell Differentiation. Neurodegener. Dis. 2006, 3, 76–86.
- le Maire, A., Grimaldi, M., Roecklin, D., Dagnino, S., Vivat-Hannah, V., Balaguer, P., et al., 2009. Activation of RXR-PPAR heterodimers by organotin environmental endocrine disruptors. EMBO Rep. 10, 367–373.
- Legler, J., Zalko, D., Jourdan, F., Jacobs, M., Fromenty, B., Balaguer, P., et al., 2020. The GOLIATH project: towards an internationally harmonised

approach for testing metabolism disrupting compounds. Int. J. Mol. Sci. 21.
- Lehmann, J.M., Moore, L.B., Smith-Oliver, T.A., Wilkison, W.O., Willson, T.M., Kliewer, S.A., 1995. An antidiabetic thiazolidinedione is a high affinity ligand for peroxisome proliferator-activated receptor γ (PPARγ). J. Biol. Chem. 270, 12953–12956.
- Li, X., Ycaza, J., Blumberg, B., 2011. The environmental obesogen tributyltin chloride acts via peroxisome proliferator activated receptor gamma to induce adipogenesis in murine 3T3-L1 preadipocytes. J. Steroid Biochem. Mol. Biol. 127, 9–15.
- Liu, L.Y.; Alexa, K.; Cortes, M.; Schatzman-Bone, S.; Kim, A.J.; Mukhopadhyay, B.; Cinar, R.; Kunos, G.; North, T.E.; Goessling, W. Cannabinoid Receptor Signaling Regulates Liver Development and Metabolism. Development 2016, 143, 609–622. https://doi.org/10.1242/dev.121731.
- Lowe, H.; Toyang, N.; Steele, B.; Bryant, J.; Ngwa, W. The Endocannabinoid System: A Potential Target for the Treatment of Various Diseases. Int. J. Mol. Sci. 2021, 22, 9472. https://doi.org/10.3390/ijms22179472.
- Lowe, H.; Toyang, N.; Steele, B.; Bryant, J.; Ngwa, W. The Endocannabinoid System: A Potential Target for the Treatment of Various Diseases. Int. J. Mol. Sci. 2021, 22, 9472. https://doi.org/10.3390/ijms22179472.
- Lu, H.; Guo, R.; Zhang, Y.; Su, S.; Zhao, Q.; Yu, Y.; Shi, H.; Sun, H.; Zhang, Y.; Li, S.; et al. Inhibition of LncRNA TCONS_00077866 Ameliorates the High Stearic Acid Diet-Induced Mouse Pancreatic β-Cell Inflammatory Response by Increasing MiR-297b-5p to Downregulate SAA3 Expression. Diabetes 2021, 70, 2275–2288. https://doi.org/10.2337/db20-1079.
- Lu, H.-C.; Mackie, K. Review of the Endocannabinoid System. Biol. Psychiatry Cogn. Neurosci. Neuroimaging 2020.
- Lutz, B. Neurobiology of cannabinoid receptor signaling. Dialog Clin. Neurosci. 2020, 22, 207–222.
- Luz, A.L., Kassotis, C.D., Stapleton, H.M., Meyer, J.N., 2018. The high-production volume fungicide pyraclostrobin induces triglyceride accumulation associated with mitochondrial dysfunction, and promotes adipocyte differentiation independent of ppargamma activation, in 3T3-L1 cells. Toxicology 393, 150–159.
- M.Weiss, J., Ivd, Veen, Boer, J., SPJv, Leeuwen, Cofino, W., Crum, S., 2013. Analytical improvements shown over four interlaboratory studies

of perfluoroalkyl substances in environmental and food samples. Trac Trends Anal. Chem. 43, 204–216.
- Ma, Z.-G.; Yuan, Y.-P.; Zhang, X.; Xu, S.-C.; Wang, S.-S.; Tang, Q.-Z. Piperine Attenuates Pathological Cardiac Fibrosis Via PPAR-γ/AKT Pathways. EBioMedicine 2017, 18, 179–187. https://doi.org/10.1016/j.ebiom.2017.03.021.
- Maccarrone, M. In vitro and in vivo models of Huntington's disease show alterations in the endocannabinoid system. FEBS J. 2013, 280, 3376–3388.
- Machado, K.d.C.; Islam, M.T.; Ali, E.S.; Rouf, R.; Uddin, S.J.; Dev, S.; Shilpi, J.A.; Shill, M.C.; Reza, H.M.; Das, A.K.; et al. A Systematic Review on the Neuroprotective Perspectives of Beta-Caryophyllene; John Wiley and Sons Ltd.: Hoboken , NJ, USA, 2018; Volume 32.
- Maffei, M.E. Plant Natural Sources of the Endocannabinoid (E)-β-Caryophyllene: A Systematic Quantitative Analysis of Published Literature. Int. J. Mol. Sci. 2020, 21, 6540. https://doi.org/10.3390/ijms21186540.
- Mannino, F.; Pallio, G.; Corsaro, R.; Minutoli, L.; Altavilla, D.; Vermiglio, G.; Allegra, A.; Eid, A.H.; Bitto, A.; Squadrito, F.; et al. Beta-Caryophyllene Exhibits Anti-Proliferative Effects through Apoptosis Induction and Cell Cycle Modulation in Multiple Myeloma Cells. Cancers 2021, 13, 5741. https://doi.org/10.3390/cancers13225741.
- Mannino, F.; Pallio, G.; Corsaro, R.; Minutoli, L.; Altavilla, D.; Vermiglio, G.; Allegra, A.; Eid, A.H.; Bitto, A.; Squadrito, F.; et al. Beta-Caryophyllene Exhibits Anti-Proliferative Effects through Apoptosis Induction and Cell Cycle Modulation in Multiple Myeloma Cells. Cancers 2021, 13, 5741. https://doi.org/10.3390/cancers13225741.
- Mantovani, A.; Dalbeni, A. Treatments for NAFLD: State of Art. Int. J. Mol. Sci. 2021, 22, 2350. https://doi.org/10.3390/ijms22052350.
- Masuno, H., Iwanami, J., Kidani, T., Sakayama, K., Honda, K., 2005. Bisphenol A accelerates terminal differentiation of 3T3-L1 cells into adipocytes through the phosphatidylinositol 3-kinase pathway. Toxicol. Sci. 84, 319–327.
- Masuno, H., Kidani, T., Sekiya, K., Sakayama, K., Shiosaka, T., Yamamoto, T., et al., 2002. Bisphenol A in combination with insulin can accelerate the conversion of 3T3- L1 fibroblasts to adipocytes. J. Lipid Res. 43, 676–684.
- Mboumba Bouassa, R.-S.; Sebastiani, G.; Di Marzo, V.; Jenabian, M.-A.; Costiniuk, C.T. Cannabinoids and Chronic Liver Diseases. Int. J. Mol. Sci. 2022, 23, 9423. https://doi.org/10.3390/ijms23169423.

- Mechoulam, R.; Gaoni, Y. A Total Synthesis of dl-Δ1-Tetrahydrocannabinol, the Active Constituent of Hashish1. J. Am. Chem. Soc.
- Meeran, M.F.N.; Al Taee, H.; Azimullah, S.; Tariq, S.; Adeghate, E.; Ojha, S. β-Caryophyllene, a Natural Bicyclic Sesquiterpene Attenuates Doxorubicin-Induced Chronic Cardiotoxicity via Activation of Myocardial Cannabinoid Type-2 (CB2) Receptors in Rats. Chem.-Biol. Interact. 2019, 304, 158–167, doi:10.1016/j.cbi.2019.02.028.
- Meerts, I.A., van Zanden, J.J., Luijks, E.A., van Leeuwen-Bol, I., Marsh, G., Jakobsson, E., et al., 2000. Potent competitive interactions of some brominated flame retardants and related compounds with human transthyretin in vitro. Toxicol. Sci. 56, 95–104.
- Mehinto, A.C., Jia, A., Snyder, S.A., Jayasinghe, B.S., Denslow, N.D., Crago, J., et al., 2015. Interlaboratory comparison of in vitro bioassays for screening of endocrine active chemicals in recycled water. Water Res. 83, 303–309.
- Mehra, A., Macdonald, I., Pillay, T.S., 2007. Variability in 3T3-L1 adipocyte differentiation depending on cell culture dish. Anal. Biochem. 362, 281–283.
- Melymuk, L., Diamond, M.L., Riddell, N., Wan, Y., Vojta, S., Chittim, B., 2018. Challenges in the analysis of novel flame retardants in indoor dust: results of the INTERFLAB 2 interlaboratory evaluation. Environ. Sci. Technol. 52, 9295–9303.
- Melymuk, L., Goosey, E., Riddell, N., Diamond, M.L., 2015. Interlaboratory study of novel halogenated flame retardants: INTERFLAB. Anal. Bioanal. Chem. 407, 6759–6769.
- Mendez-Sanchez, N.; Zamora-Valdes, D.; Pichardo-Bahena, R.; Barredo-Prieto, B.; Ponciano-Rodriguez, G.; Bermejo-Martínez, L.; Chavez-Tapia, N.C.; Baptista-González, H.A.; Uribe, M. Endocannabinoid Receptor CB2 in Nonalcoholic Fatty Liver Disease. Liver Int. 2007, 27, 215–219. https://doi.org/10.1111/j.1478-3231.2006.01401.x.
- Mlost, J.; Wąsik, A.; Starowicz, K. Role of Endocannabinoid System in Dopamine Signalling within the Reward Circuits Affected by Chronic Pain. Pharmacol. Res. 2019, 143, 40–47. https://doi.org/10.1016/j.phrs.2019.02.029.
- Mödinger, Y.; Knaub, K.; Dharsono, T.; Wacker, R.; Meyrat, R.; Land, M.H.; Petraglia, A.L.; Schön, C. Enhanced Oral Bioavailability of β-Caryophyllene in Healthy Subjects Using the VESIsorb® Formulation Technology, a Novel Self-Emulsifying Drug Delivery System (SEDDS).

Molecules 2022, 27, 2860. https://doi.org/10.3390/molecules27092860.
- Molina-Holgado, F.; Rubio-Araiz, A.; García-Ovejero, D.; Williams, R.J.; Moore, J.D.; Arévalo-Martín, Á.; Gómez-Torres, O. CB2 cannabinoid receptors promote mouse neural stem cell proliferation. Eur. J. Neurosci. 2007, 25, 629–634.
- Montagner, A.; Polizzi, A.; Fouché, E.; Ducheix, S.; Lippi, Y.; Lasserre, F.; Barquissau, V.; Régnier, M.; Lukowicz, C.; Benhamed, F.; et al. Liver PPARα Is Crucial for Whole-Body Fatty Acid Homeostasis and Is Protective against NAFLD. Gut 2016, 65, 1202–1214. https://doi.org/10.1136/gutjnl-2015-310798.
- Morgan, B.J.; Chai, S.Y.; Albiston, A.L. GLUT4 Associated Proteins as Therapeutic Targets for Diabetes. Recent. Pat. Endocr. Metab. Immune. Drug Discov. 2011, 5, 25–32.
- Niemel¨a, S., Miettinen, S., Sarkanen, J.R., Ashammakhi, N., 2008. Adipose tissue and adipocyte differentiation: molecular and cellular aspects and tissue engineering applications. In: Topics in tissue engineering, Vol. 4, 1–26.
- Nuutinen, T. Medicinal Properties of Terpenes Found in Cannabis Sativa and Humulus Lupulus. Eur. J. Med. Chem. 2018, 157, 198–228, doi:10.1016/j.ejmech.2018.07.076.
- Oddi, S.; Scipioni, L.; Maccarrone, M. Endocannabinoid system and adult neurogenesis: A focused review. Curr. Opin. Pharmacol. 2020, 50, 25–32.
- Orton, F., Rosivatz, E., Scholze, M., Kortenkamp, A., 2011. Widely used pesticides with previously unknown endocrine activity revealed as in vitro anti-androgens. Environ. Health Perspect. 119, 794–800.
- Oudin, M.J.; Gajendra, S.; Williams, G.; Hobbs, C.; Lalli, G.; Doherty, P. Endocannabinoids Regulate the Migration of Subventricular Zone-Derived Neuroblasts in the Postnatal Brain. J. Neurosci. 2011, 31, 4000–4011.
- Palazuelos, J.; Aguado, T.; Egia, A.; Mechoulam, R.; Guzmán, M.; Galve-Roperh, I. Non-psychoactive CB 2 cannabinoid agonists stimulate neural progenitor proliferation. FASEB J. 2006, 20, 2405–2407.
- Palazuelos, J.; Ortega, Z.; Díaz-Alonso, J.; Guzmán, M.; Galve-Roperh, I. CB2 Cannabinoid Receptors Promote Neural Progenitor Cell Proliferation via mTORC1 Signaling. J. Biol. Chem. 2012, 287, 1198–1209.
- Penza, M., Jeremic, M., Marrazzo, E., Maggi, A., Ciana, P., Rando, G., et al., 2011. The environmental chemical tributyltin chloride (TBT) shows

both estrogenic and adipogenic activities in mice which might depend on the exposure dose. Toxicol. Appl. Pharmacol. 255, 65–75.
- Pereira-Fernandes, A., Vanparys, C., Hectors, T.L., Vergauwen, L., Knapen, D., Jorens, P. G., et al., 2013. Unraveling the mode of action of an obesogen: mechanistic analysis of the model obesogen tributyltin in the 3T3-L1 cell line. Mol. Cell. Endocrinol. 370, 52–64.
- Pertwee, R.G. Endocannabinoids and their pharmacological actions. In Endocannabinoids; Pertwee, R.G., Ed.; Springer: Berlin, Germany, 2015; Volume 231, pp. 1–37.
- Picciolo, G.; Pallio, G.; Altavilla, D.; Vaccaro, M.; Oteri, G.; Irrera, N.; Squadrito, F. β-Caryophyllene Reduces the Inflammatory Phenotype of Periodontal Cells by Targeting CB2 Receptors. Biomedicines 2020, 8, 164. https://doi.org/10.3390/BIOMEDICINES8060164.
- Picciolo, G.; Pallio, G.; Altavilla, D.; Vaccaro, M.; Oteri, G.; Irrera, N.; Squadrito, F. β-Caryophyllene Reduces the Inflammatory Phenotype of Periodontal Cells by Targeting CB2 Receptors. Biomedicines 2020, 8, 164. https://doi.org/10.3390/BIOMEDICINES8060164.
- Pomatto, V.; Cottone, E.; Cocci, P.; Mozzicafreddo, M.; Mosconi, G.; Nelson, E.R.; Palermo, F.A.; Bovolin, P. Plasticizers Used in Food-Contact Materials Affect Adipogenesis in 3T3-L1 Cells. J. Steroid Biochem. Mol. Biol. 2018, 178, 322–332, doi:10.1016/j.jsbmb.2018.01.014.
- Powell, E.E.; Wong, V.W.-S.; Rinella, M. Non-Alcoholic Fatty Liver Disease. Lancet 2021, 397, 2212–2224. https://doi.org/10.1016/S0140-6736(20)32511-3.
- Pregno, G.; Zamburlin, P.; Gambarotta, G.; Farcito, S.; Licheri, V.; Fregnan, F.; Perroteau, I.; Lovisolo, D.; Bovolin, P. Neuregulin1/ErbB4-induced migration in ST14A striatal progenitors: Calcium-dependent mechanisms and modulation by NMDA receptor activation. BMC Neurosci. 2011, 12, 103.
- Reilly, M.P.; Rader, D.J. The Metabolic Syndrome. Circulation 2003, 108, 1546–1551, doi:10.1161/01.CIR.0000088846.10655.E0.
- Rigamonti, D.; Bauer, J.H.; De-Fraja, C.; Conti, L.; Sipione, S.; Sciorati, C.; Clementi, E.; Hackam, A.; Hayden, M.R.; Li, Y.; et al. Wild-Type Huntingtin Protects from Apoptosis Upstream of Caspase-3. J. Neurosci. 2000, 20, 3705–3713.
- Rivera, P.; Vargas, A.; Pastor, A.; Boronat, A.; López-Gambero, A.J.; Sánchez-Marín, L.; Medina-Vera, D.; Serrano, A.; Pavón, F.J.; de la Torre, R.; et al. Differential Hepatoprotective Role of the Cannabinoid CB1 and CB2 Receptors in Paracetamol-Induced Liver Injury. Br. J. Pharmacol. 2020, 177, 3309–3326. https://doi.org/10.1111/bph.15051.

- Rochester, J.R., 2013. Bisphenol a and human health: a review of the literature. Reprod. Toxicol. 42, 132–155. C.
- Rochlani Y, Pothineni NV, Kovelamudi S, Mehta JL. Metabolic syndrome: pathophysiology, management, and modulation by natural compounds. Ther Adv Cardiovasc Dis. 2017 Aug;11(8):215-225. doi: 10.1177/1753944717711379.
- Rosen, E.D., Sarraf, P., Troy, A.E., Bradwin, G., Moore, K., Milstone, D.S., et al., 1999. PPAR gamma is required for the differentiation of adipose tissue in vivo and in vitro. Mol. Cell 4, 611–617.
- Rozenfeld, R. Type I Cannabinoid Receptor Trafficking: All Roads Lead to Lysosome. Traffic 2010, 12, 12–18.
- Ruiz, D., Becerra, M., Jagai, J.S., Ard, K., Sargis, R.M., 2018. Disparities in environmental exposures to endocrine-disrupting chemicals and diabetes risk in vulnerable populations. Diabetes Care 41, 193–205.
- Saba, J.; Couselo, F.L.; Turati, J.; Carniglia, L.; Durand, D.; De Laurentiis, A.; Lasaga, M.; Caruso, C. Astrocytes from cortex and striatum show differential responses to mitochondrial toxin and BDNF: Implications for protection of striatal neurons expressing mutant huntingtin. J. Neuroinflam. 2020, 17, 1–15.
- Santos, P.S.; Oliveira, T.C.; Júnior, L.M.R.; Figueiras, A.; Nunes, L.C.C. β-Caryophyllene Delivery Systems: Enhancing the Oral Pharmacokinetic and Stability. Curr. Pharm. Des. 2018, 24, 3440–3453. https://doi.org/10.2174/1381612824666180912151412.
- Saraswathi, V.; Kumar, N.; Ai, W.; Gopal, T.; Bhatt, S.; Harris, E.N.; Talmon, G.A.; Desouza, C.V. Myristic Acid Supplementation Aggravates High Fat Diet-Induced Adipose Inflammation and Systemic Insulin Resistance in Mice. Biomolecules 2022, 12, 739. https://doi.org/10.3390/biom12060739.
- Sargis, R.M., Johnson, D.N., Choudhury, R.A., Brady, M.J., 2010. Environmental endocrine disruptors promote adipogenesis in the 3T3-L1 cell line through glucocorticoid receptor activation. Obesity Silver Spring (Silver Spring) 18, 1283–1288.
- Scandiffio, R.; Geddo, F.; Cottone, E.; Querio, G.; Antoniotti, S.; Gallo, M.P.; Maffei, M.E.; Bovolin, P. Protective Effects of (E)-β-Caryophyllene (BCP) in Chronic Inflammation. Nutrients 2020, 12, 3273. https://doi.org/10.3390/nu12113273.
- Scandiffio, R.; Geddo, F.; Cottone, E.; Querio, G.; Antoniotti, S.; Gallo, M.P.; Maffei, M.E.; Bovolin, P. Protective Effects of (E)-β-Caryophyllene (BCP) in Chronic Inflammation. Nutrients 2020, 12, 3273. https://doi.org/10.3390/nu12113273.

- Seimandi, M., Lemaire, G., Pillon, A., Perrin, A., Carlavan, I., Voegel, J.J., et al., 2005. Differential responses of PPARalpha, PPARdelta, and PPARgamma reporter cell lines to selective PPAR synthetic ligands. Anal. Biochem. 344, 8–15.
- Shahbazi, F.; Grandi, V.; Banerjee, A.; Trant, J.F. Cannabinoids and Cannabinoid Receptors: The Story so Far. iScience 2020.
- Sharma, C.; Al Kaabi, J.M.; Nurulain, S.M.; Goyal, S.N.; Kamal, M.A.; Ojha, S. Polypharmacological Properties and Therapeutic Potential of β-Caryophyllene: A Dietary Phytocannabinoid of Pharmaceutical Promise. Curr. Pharm. Des. 2016, 22, 3237–3264, doi:10.2174/1381612822666160311115226.
- Shen, O., Du, G., Sun, H., Wu, W., Jiang, Y., Song, L., et al., 2009. Comparison of in vitro hormone activities of selected phthalates using reporter gene assays. ToXicol. Lett. 191, 9–14.
- Shoemaker, J.L.; Ruckle, M.B.; Mayeux, P.R.; Prather, P.L. Agonist-Directed Trafficking of Response by Endocannabinoids Acting at CB2 Receptors. J. Pharmacol. Exp. Ther. 2005, 315, 828–838.
- Silva Figueiredo, P.; Inada, A.C.; Ribeiro Fernandes, M.; Granja Arakaki, D.; Freitas, K.D.C.; Avellaneda Guimarães, R.D.C.; Aragão do Nascimento, V.; Aiko Hiane, P. An Overview of Novel Dietary Supplements and Food Ingredients in Patients with Metabolic Syndrome and Non-Alcoholic Fatty Liver Disease. Molecules 2018, 23, 877, doi:10.3390/molecules23040877.
- Simão, J.J.; Cruz, M.M.; Abdala, F.M.; Bolsoni-Lopes, A.; Armelin-Correa, L.; Alonso-Vale, M.I.C. Palmitoleic Acid Acts on Adipose-Derived Stromal Cells and Promotes Anti-Hypertrophic and Anti-Inflammatory Effects in Obese Mice. Pharmaceuticals 2022, 15, 1194. https://doi.org/10.3390/ph15101194.
- Singh, M.K.; Yadav, R.; Bhaskar, A.K.; Sengupta, S.; Sachidanandan, C. A Diet-Independent Zebrafish Model for NAFLD Recapitulates Patient Lipid Profiles and Offers a System for Small Molecule Screening. Biochim. et Biophys. Acta (BBA)—Mol. Cell. Biol. Lipids 2023, 1868, 159246. https://doi.org/10.1016/j.bbalip.2022.159246.
- Soldati, C.; Biagioni, S.; Poiana, G.; Augusti-Tocco, G. β-Catenin and actin reorganization in HGF/SF response of ST14A cells. J. Neurosci. Res. 2008, 86, 1044–1052.
- Somm, E., Schwitzgebel, V.M., Toulotte, A., Cederroth, C.R., Combescure, C., Nef, S., et al., 2009. Perinatal exposure to bisphenol A alters early adipogenesis in the rat. Environ. Health Perspect. 117, 1549–1555.

- Songtrai, S.; Pratchayasakul, W.; Arunsak, B.; Chunchai, T.; Kongkaew, A.; Chattipakorn, N.; Chattipakorn, S.C.; Kaewsuwan, S. Cyclosorus Terminans Extract Ameliorates Insulin Resistance and Non-Alcoholic Fatty Liver Disease (NAFLD) in High-Fat Diet (HFD)-Induced Obese Rats. Nutrients 2022, 14, 4895. https://doi.org/10.3390/nu14224895.
- Spiegelman, B.M., 1998. Ppar-gamma: adipogenic regulator and thiazolidinedione receptor. Diabetes 47, 507–514.
- Stapleton, H.M., Klosterhaus, S., Eagle, S., Fuh, J., Meeker, J.D., Blum, A., et al., 2009. Detection of organophosphate flame retardants in furniture foam and U.S. House dust. Environ. Sci. Technol. 43, 7490–7495.
- Stapleton, H.M., Klosterhaus, S., Keller, A., Ferguson, P.L., van Bergen, S., Cooper, E., et al., 2011. Identification of flame retardants in polyurethane foam collected from baby products. Environ. Sci. Technol. 45, 5323–5331.
- Suijun, W.; Zhen, Y.; Ying, G.; Yanfang, W. A Role for Trans-Caryophyllene in the Moderation of Insulin Secretion. Biochem. Biophys. Res. Commun. 2014, 444, 451–454, doi:10.1016/j.bbrc.2013.11.136.
- Takeuchi, S., Iida, M., Kobayashi, S., Jin, K., Matsuda, T., Kojima, H., 2005. Differential effects of phthalate esters on transcriptional activities via human estrogen receptors alpha and beta, and androgen receptor. ToXicology 210, 223–233.
- Takooree, H.; Aumeeruddy, M.Z.; Rengasamy, K.R.R.; Venugopala, K.N.; Jeewon, R.; Zengin, G.; Mahomoodally, M.F.A. Systematic Review on Black Pepper (Piper Nigrum L.): From Folk Uses to Pharmacological Applications. Crit. Rev. Food Sci. Nutr. 2019, 59, S210–S243, doi:10.1080/10408398.2019.1565489.
- Taxvig, C., Dreisig, K., Boberg, J., Nellemann, C., Schelde, A.B., Pedersen, D., et al., 2012. Differential effects of environmental chemicals and food contaminants on adipogenesis, biomarker release and PPARgamma activation. Mol. Cell. Endocrinol.361, 106–115.
- Temkin, A.M., Bowers, R.R., Magaletta, M.E., Holshouser, S., Maggi, A., Ciana, P., et al., 2016. Effects of crude oil/dispersant miXture and dispersant components on PPARgamma activity and : identification of dioctyl sodium sulfosuccinate (DOSS; CAS #577-11-7) as a probable obesogen. Environ. Health Perspect. 124, 112–119.
- Trasande, L., Attina, T.M., Blustein, J., 2012. Association between urinary bisphenol A concentration and obesity prevalence in children and adolescents. JAMA 308, 9.
- Viveros-Paredes, J.M.; González-Castañeda, R.E.; Gertsch, J.; Chaparro-Huerta, V.; López-Roa, R.I.; Vázquez-Valls, E.; Beas-Zarate, C.; Camins-

Espuny, A.; Flores-Soto, M.E. Neuroprotective Effects of β-Caryophyllene against Dopaminergic Neuron Injury in a Murine Model of Parkinson's Disease Induced by MPTP. Pharmaceuticals 2017, 10, 60, doi:10.3390/ph10030060.

- Voet, Hd, JAHv, Rhijn, HJvd, Wiel, 1999. Inter-laboratory, time, and fitness-for-purpose aspects of effective validation. Anal. Chim. Acta 391, 159–171.
- vom Saal, F.S., Akingbemi, B.T., Belcher, S.M., Birnbaum, L.S., Crain, D.A., Eriksen, M., et al., 2007. Chapel Hill bisphenol A expert panel consensus statement: integration of mechanisms, effects in animals and potential to impact human health at current levels of exposure. Reprod. ToXicol. 24, 131–138.
- Vom Saal, F.S., Nagel, S.C., Coe, B.L., Angle, B.M., Taylor, J.A., 2012. The estrogenic endocrine disrupting chemical bisphenol A (BPA) and obesity. Mol. Cell. Endocrinol. 354, 74–84.
- Wang, Y.; Nakajima, T.; Gonzalez, F.J.; Tanaka, N. PPARs as Metabolic Regulators in the Liver: Lessons from Liver-Specific PPAR-Null Mice. Int. J. Mol. Sci. 2020, 21, 2061. https://doi.org/10.3390/ijms21062061.
- Wang, Y.; Zhang, X.; Yuan, B.; Lu, X.; Zheng, D.; Zhang, K.; Zhong, M.; Xu, X.; Duan, X. GVS-12 Attenuates Non-Alcoholic Steatohepatitis by Suppressing Inflammatory Responses via PPARγ/STAT3 Signaling Pathways. RSC Adv. 2019, 9, 9555–9564. https://doi.org/10.1039/C8RA10178G.
- Welshons, W.V., Nagel, S.C., vom Saal, F.S., 2006. Large effects from small exposures. III. Endocrine mechanisms mediating effects of bisphenol A at levels of human exposure. Endocrinology 147, S56–69.
- Wong, J., Hao, C., Zhang, K., Yang, P., Banerjee, K., Hayward, D., et al., 2010. Development and interlaboratory validation of a QuEChERS-based liquid chromatography-tandem mass spectrometry method for multiresidue pesticide analysis. J. Agric. Food Chem. 58, 5897–5903.
- Wu, C.; Jia, Y.; Lee, J.H.; Jun, H.-J.; Lee, H.-S.; Hwang, K.-Y.; Lee, S.-J. Trans-Caryophyllene Is a Natural Agonistic Ligand for Peroxisome Proliferator-Activated Receptor-α. Bioorganic Med. Chem. Lett. 2014, 24, 3168–3174, doi:10.1016/j.bmcl.2014.04.112.
- Wu, C.; Jia, Y.; Lee, J.H.; Jun, H.J.; Lee, H.S.; Hwang, K.Y.; Lee, S.J. Trans-Caryophyllene Is a Natural Agonistic Ligand for Peroxisome Proliferator-Activated Receptor-α. Bioorganic Med. Chem. Lett. 2014, 24, 3168–3174. https://doi.org/10.1016/j.bmcl.2014.04.112.

- Wu, L.; Guo, C.; Wu, J. Therapeutic Potential of PPARγ Natural Agonists in Liver Diseases. J. Cell. Mol. Med. 2020, 24, 2736–2748. https://doi.org/10.1111/jcmm.15028.
- Yamaguchi, M.; Levy, R.M. β-Caryophyllene Promotes Osteoblastic Mineralization, and Suppresses Osteoclastogenesis and Adipogenesis in Mouse Bone Marrow Cultures in Vitro. Exp. Ther. Med. 2016, 12, 3602–3606, doi: 10.3892/etm.2016.3818.
- Yang, M.; Lv, Y.; Tian, X.; Lou, J.; An, R.; Zhang, Q.; Li, M.; Xu, L.; Dong, Z. Neuroprotective Effect of β-Caryophyllene on Cerebral Ischemia-Reperfusion Injury via Regulation of Necroptotic Neuronal Death and Inflammation: In Vivo and in Vitro. Front. Neurosci. 2017, 11, doi:10.3389/fnins.2017.00583.
- Younis, N.S.; Mohamed, M.E. β-Caryophyllene as a Potential Protective Agent Against Myocardial Injury: The Role of Toll-Like Receptors. Molecules 2019, 24, 1929, doi:10.3390/molecules24101929.
- Youssef, D.A.; El-Fayoumi, H.M.; Mahmoud, M.F. Beta-Caryophyllene Protects against Diet-Induced Dyslipidemia and Vascular Inflammation in Rats: Involvement of CB2 and PPAR-γ Receptors. Chem.-Biol. Interact. 2019, 297, 16–24, doi:10.1016/j.cbi.2018.10.010.
- Youssef, D.A.; El-Fayoumi, H.M.; Mahmoud, M.F. Beta-Caryophyllene Alleviates Diet-Induced Neurobehavioral Changes in Rats: The Role of CB2 and PPAR-γ Receptors. Biomed. Pharmacother. 2019, 110, 145–15, doi:10.1016/j.biopha.2018.11.039.
- Youssef, D.A.; El-Fayoumi, H.M.; Mahmoud, M.F. Beta-Caryophyllene Protects against Diet-Induced Dyslipidemia and Vascular Inflammation in Rats: Involvement of CB2 and PPAR-γ Receptors. Chem. -Biol. Interact. 2019, 297, 16–24. https://doi.org/10.1016/j.cbi.2018.10.010.
- Yovas, A.; Manjusha, W.A.; Ponnian, S.M.P. β-Caryophyllene Modulates B-Cell Lymphoma Gene-2 Family Genes and Inhibits the Intrinsic Pathway of Apoptosis in Isoproterenol-Induced Myocardial Infarcted Rats; A Molecular Mechanism. Eur. J. Pharmacol. 2022, 932, 175181. https://doi.org/10.1016/j.ejphar.2022.175181.
- Yovas, A.; Manjusha, W.A.; Ponnian, S.M.P. β-Caryophyllene Modulates B-Cell Lymphoma Gene-2 Family Genes and Inhibits the Intrinsic Pathway of Apoptosis in Isoproterenol-Induced Myocardial Infarcted Rats; A Molecular Mechanism. Eur. J. Pharmacol. 2022, 932, 175181. https://doi.org/10.1016/j.ejphar.2022.175181.
- Yu, S.; Matsusue, K.; Kashireddy, P.; Cao, W.-Q.; Yeldandi, V.; Yeldandi, A.V.; Rao, M.S.; Gonzalez, F.J.; Reddy, J.K. Adipocyte-Specific Gene Expression and Adipogenic Steatosis in the Mouse Liver Due to

Peroxisome Proliferator-Activated Receptor Gamma1 (PPARgamma1) Overexpression. J. Biol. Chem. 2003, 278, 498–505. https://doi.org/10.1074/jbc.M210062200.

- Zava, D.T., Wyler-von Ballmoos, A., Goldhirsch, A., Roos, W., Takahashi, A., Eppenberger, U., et al., 1982. A quality control study to assess the inter-laboratory variability of routine estrogen and progesterone receptor assays. Eur. J. Cancer Clin. Oncol. 18, 713–721.
- Zebisch, K., Voigt, V., Wabitsch, M., Brandsch, M., 2012. Protocol for effective differentiation of 3T3-L1 cells to adipocytes. Anal. Biochem. 425, 88–90.
- Zenbio Inc, 2015. 3T3-L1 Cell Care Manual - Maintenance and Differentiation of Preadipocytes to Adipocytes. Available: http://www.zen-bio.com/pdf/ ZBM0009.013T3L1CareprotocolRV08.08.pdf [accessed 30 September 2015.
- Zhao, Y., Zhang, K., Giesy, J.P., Hu, J., 2015. Families of nuclear receptors in vertebrate models: characteristic and comparative toxicological perspective. Sci. Rep. 5, 8554.
- Zhu, X.; Bian, H.; Wang, L.; Sun, X.; Xu, X.; Yan, H.; Xia, M.; Chang, X.; Lu, Y.; Li, Y.; et al. Berberine Attenuates Nonalcoholic Hepatic Steatosis through the AMPK-SREBP-1c-SCD1 Pathway. Free. Radic. Biol. Med. 2019, 41, 192–204. https://doi.org/10.1016/j.freeradbiomed.2019.06.019.

Published results

nutrients

MDPI

Review

Protective Effects of (*E*)-β-Caryophyllene (BCP) in Chronic Inflammation

Rosaria Scandiffio [1,2], Federica Geddo [1], Erika Cottone [1], Giulia Querio [1], Susanna Antoniotti [1], Maria Pia Gallo [1], Massimo E. Maffei [2] and Patrizia Bovolin [1,*]

[1] Department of Life Sciences and Systems Biology, University of Turin, Via Accademia Albertina 13, 10123 Turin, Italy; rosaria.scandiffio@unito.it (R.S.); federica.geddo@unito.it (F.G.); erika.cottone@unito.it (E.C.); giulia.querio@unito.it (G.Q.); susanna.antoniotti@unito.it (S.A.); mariapia.gallo@unito.it (M.P.G.)

[2] Plant Physiology Unit, Department of Life Sciences and Systems Biology, University of Turin, Via Quarello 15/a, 10135 Turin, Italy; massimo.maffei@unito.it

* Correspondence: patrizia.bovolin@unito.it

Received: 30 September 2020; Accepted: 21 October 2020; Published: 26 October 2020

Abstract: (*E*)-β-caryophyllene (BCP) is a bicyclic sesquiterpene widely distributed in the plant kingdom, where it contributes a unique aroma to essential oils and has a pivotal role in the survival and evolution of higher plants. Recent studies provided evidence for protective roles of BCP in animal cells, highlighting its possible use as a novel therapeutic tool. Experimental results show the ability of BCP to reduce pro-inflammatory mediators such as tumor necrosis factor-alfa (TNF-α), interleukin-1β (IL-1β), interleukin-6 (IL-6), nuclear factor kappa-light-chain-enhancer of activated B cells (NF-κB), thus ameliorating chronic pathologies characterized by inflammation and oxidative stress, in particular metabolic and neurological diseases. Through the binding to CB2 cannabinoid receptors and the interaction with members of the family of peroxisome proliferator-activated receptors (PPARs), BCP shows beneficial effects on obesity, non-alcoholic fatty liver disease/nonalcoholic steatohepatitis (NAFLD/NASH) liver diseases, diabetes, cardiovascular diseases, pain and other nervous system disorders. This review describes the current knowledge on the biosynthesis and natural sources of BCP, and reviews its role and mechanisms of action in different inflammation-related metabolic and neurologic disorders.

Keywords: (*E*)-β-caryophyllene; biosynthesis and distribution; inflammation; metabolic disorders; obesity; steatosis; type II diabetes; cardiovascular disorders; pain; neurodegenerative diseases

1. Introduction

The scientific interest for natural compounds as novel potential drugs has increased exponentially in the last few years, along with the number of trials and studies on nutraceuticals and herbal extracts, aimed to test their effects on many disorders, including obesity, type II diabetes (T2D), cardiovascular disease (CVD), NAFLD and also cancer [1–4].

The sesquiterpene hydrocarbon (*E*)-β-caryophyllene (BCP) is one of the most studied and promising natural compounds [5–10]. In recent years, modulatory and pharmacological effects of BCP have been demonstrated in numerous organs such as liver [11], kidney [12] and brain [13]. BCP has been reported to exert therapeutic effects as antioxidant [11], anti-inflammatory [14] and anticancer [12,15]. Importantly, BCP has been identified as a fully selective agonist of CB2 cannabinoid receptors [16], one of the key members of the endocannabinoid system (ECS). The ECS is an endogenous system exerting regulatory control on food intake, metabolism and storage of calories and for this reason it represents a potential pharmacotherapeutic target for a wide range of metabolic disorders such

as obesity, dyslipidemia, steatosis, diabetes and eating disorders [17]. The ECS is also involved in the regulation of inflammation [18] and in the modulation of depression, schizophrenia and chronic pain [6,19–21]. The selectivity of BCP for CB2 receptors avoids potential psychotropic effects mediated by brain CB1 cannabinoid receptor, being CB2 receptors mainly expressed in peripheral tissues and in central nervous system (CNS) immune cells [5,16]. Apart from CB2 receptors, BCP has been recently demonstrated to interact with members of the family of peroxisome proliferator-activated receptors (PPARs), in particular PPARα and γ, transcriptional factors belonging to the ligand-activated nuclear receptor superfamily [10,22,23].

This review will first present the molecular features, biosynthesis and distribution of BCP in plants, followed by current information on the molecular targets of BCP in animal cells. Finally, the beneficial effects of BCP on human health will be discussed; since many of them have been already extensively reviewed [5–7,9,24,25], this review will specifically focus on BCP effects in metabolic and neurological diseases/disorders, with special emphasis on those characterized by chronic inflammation.

2. Plant Distribution, Biosynthesis and Molecular Biology of BCP

BCP, a bicyclic sesquiterpene, is widely distributed in the plant kingdom. It is a secondary metabolite belonging to the macro group of terpenes, it exerts a pivotal role in the survival and evolution of higher plants and contributes to the unique aroma of essential oils extracted from numerous species [26]. BCP is one of the most widespread sesquiterpenes in floral volatiles, occurring in more than 50% of angiosperm families [27]. A recent study identified several plants able to produce high percentages and high yields of BCP [28]. The work, out of more than 300 selected species, identified top species like *Copaifera langsdforffii*, *Cananga odorata*, *Humulus lupulus*, *Piper nigrum* and *Syzygium aromaticum*, which provide a high percentage of BCP along with interesting essential oil yields. These species possess a high potential for BCP utilization; however, only a skillful molecular fractionation of the essential oil allows the removal of undesired or even toxic terpenes that sometimes may be present along with BCP [28]. For instance, essential oils from *S. aromaticum* (also known as clove oil) may contain relatively high percentages of the toxic compound eugenol. This compound may form eugenol–quinone methides in hepatocytes, which are responsible for the cytotoxicity mediated by eugenol; finally, methyl eugenol, a derivative of eugenol, is also hepatotoxic [29]. With the due fractionation, the high percentages of BCP provided by these plants can be used for the preparation of new drugs or dietary supplements aimed to improve health, prevent lifestyle illnesses and act as a valid support for chronical diseases such as pain, metabolic and neurological disorders [28].

Due to the wide variety of plants producing BCP, the chemical synthesis of BCP appears to be an inconvenient strategy. For instance, a chemical method for BCP synthesis required eight steps including reduction, dehydration by Mitsunobu activation, diastereoselective reduction, selective tosylation, deprotonation, carbonyl-forming elimination, desilation and wittig methylenation [30]. Another way of producing BCP could be through microbial fermentation, because microorganisms grow rapidly. Although significant BCP yields have been obtained by employing a multi-step metabolic engineering strategy to increase precursor and cofactor supplies for BCP production [31], the costs for biotechnological applications are still too high when compared to essential oil costs and yields.

Thus, plants remain the main factories for BCP synthesis. In plants, terpenes are synthesized by terpene synthases (TPSs) which accept the ubiquitous prenyl diphosphates geranyl diphosphate (GPP), farnesyl diphosphate (FPP) and geranylgeranyl diphosphate (GGPP) as substrates and convert them into the different mono-, sesqui- and diterpene skeletons, respectively [32]. In the biochemical pathway that leads to BCP, the five-carbon building blocks isopentenyl diphosphate (IPP) and its allylic isomer dimethylallyl diphosphate (DMAPP) originate from two alternative pathways: the cytosolic mevalonate (MVA) pathway and the plastidial methylerythritol phosphate (MEP) pathway [32]. However, there is no compartmental separation of the two pathways and the extent of this cross-talk depends on the species and the physiological conditions [33].

The condensation of one DMAPP and two IPP molecules catalyzed by farnesyl diphosphate synthase (FPPS) leads to the formation of farnesyl diphosphate (FPP) in the cytosol [34]. FPP serves as substrate for TPSs for synthesizing BCP and the reaction starts with FPP ionization to a *trans*-farnesyl cation [35]. This is then followed by a series of complex chemical mechanisms involving isomerizations, cyclizations, and rearrangements catalyzed by TPSs, which generate humulyl cation, caryophyllyl cation and eventually BCP [36] (Figure 1).

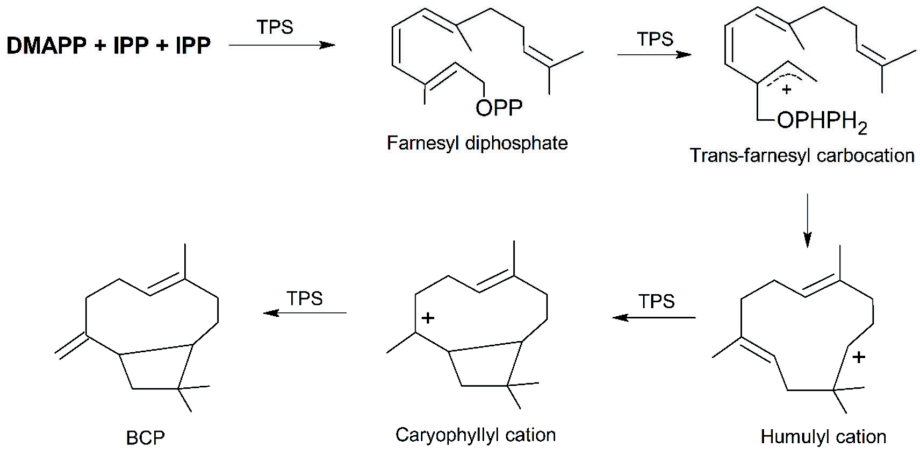

Figure 1. Simplified mechanism of the formation of (*E*)-β-caryophyllene (BCP) from DMAPP and IPP. Abbreviations: DMAPP, dimethylallyl diphosphate; IPP, isopentenyl diphosphate; TPS, terpene synthase. Modified from [36].

The BCP synthase (BCS) gene is characterized by the GVYXEP consensus sequence common to angiosperm sesquiterpene synthases [37], a conserved aspartate-rich region (DDxxD), which is crucial for the substrate binding [38] and by the xDx6E motif for metal cofactor binding [39]. A $RR(X)_8W$ motif, which is present in the *N*-terminal region and downstream of the *N*-terminal transit peptide, is assumed to participate in the ionization of the substrate [40] and is characteristic of the majority of the members of the terpene synthase subfamilies TPS-a and TPS-b [37]. Another conserved region, the RxR motif, is located 35 amino acids upstream of the DDxxD motif and is known to form the complex of diphosphate group after substrate ionization [41].

The role of BCP in plants is directly connected to plant defense and attraction. BCP is the main product of *Gossypium hirsutum* terpene synthase 1 (GhTPS1) and the expression of *GhTPS1* is induced in leaves of methyl jasmonate (MeJA)-treated cotton plants [42,43]. In *Medicago truncatula*, the MEP pathway-derived BCP is the main product of the terpene synthase 1 (MtTPS1); in this case the gene is induced by jasmonate (JA) and by the combination of JA and the ethylene precursor 1-aminocyclopropane-1-carboxylic acid (ACC) [44].

In grapevine five genes are known to code for BCP synthases [45] but only one (*VvGwECar2*) is actually expressed in all plant tissues and therefore accounts for most of the volatile production in vegetative parts and berries [46]. In this plant, flowers express two other genes (*VvGwECar1* and *VvPNECar2*) that seem to play an important role in these organs [47]. Biochemical analysis of *Oryza sativa* terpene synthase 1 (OryzaTPS1), coded by a rice terpene synthase gene involved in indirect defense against insects, showed that the enzyme functions as a BCS [48].

A partial cDNA for the BCP synthase gene (*MmCS*) was isolated from the expressed sequence tag (EST) library of *Mikania micrantha* leaves. *MmCS* expression was significantly increased in *M. micrantha* leaves within 3-days after wounding [49] and was found to be induced by high CO_2 levels [50]. The Japanese pepper (*Zanthoxylum piperitum*) produces BCP in the secretory cavities. In this plant,

the BCS ZpTPS1 specifically accepts the substrate FPP and is responsible for the biosynthesis of BCP [51]. In the flowers of the model plant *Arabidopsis thaliana*, the expression of terpene synthases can be induced by the phytohormones gibberellin (GA) and JA, and their induction increases the expression of *TPS21,* which encodes an enzyme that converts farnesyl diphosphate into BCP [52,53]. *TPS21* overexpression also demonstrated that BCP served as a defense against pathogens that invade floral tissues [35]. In *Liquidambar formosana*, the characterization of the BCS *LfTPS04* showed that seasonal differences in BCP content were correlated to the sesquiterpene synthase gene expression [54]. Expression patterns of BCP synthase gene during the development of *Artemisia annua* were observed in response to wounding and elicitation [55], whereas in *Pinus sylvestris* (Scots pine), insect oviposition enhances the transcription of the BCP/α-humulene synthase (*PsTPS1*), which in turn induces the attraction of an insect parasitoid [56]. Finally, in black pepper (*Piper nigrum*), *PnTPS1* produced BCP as a main product and α-humulene as a minor compound. The transcript level of *PnTPS1* correlated with the predominant BCP biosynthesis in black pepper, defining it as a relevant source of BCP [57].

3. Molecular Targets of BCP Action in Animal Cells

Apart from the functions of BCP in plants, recent studies outlined also a role of BCP in animal cells, highlighting its possible use as a novel therapeutic tool. Although the mechanism of action is not yet fully understood, studies indicate that BCP could act in animal cells through the specific binding to the CB2 receptor, a member of the endocannabinoid system [16], as well as the activation of PPARs, in particular PPARα and γ [10,22,23].

In the next few paragraphs, we will therefore describe more in detail these two classes of receptors.

3.1. CB2 Receptors

The cannabinoid receptors CB2 and CB1 belong to the endocannabinoid system, along with their natural ligands, the endocannabinoids, e.g., anandamide (AEA) and 2-arachidonoylglycerol (2-AG), and a plethora of enzymes involved in their biosynthesis and inactivation [58,59]. Nevertheless, exogenous cannabinoids do exist, the most potent of which is Δ^9-tetrahydrocannabinol (THC), a well-known terpenoid present in *Cannabis sativa* var. *indica*, responsible for the psychoactive effects of marijuana [60]. The endocannabinoid system shares mediators and overlaps with metabolic processes of other signaling pathways; thus, a wider endocannabinoid-related network has been identified as "expanded endocannabinoid system" or "endocannabinoidome" [61].

Both CB1 and CB2 receptors are G-protein coupled receptors, with an extracellular *N*-terminal domain, seven transmembrane alpha-helices and an intracellular C-terminus [62,63]. They show 44% overall amino acid similarity and 68% homology in the transmembrane domain [63]; one of the most different regions is the one located in the extracellular domain, which is responsible for cannabinoid binding [64]. Both receptors signal through $G_{i/o}$ proteins, thus they can inhibit adenylyl cyclase and activate mitogen-activated protein kinases (MAPKs). Worthy of note is the fact that MAPKs could regulate the activation of PPARs via direct phosphorylation. Differently from CB2 receptor, CB1-coupled $G_{i/o}$ proteins can mediate activation of A-type and inwardly rectifying potassium channels, and inhibition of N- and P/Q-type calcium currents; in addition, CB1 receptors can signal through G_s proteins [65].

CB1 is the most abundant and widespread G-protein coupled receptor in the mammalian brain, being highly expressed by presynaptic termini of neurons in the cortex, amygdala, hippocampus, basal ganglia, and cerebellum, where its activation modulates neurotransmitter release [66]. Notably, CB1 is present also in many peripheral sites, including spleen, lung, thymus, heart [67].

On the other hand, CB2 receptors, are mostly distributed peripherally, in the cells of the immune system [68] and indeed the main role of CB2 seems to be immune modulation. However, recent studies showed low levels of CB2 also in the central nervous system [69], especially in microglial cells and its activation in association with neurodegenerative disorders [70].

The endocannabinoid system, due to its wide distribution, regulates various physiological functions, such as neurogenesis and neurodegeneration, cognitive and mood regulation, appetite and metabolism, muscle contractility, inflammation and immune functions [67].

In 2008, Gertsch and colleagues [16] showed that BCP is able to elicit some of its effects by acting as a fully functional agonist of the CB2 receptor. Notably, BCP binds selectively CB2 receptors, since it lacks significant binding activity to the human CB1 (hCB1) receptor, and it is unable to displace high-affinity ligands from hCB1. BCP was shown to bind hCB2 with an inhibitory constant K_i of 155 ± 4 nM, a binding affinity about 150 times lower than the potent high affinity cannabinoid ligand WIN55,212-2 (whose K_i for hCB2 is 1.2 nM). BCP, likely in its bioactive ββ conformation, binds to the hydrophobic region of the amphipathic hCB2 receptor binding pocket, being the putative binding site located adjacent to helices III, V, VI, and VII at the near extracellular site of the seven transmembrane domain. BCP acts as a full CB2 receptor ligand, since its binding activates CB2-mediated intracellular signaling, e.g., adenylate cyclase inhibition, intracellular calcium release and mitogen-activated kinases Erk1/2 and p38 activation [16]. Notably, BCP was shown to lead to anti-inflammatory effects, inhibiting lipopolysaccharide (LPS)-induced TNF and IL-1β expression in peripheral blood and attenuating LPS-stimulated Erk1/2 and JNK1/2 phosphorylation in monocytes. CB2-mediated BCP anti-inflammatory effects were also observed in an in vivo model, where BCP (5 and 10 mg/kg body weight), orally administered 1 h before carrageenan treatment, strongly reduces inflammatory response in wild-type mice but not in CB2 deficient mice [16].

Recent studies have demonstrated a role of BCP, through the activation of CB2 receptors, in the modulation of different processes. A specific BCP-mediated CB2 receptor activation has been demonstrated to be at the base for example of tumor suppression in glioblastoma where it has anti-proliferative effects and plays an anti-inflammatory activity through the modulation of NF-κB and PPARγ [71]. In LPS-induced interstitial cystitis in mice, the intravesical instillation or the oral treatment with BCP (100 mg/kg) resulted in a significant decrease in the number of adherent leukocytes, thus confirming an anti-inflammatory activity in bladder inflammation [72]. In another study [73], BCP (25 mg/kg) was able to prevent nucleoside reverse transcriptase inhibitors (NRTI)-induced neuropathic pain in mice, in a CB2 cannabinoid receptor-dependent manner; also, BCP treatment prevented the induced upregulation of inflammatory cytokines mRNA transcripts (i.e., Interferon γ, IL-6β and TNFα).

3.2. PPARs

PPARs are transcriptional factors belonging to the ligand-activated nuclear receptor superfamily involved in both metabolic and inflammatory responses (recently reviewed by Hong et al. [74]). The existence of receptors that could mediate peroxisome proliferation was first hypothesized in 1983 by Lalwani et al. [75]. PPARα (also called NR1C1) was later identified [76] as a new member of the steroid hormone receptor superfamily, that could be activated by different molecules, such as fatty acids and fibrates, a widely used class of hypolipidemic drugs. Further on, other members of PPARs family were discovered [77], namely PPARβ/δ (NR1C2) and PPARγ (NR1C3). PPARβ/δ is activated by saturated and polyunsaturated fatty acids and eicosanoids, as well as synthetic ligands. PPARγ is instead a specific receptor for thiazolidinediones (TZDs), such as troglitazone, rosiglitazone and pioglitazone, widely used for T2D treatment [74].

Although PPARs share high structural homologies, they are encoded by different genes, have different ligands, are expressed in different tissues and regulate different biological processes [74].

PPARα is abundantly expressed in the liver, where it acts as the master regulator of hepatic lipid metabolism [10,78,79]. PPARα is also present in the brown adipose tissue, heart, kidney and muscles [80]. PPARβ/δ is expressed in skeletal muscle, heart, gastrointestinal tract, adipose tissue, where it regulates fatty acid metabolism [81]. PPARγ is actually considered the master gene of adipogenesis, being mostly expressed in white and brown adipose tissue, but also the large intestine and the spleen [10,82]. Two major PPARγ isoforms, derived from alternative promoter usage, have been described. While

PPARγ1 is expressed in many different tissues, PPARγ2 is specifically expressed in adipose tissue, although it can be induced in other districts by a high-fat diet [83,84]. PPARγ participates into the programmed differentiation of adipocytes by enhancing the 5′-adenosine monophosphate-activated protein kinase (AMPK) activity, a master energy sensor which regulates diverse metabolic pathways, increases mitochondrial activity and biogenesis in muscles and is responsible for the inhibition of adipogenesis [9,85]; moreover, PPARγ is an insulin sensitizer also involved in glucose homeostasis [74].

PPARs are ligand-activated nuclear receptors, that enhance the transcription of specific genes. They are characterized by 13 helices and a small four beta-sheets with a large hydrophobic binding pocket. Ligand binding induces a conformational change of the ligand-binding region and allow PPARs to form heterodimers with the retinoid-X-receptor (RXR); after activation, PPAR-RXR heterodimers can bind to specific DNA sequences (PPAR response elements, PPREs), which in turn stimulate the transcription of target genes [86]. The function of PPARs can be stimulated by the presence of specific coactivators or inhibited by corepressors, depending on the different tissues [87].

BCP has been demonstrated to interact with and to up-regulate members of the PPARs family. In particular, it can activate PPARα through a direct interaction with the ligand-binding pocket, thus regulating lipid metabolism [23].

Furthermore, studies indicate the triggering of PPARγ via a BCP-mediated CB2 receptor activation [88,89]. In this respect, PPARγ was demonstrated to be involved in BCP-dependent neuroprotection [90] and tumor suppression functions [71], as well as hypolipidemic effects and vascular inflammation amelioration [10], anxiolytic, anti-oxidant, anti-arthritic and anti-inflammatory effects [22,48,91].

4. Protective Effects of BCP on Metabolic and Neural Disorders Characterized by Inflammatory States

Recently, a growing number of studies has described multiple protective effects of BCP in several metabolic and neural disorders. Notably, these disorders are mostly characterized by chronic inflammation. In the next subsections, first the general features of chronic inflammation will be presented, followed by description of the protective and anti-inflammatory effects exerted by BCP in specific metabolic and neurologic diseases.

4.1. Chronic Inflammation as a Common Theme of Many Metabolic and Neurological Disorders

During the last decades, the complex phenomenon of inflammation has been extensively studied, and it has become clear that this condition is a fundamental feature of metabolic disorders such as obesity, type II diabetes (T2D), nonalcoholic steatohepatitis (NASH), NAFLD [92–95] and also neurological disorders, e.g., chronic pain, Parkinson's and Alzheimer's diseases [21,96,97].

The process of inflammation constitutes the tissue response to injury, and can be divided into acute and chronic inflammation. The first one is characterized by increased blood flow and vascular permeability, along with accumulation of inflammatory mediators such as cytokines, and immune cells, like neutrophils. The resolution of acute inflammation occurs rapidly [98]. Chronic inflammation involves progressive changes in inflammatory cells and the coexistence of tissue destruction and repair; it can become pathological because of the loss of tolerance or regulatory processes. Obesity and metabolic syndrome lead to an inflammatory state that differ from the classical response, being the inflammatory process systemic and characterized by a chronic low-intensity reaction [99]. During the first stages of white adipose tissue expansion, typical of an overweight condition, a set of acute pro-inflammatory mediators is required to support the remodeling of healthy adipose depots; however, if lipid accumulation progresses and the pro-inflammatory molecules persist, a state of chronic low-level inflammation is established, a typical scenario of an obesity condition. Recent studies showed that local infiltration of immune cells and enhanced production of pro-inflammatory cytokines lead to a condition that could generate insulin resistance, defective insulin secretion, and disruption of other aspects of energy homeostasis [93,94,100]. This chronic, low-grade, metabolically triggered inflammation is also

called metaflammation, a condition mainly generated by metabolic excess and occurring in several metabolic tissues, including adipose tissue, pancreas, liver, muscle, brain, and heart [101–103].

The chronic inflammatory response develops from the interaction between adipose tissue resident immune cells, including macrophages, and the immune system, skewed to a proinflammatory phenotype. Under physiological conditions, immune cells coordinately regulate tissue integrity and metabolism by controlling the activity of subsets of T lymphocytes. These cells release a cascade of cytokines that regulate other immune cells such as mast cells, eosinophils and others, maintaining resident macrophages in a M2-polarized phenotype, therefore acting toward an anti-inflammatory and immunoregulatory direction [94,104].

Conversely, under pathological conditions like obesity, fatty liver disease and T2D, immune cells withstand changes such as the recruitment of M1-polarized macrophages, which display a more proinflammatory phenotype and secrete proinflammatory cytokines such as TNF-α,IL-1, IL-6, IL-12 and C-reactive protein [94,105–107].

The hypothesis that inflammation is linked to metabolic conditions was formulated in 1993 with the publication by Hotamisligil and colleagues, demonstrating that adipocytes constitutively express TNF-α, whose expression is noticeably increased in adipocytes of obese animal models (ob/ob mouse, db/db mouse and fa/fa Zucker rat) [108,109]. Nowadays, almost 30 years later, the link between obesity, diabetes and chronic inflammation has been confirmed [93,109] and it has been also proved that mice lacking functional TNF-α are more insulin sensitive and glucose tolerant than wild type animals [106,110]. Moreover, TNF-α is overexpressed in the adipose and muscle tissues of obese humans, and its exogenous dragging leads to insulin resistance [92,111].

Metabolic, inflammatory and innate immune processes are also regulated by lipids [92,112] through the action of PPARs and liver X receptor (LXR) families. Activation of these transcription factors inhibits the expression of several genes involved in the inflammatory response in macrophages and adipocytes, therefore suppressing the production of proinflammatory cytokines [92,113,114].

In this complex scenario, the Toll-Like receptor (TLRs) pathway plays a crucial role; in fact, it has been demonstrated that fatty acids may also bind to Toll-like receptors, inducing the synthesis of inflammatory markers in macrophages and exacerbating insulin resistance [107,115]. TLRs are a family of transmembrane receptors that recognize a variety of pathogen-associated molecular patterns (PAMPs), playing a fundamental role in the innate immune system. Presumably reflecting structural similarity between microbial and host membrane lipids, the subfamily of TLR2 and TLR4 have been reported also to recognize select host lipids and to play important roles in the pathogenesis of insulin resistance and obesity [99,115].

Hypertrophic obesity leads to a dysregulated subcutaneous adipose tissue and the accumulation of ectopic fat in many depots, such as in liver, where inflammation and hepatocyte injury are the hallmarks of NASH and NAFLD [95,116]. The innate immune system plays a fundamental role also in triggering and amplifying hepatic inflammation in liver lipid disorders. Activation of the inflammatory response pathway results from abnormal accumulation of lipids and consequent lipotoxicity [95]. It has been demonstrated that PPARα plays central role in this context, exerting anti-inflammatory activities in murine models of systemic inflammation. In fact, PPARα agonists specifically attenuate IL-6 concentration *in vitro* and *in vivo* [117,118].

Inflammatory reaction can also occur in chronic nervous system diseases, being neuroinflammation a central pathological feature of several neurological disorders such as Alzheimer's disease, Parkinson's disease and multiple sclerosis. Acting as a mediator in neurodegenerative pathologies, neuroinflammation causes microglia activation, mitochondrial dysfunction, as well as release of pro-inflammatory cytokines and reactive oxygen species (ROS) production [119].

4.2. Protective Effects of BCP on Metabolic Disorders Characterized by Chronic Inflammation

The current increase in metabolic diseases such as obesity, T2D, liver lipid disorders, and the complex framework of metabolic syndrome (MetS) is now considered a sort of epidemics caused by

multiple factors, including loss of exercise, aging, wrong diet, genetic background and exposure to endocrine disruptors [120–122]. Most single metabolic diseases and complex syndromes such as MetS are characterized by inflammation, often becoming chronic and leading to CVD [123–125].

To cope with this global complex problem, several strategies are needed. Thanks to the growing data in this field, natural compounds are becoming an important approach to promote health and ameliorate metabolic disorder conditions [1,123,126–130].

Recently, a growing number of reports has described multiple protective effects of BCP in several metabolic disorders (see Table 1). In particular, BCP has been shown to actively promote the inhibition of lipid accumulation, fatty acids oxidation, decrease of visceral fat index, reduction of total cholesterol, triglycerides, and low density lipoprotein (LDL) cholesterol levels, decrease of hepatic 3-hydroxy-3-methylglutayl coenzyme A (HMG-CoA) reductase activity, reduction of body weight in animal models and action as insulinotropic agent [5,10,78,126,131–136]. Notably, the effectiveness of BCP as anti-inflammatory agent is at least partly due to its ability to inhibit the main inflammatory mediators, e.g., inducible nitric oxide synthase (iNOS), IL-1β, IL-6, TNF-α, NF-κB, cyclooxygenase 1 (COX-1) and cyclooxygenase 2 (COX-2) [5,10,16,137].

The next subsections will describe the current knowledge about BCP action in different inflammation-related metabolic diseases.

Table 1. Evidence of a role of BCP on metabolic diseases.

Disease	Main Metabolic Effect	Experimental Model	BCP Administration	References
Obesity and dyslipidemia	Decrease of visceral fat index. LDL and VLDL	Wistar rats fed with HFFD	30 mg/Kg b.w./day for 4 weeks by oral gavage	[10]
	Inhibition of adipogenesis	Bone marrow cells	0.1–100 μM for 3–4 days in differentiation medium	[85]
	Inhibition of lipid accumulation	Preadipocytes (3T3-L1 cells)	1 nM–10 μM for 9 days in differentiation medium	[133]
			5 or 10 μM for 6 days in differentiation medium	[134]
	Suppression of body weight gain	HFD-fed C57BL/6N mice	0.15% or 0.3% supplemented diets for 16 weeks	[134]
			0.02% or 0.2% supplemented diets for 4 and 8 weeks	[136]
	Reduction of total cholesterol, triglycerides, and LDL cholesterol levels	Hypercholesterolemic Wistar rats	1 mL/Kg b.w. for 3 days by oral gavage	[126]
			30 mg/Kg b.w./day for 4 weeks by oral gavage	[135]
Hepatic steatosis	Decrease of hepatic HMG-CoA reductase activity	Hypercholesterolemic Wistar rats	1 mL/Kg b.w. for 3 days by oral gavage	[126]
			30 mg/Kg b.w./day for 4 weeks by oral gavage	[135]
	Inhibition of palmitate-inducible lipid accumulation Downregulation of FAS and upregulation of ATGL Reduction of triglycerides. increase of FFA uptake and FFA oxidation	Human hepatocyte cell line (HepG2)	5 μM for 24h in serum free medium	[78]
			1, 10 or 100 μM for 24h	[23]
T2D	Increase of glucose uptake and GLUT4 translocation	Skeletal myotubes (C2C12 cells)	1, 10, 100 nM for 30 min in glucose and serum free medium	[133]
	Decrease of blood glucose levels and proinflammatory cytokines levels Increase of plasma insulin	Streptozotocin-Induced Diabetic rats	200 mg/Kg b.w. for 45 days by oral gavage	[138,139]
	Decrease of fasting blood glucose and fasting insulin	Wistar rats fed with a HFFD	30 mg/Kg b.w./day for 4 weeks by oral gavage	[10]
Cardiovascular disorders	Reduction of atherogenic and coronary risk index	Hypercholesterolemic Wistar rats	30 mg/Kg b.w./day for 4 weeks by oral gavage	[10]
	Protective role against isoproterenol-induced myocardial infarction	Male Sprague–Dawley rats	100 or 200 mg/Kg b.w/day for 21 days orally	[140]
	Protective effect against Doxorubicin-induced inflammation in the myocardium	Male Wistar Rats	25, 50, 100 mg/Kg b.w. for 5 days by intraperitoneal injection	[141]
			25 mg/Kg b.w. for 6 days a week for 5 weeks by intraperitoneal injection	[142]

HFFD: high fat/fructose diet; HFD: high fat diet; LDL: low density lipoprotein; HMG-CoA: Hydroxy methylglutaryl-Coenzyme A; FAS: fatty acid synthase; ATGL: adipose triglyceride lipase; GLUT4: glucose transporter 4; VLDL: very low density lipoprotein; FFA: free fatty acids.

4.2.1. Obesity and Dyslipidemia

Obesity is a chronic metabolic disease characterized by excessive fat accumulation in adipose tissue [129]. The prevalence of obesity has increased globally over the last two decades [125], as a consequence of our evolutionary history [143]. Obesity is a multifactorial disease, caused by interactions between environment, lifestyle and genetics. Comprehension of these multiple factors is still ongoing and necessary for developing efficient strategies for obesity prevention and treatment [122].

According to the World Health Organization's report dated April 2020, worldwide obesity has nearly tripled since 1975. In 2016, more than 1.9 billion adults were overweight; of these, over 650 million were obese. Moreover, in 2019 an estimated 38.2 million children under the age of 5 were overweight or obese. Once considered a problem only for high-income countries, overweight and obesity are now on the rise in low- and middle-income countries, particularly in urban settings. In Africa, the number of overweight children under 5 has increased by nearly 24% percent since 2000. Almost half of the children under 5 who were overweight or obese in 2019 lived in Asia [144].

Obesity correlates with cardiovascular risk, since it is associated with increased fasting plasma triglycerides and low density lipoprotein (LDL) cholesterol, low levels of high density lipoprotein (HDL) cholesterol, elevated blood glucose and insulin levels, and high blood pressure [145]. Specifically, the elevation of lipids in the blood is a condition called dyslipidemia, nowadays considered the major risk factor for the development of atherosclerotic disease and subsequent cardiovascular disease [146,147].

As mentioned before, obesity and overweight are characterized by chronic, low-grade inflammation, which perpetuates the disease and is associated with multiple complications [148], including the increase of inflammatory markers in liver, adipose tissue, skeletal muscle, pancreatic islets, and brain. Although the relationships between these events in rodents or obese humans remain poorly understood [94], in the last few years it has been suggested that adipocyte dysfunction is the trigger of obesity-related inflammation [149].

Several studies have been focused on possible strategies to treat obesity. Among the approaches based on natural compounds and bioactive molecules, the use of BCP has been tested both *in vivo* and *in vitro*. In this regard, we recently demonstrated an *in vitro* anti-obesogenic effect of 1 nM–10 μM BCP extracted from *Piper nigrum* and showed that it was able to reduce intracellular triglycerides accumulation without interfering with adipocyte number in the murine 3T3-L1 adipocytes [133]. The same *in vitro* model was already used to prove that dietary 5 or 10 μM BCP inhibits lipid accumulation in adipocytes and 0.15%–0.3% BCP dietary supplementation suppresses *in vivo* body weight gain and fasting blood glucose levels in high fat diet (HFD)-fed mice [134].

Another *in vitro* study tested the effects of 0.1–100 μM BCP on osteoblastic mineralization, osteoclastogenesis and adipogenesis in a bone marrow mesenchymal stem cells (MSC) model, demonstrating that BCP significantly suppresses the differentiation of bone marrow cells into adipocytes in a dose-dependent manner [85]. In an *in vivo* experiment on Wistar rats fed with high fat/fructose diet (HFFD), the effect of 30 mg/Kg b.w. /day BCP administration for 4 weeks by oral gavage on diet-induced dyslipidemia and inflammation was assessed [10]. In this study, BCP was able to decrease the visceral fat index, total cholesterol, LDL, very low density lipoprotein (VLDL), and pro-inflammatory cytokines (TNF-α and NF-κB). These effects were reversed by treatment with CB2 and PPAR-γ antagonists, suggesting that BCP activity is mediated by direct binding to CB2 receptors and by the activation of PPAR-γ, possibly through a cross-talk between these two receptor systems [10].

The effect of BCP on hypercholesterolemia was tested in a rat model of Triton-induced hyperlipidemia; 30 mg/Kg b.w. BCP was found to reduce total cholesterol, triglycerides, and LDL cholesterol levels in hypercholesterolemic animals and to exert hypolipidemic effects via inhibition of the hepatic HMG-CoA reductase [126]. The hypocholesterolemic effect of 30 mg/Kg b.w. BCP was also demonstrated in rats fed with cholesterol and fat enriched diet (HCFD); a significant decrease in serum total cholesterol and LDL, and an increase in HDL levels were observed also in this case [135].

In a mouse model of nonalcoholic steatohepatitis, 0.02% and 0.2% BCP supplementation in the diet exerted an antioxidant action and reduced hepatic steatosis as well as liver inflammation and fibrosis [136].

4.2.2. NAFLD and NASH

Liver diseases are among the major causes of illness worldwide, and are caused by viral infections, alcohol abuse, abnormal dietary fat ingestion. In particular, NAFLD and the consequent NASH are considered as hepatic manifestation of MetS and strictly correlate with insulin resistance, obesity, dyslipidemia, atherosclerosis, and hypertension [116,150,151]. NAFLD is characterized by excess accumulation of triglycerides in hepatocytes due to both increased ingestion of free fatty acids (FFAs) and *de novo* hepatic lipogenesis. The accumulation of lipids causes oxidative stress and inflammatory response leading to NASH, which may progress to cirrhosis and liver cancer [78,116,150].

There is multiple scientific evidence on the beneficial effects of BCP on NAFLD and NASH experimental models. Clove extract (5 μM) was demonstrated to potently suppress the palmitate-induced lipid accumulation in human HepG2 hepatocytes, used as a model of *in vitro* NAFLD [78]. The major active molecule was found to be BCP, exerting its effects by binding to CB2 receptors, with subsequent AMPK phosphorylation, which in turn led to the upregulation of the lipolytic enzyme adipose triglyceride lipase (ATGL) and the downregulation of the lipogenic enzyme fatty acid synthase (FAS). In another *in vitro* study on HepG2 cells, BCP stimulation (1, 10 or 100 μM) led to a significant reduction of intracellular triglycerides and an increase of hepatic FFA uptake and FFA oxidation, via a PPARα-dependent mechanism [23].

In hypercholesterolemic Wistar rats fed with high cholesterol and fat diet, 1 mL/Kg b.w. or 30 mg/Kg b.w. BCP administration correlated with decreased hepatomegaly, lower hepatic lipid accumulation and steatosis, and decreased aspartate aminotransferase (AST) and alanine aminotransferase (ALT) activities; the hypolipidemic effects were mediated through inhibition of the hepatic HMG-CoA reductase [126,135].

In mice fed with methionine- and choline-deficient diet (MCD) reproducing the histopathological features of human NASH, BCP administration (0.2% of total diet for 8 weeks) exerted beneficial effects against hepatic steatosis, liver damage and inflammation found in the development and progression of NASH [136].

4.2.3. Diabetes

T2D is considered one of the most important chronic diseases with severe complications, responsible for elevated indexes of morbidity and mortality [152]. The combination of genetic factors associated with impaired insulin secretion, insulin resistance, environmental factors, including overeating, aging, obesity and lack of exercise, typically accounts for T2D [153]. Moreover, insulin resistance can be a consequence of a reduction of insulin receptors numbers or a failure in insulin-receptor binding or in glucose transportation into the cell by the glucose transporter GLUT4 [152]. Inflammatory pathways have been suggested as the underlying and unifying pathogenic mediators for obesity and diabetes mellitus [154]. Indeed, an increase in body weight results in a dysfunction of the adipose tissue, with a greater release of proinflammatory cytokines, such as IL-6 and TNF-α. These molecules, together with increased FFA, can alter insulin sensitivity by stimulating the phosphorylation of serine instead of tyrosine residues in insulin receptor substrate-1 (IRS-1), thereby preventing the activation of insulin signaling pathway and making tissues less responsive to its action until insulin resistance [152,155].

Both *in vivo* and *in vitro* studies suggested a potential impact BCP on glucose metabolism. In particular, by *in vitro* analysis in skeletal myotubes (C2C12 cells) we demonstrated that 1, 10 and 100 nM of BCP was as efficient as insulin in stimulating cellular glucose uptake [133]. Besides, BCP induced the translocation of the GLUT4 storage vesicles to the plasma membrane of C2C12 cells, a process that, mainly in skeletal muscle and in adipose tissue, is directly correlated with the ability to lower elevated blood glucose levels. Other studies demonstrated that BCP induces insulin secretion in

rat insulinoma (RIN-5F cells) [131], and in mouse pancreatic β−(MIN) cell line, through activation of CB2 and small G proteins ADP ribosylation factor (Arf)6, Ras-related C3 botulinum toxin substrate (Rac)1 and Cell division control protein (Cdc) 42 [156].

In streptozotocin (STZ)-induced diabetic rats (40 mg/Kg b.w.), the oral administration of 200 mg/Kg b.w. BCP significantly decreased blood glucose levels and increased plasma insulin; BCP increased the activity of metabolic enzymes such as hexokinase, pyruvate kinase and glucose-6-phosphate dehydrogenase in liver, kidney and skeletal muscle; BCP also reversed the activity of gluconeogenic enzymes that are deficient in diabetic rats, proving that it could normalize carbohydrate metabolism by enhancing glucose utilization and decreasing hepatic glucose production. Immunohistochemical analysis of pancreas sections demonstrated that BCP treatment improved tissue structure and increased insulin-secreting cell number, suggesting an insulinotropic effect of BCP [138]. In another study, oral administration of 200 mg/Kg b.w. BCP to STZ-induced diabetic rats significantly improved the levels of antioxidant enzymes, decreased lipid peroxidative markers in plasma and pancreatic tissues and reversed proinflammatory cytokines (TNF-α and IL-6) to near normal levels, thus indicating a relevant anti-inflammatory role of BCP in preventing diabetes-induced oxidative stress and associated complications [139].

An *ex vivo* and *in vivo* study in diabetic rats, also suggested an antidiabetic effect of BCP alone or in combination with dietary supplementation of L-arginine, that displays pancreatic β cell regenerative effects through nitric oxide (NO) modulation [131].

The protective effects of 30 mg/Kg b.w. BCP treatment on metabolic alterations were also highlighted in rats receiving a high fat/fructose diet (HFFD) that causes insulin resistance and obesity, where BCP administration prevented HFFD-induced elevation of adipose-index, hyperglycemia and hyperinsulinemia, acting through the activation of CB2 receptors [10].

4.2.4. Cardiovascular Disorders

Metabolic dysfunctions are strictly related to cardiovascular inflammatory responses [157]. In particular, diet-induced disorders augment atherogenic complications and exacerbate vascular inflammation, leading to several detrimental outcomes as vascular wall thickness, platelet activation and predisposition to thrombosis [158,159]. This atherosclerotic process underlies ischemic diseases, among which myocardial infarction, the leading cause of death worldwide. Current established therapeutic options to prevent and treat atherosclerosis include inhibitors of cholesterol synthesis (statins), inhibitors of fat breakdown in adipose tissue (niacin), inhibitors of platelet aggregation (aspirin) and antihypertensive drugs (β-blockers, renin-angiotensin system inhibitors) [160].

Among new experimental strategies, the use of plant-derived bioactive compounds, in combination with drugs or used as preventive intervention from early life, represents a promising approach. Anti-atherosclerotic properties have been shown by several bioactive compounds, such as Omega-3 fatty acids, phytosterols, phenolic compounds [161], and, very recently, BCP. In particular the role of BCP in the regulation of the inflammatory cascade has been investigated in order to evaluate its use as a therapeutic agent against cardiovascular damage. In this regard, rats fed with a high fat/high fructose diet showed an ameliorated lipid profile (higher levels of HDL and lower levels of triglycerides, total cholesterol, LDL and VLDL) when supplemented with BCP. Furthermore, 30 mg/Kg b.w. BCP induced a reduction in pro-inflammatory cytokines TNF-α and NF-kB and no expression of adhesion molecule vascular cell adhesion molecule (VCAM)-1 in the aorta, underlining a positive effect of the molecule against atherosclerotic burden [10]. Furthermore, oral administration of BCP to hypercholesterolemic rats reduces atherogenic index and coronary risk index, preventing cardiovascular damage [10,162].

Occlusion of vascular wall could be a possible exacerbation of atherosclerosis, thus causing ischemic tissue damage with improper tissue blood supply. When the heart is involved in prolonged ischemic condition, myocardial infarction can develop, thus causing loss of cardiac cells and impaired organ function. Younis and colleagues showed the protective role of 100 or 200 mg/Kg b.w. BCP against

isoproterenol-induced myocardial infarction, underlining the reduction of the inflammatory response induced by the treatment through a CB2-independent pathway. Indeed, orally administered BCP inactivated the heat shock protein (HSP)-60/Toll-like Receptor (TLR)/ Myeloid differentiation primary response (MyD) 88/NF-kB pathway thus protecting the heart from pro-inflammatory cytokines and chemokines rising and reducing infarct size [140].

Among drug-mediated cardiotoxic inflammation, the deleterious effect of doxorubicin, an anthracycline used in chemotherapy, has been underlined. Doxorubicin treatment induced the expression of NF-kB and activation of pro-inflammatory cytokines and chemokines that are involved in the progression of the inflammatory response in the cardiac tissue [163]. Intraperitoneal injection of 25–100 mg/Kg b.w. BCP showed protective effects against doxorubicin toxicity, in fact, it reduced the expression of NF-kB, TNF-α, IL-1β and IL-6, and down-regulated COX-2 and iNOS, thus attenuating inflammatory response in the myocardium without altering the antitumor effect of the drug and suggesting the possible use of BCP to prevent cardiac damage induced by doxorubicin [141,142].

4.3. Activity of BCP in Pain and Other Nervous System Disorders

Acute and especially chronic pain is a serious social burden and it has been estimated that around 10% of population worldwide suffers from long-lasting pain [164]. The neuroprotective role of cannabinoids against pain and neurodegenerative diseases has been extensively demonstrated [165]. Moreover, the endocannabinoid system seems to play an important role on inflammation and nociception with analgesic effects in numerous pain conditions, frequently in hyperalgesic and inflammatory states [165]. In inflammatory hyperalgesia, CB2 receptors localized on mast and immune cells could possibly achieve pain inhibition by the reduction of prostanoids or cytokines release, which are responsible for peripheral nociceptor sensitization [7]. This evidence is of particular relevance, since, as we already mentioned, CB2 receptors can be activated by BCP binding. Indeed, several studies demonstrated the efficacy of BCP to treat neuropathies and pain [21,73].

Due to its lipophilicity, BCP easily penetrates cell membranes, while still presenting good oral bioavailability and a very large therapeutic window, with an oral 50% lethal dose (LD_{50}) of more than 5000 mg/kg in rats [7]. Significant and dose-dependent antinociceptive response was produced by BCP without the presence of gastric damage [166]. Antiallodynic actions of BCP are exerted only through activation of local peripheral CB2 [7]. In neuropathic pain models, BCP reduced spinal neuroinflammation and the oral administration was more effective than the subcutaneously injected synthetic CB2 agonist JWH-133. Thus, BCP may be highly effective in the treatment of long-lasting, debilitating pain states [167]. BCP also prevents nucleoside reverse transcriptase inhibitors-induced mechanical allodynia, possibly via reducing the inflammatory response, and attenuates mechanical allodynia through CB2 receptor activation [73]. BCP induces decrement in expression of COX-2 and iNOS, which could suppress NF-κB activation and as a consequence promote analgesia [168]. Recently, BCP was found to attenuate mechanical allodynia induced by paclitaxel, a drug used in chemotherapy, in a CB2-dependent manner. Moreover, BCP was able to attenuate the development of paclitaxel-induced peripheral neuropathy by reducing mitogen-activated protein kinases (p38MAPK) and NF-kB activation and increased ionized calcium-binding adaptor molecule-1 (Iba-1) and IL-1β immunoreactivity promoted by paclitaxel [169].

Interestingly, BCP can diminish acute and chronic pain not only through the endocannabinoid system, but also through the opioid system [21]. This latter mechanism involves the participation of benzodiazepine and serotonin 1A (5-HT1A) receptors, as well as nitric oxide [170]. BCP is able to indirectly activate the opioid system through β-endorphin release, which in turn activates μ-opioid receptors on primary afferent neurons [166]. The role of the opioid system is further demonstrated by blockade with naloxone, resulting in the abolishment of BCP analgesic effects in acute and chronic pain models [171].

The degeneration of axons is a critical event in many neurodegenerative conditions including stroke, glaucoma, motor neuropathies, amyotrophic lateral sclerosis (ALS), Alzheimer's, Parkinson's

and Huntington's diseases [172,173]. BCP could have a beneficial role in inducing neuritogenesis through the activation of tropomyosin receptor kinase A (TrkA) receptors by a mechanism independent of nerve growth factor (NGF) or cannabinoid receptors [5].

Parkinson's disease (PD) is a long-term neurodegenerative disorder characterized by progressive dopaminergic neurons loss in the substantia nigra pars compacta (SNc). Treatment of mice with BCP rescued dopaminergic neurons and decreased microglia and astrocyte activation, as evidenced by reduced levels of Iba-1 and glial fibrillary acidic protein (GFAP) expression [6]. BCP, in addition to attenuation of pro-inflammatory cytokines and inflammatory mediators such as COX-2 and iNOS, also restored antioxidant enzymes and inhibited lipid peroxidation as well as glutathione depletion [174]. BCP acts via multiple neuroprotective mechanisms in murine models, thus it may be viewed as a potential treatment and/or preventative agent for PD [175].

Administration of BCP protects against cerebral ischemic injury in rats and reduces astrogliosis and microglial activation in a transgenic mouse model of Alzheimer's disease [89].

A beneficial effect of BCP was also found for multiple sclerosis, also known as encephalomyelitis disseminata, the most common inflammatory and demyelinating autoimmune disease of the central nervous system. BCP reduced the clinical score and severity of experimental autoimmune encephalomyelitis and inhibited H_2O_2, NO, TNF-α, interferon-γ (IFN-γ), and IL-17 production. Moreover, BCP treatment significantly reduced the numbers of inflammatory infiltrates and attenuated neurological damages in the CNS of experimental autoimmune encephalomyelitis mice [176].

Epilepsy is a neurological disease, and recurrent epileptic seizures and behavioral comorbidities such as depression, anxiety, psychosis, and cognitive deficits largely affect the quality of life of the patients with epilepsy and their families [177]. BCP was found to display anticonvulsant activity against seizures induced by pentylenetetrazole in mice. Since no adverse effects were observed when BCP was administered at the concentration of 100 mg/kg b.w., and because of the lack of genotoxicity [178], this compound was considered a potential new anticonvulsant drugs [179]. Moreover, BCP was clinically useful as an adjunct treatment against seizure spread and status epilepticus and concomitant oxidative stress, neurotoxicity and cognitive impairments [180].

As a summary of the experimental evidence reported in this review, Figure 2 schematizes the major currently known positive effects of BCP on metabolic and neurological disorders.

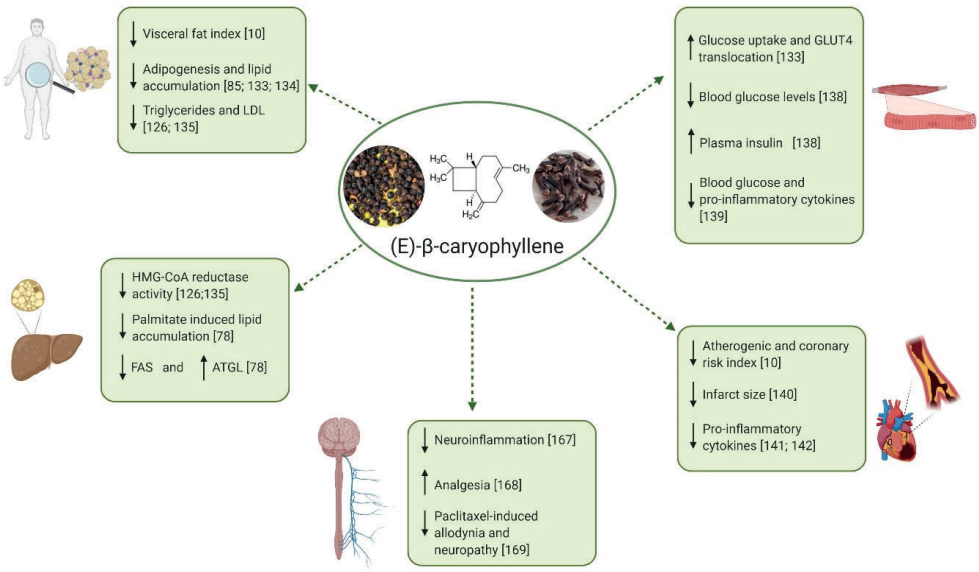

Figure 2. Positive effects of BCP on metabolic and neurological disorders. Scheme created with BioRender.com. ↓: reduction; ↑: increase; LDL: Low density lipoproteins; HMG-CoA: Hydroxy methylglutaryl-Coenzyme A; FAS: fatty acid synthase; ATGL: adipose triglyceride lipase; GLUT4: glucose transporter 4.

5. Conclusions

The bicyclic sesquiterpene BCP is a natural compound widely present in the plant kingdom and obtained in high concentrations from the essential oils of several plants. As a secondary metabolite, particularly present in both vegetative and reproductive parts, BCP is primarily involved in plant defense and attraction. Recent studies outlined a protective role of BCP also in animal cells, underlining its beneficial effects against many diseases. These results have been summarized in previous reviews; the present review specifically focused on BCP action on diseases characterized by chronic inflammation.

Chronic inflammation is a common theme of many metabolic and neurologic disorders. The definition of new therapeutic approaches based on natural compounds could represent a promising way to complement, or even replace, currently administered drugs. The data accumulated so far both in *in vivo* and *in vitro* studies show that BCP is a good candidate in the treatment of chronic inflammation due to its specific molecular targets and very low toxicity. In fact, it is now widely accepted that this sesquiterpene acts on several molecular pathways implicated in the generation of inflammatory states and is able to reduce several pro-inflammatory mediators, including IL-1β, IL-6, TNF-α, NF-κB. The molecular mechanisms underlying BCP effects are only beginning to be unraveled. The available data suggest that BCP is able to exert its potent anti-inflammatory effects through multiple mechanisms mostly initiated by the binding of BCP to CB2 receptors. Subsequent steps likely depend on the cell type and grade of the inflammatory state. Recently, BCP activation of PPARs, a class of nuclear receptors involved both in metabolic and inflammatory responses, has been clearly demonstrated. Direct binding of BCP has been shown only for PPARα, while available data suggest CB2-mediated PPARγ activation. Further clarification of the molecular details involved in this receptor-cross-talk will strengthen the possible therapeutic use of BCP.

Although further studies are needed to better define the systemic effects of BCP in animals, the promising results obtained so far in preclinical studies on models of metabolic and neurologic disorders strongly suggest that BCP constitute an attractive molecule for the treatment of diseases characterized by chronic inflammation.

Author Contributions: M.E.M. and P.B. conceptualized the manuscript; R.S., F.G., E.C., G.Q. drafted the manuscript; R.S., F.G., G.Q. and M.E.M. prepared the figures and table; E.C., S.A., M.P.G., M.E.M. and P.B. revised and edited the manuscript; P.B. supervised the manuscript preparation. All authors have read and agreed to the published version of the manuscript.

Funding: This work was supported by the local funding of the University of Turin and by "Fondazione Cassa di Risparmio di Torino" (Erogazioni Ordinarie 2018, grant number ID 61356).

Conflicts of Interest: The authors declare no conflict of interest. The funders had no role in the conceptualization and writing of the manuscript.

References

1. Waltenberger, B.; Mocan, A.; Šmejkal, K.; Heiss, E.H.; Atanasov, A.G. Natural products to counteract the epidemic of cardiovascular and metabolic disorders. *Molecules* **2016**, *21*, 807. [CrossRef] [PubMed]
2. Amirkia, V.; Heinrich, M. Natural products and drug discovery: A survey of stakeholders in industry and academia. *Front. Pharmacol.* **2015**, *6*, 237. [CrossRef] [PubMed]
3. Cefalu, W.; Ye, J.; Wang, Z. Efficacy of dietary supplementation with botanicals on carbohydrate metabolism in humans. *Endocr. Metab. Immune Disord. Targets* **2008**, *8*, 78–81. [CrossRef] [PubMed]
4. David, B.; Wolfender, J.L.; Dias, D.A. The pharmaceutical industry and natural products: Historical status and new trends. *Phytochem. Rev.* **2015**, *14*, 299–315. [CrossRef]
5. Francomano, F.; Caruso, A.; Barbarossa, A.; Fazio, A.; La Torre, C.; Ceramella, J.; Mallamaci, R.; Saturnino, C.; Iacopetta, D.; Sinicropi, M.S. β-caryophyllene: A sesquiterpene with countless biological properties. *Appl. Sci.* **2019**, *9*, 5420. [CrossRef]
6. Machado, K.D.C.; Islam, M.T.; Ali, E.S.; Rouf, R.; Uddin, S.J.; Dev, S.; Shilpi, J.A.; Shill, M.C.; Reza, H.M.; Das, A.K.; et al. A systematic review on the neuroprotective perspectives of beta-caryophyllene. *Phyther. Res.* **2018**, *32*, 2376–2388. [CrossRef] [PubMed]
7. Fidyt, K.; Fiedorowicz, A.; Strządała, L.; Szumny, A. B-Caryophyllene and B-Caryophyllene Oxide—Natural compounds of anticancer and analgesic properties. *Cancer Med.* **2016**, *5*, 3007–3017. [CrossRef] [PubMed]
8. Sut, S.; Maggi, F.; Nicoletti, M.; Baldan, V.; Dall'Acqua, S. New drugs from old natural compounds: Scarcely investigated sesquiterpenes as new possible therapeutic agents. *Curr. Med. Chem.* **2017**, *25*, 1241–1258. [CrossRef]
9. Sharma, C.; Al Kaabi, J.M.; Nurulain, S.N.; Goyal, S.; Amjad Kamal, M.; Ojha, S. Polypharmacological properties and therapeutic potential of β-caryophyllene: A dietary phytocannabinoid of pharmaceutical promise. *Curr. Pharm. Des.* **2016**, *22*, 3237–3264. [CrossRef] [PubMed]
10. Youssef, D.A.; El-Fayoumi, H.M.; Mahmoud, M.F. Beta-caryophyllene protects against diet-induced dyslipidemia and vascular inflammation in rats: Involvement of CB2 and PPAR-γ receptors. *Chem. Biol. Interact.* **2019**, *297*, 16–24. [CrossRef]
11. Calleja, M.A.; Vieites, J.M.; Montero-Meterdez, T.; Torres, M.I.; Faus, M.J.; Gil, A.; Suárez, A. The antioxidant effect of β-caryophyllene protects rat liver from carbon tetrachloride-induced fibrosis by inhibiting hepatic stellate cell activation. *Br. J. Nutr.* **2013**, *109*, 394–401. [CrossRef]
12. Horváth, B.; Mukhopadhyay, P.; Kechrid, M.; Patel, V.; Tanchian, G.; Wink, D.A.; Gertsch, J.; Pacher, P. β-caryophyllene ameliorates cisplatin-induced nephrotoxicity in a cannabinoid 2 receptor-dependent manner. *Free Radic. Biol. Med.* **2012**, *52*, 1325–1333. [CrossRef] [PubMed]
13. Javed, H.; Azimullah, S.; Haque, M.E.; Ojha, S.K. Cannabinoid type 2 (CB2) receptors activation protects against oxidative stress and neuroinflammation associated dopaminergic neurodegeneration in rotenone model of Parkinson's disease. *Front. Neurosci.* **2016**, *10*, 321. [CrossRef] [PubMed]
14. Picciolo, G.; Pallio, G.; Altavilla, D.; Vaccaro, M.; Oteri, G.; Irrera, N.; Squadrito, F. β-Caryophyllene reduces the inflammatory phenotype of periodontal cells by targeting CB2 receptors. *Biomedicines* **2020**, *8*, 164. [CrossRef] [PubMed]
15. Legault, J.; Pichette, A. Potentiating effect of β-caryophyllene on anticancer activity of α-humulene, isocaryophyllene and paclitaxel. *J. Pharm. Pharmacol.* **2007**, *59*, 1643–1647. [CrossRef]
16. Gertsch, J.; Leonti, M.; Raduner, S.; Racz, I.; Chen, J.Z.; Xie, X.Q.; Altmann, K.H.; Karsak, M.; Zimmer, A. Beta-caryophyllene is a dietary cannabinoid. *Proc. Natl. Acad. Sci. USA* **2008**, *105*, 9099–9104. [CrossRef]
17. Gatta-Cherifi, B.; Cota, D. Endocannabinoids and metabolic disorders. *Handb. Exp. Pharmacol.* **2015**, *231*, 367–391. [CrossRef] [PubMed]

18. Turcotte, C.; Chouinard, F.; Lefebvre, J.S.; Flamand, N. Regulation of inflammation by cannabinoids, the endocannabinoids 2-arachidonoyl-glycerol and arachidonoyl-ethanolamide, and their metabolites. *J. Leukoc. Biol.* **2015**, *97*, 1049–1070. [CrossRef]
19. Mlost, J.; Wąsik, A.; Starowicz, K. Role of endocannabinoid system in dopamine signalling within the reward circuits affected by chronic pain. *Pharmacol. Res.* **2019**, *143*, 40–47. [CrossRef]
20. Leweke, F.M.; Mueller, J.K.; Lange, B.; Fritze, S.; Topor, C.E.; Koethe, D.; Rohleder, C. Role of the endocannabinoid system in the pathophysiology of schizophrenia: Implications for pharmacological intervention. *CNS Drugs* **2018**, *32*, 605–619. [CrossRef]
21. Paula-Freire, L.I.G.; Andersen, M.L.; Gama, V.S.; Molska, G.R.; Carlini, E.L.A. The oral administration of trans-caryophyllene attenuates acute and chronic pain in mice. *Phytomedicine* **2014**, *21*, 356–362. [CrossRef]
22. Irrera, N.; D'ascola, A.; Pallio, G.; Bitto, A.; Mazzon, E.; Mannino, F.; Squadrito, V.; Arcoraci, V.; Minutoli, L.; Campo, G.M.; et al. β-Caryophyllene mitigates collagen antibody induced arthritis (CAIA) in mice through a cross-talk between CB2 and PPAR-γ receptors. *Biomolecules* **2019**, *9*, 326. [CrossRef] [PubMed]
23. Wu, C.; Jia, Y.; Lee, J.H.; Jun, H.J.; Lee, H.S.; Hwang, K.Y.; Lee, S.J. Trans-Caryophyllene is a natural agonistic ligand for peroxisome proliferator-activated receptor-α. *Bioorg. Med. Chem. Lett.* **2014**, *24*, 3168–3174. [CrossRef]
24. Johnson, S.A.; Rodriguez, D.; Allred, K. A systematic review of essential oils and the endocannabinoid system: A connection worthy of further exploration. *Evid. Complement. Altern. Med.* **2020**, *2020*, 8035301. [CrossRef]
25. Gonçalves, E.C.D.; Baldasso, G.M.; Bicca, M.A.; Paes, R.S.; Capasso, R.; Dutra, R.C. erpenoids, cannabimimetic ligands, beyond the cannabis plant. *Molecules* **2020**, *25*, 1567. [CrossRef] [PubMed]
26. Tetali, S.D. Terpenes and isoprenoids: A wealth of compounds for global use. *Planta* **2019**, *249*, 1–8. [CrossRef] [PubMed]
27. Knudsen, J.T.; Eriksson, R.; Gershenzon, J. Diversity and Distribution of Floral Scent. *Bot. Rev.* **2006**, *72*, 1. [CrossRef]
28. Maffei, M.E. Plant natural sources of the endocannabinoid (E)-β-caryophyllene: A systematic quantitative analysis of published literature. *Int. J. Mol. Sci.* **2020**, *21*, 6540. [CrossRef]
29. Martins, C.; Rueff, J.; Rodrigues, A.S. Genotoxic alkenylbenzene flavourings, a contribution to risk assessment. *Food Chem. Toxicol.* **2018**, *118*, 861–879. [CrossRef]
30. Larionov, O.V.; Corey, E.J. An unconventional approach to the enantioselective synthesis of caryophylloids. *J. Am. Chem. Soc.* **2008**, *130*, 2954–2955. [CrossRef]
31. Yang, J.; Li, Z.; Guo, L.; Du, J.; Bae, H.J. Biosynthesis of β-caryophyllene, a novel terpene-based high-density biofuel precursor, using engineered *Escherichia coli*. *Renew. Energy* **2016**, *99*, 216–223. [CrossRef]
32. Maffei, M.E. *Plant Bioactive Molecules*; Cambridge Scholars Publishing: New Castle upon Tyne, UK, 2018; ISBN 978-1-5275-1314-3.
33. Hemmerlin, A.; Hoeffler, J.F.; Meyer, O.; Tritsch, D.; Kagan, I.A.; Grosdemange-Billiard, C.; Rohmer, M.; Bach, T.J. Cross-talk between the cytosolic mevalonate and the plastidial methylerythritol phosphate pathways in tobacco bright yellow-2 cells. *J. Biol. Chem.* **2003**, *278*, 26666–26676. [CrossRef]
34. Despinasse, Y.; Fiorucci, S.; Antonczak, S.; Moja, S.; Bony, A.; Nicolè, F.; Baudino, S.; Magnard, J.L.; Jullien, F. Bornyl-diphosphate synthase from *Lavandula angustifolia*: A major monoterpene synthase involved in essential oil quality. *Phytochemistry* **2017**, *137*, 24–33. [CrossRef] [PubMed]
35. Huang, M.; Sanchez-Moreiras, A.M.; Abel, C.; Sohrabi, R.; Lee, S.; Gershenzon, J.; Tholl, D. The major volatile organic compound emitted from *Arabidopsis thaliana* flowers, the sesquiterpene (E)-β-caryophyllene, is a defense against a bacterial pathogen. *New Phytol.* **2012**, *193*, 997–1008. [CrossRef]
36. He, S.M.; Wang, X.; Yang, S.C.; Dong, Y.; Zhao, Q.M.; Yang, J.L.; Cong, K.; Zhang, J.J.; Zhang, G.H.; Wang, Y.; et al. De novo transcriptome characterization of rhodomyrtus tomentosa leaves and identification of genes involved in α/β-pinene and β-caryophyllene biosynthesis. *Front. Plant Sci.* **2018**, *9*, 1231. [CrossRef]
37. Bohlmann, J.; Meyer-Gauen, G.; Croteau, R. Plant terpenoid synthases: Molecular biology and phylogenetic analysis. *Proc. Natl. Acad. Sci. USA* **1998**, *95*, 4126–4133. [CrossRef]
38. Rynkiewicz, M.J.; Cane, D.E.; Christianson, D.W. Structure of trichodiene synthase from *Fusarium sporotrichioides* provides mechanistic inferences on the terpene cyclization cascade. *Proc. Natl. Acad. Sci. USA* **2001**, *98*, 13543–13548. [CrossRef]

39. Degenhardt, J.; Köllner, T.G.; Gershenzon, J. Monoterpene and sesquiterpene synthases and the origin of terpene skeletal diversity in plants. *Phytochemistry* **2009**, *70*, 1621–1637. [CrossRef] [PubMed]
40. Williams, D.C.; McGarvey, D.J.; Katahira, E.J.; Croteau, R. Truncation of limonene synthase preprotein provides a fully active "pseudomature" form of this monoterpene cyclase and reveals the function of the amino-terminal arginine pair. *Biochemistry* **1998**, *37*, 12213–12220. [CrossRef] [PubMed]
41. Starks, C.M.; Back, K.; Chappell, J.; Noel, J.P. Structural basis for cyclic terpene biosynthesis by tobacco 5-epi-aristolochene synthase. *Science* **1997**, *277*, 1815–1820. [CrossRef]
42. Yang, C.Q.; Wu, X.M.; Ruan, J.X.; Hu, W.L.; Mao, Y.B.; Chen, X.Y.; Wang, L.J. Isolation and characterization of terpene synthases in cotton (*Gossypium hirsutum*). *Phytochemistry* **2013**, *96*, 46–56. [CrossRef] [PubMed]
43. Huang, X.; Xiao, Y.; Köllner, T.G.; Zhang, W.; Wu, J.; Wu, J.; Guo, Y.; Zhang, Y. Identification and characterization of (E)-β-caryophyllene synthase and α/β-pinene synthase potentially involved in constitutive and herbivore-induced terpene formation in cotton. *Plant Physiol. Biochem.* **2013**, *73*, 302–308. [CrossRef]
44. Stefan, G.A.; Massimo, G.; Ma, V.; Bossi, S.; Schulze, B.; Leitner, M.; Mithöfer, A.; Boland, W. Herbivore-induced terpenoid emission in *Medicago truncatula*: Concerted action of jasmonate, ethylene and calcium signaling. *Planta* **2008**, 453–464. [CrossRef]
45. Martin, D.M.; Aubourg, S.; Schouwey, M.B.; Daviet, L.; Schalk, M.; Toub, O.; Lund, S.T.; Bohlmann, J. Functional annotation, genome organization and phylogeny of the grapevine (*Vitis vinifera*) terpene synthase gene family based on genome assembly, FLcDNA cloning, and enzyme assays. *BMC Plant Biol.* **2010**, *10*, 226. [CrossRef] [PubMed]
46. Matarese, F.; Cuzzola, A.; Scalabrelli, G.; D'Onofrio, C. Expression of terpene synthase genes associated with the formation of volatiles in different organs of *Vitis vinifera*. *Phytochemistry* **2014**, *105*, 12–24. [CrossRef] [PubMed]
47. Salvagnin, U.; Carlin, S.; Angeli, S.; Vrhovsek, U.; Anfora, G.; Malnoy, M.; Martens, S. Homologous and heterologous expression of grapevine E-(β)-caryophyllene synthase (VvGwECar2). *Phytochemistry* **2016**, *131*, 76–83. [CrossRef] [PubMed]
48. Chen, H.; Li, G.; Köllner, T.G.; Jia, Q.; Gershenzon, J.; Chen, F. Positive Darwinian selection is a driving force for the diversification of terpenoid biosynthesis in the genus Oryza. *BMC Plant Biol.* **2014**, *14*, 1–12. [CrossRef]
49. Ruilong, W.; Shaolin, P.; Rensen, Z.; Ling, W.D.; Zengfu, X.U. Cloning, expression and wounding induction of β-caryophyllene synthase gene from *Mikania micrantha* H.B.K. and allelopathic potential of β-caryophyllene. *Allelopath. J.* **2009**, *24*, 35–44.
50. Wang, R.L.; Staehelin, C.; Peng, S.L.; Wang, W.T.; Xie, X.M.; Lu, H.N. Responses of *Mikania micrantha*, an invasive weed to elevated CO2: Induction of β-caryophyllene synthase, changes in emission capability and allelopathic potential of β-caryophyllene. *J. Chem. Ecol.* **2010**, *36*, 1076–1082. [CrossRef]
51. Fujita, Y.; Koeduka, T.; Aida, M.; Suzuki, H.; Iijima, Y.; Matsui, K. Biosynthesis of volatile terpenes that accumulate in the secretory cavities of young leaves of Japanese pepper (*Zanthoxylum piperitum*): Isolation and functional characterization of monoterpene and sesquiterpene synthase genes. *Plant Biotechnol.* **2017**, *34*, 17–28. [CrossRef]
52. Chen, F.; Tholl, D.; D'Auria, J.C.; Farooq, A.; Pichersky, E.; Gershenzon, J. Biosynthesis and emission of terpenoid volatiles from *Arabidopsis* flowers. *Plant Cell* **2003**, *15*, 481–494. [CrossRef] [PubMed]
53. Hong, G.J.; Xue, X.Y.; Mao, Y.B.; Wang, L.J.; Chen, X.Y. *Arabidopsis* MYC2 interacts with DELLA proteins in regulating sesquiterpene synthase gene expression. *Plant Cell* **2012**, *24*, 2635–2648. [CrossRef] [PubMed]
54. Chuang, L.; Wen, C.H.; Lee, Y.R.; Lin, Y.L.; Hsu, L.R.; Wang, S.Y.; Chu, F.H. Identification, functional characterization, and seasonal expression patterns of five sesquiterpene synthases in *Liquidambar formosana*. *J. Nat. Prod.* **2018**, *81*, 1162–1172. [CrossRef]
55. Cai, Y.; Jia, J.W.; Crock, J.; Lin, Z.X.; Chen, X.Y.; Croteau, R. A cDNA clone for β-caryophyllene synthase from *Artemisia annua*. *Phytochemistry* **2002**, *61*, 523–529. [CrossRef]
56. Köpke, D.; Beyaert, I.; Gershenzon, J.; Hilker, M.; Schmidt, A. Species-specific responses of pine sesquiterpene synthases to sawfly oviposition. *Phytochemistry* **2010**, *71*, 909–917. [CrossRef]
57. Jin, Z.; Kwon, M.; Lee, A.R.; Ro, D.K.; Wungsintaweekul, J.; Kim, S.U. Molecular cloning and functional characterization of three terpene synthases from unripe fruit of black pepper (*Piper nigrum*). *Arch. Biochem. Biophys.* **2018**, *638*, 35–40. [CrossRef]

58. Di Marzo, V. New approaches and challenges to targeting the endocannabinoid system. *Nat. Rev. Drug Discov.* **2018**, *17*, 623–639. [CrossRef] [PubMed]
59. Shahbazi, F.; Grandi, V.; Banerjee, A.; Trant, J.F. Cannabinoids and cannabinoid receptors: The story so far. *iScience* **2020**, *23*, 101301. [CrossRef]
60. Mechoulam, R.; Gaoni, Y. A total synthesis of dl-Δ1-tetrahydrocannabinol, the active constituent of hashish. *J. Am. Chem. Soc.* **1965**, *87*, 3273–3275. [CrossRef]
61. Di Marzo, V.; Piscitelli, F. The endocannabinoid system and its modulation by phytocannabinoids. *Neurotherapeutics* **2015**, *12*, 692–698. [CrossRef]
62. Matsuda, L.A.; Lolait, S.J.; Brownstein, M.J.; Young, A.C.; Bonner, T.I. Structure of a cannabinoid receptor and functional expression of the cloned cDNA. *Nature* **1990**, *346*, 561–564. [CrossRef]
63. Munro, S.; Thomas, K.L.; Abu-Shaar, M. Molecular characterization of a peripheral receptor for cannabinoids. *Nature* **1993**, *365*, 61–65. [CrossRef] [PubMed]
64. Shao, Z.; Yin, J.; Chapman, K.; Grzemska, M.; Clark, L.; Wang, J.; Rosenbaum, D.M. High-resolution crystal structure of the human CB1 cannabinoid receptor. *Nature* **2016**, *540*, 602–606. [CrossRef]
65. Pertwee, R.G. Endocannabinoids and their pharmacological actions. *Handb. Exp. Pharmacol.* **2015**, *231*, 1–37. [CrossRef]
66. Busquets-Garcia, A.; Bains, J.; Marsicano, G. CB 1 receptor signaling in the brain: Extracting specificity from ubiquity. *Neuropsychopharmacology* **2018**, *43*, 4–20. [CrossRef]
67. Maccarrone, M.; Bab, I.; Bíró, T.; Cabral, G.A.; Dey, S.K.; Di Marzo, V.; Konje, J.C.; Kunos, G.; Mechoulam, R.; Pacher, P.; et al. Endocannabinoid signaling at the periphery: 50 years after THC. *Trends Pharmacol. Sci.* **2015**, *36*, 277–296. [CrossRef]
68. Galiègue, S.; Mary, S.; Marchand, J.; Dussossoy, D.; Carrière, D.; Carayon, P.; Bouaboula, M.; Shire, D.; LE Fur, G.; Casellas, P. Expression of central and peripheral cannabinoid receptors in human immune tissues and leukocyte subpopulations. *Eur. J. Biochem.* **1995**, *232*, 54–61. [CrossRef]
69. Gong, J.P.; Onaivi, E.S.; Ishiguro, H.; Liu, Q.R.; Tagliaferro, P.A.; Brusco, A.; Uhl, G.R. Cannabinoid CB2 receptors: Immunohistochemical localization in rat brain. *Brain Res.* **2006**, *1071*, 10–23. [CrossRef] [PubMed]
70. Aymerich, M.S.; Aso, E.; Abellanas, M.A.; Tolon, R.M.; Ramos, J.A.; Ferrer, I.; Romero, J.; Fernández-Ruiz, J. Cannabinoid pharmacology/therapeutics in chronic degenerative disorders affecting the central nervous system. *Biochem. Pharmacol.* **2018**, *157*, 67–84. [CrossRef] [PubMed]
71. Irrera, N.; D'ascola, A.; Pallio, G.; Bitto, A.; Mannino, F.; Arcoraci, V.; Rottura, M.; Ieni, A.; Minutoli, L.; Metro, D.; et al. β-caryophyllene inhibits cell proliferation through a direct modulation of CB2 receptors in glioblastoma cells. *Cancers* **2020**, *12*, 1038. [CrossRef]
72. Berger, G.; Arora, N.; Burkovskiy, I.; Xia, Y.; Chinnadurai, A.; Westhofen, R.; Hagn, G.; Cox, A.; Kelly, M.; Zhou, J.; et al. Experimental cannabinoid 2 receptor activation by phyto-derived and synthetic cannabinoid ligands in LPS-Induced interstitial cystitis in mice. *Molecules* **2019**, *24*, 4239. [CrossRef]
73. Aly, E.; Khajah, M.A.; Masocha, W. β-caryophyllene, a CB2-receptor-selective phytocannabinoid, suppresses mechanical allodynia in a mouse model of antiretroviral-induced neuropathic pain. *Molecules* **2020**, *25*, 106. [CrossRef] [PubMed]
74. Hong, F.; Pan, S.; Guo, Y.; Xu, P.; Zhai, Y. PPARs as nuclear receptors for nutrient and energy metabolism. *Molecules* **2019**, *24*, 2545. [CrossRef] [PubMed]
75. Lalwani, N.D.; Fahl, W.E.; Reddy, J.K. Detection of a nafenopin-binding protein in rat liver cytosol associated with the induction of peroxisome proliferation by hypolipidemic compounds. *Biochem. Biophys. Res. Commun.* **1983**, *116*, 388–393. [CrossRef]
76. Issemann, I.; Green, S. Activation of a member of the steroid hormone receptor superfamily by peroxisome proliferators. *Nature* **1990**, *347*, 645–650. [CrossRef]
77. Dreyer, C.; Krey, G.; Keller, H.; Givel, F.; Helftenbein, G.; Wahli, W. Control of the peroxisomal β-oxidation pathway by a novel family of nuclear hormone receptors. *Cell* **1992**, *68*, 879–887. [CrossRef]
78. Kamikubo, R.; Kai, K.; Tsuji-Naito, K.; Akagawa, M. β-Caryophyllene attenuates palmitate-induced lipid accumulation through AMPK signaling by activating CB2 receptor in human HepG2 hepatocytes. *Mol. Nutr. Food Res.* **2016**, *60*, 2228–2242. [CrossRef]
79. Kersten, S.; Stienstra, R. The role and regulation of the peroxisome proliferator activated receptor alpha in human liver. *Biochimie* **2017**, *136*, 75–84. [CrossRef]

80. Corrales, P.; Izquierdo-Lahuerta, A.; Medina-Gómez, G. Maintenance of kidney metabolic homeostasis by PPAR gamma. *Int. J. Mol. Sci.* **2018**, *19*, 2063. [CrossRef]
81. Vázquez-Carrera, M. Unraveling the effects of PPARβ/δ on insulin resistance and cardiovascular disease. *Trends Endocrinol. Metab.* **2016**, *27*, 319–334. [CrossRef]
82. Janani, C.; Ranjitha Kumari, B.D. PPAR gamma gene—A review. *Diabetes Metab. Syndr. Clin. Res. Rev.* **2015**, *9*, 46–50. [CrossRef] [PubMed]
83. Kliewer, S.A.; Forman, B.M.; Blumberg, B.; Ong, E.S.; Borgmeyer, U.; Mangelsdorf, D.J.; Umesono, K.; Evans, R.M. Differential expression and activation of a family of murine peroxisome proliferator-activated receptors. *Proc. Natl. Acad. Sci. USA* **1994**, *91*, 7355–7359. [CrossRef] [PubMed]
84. Tontonoz, P.; Graves, R.A.; Budavari, A.I.; Erdjument-bromage, H.; Lui, M.; Hu, E.; Tempst, P.; Spiegelman, B.M. Adipocyte-specific transcription factor ARF6 is a heterodimeric complex of two nuclear hormone receptors, PPAR7 and RXRa. *Nucleic Acids Res.* **1994**, *22*, 5628–5634. [CrossRef] [PubMed]
85. Yamaguchi, M.; Levy, R.M. β-caryophyllene promotes osteoblastic mineralization, and suppresses osteoclastogenesis and adipogenesis in mouse bone marrow cultures *in vitro*. *Exp. Ther. Med.* **2016**, *12*, 3602–3606. [CrossRef]
86. Berger, J.; Moller, D.E. The mechanisms of action of PPARs. *Annu. Rev. Med.* **2002**, *53*, 409–435. [CrossRef]
87. Viswakarma, N.; Jia, Y.; Bai, L.; Vluggens, A.; Borensztajn, J.; Xu, J.; Reddy, J.K. Coactivators in PPAR-regulated gene expression. *PPAR Res.* **2010**, *2010*, 250126. [CrossRef]
88. Bento, A.F.; Marcon, R.; Dutra, R.C.; Claudino, R.F.; Cola, M.; Leite, D.F.P.; Calixto, J.B. β-caryophyllene inhibits dextran sulfate sodium-induced colitis in mice through CB2 receptor activation and PPARγ pathway. *Am. J. Pathol.* **2011**, *178*, 1153–1166. [CrossRef]
89. Cheng, Y.; Dong, Z.; Liu, S. β-caryophyllene ameliorates the Alzheimer-like phenotype in APP/PS1 mice through CB2 receptor activation and the PPARγ pathway. *Pharmacology* **2014**, *94*, 1–12. [CrossRef]
90. Askari, V.R.; Shafiee-Nick, R. Promising neuroprotective effects of β-caryophyllene against LPS-induced oligodendrocyte toxicity: A mechanistic study. *Biochem. Pharmacol.* **2019**, *159*, 154–171. [CrossRef]
91. Youssef, D.A.; El-Fayoumi, H.M.; Mahmoud, M.F. Beta-caryophyllene alleviates diet-induced neurobehavioral changes in rats: The role of CB2 and PPAR-γ receptors. *Biomed. Pharmacother.* **2019**, *110*, 145–154. [CrossRef]
92. Hotamisligil, G.S. Inflammation and metabolic disorders. *Nature* **2006**, *444*, 860–867. [CrossRef]
93. Wellen, K.E.; Hotamisligil, G.S. Inflammation, stress, and diabetes. *J. Clin. Investig.* **2005**, *115*, 1111–1119. [CrossRef] [PubMed]
94. Saltiel, A.R.; Olefsky, J.M. Inflammatory mechanisms linking obesity and metabolic disease. *J. Clin. Investig.* **2017**, *127*, 1–4. [CrossRef] [PubMed]
95. Arrese, M.; Cabrera, D.; Kalergis, A.M.; Feldstein, A.E. Innate immunity and inflammation in NAFLD/NASH. *Dig. Dis. Sci.* **2016**, *61*, 1294–1303. [CrossRef]
96. Joshi, N.; Singh, S. Updates on immunity and inflammation in Parkinson disease pathology. *J. Neurosci. Res.* **2018**, *96*, 379–390. [CrossRef]
97. Forloni, G.; Balducci, C. Alzheimer's disease, oligomers, and inflammation. *J. Alzheimer's Dis.* **2018**, *62*, 1261–1276. [CrossRef] [PubMed]
98. Feghali, C.A.; Wright, T.M. Cytokines in acute and chronic inflammation. *Front. Biosci.* **1997**, *2*, d12–d26. [CrossRef] [PubMed]
99. Rogero, M.M.; Calder, P.C. Obesity, inflammation, toll-like receptor 4 and fatty acids. *Nutrients* **2018**, *10*, 432. [CrossRef]
100. Villarroya, F.; Cereijo, R.; Gavaldà-Navarro, A.; Villarroya, J.; Giralt, M. Inflammation of brown/beige adipose tissues in obesity and metabolic disease. *J. Intern. Med.* **2018**, *284*, 492–504. [CrossRef]
101. Hotamisligil, G.S. Inflammation, metaflammation and immunometabolic disorders. *Nature* **2017**, *542*, 177–185. [CrossRef]
102. Ertunc, M.E.; Hotamisligil, G.S. Lipid signaling and lipotoxicity in metaflammation: Indications for metabolic disease pathogenesis and treatment. *J. Lipid Res.* **2016**, *57*, 2099–2114. [CrossRef]
103. Caputo, T.; Gilardi, F.; Desvergne, B. From chronic overnutrition to metaflammation and insulin resistance: Adipose tissue and liver contributions. *FEBS Lett.* **2017**, *591*, 3061–3088. [CrossRef] [PubMed]
104. Shapouri-Moghaddam, A.; Mohammadian, S.; Vazini, H.; Taghadosi, M.; Esmaeili, S.A.; Mardani, F.; Seifi, B.; Mohammadi, A.; Afshari, J.T.; Sahebkar, A. Macrophage plasticity, polarization, and function in health and disease. *J. Cell. Physiol.* **2018**, *233*, 6425–6440. [CrossRef]

105. Lumeng, C.N.; Bodzin, J.L.; Saltiel, A.R. Obesity induces a phenotypic switch in adipose tissue macrophage polarization. *J. Clin. Investig.* **2007**, *117*, 175–184. [CrossRef] [PubMed]
106. Mclaughlin, T.; Ackerman, S.E.; Shen, L.; Engleman, E. Role of innate and adaptive immunity in obesity-associated metabolic disease. *J. Clin. Investig.* **2017**, *127*, 5–13. [CrossRef] [PubMed]
107. De Heredia, F.P.; Gómez-Martínez, S.; Marcos, A. Chronic and degenerative diseases: Obesity, inflammation and the immune system. *Proc. Nutr. Soc.* **2012**, *71*, 332–338. [CrossRef] [PubMed]
108. Dandona, P.; Aljada, A.; Bandyopadhyay, A. Inflammation: The link between insulin resistance, obesity and diabetes. *Trends Immunol.* **2004**, *25*, 4–7. [CrossRef]
109. Hotamisligil, G.S.; Shargill, N.S.; Spiegelman, B.M. Adipose expression of tumor necrosis factor-α: Direct role in obesity-linked insulin resistance. *Science* **1993**, *259*, 87–91. [CrossRef]
110. Uysal, K.T.; Wiesbrock, S.M.; Marino, M.W.; Hotamisligil, G.S. Protection from obesity-induced insulin resistance in mice lacking TNF- α function. *Nature* **1997**, *389*, 610–614. [CrossRef]
111. Kern, P.A.; Saghizadeh, M.; Ong, J.M.; Bosch, R.J.; Deem, R.; Simsolo, R.B. The expression of tumor necrosis factor in human adipose tissue: Regulation by obesity, weight loss, and relationship to lipoprotein lipase. *J. Clin. Investig.* **1995**, *95*, 2111–2119. [CrossRef]
112. Yu, C.; Chen, Y.; Cline, G.W.; Zhang, D.; Zong, H.; Wang, Y.; Bergeron, R.; Kim, J.K.; Cushman, S.W.; Cooney, G.J.; et al. Mechanism by which fatty acids inhibit insulin activation of insulin receptor substrate-1 (IRS-1)-associated phosphatidylinositol 3-kinase activity in muscle. *J. Biol. Chem.* **2002**, *277*, 50230–50236. [CrossRef] [PubMed]
113. Glass, C.K.; Ogawa, S. Combinatorial roles of nuclear receptors in inflammation and immunity. *Nat. Rev. Immunol.* **2006**, *6*, 44–55. [CrossRef] [PubMed]
114. Chawla, A.; Repa, J.J.; Evans, R.M.; Mangelsdorf, D.J. Nuclear receptors and lipid physiology: Opening the x-files. *Science* **2001**, *294*, 1866–1870. [CrossRef] [PubMed]
115. Fessler, M.B.; Rudel, L.L.; Brown, J.M. Toll-like receptor signaling links dietary fatty acids to the metabolic syndrome. *Curr. Opin. Lipidol.* **2009**, *20*, 379–385. [CrossRef] [PubMed]
116. Engin, A. Non-alcoholic fatty liver disease. *Adv. Exp. Med. Biol.* **2017**, *960*, 443–467. [CrossRef] [PubMed]
117. Pawlak, M.; Lefebvre, P.; Staels, B. Molecular mechanism of PPARα action and its impact on lipid metabolism, inflammation and fibrosis in non-alcoholic fatty liver disease. *J. Hepatol.* **2015**, *62*, 720–733. [CrossRef]
118. Gervois, P.; Kleemann, R.; Pilon, A.; Percevault, F.; Koenig, W.; Staels, B.; Kooistra, T. Global suppression of IL-6-induced acute phase response gene expression after chronic in vivo treatment with the peroxisome proliferator-activated receptor-α activator fenofibrate. *J. Biol. Chem.* **2004**, *279*, 16154–16160. [CrossRef]
119. Seo, D.Y.; Heo, J.W.; Ko, J.R.; Kwak, H.B. Exercise and neuroinflammation in health and disease. *Int. Neurourol. J.* **2019**, *23*, S82–S92. [CrossRef]
120. Heindel, J.J.; Blumberg, B.; Cave, M.; Machtinger, R.; Mantovani, A.; Mendez, M.A.; Nadal, A.; Palanza, P.; Panzica, G.; Sargis, R.; et al. Metabolism disrupting chemicals and metabolic disorders. *Reprod. Toxicol.* **2017**, *68*, 3–33. [CrossRef]
121. Scotti, L.; Monteiro, A.F.M.; de Oliveira Viana, J.; Mendonça Junior, F.J.B.; Ishiki, H.M.; Tchouboun, E.N.; Santos, R.; Scotti, M.T. Multi-target drugs against metabolic disorders. *Endocr. Metab. Immune Disord. Drug Targets* **2018**, *19*, 402–418. [CrossRef]
122. van Dijk, S.J.; Tellam, R.L.; Morrison, J.L.; Muhlhausler, B.S.; Molloy, P.L. Recent developments on the role of epigenetics in obesity and metabolic disease. *Clin. Epigenetics* **2015**, *7*. [CrossRef]
123. Rochlani, Y.; Pothineni, N.V.; Kovelamudi, S.; Mehta, J.L. Metabolic syndrome: Pathophysiology, management, and modulation by natural compounds. *Ther. Adv. Cardiovasc. Dis.* **2017**, *11*, 215–225. [CrossRef] [PubMed]
124. Galassi, A.; Reynolds, K.; He, J. Metabolic syndrome and risk of cardiovascular disease: A meta-analysis. *Am. J. Med.* **2006**, *119*, 812–819. [CrossRef] [PubMed]
125. Neeland, I.J.; Poirier, P.; Després, J.P. Cardiovascular and metabolic heterogeneity of obesity: Clinical challenges and implications for management. *Circulation* **2018**, *137*, 1391–1406. [CrossRef]
126. Baldissera, M.D.; Souza, C.F.; Grando, T.H.; Doleski, P.H.; Boligon, A.A.; Stefani, L.M.; Monteiro, S.G. Hypolipidemic effect of β-caryophyllene to treat hyperlipidemic rats. *Naunyn. Schmiedebergs. Arch. Pharmacol.* **2017**, *390*, 215–223. [CrossRef]
127. Ríos, J.L.; Francini, F.; Schinella, G.R. Natural products for the treatment of type 2 diabetes mellitus. *Planta Med.* **2015**, *81*, 975–994. [CrossRef] [PubMed]

128. Tran, N.; Pham, B.; Le, L. Bioactive compounds in anti-diabetic plants: From herbal medicine to modern drug discovery. *Biology* **2020**, *9*, 252. [CrossRef]
129. Cheng, C.; Zhuo, S.; Zhang, B.; Zhao, X.; Liu, Y.; Liao, C.; Quan, J.; Li, Z.; Bode, A.M.; Cao, Y.; et al. Treatment implications of natural compounds targeting lipid metabolism in nonalcoholic fatty liver disease, obesity and cancer. *Int. J. Biol. Sci.* **2019**, *15*, 1654–1663. [CrossRef]
130. Xu, G.; Huang, K.; Zhou, J. Hepatic AMP Kinase as a potential target for treating nonalcoholic fatty liver disease: Evidence from studies of natural products. *Curr. Med. Chem.* **2017**, *25*, 889–907. [CrossRef]
131. Kumawat, V.S.; Kaur, G. Insulinotropic and antidiabetic effects of β-caryophyllene with L-arginine in type 2 diabetic rats. *J. Food Biochem.* **2020**, *44*, e13156. [CrossRef]
132. Zheng, X.; Sun, T.; Wang, X. Activation of type 2 cannabinoid receptors (CB2R) promotes fatty acid oxidation through the SIRT1/PGC-1α pathway. *Biochem. Biophys. Res. Commun.* **2013**, *436*, 377–381. [CrossRef] [PubMed]
133. Geddo, F.; Scandiffio, R.; Antoniotti, S.; Cottone, E.; Querio, G.; Maffei, M.E.; Bovolin, P.; Gallo, M.P. Pipenig®-FL, a fluid extract of black pepper (*Piper nigrum L.*) with a high standardized content of trans-β-caryophyllene, reduces lipid accumulation in 3T3-L1 preadipocytes and improves glucose uptake in C2C12 myotubes. *Nutrients* **2019**, *11*, 2788. [CrossRef] [PubMed]
134. Jung, J.I.; Kim, E.J.; Kwon, G.T.; Jung, Y.J.; Park, T.; Kim, Y.; Yu, R.; Choi, M.-S.; Chun, H.S.; Kwon, S.-H.; et al. β-Caryophyllene potently inhibits solid tumor growth and lymph node metastasis of B16F10 melanoma cells in high-fat diet-induced obese C57BL/6N mice. *Carcinogenesis* **2015**, *36*, 1028–1039. [CrossRef] [PubMed]
135. Harb, A.A.; Bustanji, Y.K.; Abdalla, S.S. Hypocholesterolemic effect of β-caryophyllene in rats fed cholesterol and fat enriched diet. *J. Clin. Biochem. Nutr.* **2018**, *62*, 230–237. [CrossRef]
136. Arizuka, N.; Murakami, T.; Suzuki, K. The effect of β-caryophyllene on nonalcoholic steatohepatitis. *J. Toxicol. Pathol.* **2017**, *30*, 263–273. [CrossRef]
137. Ames-Sibin, A.P.; Barizão, C.L.; Castro-Ghizoni, C.V.; Silva, F.M.S.; Sá-Nakanishi, A.B.; Bracht, L.; Bersani-Amado, C.A.; Marçal-Natali, M.R.; Bracht, A.; Comar, J.F. β-Caryophyllene, the major constituent of copaiba oil, reduces systemic inflammation and oxidative stress in arthritic rats. *J. Cell. Biochem.* **2018**, *119*, 10262–10277. [CrossRef]
138. Basha, R.H.; Sankaranarayanan, C. β-Caryophyllene, a natural sesquiterpene, modulates carbohydrate metabolism in streptozotocin-induced diabetic rats. *Acta Histochem.* **2014**, *116*, 1469–1479. [CrossRef]
139. Basha, R.H.; Sankaranarayanan, C. β-Caryophyllene, a natural sesquiterpene lactone attenuates hyperglycemia mediated oxidative and inflammatory stress in experimental diabetic rats. *Chem. Biol. Interact.* **2016**, *245*, 50–58. [CrossRef]
140. Younis, N.S.; Mohamed, M.E. β-Caryophyllene as a potential protective agent against myocardial injury: The role of Toll-like receptors. *Molecules* **2019**, *24*, 1929. [CrossRef]
141. Al-Taee, H.; Azimullah, S.; Meeran, M.F.N.; Alaraj Almheiri, M.K.; Al Jasmi, R.A.; Tariq, S.; AB Khan, M.; Adeghate, E.; Ojha, S. β-caryophyllene, a dietary phytocannabinoid attenuates oxidative stress, inflammation, apoptosis and prevents structural alterations of the myocardium against doxorubicin-induced acute cardiotoxicity in rats: An in vitro and in vivo study. *Eur. J. Pharmacol.* **2019**, *858*, 172467. [CrossRef]
142. Meeran, M.F.N.; Al Taee, H.; Azimullah, S.; Tariq, S.; Adeghate, E.; Ojha, S. β-Caryophyllene, a natural bicyclic sesquiterpene attenuates doxorubicin-induced chronic cardiotoxicity via activation of myocardial cannabinoid type-2 (CB2) receptors in rats. *Chem. Biol. Interact.* **2019**, *304*, 158–167. [CrossRef] [PubMed]
143. Speakman, J.R.; O'rahilly, S. Fat: An evolving issue. *Dis. Model. Mech.* **2012**, *5*, 569–573. [CrossRef]
144. Obesity and Overweight. Available online: https://www.who.int/news-room/fact-sheets/detail/obesity-and-overweight (accessed on 20 August 2020).
145. Klop, B.; Elte, J.W.F.; Cabezas, M.C. Dyslipidemia in obesity: Mechanisms and potential targets. *Nutrients* **2013**, *5*, 1218–1240. [CrossRef] [PubMed]
146. Anderson, T.J.; Mancini, G.B.J.; Genest, J.; Grégoire, J.; Lonn, E.M.; Hegele, R.A. The new dyslipidemia guidelines: What is the debate? *Can. J. Cardiol.* **2015**, *31*, 605–612. [CrossRef] [PubMed]
147. Wickramasinghe, M.; Weaver, J.U. Lipid disorders in obesity. In *Practical Guide to Obesity Medicine*; Elsevier: Amsterdam, The Netherlands, 2018; pp. 99–108. [CrossRef]
148. Izaola, O.; de Luis, D.; Sajoux, I.; Domingo, J.C.; Vidal, M. Inflamación y obesidad (Lipoinflamación). *Nutr. Hosp.* **2015**, *31*, 2352–2358. [CrossRef] [PubMed]

149. Maurizi, G.; Della Guardia, L.; Maurizi, A.; Poloni, A. Adipocytes properties and crosstalk with immune system in obesity-related inflammation. *J. Cell. Physiol.* **2018**, *233*, 88–97. [CrossRef] [PubMed]
150. Idilman, I.S.; Ozdeniz, I.; Karcaaltincaba, M. Hepatic steatosis: Etiology, patterns, and quantification. *Semin. Ultrasound CT MRI* **2016**, *37*, 501–510. [CrossRef]
151. de Alwis, N.M.W.; Day, C.P. Non-alcoholic fatty liver disease: The mist gradually clears. *J. Hepatol.* **2008**, *48*, S104–S112. [CrossRef]
152. Cruz, N.G.; Sousa, L.P.; Sousa, M.O.; Pietrani, N.T.; Fernandes, A.P.; Gomes, K.B. The linkage between inflammation and Type 2 diabetes mellitus. *Diabetes Res. Clin. Pract.* **2013**, *99*, 85–92. [CrossRef]
153. Halim, M.; Halim, A. The effects of inflammation, aging and oxidative stress on the pathogenesis of diabetes mellitus (type 2 diabetes). *Diabetes Metab. Syndr. Clin. Res. Rev.* **2019**, *13*, 1165–1172. [CrossRef]
154. Lontchi-Yimagou, E.; Sobngwi, E.; Matsha, T.E.; Kengne, A.P. Diabetes mellitus and inflammation. *Curr. Diab. Rep.* **2013**, *13*, 435–444. [CrossRef] [PubMed]
155. Calle, M.C.; Fernandez, M.L. Inflammation and type 2 diabetes. *Diabetes Metab.* **2012**, *38*, 183–191. [CrossRef] [PubMed]
156. Suijun, W.; Zhen, Y.; Ying, G.; Yanfang, W. A role for trans-caryophyllene in the moderation of insulin secretion. *Biochem. Biophys. Res. Commun.* **2014**, *444*, 451–454. [CrossRef] [PubMed]
157. Christia, P.; Frangogiannis, N.G. Targeting inflammatory pathways in myocardial infarction. *Eur. J. Clin. Investig.* **2013**, *43*, 986–995. [CrossRef] [PubMed]
158. Wong, B.W.; Meredith, A.; Lin, D.; McManus, B.M. The biological role of inflammation in atherosclerosis. *Can. J. Cardiol.* **2012**, *28*, 631–641. [CrossRef]
159. Raggi, P.; Genest, J.; Giles, J.T.; Rayner, K.J.; Dwivedi, G.; Beanlands, R.S.; Gupta, M. Role of inflammation in the pathogenesis of atherosclerosis and therapeutic interventions. *Atherosclerosis* **2018**, *276*, 98–108. [CrossRef]
160. Weber, C.; Noels, H. Atherosclerosis: Current pathogenesis and therapeutic options. *Nat. Med.* **2011**, *17*, 1410–1422. [CrossRef]
161. Scolaro, B.; Soo Jin Kim, H.; de Castro, I.A. Bioactive compounds as an alternative for drug co-therapy: Overcoming challenges in cardiovascular disease prevention. *Crit. Rev. Food Sci. Nutr.* **2018**, *58*, 958–971. [CrossRef]
162. Baldissera, M.D.; Souza, C.F.; Grando, T.H.; Stefani, L.M.; Monteiro, S.G. β-caryophyllene reduces atherogenic index and coronary risk index in hypercholesterolemic rats: The involvement of cardiac oxidative damage. *Chem. Biol. Interact.* **2017**, *270*, 9–14. [CrossRef]
163. Octavia, Y.; Tocchetti, C.G.; Gabrielson, K.L.; Janssens, S.; Crijns, H.J.; Moens, A.L. Doxorubicin-induced cardiomyopathy: From molecular mechanisms to therapeutic strategies. *J. Mol. Cell. Cardiol.* **2012**, *52*, 1213–1225. [CrossRef]
164. Wong, J.J.; Côté, P.; Tricco, A.C.; Rosella, L.C. Examining the effects of low back pain and mental health symptoms on healthcare utilisation and costs: A protocol for a population-based cohort study. *BMJ Open* **2019**, *9*, e031749. [CrossRef] [PubMed]
165. Rom, S.; Persidsky, Y. Cannabinoid receptor 2: Potential role in immunomodulation and neuroinflammation. *J. Neuroimmune Pharmacol.* **2013**, *8*, 608–620. [CrossRef]
166. Ibrahim, M.M.; Porreca, F.; Lai, J.; Albrecht, P.J.; Rice, F.L.; Khodorova, A.; Davar, G.; Makriyannis, A.; Vanderah, T.W.; Mata, H.P.; et al. CB2 cannabinoid receptor activation produces antinociception by stimulating peripheral release of endogenous opioids. *Proc. Natl. Acad. Sci. USA* **2005**, *102*, 3093–3098. [CrossRef]
167. Klauke, A.L.; Racz, I.; Pradier, B.; Markert, A.; Zimmer, A.M.; Gertsch, J.; Zimmer, A. The cannabinoid CB2 receptor-selective phytocannabinoid beta-caryophyllene exerts analgesic effects in mouse models of inflammatory and neuropathic pain. *Eur. Neuropsychopharmacol.* **2014**, *24*, 608–620. [CrossRef]
168. Fernandes, E.S.; Passos, G.F.; Medeiros, R.; da Cunha, F.M.; Ferreira, J.; Campos, M.M.; Pianowski, L.F.; Calixto, J.B. Anti-inflammatory effects of compounds alpha-humulene and (-)-trans-caryophyllene isolated from the essential oil of *Cordia verbenacea*. *Eur. J. Pharmacol.* **2007**, *569*, 228–236. [CrossRef] [PubMed]
169. Segat, G.C.; Manjavachi, M.N.; Matias, D.O.; Passos, G.F.; Freitas, C.S.; Costa, R.; Calixto, J.B. Antiallodynic effect of β-caryophyllene on paclitaxel-induced peripheral neuropathy in mice. *Neuropharmacology* **2017**, *125*, 207–219. [CrossRef] [PubMed]

170. Hernandez-Leon, A.; González-Trujano, M.E.; Narváez-González, F.; Pérez-Ortega, G.; Rivero-Cruz, F.; Aguilar, M.I. Role of β-caryophyllene in the antinociceptive and anti-inflammatory effects of *Tagetes lucida* Cav. Essential oil. *Molecules* **2020**, *25*, 675. [CrossRef]
171. Katsuyama, S.; Mizoguchi, H.; Kuwahata, H.; Komatsu, T.; Nagaoka, K.; Nakamura, H.; Bagetta, G.; Sakurada, T.; Sakurada, S. Involvement of peripheral cannabinoid and opioid receptors in β-caryophyllene-induced antinociception. *Eur. J. Pain* **2013**, *17*, 664–675. [CrossRef] [PubMed]
172. Wang, J.T.; Medress, Z.A.; Barres, B.A. Axon degeneration: Molecular mechanisms of a self-destruction pathway. *J. Cell Biol.* **2012**, *196*, 7–18. [CrossRef] [PubMed]
173. Neukomm, L.J.; Freeman, M.R. Diverse cellular and molecular modes of axon degeneration. *Trends Cell Biol.* **2014**, *S24*, 515–523. [CrossRef]
174. Ojha, S.; Javed, H.; Azimullah, S.; Haque, M.E. β-Caryophyllene, a phytocannabinoid attenuates oxidative stress, neuroinflammation, glial activation, and salvages dopaminergic neurons in a rat model of Parkinson disease. *Mol. Cell. Biochem.* **2016**, *418*, 59–70. [CrossRef] [PubMed]
175. Viveros-Paredes, J.M.; González-Castañeda, R.E.; Gertsch, J.; Chaparro-Huerta, V.; López-Roa, R.I.; Vázquez-Valls, E.; Beas-Zarate, C.; Camins-Espuny, A.; Flores-Soto, M.E. Neuroprotective Effects of β-caryophyllene against dopaminergic neuron injury in a murine model of Parkinson's disease induced by MPTP. *Pharmaceuticals* **2017**, *10*, 60. [CrossRef]
176. Fontes, L.B.A.; Dias, D.D.S.; Aarestrup, B.J.V.; Aarestrup, F.M.; Da Silva Filho, A.A.; do Corrêa, J.O.A. β-Caryophyllene ameliorates the development of experimental autoimmune encephalomyelitis in C57BL/6 mice. *Biomed. Pharmacother.* **2017**, *91*, 257–264. [CrossRef] [PubMed]
177. Fisher, R.S.; Van Emde Boas, W.; Blume, W.; Elger, C.; Genton, P.; Lee, P.; Engel, J. Response: Definitions proposed by the International League Against Epilepsy (ILAE) and the International Bureau for Epilepsy (IBE). *Epilepsia* **2005**, *46*, 1701–1702. [CrossRef]
178. Álvarez-González, I.; Madrigal-Bujaidar, E.; Castro-García, S. Antigenotoxic capacity of beta-caryophyllene in mouse, and evaluation of its antioxidant and GST induction activities. *J. Toxicol. Sci.* **2014**, *39*, 849–859. [CrossRef]
179. De Oliveira, C.C.; de Oliveira, C.V.; Grigoletto, J.; Ribeiro, L.R.; Funck, V.R.; Grauncke, A.C.B.; de Souza, T.L.; Souto, N.S.; Furian, A.F.; Menezes, I.R.A.; et al. Anticonvulsant activity of β-caryophyllene against pentylenetetrazol-induced seizures. *Epilepsy Behav.* **2016**, *56*, 26–31. [CrossRef]
180. Tchekalarova, J.; da Conceição Machado, K.; Gomes Júnior, A.L.; de Carvalho Melo Cavalcante, A.A.; Momchilova, A.; Tzoneva, R. Pharmacological characterization of the cannabinoid receptor 2 agonist, β-caryophyllene on seizure models in mice. *Seizure* **2018**, *57*, 22–26. [CrossRef]

nutrients

MDPI

Article

PipeNig®-FL, a Fluid Extract of Black Pepper (*Piper Nigrum* L.) with a High Standardized Content of *Trans*-β-Caryophyllene, Reduces Lipid Accumulation in 3T3-L1 Preadipocytes and Improves Glucose Uptake in C2C12 Myotubes

Federica Geddo [1,†], Rosaria Scandiffio [1,†], Susanna Antoniotti [1], Erika Cottone [1], Giulia Querio [1], Massimo E. Maffei [2], Patrizia Bovolin [1] and Maria Pia Gallo [1,*]

[1] Department of Life Sciences and Systems Biology, University of Turin, Via Accademia Albertina 13, 10123 Turin, Italy; federica.geddo@unito.it (F.G.); rosaria.scandiffio@unito.it (R.S.); susanna.antoniotti@unito.it (S.A.); erika.cottone@unito.it (E.C.); giulia.querio@unito.it (G.Q.); patrizia.bovolin@unito.it (P.B.)

[2] Plant Physiology Unit, Department of Life Sciences and Systems Biology, University of Turin, Via Quarello 15/a, 10135 Turin, Italy; massimo.maffei@unito.it

* Correspondence: mariapia.gallo@unito.it; Tel.: +39-011-670-4671

† These authors equally contributed to this work.

Received: 10 October 2019; Accepted: 13 November 2019; Published: 15 November 2019

Abstract: *Trans*-β-caryophyllene (BCP) is a natural sesquiterpene hydrocarbon with several important pharmacological activities, including antioxidant, anti-inflammatory, anticancer, and cardioprotective functions. These properties are mainly due to its selective interaction with the peripherally expressed cannabinoid receptor 2. In addition, BCP activates peroxisome proliferated activator receptors α and γ and inhibits the Toll-like receptor signaling pathway. Given the growing scientific interest in BCP, the aim of our study was to investigate the metabolic effects of a black pepper extract (PipeNig®-FL), containing a high standardized content of BCP. In particular our interest was focused on its potential activity on lipid accumulation and glucose uptake. The extract PipeNig®-FL was chemically characterized by gas chromatography–mass spectrometry (GC–MS) and gas chromatography with flame-ionization detection (GC–FID), confirming a high content (814 mg/g) of BCP. Experiments were performed on 3T3-L1 preadipocytes and on C2C12 myotubes. Lipid content following 3T3-L1 adipogenic differentiation was quantified with AdipoRed fluorescence staining. Glucose uptake and GLUT4 membrane translocation were studied in C2C12 myotubes with the fluorescent glucose analog 2-NBDG and by immunofluorescence analysis. Here we show that PipeNig®-FL reduces 3T3-L1 adipocyte differentiation and lipid accumulation. Moreover, acute exposure of C2C12 myotubes to PipeNig®-FL improves glucose uptake activity and GLUT4 migration. Taken together, these results reveal interesting and novel properties of BCP, suggesting potential applications in the prevention of lipid accumulation and in the improvement of glucose uptake.

Keywords: *trans*-β-caryophyllene; adipogenesis; lipid accumulation; glucose uptake; GLUT4; black pepper

1. Introduction

Metabolic syndrome is a non-communicable disease characterized by visceral adiposity, insulin resistance, hyperlipidemia, hypertension and a chronic low-grade inflammatory state, often dragging into the onset of type 2 diabetes, coronary disease, stroke, and other disabilities. This chronic illness

represents a major health hazard in the modern population, being rapidly spread from Western to developing countries [1]. The multiple biological mechanisms included in metabolic syndrome provide a complex interorgan communication, involving adipokines, macrophages, endoplasmic reticulum stress, thyroid hormones, beta adrenergic hormones, gut microbiome and other factors, where epigenetic drivers represent the major component with respect to genetic predisposition [1]. The pharmacological treatment of metabolic syndrome commonly involves anti-obesity drugs, thiazolidinediones (TZDs), metformin, statins, fibrates and several other drugs [2], but its management chiefly lies in the adoption of a healthy lifestyle [3]. In this perspective, many studies and clinical trials highlight some quality diets, such as the Mediterranean diet, the Nordic diet, and the Dietary Approaches to Stop Hypertension (DASH) diet, to protect against metabolic syndrome or to improve its phenotype. Moreover, plants and plant-derived molecules have received great attention as complementary supports in managing metabolic dysfunctions [4]. As an example, *Piper nigrum*, a widely used spice, has been present in traditional medicine of different countries all over the world since ancient times due to the beneficial effects of its biologically active extracts, underlining its possible use in the treatment of metabolic syndrome or other related conditions [5]. Among active compounds naturally present in *Piper nigrum*, the dietary cannabinoid *trans*-β-caryophyllene (BCP) could be considered as a possible key component in the treatment of obesity and type 2 diabetes in the metabolic syndrome scenario [6].

BCP is a bicyclic sesquiterpene hydrocarbon, highly present in a consistent number of plant-derived essential oils, such as balsams of *Copaiba* spp. (up to 53%), black pepper (*Piper nigrum*, up to 70%), lemon balm (*Melissa officinalis*, up to 19%), cloves (*Syzygium aromaticum*, up to 12%) and hops (*Humulus lupulus*, up to 9%) [7]. The Research Institute for Fragrance Materials (RIFM) evaluated BCP safety [8] and it has been approved by the Food and Drug Administration and by the European Food Safety Authority as a flavoring agent, usable in cosmetic and food additives. In recent years, many studies reported the beneficial properties of BCP against several disorders, in particular cancer, chronic pain and inflammation; among the main ones, recent findings showed chemosensitizing properties for doxorubicin chemotherapy [9], sorafenib [10], and 5-fluorouracil and oxaliplatin [11], neuroprotective effects against cerebral ischemia reperfusion injury [12] and dopaminergic neuron injury [13], cardioprotective features against myocardial infarction [14] and doxorubicin toxicity [15] and, especially, a significant impact in the metabolic syndrome context. BCP has indeed been highlighted as a hypocholesterolemic and insulinotropic agent in high-fat diet-fed [16,17], or in streptozotocin-induced, diabetic rats [18,19], where it showed non-clinical toxicity and an absence of adverse effects [20]. BCP can act as a selective agonist of cannabinoid receptor 2 (CB2) [21], can directly activate peroxisome proliferator-activated receptor-α (PPAR α) [22], involved mainly in liver metabolism, and triggers the activation of PPPAR γ [17], a master regulator of adipogenesis, possibly through an indirect mechanism [23]. Therefore, BCP may represent a promising treatment for several metabolic disorders.

The effects of BCP on adipose tissue have never been addressed before, and so far, all studies on the BCP effects on glucose metabolism have been reported only in vivo. In vitro studies are a fundamental step for initial screening of potential cellular targets and characterization of the cellular mechanisms of bioactive molecules. Moreover, in the aim of a dietary approach, natural plant extracts with a high and standardized content of BCP could have a more suitable impact with respect to plain/synthetic BCP. Therefore, the present study was designed to evaluate the chemical characterization of a black pepper extract with a high content of BCP (PipeNig®-FL) produced by Biosfered Srl (Italy), and to study its effects on lipid accumulation and glucose uptake in in vitro models. The efficacy of the product was evaluated in two different cellular models, 3T3-L1 and C2C12, by assessing triglycerides accumulation in adipocytes and both glucose uptake and GLUT4 translocation in skeletal muscle myotubes.

2. Materials and Methods

2.1. Reagents

PipeNig®-FL (batch number PNF01-1907001), a *Piper nigrum* L. (black pepper) liquid extract, was kindly provided by Biosfered Srl (Torino, Italy). Certificate of analysis, technical sheets and materials safety data sheet of PipeNig®-FL are available from Biosfered upon request. The method of extraction and production of PipeNig®-FL are covered by the company trade secrets. PipeNig®-FL contains BCP at a concentration of 3.5 M in rice oil. For experiments, a stock solution of 1 M in DMSO was obtained, then diluted in culture medium for cell treatments. Concentrations reported in this work refer to those of BCP in each dilution.

NucBlue™ Live ReadyProbes™ Reagent and 2-(7-Nitrobenz-2-oxa-1,3-diazol-4-yl)Amino)-2-Deoxyglucose) (2-NBDG) were obtained from Invitrogen (Carlsbad, CA, USA); CellTiter-Glo® Luminescent Cell Viability and CellTiter 96® AQueous One Solution Cell Proliferation Assays were from Promega (Madison, WI, USA); anti-GLUT4 primary antibody and anti-rabbit secondary antibody Alexa Fluor 568 were from ThermoFisher Scientific (Waltham, MA, USA). Human insulin was used for cell treatments. Unless otherwise specified, all chemicals were purchased from Sigma Aldrich (St. Louis, MO, USA).

2.2. Gas-Chromatographic Analyses of PipeNig®-FL

PipeNig®-FL was analyzed by gas-chromatography (mod. 6890N, Agilent Technologies, Santa Clara, CA, USA) coupled with mass spectrometry (mod. 5973A, Agilent Technologies) (GC–MS). Compounds were separated on a Zebron ZB-5MS (mod. 7HG-G010-11, Phenomenex, Torrance, CA, USA) capillary column (stationary phase: 95% polydimethyl siloxane—5% diphenyl, 30 m length, 250 μm internal diameter, 0.25 μm film thickness) with the following temperature program: 60 °C for 5 min followed by a temperature rise at a 3 °C min^{-1} rate to 270 °C (held for 5 min). Carrier gas was He with a constant flow of 1 mL min^{-1}, transfer line temperature to MSD was 280 °C, ionization energy (EI) 70 eV, and full scan range 50–300 m/z. Separated compounds were identified by pure standard comparison, by comparison of their mass spectra with those of reference substances and by comparison with the NIST mass spectral search software v2.0 using the libraries NIST 98 library. Quantitative analyses were confirmed by gas chromatography coupled with flame ionization detector (GC–FID) (mod. 6890N, Agilent Technologies); analyses performed with the same column and GC conditions as above.

2.3. Cell Cultures

3T3-L1 preadipocytes (ATCC® CL-173™; Lot No 70009858, ATCC, Manassas, VA, USA) were cultured in high-glucose (4.5 g/L) Dulbecco's modified Eagle's medium (DMEM) supplemented with 10% calf serum, 2 mM L-glutamine, 50 IU/mL penicillin, and 50 μg/mL streptomycin [24]. For experiments, 5×10^3 cells/well were seeded in 96-black well clear bottom plates (Greiner Bio-One, Frickenhausen, Germany). Two days after reaching confluence (day 0), cells were exposed to the differentiation medium (MDI; which was DMEM containing 10% fetal bovine serum (FBS), 1 μg/mL insulin, 0.25 μM dexamethasone, 0.5 mM isobutylmethylxanthine). Two days later (day 2), MDI was replaced with maintenance medium (MM; which was DMEM 10% FBS, 1 μg/mL insulin). Fresh medium was provided every two days. Experiments ended after 9 days from the beginning of the differentiation (day 9).

The mouse myoblast cell line C2C12 (ECACC 91031101, lot 17I044) was purchased from the European Collection of Authenticated Cell Cultures (ECACC, Salisbury, UK) and cultured in high-glucose DMEM supplemented with 10% FBS, 1% penicillin/streptomycin and 2 mM L-glutamine in a humidified atmosphere of 5% CO_2 at 37 °C. Cultures were plated at a density of 2×10^3 cells per cm^2 on tissue plastic dishes (Becton Dickinson, Franklin Lakes, NJ, USA) and sub-cultured before reaching 70% confluence. For experiments, cells were seeded at a density respectively of 2×10^3 cells/cm^2 in

96-well plates or 10×10^3 cell/cm^2 on coverslips or glass bottom dishes (VWR Int., Radnor, PA, USA), to enhance adhesion. After cells reached confluence, differentiation was induced by changing the medium to DMEM supplemented with 2% horse serum (HS). Cells were allowed to differentiate for additional 5 to 7 days. The day before glucose uptake and GLUT4 translocation experiments, C2C12 cells were starved in DMEM glucose and serum free for 24 h.

2.4. Cell Viability

The viability of 3T3-L1 cells was evaluated at the end of the experiments (day 9) by CellTiter-Glo® Luminescent Cell Viability Assay, based on the quantitation of ATP, which signals the presence of metabolically active cells. After AdipoRed™/NucBlue™ quantification (see belove), the dye mixture was removed from the cell cultures and CellTiter-Glo® reagent, diluted 1:1 in phosphate-buffered saline (PBS), was added. Cells were incubated at room temperature in the dark for 10 min, then luminescence was detected and quantified with FilterMax F5™ Multi-Mode microplate reader (Molecular Devices, Sunnyvale, CA, USA). The values of luminescence are directly proportional to the number of viable cells. Data from three independent experiments were expressed as percentage referred to control condition; these values were then summarized to calculate mean ± standard error of the mean (SEM).

C2C12 cell viability was evaluated by the CellTiter 96® AQueous One Solution Cell Proliferation Assay, using the tetrazolium compound [3-(4,5-dimethylthiazol-2-yl)-5-(3-carboxymethoxyphenyl)-2-(4-sulfophenyl)-2H-tetrazolium, inner salt (MTS), that is bioreduced by metabolically active cells into a colored formazan product soluble in tissue culture medium. C2C12 cells, grown and differentiated into 96-well plates, were treated in 50 μL DMEM + 2% HS with different concentrations of PipeNig®-FL for one hour; during the last 30 min, 10 μL of MTS were added to each well (six wells for each condition). Formazan product was measured with FilterMax F5 microplate reader at 450 nm; absorbance is directly proportional to the number of viable cells. Data from three independent experiments were expressed as percentage referred to control condition; these values were then summarized to calculate mean ± SEM.

2.5. Quantification of Adipocyte Lipid Accumulation and DNA Staining

The 3T3-L1 cells, grown in 96-black well clear bottom plates, were exposed to PipeNig®-FL from day 0 to day 9 (whole differentiation period treatment), at scalar dilutions ranging from 1 nM to 10 μM (maximum DMSO concentration: 0.1%). Control cells were treated with 0.1% DMSO. Experiments were repeated three times (four wells for each condition), using cells at different passage numbers (p3–p5). At the end of the experiments (day 9 after the induction of differentiation), lipid accumulation was quantified by using AdipoRed™ assay reagent (Lonza, Walkersville, MD, USA), while the DNA content was estimated by NucBlue™ staining. Briefly, medium was removed from 3T3-L1 cultures and cells were rinsed with PBS, subsequently replaced with a dye mixture containing AdipoRed™ and NucBlue™ assay reagents diluted in PBS (25 μL and 1 drop, respectively, per mL of PBS). After 40 min of incubation at room temperature in the dark, fluorescence was measured with Filtermax F5 microplate reader respectively with excitation at 485 nm and emission at 535 nm for AdipoRed™ and excitation at 360 nm and emission at 460 nm for NucBlue™ quantification. Data from three independent experiments were expressed as percentage referred to control condition; these values were then summarized to calculate mean ± SEM.

2.6. Glucose Uptake Measurements

C2C12 cells, plated and differentiated on glass bottom dishes, after 24 h without glucose and serum, were treated with a different concentration of PipeNig®-FL (1–10–100 nM), and simultaneously loaded with 100 μM of 2-NBDG in glucose and serum-free DMEM, for 30 min in the dark. Insulin (25 nM) was used as a positive control. After two washes in PBS, cells were observed in confocal microscopy. Fluorescence images at 488 nm were acquired using an Olympus Fluoview 200 laser scanning confocal system (Olympus America Inc., Melville, NY, USA) mounted on an inverted IX70 Olympus microscope,

equipped with a 60X Uplan FI (NA 1.25) oil-immersion objective. Fluorescence variations were calculated with the definition and measurement of regions of interest (ROIs) using the ImageJ software (Rasband, W.S., U. S. National Institutes of Health, Bethesda, MA, USA; http://rsb.info.nih.gov/ij/, 1997–2008). Data from four independent experiments were evaluated as mean fluorescence/area and expressed as percentage referred to control condition; these values were then summarized to calculate mean ± SEM.

2.7. GLUT4 Translocation Analysis

C2C12 cells were grown and differentiated on glass coverslips. After 24 h without glucose and serum, cells were treated with insulin 25 nM or different concentration of PipeNig®-FL (1–10–100 nM) for 30 min in glucose and serum-free DMEM. Then cells were fixed for 40 min in 4% paraformaldehyde dissolved in 0.1 M phosphate buffer, pH 7.3. After three washes with PBS, cells were incubated for 20 min with 0.3% Triton and 1% bovine serum albumin in PBS and stained for 24 h at 4 °C with the primary polyclonal antibody anti-GLUT4, 1:100. Cover slides were washed twice with PBS and incubated for 1 h at room temperature with the secondary antibody, anti-rabbit Alexa Fluor 568, 1:1000. After two washes in PBS, coverslips were mounted on standard slides with DABCO and observed after 24 h under confocal microscope. GLUT4 staining measurements of both cell periphery and cell interior were performed with the ABSnake plugin of the ImageJ software [25]. Briefly, for each myotube the ABSnake plugin was employed to design a ROI band of 1.45 μm around the plasma membrane and the fluorescence intensities of both the band and the cellular inside were collected. Data from three independent experiments were expressed as peripheral/internal fluorescence and summarized to calculate mean ± SEM.

2.8. Statistical Analysis

Data are expressed as mean ± standard error of the mean (SEM); statistical analysis was performed using ANOVA (one-way analysis of variance) followed by Bonferroni's multiple comparison test. Differences with $p < 0.05$ were considered statistically significant.

3. Results

3.1. Chemical Composition of PipeNig®-FL

The chemical composition of PipeNig®-FL was assessed by GC–MS and quantified by GC–FID, as specified in the Materials and Methods section. The extract is characterized by a high content and percentage of the sesquiterpene hydrocarbon BCP, followed by minor mono and sesquiterpenes as depicted in Figure 1 and listed in Table 1. In particular, the total standardized content of PipeNig®-FL was higher than 800 mg g^{-1} of product, in agreement with what is specified by the producer. Amounts ranging from 0.5 to 7.8 mg g^{-1} were represented by monoterpenes (with limonene being the most abundant), whereas, among sesquiterpenes, α-caryophyllene showed the highest amount. In terms of relative percentage, BCP reached a level of almost 88%, whereas total percentage of all other identified compounds was around 8% (Table 1).

Concentrations reported in this work for experiments with cell cultures refer to those of BCP contained in each dilution of PipeNig®-FL.

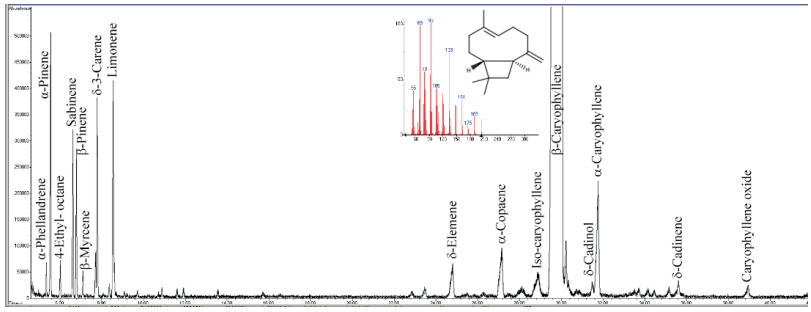

Figure 1. Gas chromatography–mass spectrometry (GC–MS) total ion current gas-chromatogram of PipeNig®-FL. The main compound *trans*-β-caryophyllene (BCP) is out of scale in order to evidence the other minor monoterpenes and sesquiterpenes that characterize the chemical composition of PipeNig®-FL. The inset shows the chemical formula and the mass spectrum of BCP. The y axis is the total ion current; the x axis represents time (in min).

Table 1. Chemical composition of PipeNig®-FL by gas chromatography coupled to mass spectrometry. Content is calculated based on gas chromatography with flame-ionization detection (GC–FID) analysis. R.T., retention time.

Compound	R.T.	Content (mg g^{-1})	Relative %
α-Phellandrene	5.35	0.47	0.11
α-Pinene	5.55	4.06	0.95
4-ethyl-octane	6.02	0.64	0.15
Sabinene	6.62	2.93	0.69
β-Pinene	6.79	2.76	0.65
β-Myrcene	7.11	1.10	0.12
δ-3-Carene	7.79	3.85	0.90
Limonene	8.55	7.84	1.10
δ-Elemene	24.79	2.21	0.52
α-Copaene	27.15	3.37	0.75
Isocaryophyllene	28.86	1.18	0.28
β-Caryophyllene	29.94	814.44	87.61
δ-Cadinol	31.49	0.70	0.16
α-Caryophyllene	31.75	6.13	1.43
δ-Cadinene	35.61	0.74	0.17
Caryophyllene oxide	38.94	0.79	0.18

3.2. Effects of PipeNig®-FL on 3T3-L1 Adipocyte Cell Viability

The long-term viability of 3T3-L1 cells treated with a wide range of PipeNig®-FL concentrations (100 nM, 1 µM, 10 µM, 100 µM, 1 mM, 10 mM) was determined by the CellTiter-Glo® viability assay, a method based on measurement of ATP content, whose amount is directly proportional to the number of metabolically active cells present in culture. As shown in Figure 2, after 9 days from the beginning of adipocyte differentiation (see Materials and Methods section), cell viability was affected only at very high PipeNig®-FL concentrations (1 mM and 10 mM), with only a minor, not statistically significant decrease at 100 µM. Based on these results, concentrations up to 10 µM were chosen for subsequent experiments. Mean values of luminescence signal from three independent experiments were as follow: CTRL (DMSO 0.1%): 100 ± 0.20, PipeNig®-FL 100 nM: 92.31 ± 0.13, PipeNig®-FL 1 µM: 92.65 ± 1.01, PipeNig®-FL 10 µM: 87.86 ± 0.83, PipeNig®-FL 100 µM: 77.55 ± 2.12, PipeNig®-FL 1 mM: 1.46 ± 1.32, PipeNig®-FL 10 mM: 0.93 ± 0.12.

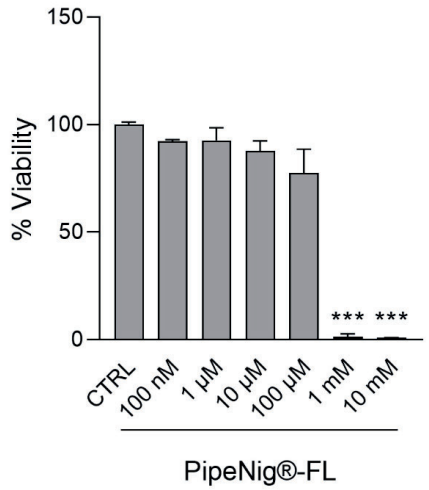

Figure 2. PipeNig®-FL affects 3T3-L1 cell viability only at high (millimolar) concentrations. 3T3-L1 cells were induced to differentiate into adipocytes for 9 days and treated with increasing concentrations of PipeNig®-FL for the entire differentiation period. The bar graph summarizes cell viability based on ATP content. Data in percentage referred to control condition are represented as the mean ± standard error of the mean (SEM) of three independent experiments. *** $p < 0.001$ vs. control.

3.3. PipeNig®-FL Reduces Intracellular Lipid Accumulation in 3T3-L1 Cells without Altering the Cell Number

The potential antiadipogenic activity of PipeNig®-FL was assayed on the murine 3T3-L1 preadipocyte cell line, a commonly used cell model for adipose cell biology research [26]. Since antiadipogenic effects can be exerted by reducing both intracellular lipid accumulation and/or the number of adipocytes (either by decreasing cell proliferation or inducing cell death), we simultaneously assayed triglyceride accumulation (AdipoRed™ assay) and cell number (NucBlue™ staining, measuring DNA content). Confluent preadipocytes, cultured in 96-well plates, were induced to start adipogenic differentiation and were treated throughout the differentiation period (9 days) with a vehicle only (0.1% DMSO; differentiated control) or with 1 nM, 10 nM, 1 µM, 10 µM PipeNig®-FL. Higher PipeNig®-FL doses were not used, based on the cell viability data reported above. After 9 days from the beginning of adipocyte differentiation, AdipoRed™/NucBlue™ stainings were performed on 3T3-L1 adipocytes (Figure 3A). Trygliceride accumulation and DNA content were calculated as percentage change from differentiated DMSO-treated controls (Figure 3B,C). The DNA content was used to normalize total triglyceride values to obtain triglyceride content per unit DNA (as a proxy for triglycerides accumulation per cell).

As shown in (Figure 3B), triglyceride accumulation per well was reduced in PipeNig®-FL treated 3T3-L1 cells compared to differentiated control cells; in particular, statistically significant reductions were obtained after treatment with PipeNig®-FL 10 nM, 1 µM and 10 µM. Mean values of fluorescence signal from three independent experiments were as follow: undifferentiated cells: 7.85 ± 2.36, differentiated CTRL: 100 ± 0.20, PipeNig®-FL 1n M: 63.64 ± 2.37, PipeNig®-FL 10 nM: 61.72 ± 1.35, PipeNig®-FL 1 µM: 59.00 ± 2.42, PipeNig®-FL 10 µM: 57.91 ± 3.05.

DNA content was not significantly different in PipeNig®-FL treated cells and control cells, thus indicating that the decrease in lipid accumulation exerted by PipeNig®-FL is not due to a decrease in cell proliferation or to cytotoxic effects (Figure 3C). Mean values of fluorescence signal from three independent experiments were as follows: undifferentiated cells: 81.23 ± 1.36, differentiated control: 100 ± 0.20, PipeNig®-FL 1n M: 91.63 ± 1.39, PipeNig®-FL 10 nM: 86.76 ± 0.96, PipeNig®-FL 1 µM: 90.43 ± 2.03, PipeNig®-FL 10 µM: 90.72 ± 1.92.

On the other hand, a significant reduction in intracellular lipid content per cell was found at all concentrations (Figure 3D); mean values of fluorescence signal from three independent experiments were as follow: undifferentiated cells: 10.63 ± 3.62, differentiated CTRL: 100 ± 0.30, PipeNig®-FL 1 nM: 68.68 ± 1.12, PipeNig®-FL 10 nM: 71 ± 0.88, PipeNig®-FL 1 μM: 64.74 ± 1.01, PipeNig®-FL 10 μM: 62.57 ± 1.31.

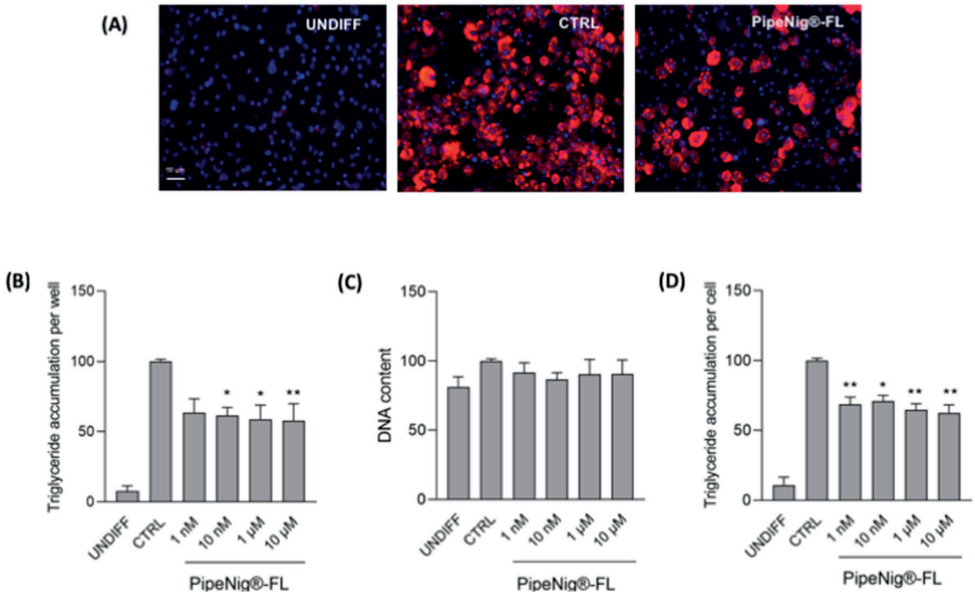

Figure 3. PipeNig®-FL reduces intracellular lipid accumulation in 3T3-L1 cells without altering the cell number. (**A**) Representative images of AdipoRed (red) and NucBlue (blue) staining of undifferentiated preadipocytes (UNDIFF), differentiated control adipocytes (CTRL) and 10 μM PipeNig®-FL-treated 3T3-L1 adipocytes after 9 days of differentiation. Scale bar 50 μm. (**B**) Bar graph summarizing AdipoRed staining experiments to assess lipid accumulation on undifferentiated cells, differentiated control and 3T3-L1 adipocytes treated with various concentrations of PipeNig®-FL for 9 days, showing triglyceride accumulation per well. (**C**) Bar graph summarizing NucBlue staining experiments to assess variations in the number of cells, showing DNA content per well. (**D**) Bar graph showing triglyceride accumulation per cell, calculated as the ratio of AdipoRed and NucBlue staining. Data in percentage referred to differentiated control condition are represented as the mean ± SEM of three independent experiments. * $p < 0.05$; ** $p < 0.01$ vs. control.

3.4. PipeNig®-FL Does Not Affect Cell Viability on C2C12 Muscle Cell

In order to investigate the effect of PipeNig®-FL on C2C12 viability, differentiated cells were treated with increasing concentration of PipeNig®-FL (100 nM, 50 μM, 200 μM, 1 mM, 10 mM) for 1 h. The MTS assay was performed in the last 30 min of treatment. The time considered to evaluate the toxicity of PipeNig®-FL was related to experiments on glucose metabolism that were done in a short time of treatment. As shown in Figure 4, acute exposure (1 h) to PipeNig®-FL even at the highest doses did not affect significantly ($p < 0.05$) cell viability. Mean values of Abs at 450 nm from three independent experiments were as follows: CTRL: 99.61 ± 1.48, PipeNig®-FL 100 nM: 100.72 ± 1.32, PipeNig®-FL 50 μM: 98.90 ± 1.78, PipeNig®-FL 200 μM: 101.27 ± 2.04, PipeNig®-FL 1 mM: 101.76 ± 1.39, PipeNig®-FL 10 mM: 92.13 ± 2.34.

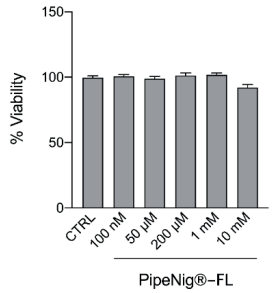

Figure 4. PipeNig®-FL does not have any effects on cell viability in C2C12 muscle cell. C2C12 cells were treated with increasing concentration of PipeNig®-FL for 1h. Data in percentage referred to control condition are represented as the mean ± SEM (n = 3).

3.5. PipeNig®-FL Improves Glucose Uptake in C2C12 Myotubes

To verify the potential role of PipeNig®-FL on glucose uptake in skeletal muscle cells, we performed confocal microscopy analyses by using a fluorescent D-glucose analog, 2-NBDG. Cells were incubated simultaneously with either 100 µM 2-NBDG and different concentrations of PipeNig®-FL (1–10–100 nM) without insulin while insulin alone (25 nM) was used as positive control, for 30 min in the dark. Doses of PipeNig®-FL were chosen in the nM range as for insulin, since we have previously verified that stimulation with PipeNig®-FL 100 nM for 1 h did not produce cytotoxic effects. A significant increase of glucose uptake was observed in treated cells with respect to control cells, whereas no differences were observed between insulin and PipeNig®-FL treatments or among PipeNig®-FL concentrations (Figure 5). Values of mean fluorescence/area from four independent experiments were as follows: CTRL: 100.13 ± 4.69, n cells = 68; insulin: 130.10 ± 6.21, n cells = 89; PipeNig®-FL 1 nM: 144.04 ± 7.95, n cells = 45; PipeNig®-FL 10 nM: 133.00 ± 6.73, n cells = 75; PipeNig®-FL 100 nM: 140.72 ± 9.64, n cells = 56.

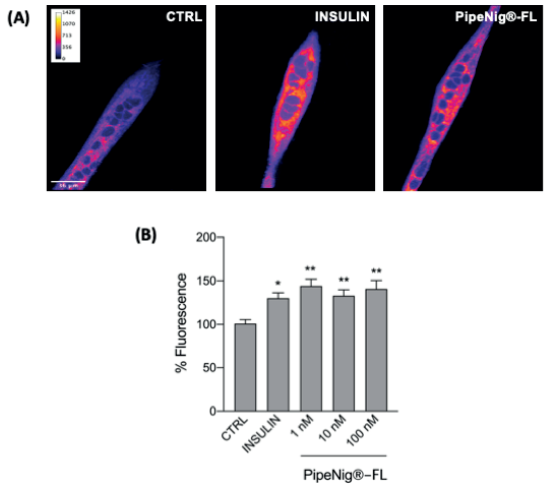

Figure 5. PipeNig®-FL stimulates glucose uptake. (**A**) Representative confocal images of C2C12 myotubes incubated with the fluorescent glucose analog 2-NBDG for 30 min. Images are presented in pseudocolor (LUT = fire) to better show the fluorescence intensity variations. Insulin (25 nm) was used as a positive control. Scale bar 36 µm. (**B**) Bar graph summarizing the experiments of fluorescent glucose uptake. Data in percentage referred to control condition are represented as the mean ± SEM (n = 4). * $p < 0.05$; ** $p < 0.01$ vs. control.

3.6. PipeNig®-FL Induces GLUT4 Translocation in C2C12 Cells

To confirm the involvement of PipeNig®-FL on glucose metabolism, we carried out immunofluorescence experiments using GLUT4 antibody, followed by a detailed image analysis of peripheral vs. internal fluorescence staining. Cells were treated with insulin (25 nM) or different concentrations of PipeNig®-FL (1–10–100 nM) without insulin, for 30 min. An evident translocation of the glucose transporter from the cytosol to the plasma membrane was observed in treated cells with respect to control cells, whereas there were no significant differences in staining among treatments (Figure 6). Values of peripheral vs. internal GLUT4 staining from three independent experiments were as follows: CTRL: 160.36 ± 18.21, n cells = 19; insulin: 282.73 ± 25.00, n cells = 21; PipeNig®-FL 1 nM: 259.26 ± 18.60, n cells = 20; PipeNig®-FL 10 nM: 336.40 ± 14.96, n cells = 18; PipeNig®-FL 100 nM: 270.96 ± 31.36, n cells = 16.

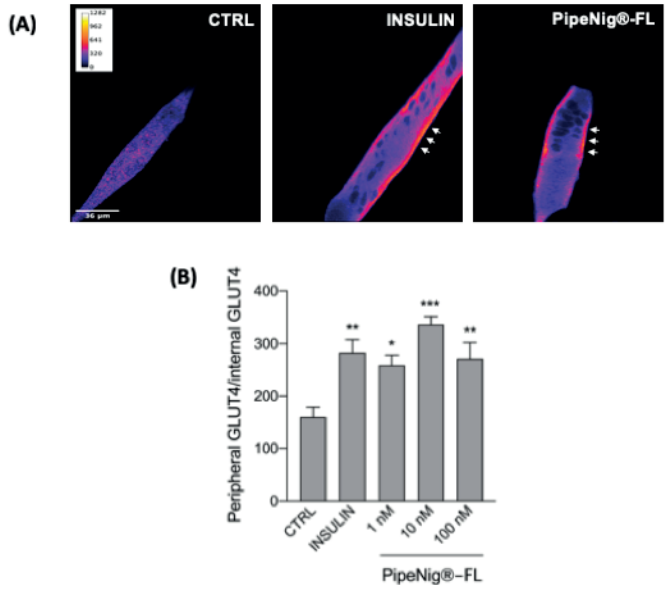

Figure 6. PipeNig®-FL induces GLUT4 translocation to the plasma membrane. (**A**) Confocal images of a representative experiment of GLUT4 immunofluorescence staining. After PipeNig®-FL stimulation (1–10–100 nM) the fluorescent signal is clearly localized to the peripheral plasmalemma, thus suggesting the GLUT4 translocation. Images are presented in pseudocolor (LUT = fire) to better show the fluorescence intensity variations. Insulin (25 nM) was used as a positive control. Scale bar 36 μm. (**B**) Bar graph representing the ratio peripheral vs. internal GLUT4 fluorescence intensity. Data are represented as the mean ± SEM of three independent experiments. * $p < 0.05$; ** $p < 0.01$; *** $p < 0,001$ vs. control.

4. Discussion

This study focuses on two goals: 1. the chemical characterization of a black pepper extract with a high content of BCP (PipeNig®-FL). 2. the in vitro investigation of the biological activities of PipeNig®-FL in adipocytes and skeletal myotubes. The present results highlight the high performance of the extract regarding its BCP content (>80%) and underline its beneficial metabolic properties, in terms of reduced lipid accumulation in adipocytes and improved glucose uptake activity in myotubes.

The attractiveness of BCP, a sesquiterpene produced by a consistent number of plant species, arises from its pharmacological feature as a CB2 receptor full agonist, which makes BCP the only phytoendocannabinoid found beyond the *Cannabis* genus to date [27], with the advantage

of lacking any psychotropic effect. In addition to CB2 receptors, BCP also activates peroxisome proliferator-activated receptor α and γ (PPARα-γ) [22,23], making it suitable to interfere with several metabolic pathways and pathological conditions, including apoptotic, inflammatory, cholesterolemic and behavioral disorders. In line with this, BCP has been demonstrated to possess anticancerogenic, neuroprotective, cardioprotective, hepatoprotective, gastroprotective, nephroprotective, antiinflammatory and immunomodulatary properties [27,28]. In particular, several studies recently pointed out potential counteractive functions of BCP against metabolic syndrome [16–19,29]. Grounding on these premises, the use of a plant-derived extract with a high and standardized BCP content represents a high-impact goal in the cross-sectional fields of plant food-nutrition-human health. In this perspective, the objective of our studies was to evaluate the properties of PipeNig®-FL to reduce lipid accumulation and induce glucose uptake.

The chemical analysis of PipeNig®-FL reveals a high content of BCP, in line with what is declared by the producer. The general GC profile is in line with the chemical composition of a typical black pepper oil [30,31] and confirms the presence of minor monoterpenes and sesquiterpenes as well as the complete absence of piperine.

We verified the suitability of PipeNig®-FL for in vitro cellular studies, by performing viability tests on 3T3-L1 preadipocytes and C2C12 myotubes. As shown in Figure 2, long-term 3T3-L1 treatment with PipeNig®-FL (9 days) did not cause any cell damage in the physiologically active range (100 nM–100 μM), only affecting cell viability at much higher concentrations (1–10 mM), while C2C12 viability (Figure 4) was unaffected by acute exposure to PipeNig®-FL (1 h, 100 nM–10 mM). Moreover, a previous study in mice reported the absence of toxicity of both acute (300 and 2000 mg/kg) and repeated doses of BCP [20], and BCP has been approved by United States Food and Drug Administration and European agencies as food additive, taste enhancer and flavoring agent [7].

We further tested the properties of PipeNig®-FL as a lipid accumulation-inhibitor during the 3T3-L1 cell differentiation process. The development of obesity is characterized by an increase in the number of fat cells (hyperplasia) and their lipid content (hypertrophy), as a result of cell proliferation and differentiation. In our experiments PipeNig®-FL led to a significant decrease in the lipid content per cell, without affecting cell proliferation, thus suggesting a role in reducing adipocyte-hypertrophic response typically present in the energy overload conditions that characterizes metabolic syndrome [32].

Previous in vitro studies on bone marrow mesenchymal stem cells showed enhanced osteoblast differentiation and reduced adipogenesis induced by synthetic BCP [33]. Moreover, recent in vivo studies in rats exposed to fat enriched diet highlighted hypocholesterolemic and protective effects of BCP [16,23], proving the involvement of several mechanisms, as the inhibition of endogenous hepatic cholesterol synthesis [16], the stimulation of the activity of antioxidant enzymes [16] and the engagement of both CB2 and PPARγ receptors [16]. In this scenario, our results of reduced adipogenesis induced by PipeNig®-FL in 3T3-L1 pre-adipocytes strengthen the message from data obtained with synthetic BCP in bone marrow cells, and support the effectiveness of the extract respect to its high BCP content.

In addition to its anti-obesogenic properties, our further experiments on skeletal myotubes highlighted PipeNig®-FL capability to be a glucose uptake inducer: as shown in Figure 5, PipeNig®-FL was as efficient as insulin in stimulating cellular glucose uptake. In 2014 Basha and Sankaranarayanan [18] reported an insulinomimetic effect of BCP (200 mg/kg) in streptozotocin-induced diabetic rats. In particular they showed a significant decrease in blood glucose levels and a significant increase in the activity of hexokinase, pyruvate kinase and glucose-6-phosphate dehydrogenase in liver, kidney and skeletal muscle [18]. Moreover, other studies in similar animal models [19] and in isolated pancreatic beta cells [34] reported antidiabetic properties of BCP through an enhanced insulin release. To gain better understanding of the mechanisms involved in glucose uptake, we performed immunofluorescence GLUT4 staining in insulin and PipeNig®-FL-treated myotubes, showing a significant plasma membrane GLUT4 translocation in both conditions (Figure 6) respect to control. Thus the attractive novelty of these results is to show, for the first time, a direct acute

effect of a BCP-enriched extract in promoting glucose uptake in skeletal myotubes, likely through an improvement of GLUT4 trafficking toward the plasma membrane. Translocation of GLUT4 storage vesicles to the plasma membrane, mainly in skeletal muscle and adipose tissue, is directly correlated with the ability to lower elevated blood glucose. Moreover, GLUT4 levels are significantly decreased in the skeletal muscle of type 2 diabetic patients and in insulin resistant patients [35]. The development of therapeutic compounds able to induce GLUT4 expression/translocation can thus improve insulin sensitivity and reduce insulin resistance. Several plant-derived bioactive molecules have been listed as stimulators of GLUT4 translocation and/or expression, among these resveratrol, chlorogenic acid, daidzein (an isoflavone found in soybeans), curcumin and astaxanthin, affecting different key-points in the intracellular cascade involved in vesicle trafficking [36]. As a major component of PipeNig®-FL, BCP could now be included in this list.

5. Conclusions

The main limitation of our study resides in the experimental models, since we tested the effects of PipeNig®-FL on cell lines of preadipocytes and skeletal myotubes. On the other hand, in vitro approaches account for important advantages, as results reflect direct effects of PipeNig®-FL on specific cellular processes, avoiding complex multi-organ interactions typical of in vivo models. At present, we do not provide a detailed analysis on the complex molecular/functional signatures of reduced lipidogenesis activated by PipeNig®-FL in 3T3-L1 cells. Future experiments should be directed to gain further information on the molecular mechanisms initiated by PipeNig®-FL and to confirm its properties as anti-lipidogenic and glucose uptake inducer in animal models.

In conclusion, giving its high content in BCP, PipeNig®-FL could represent a promising novel bioactive complex deserving both molecular investigations and in vivo studies in order to support its role as a beneficial metabolic modulator.

Author Contributions: Conceptualization, P.B., M.P.G. and M.E.M.; methodology, S.A. and E.C.; software, F.G. and R.S.; validation, S.A. and E.C.; formal analysis, S.A., E.C., F.G. and R.S.; investigation, S.A., E.C., F.G., G.Q. and R.S.; resources, M.E.M.; data curation, S.A., E.C., F.G., G.Q. and R.S.; writing—original draft preparation, P.B., M.P.G. and M.E.M.; writing—review and editing, P.B., M.P.G. and M.E.M.; supervision, P.B., M.P.G. and M.E.M.; project administration, P.B., M.P.G. and M.E.M.; funding acquisition, M.E.M.

Funding: This research was funded by "Fondazione Cassa di Risparmio di Torino" (Erogazioni Ordinarie 2018, grant number ID 61356).

Acknowledgments: We thank Biosfered S.r.l. for kindly providing PipeNig®-FL and other chemical reagents and partly supporting the research.

Conflicts of Interest: MEM is also currently a fellow of the Biosfered Srl company. No patents are pending and Biosfered supported the study by providing PipeNig®-FL and other chemical reagents and partly supporting the research. Biosfered did not interfere with the design, analysis, and decision to publish this paper. The remaining authors declare that the research was conducted in the absence of any commercial or financial relationships that could be construed as a potential conflict of interest.

References

1. Reilly, M.P.; Rader, D.J. The Metabolic Syndrome. *Circulation* **2003**, *108*, 1546–1551. [CrossRef]
2. Ammazzalorso, A.; Maccallini, C.; Amoia, P.; Amoroso, R. Multitarget PPARγ Agonists as Innovative Modulators of the Metabolic Syndrome. *Eur. J. Med. Chem.* **2019**, *173*, 261–273. [CrossRef] [PubMed]
3. Aguilar-Salinas, C.A.; Viveros-Ruiz, T. Recent Advances in Managing/Understanding the Metabolic Syndrome. *F1000Res* **2019**, *8*. [CrossRef] [PubMed]
4. Silva Figueiredo, P.; Inada, A.C.; Ribeiro Fernandes, M.; Granja Arakaki, D.; Freitas, K.D.C.; Avellaneda Guimarães, R.D.C.; Aragão do Nascimento, V.; Aiko Hiane, P. An Overview of Novel Dietary Supplements and Food Ingredients in Patients with Metabolic Syndrome and Non-Alcoholic Fatty Liver Disease. *Molecules* **2018**, *23*, 877. [CrossRef] [PubMed]
5. Ding, Y.; Gu, Z.; Wang, Y.; Wang, S.; Chen, H.; Zhang, H.; Chen, W.; Chen, Y.Q. Beyond Cannabis: Plants and the Endocannabinoid System. *Trends Pharmacol. Sci.* **2016**, *37*, 594–605. [CrossRef]

6. Takooree, H.; Aumeeruddy, M.Z.; Rengasamy, K.R.R.; Venugopala, K.N.; Jeewon, R.; Zengin, G.; Mahomoodally, M.F.A. Systematic Review on Black Pepper (*Piper Nigrum* L.): From Folk Uses to Pharmacological Applications. *Crit. Rev. Food Sci. Nutr.* **2019**, *59*, S210–S243. [CrossRef]
7. Sharma, C.; Al Kaabi, J.M.; Nurulain, S.M.; Goyal, S.N.; Kamal, M.A.; Ojha, S. Polypharmacological Properties and Therapeutic Potential of β-Caryophyllene: A Dietary Phytocannabinoid of Pharmaceutical Promise. *Curr. Pharm. Des.* **2016**, *22*, 3237–3264. [CrossRef]
8. Api, A.M.; Belsito, D.; Botelho, D.; Bruze, M.; Burton, G.A.; Buschmann, J.; Dagli, M.L.; Date, M.; Dekant, W.; Deodhar, C.; et al. RIFM Fragrance Ingredient Safety Assessment, β-Caryophyllene Alcohol, CAS Registry Number 472-97-9. *Food Chem. Toxicol.* **2018**, *122*, S566–S572. [CrossRef]
9. Di Giacomo, S.; DI Sotto, A.; Mazzanti, G.; Wink, M. Chemosensitizing Properties of β-Caryophyllene and β-Caryophyllene Oxide in Combination with Doxorubicin in Human Cancer Cells. *Anticancer Res.* **2017**, *37*, 1191–1196. [CrossRef]
10. Di Giacomo, S.; Briz, O.; Monte, M.J.; Sanchez-Vicente, L.; Abete, L.; Lozano, E.; Mazzanti, G.; Di Sotto, A.; Marin, J.J.G. Chemosensitization of Hepatocellular Carcinoma Cells to Sorafenib by β-Caryophyllene Oxide-Induced Inhibition of ABC Export Pumps. *Arch. Toxicol.* **2019**, *93*, 623–634. [CrossRef]
11. Ambrož, M.; Šmatová, M.; Šadibolová, M.; Pospíšilová, E.; Hadravská, P.; Kašparová, M.; Skarková, V.H.; Králová, V.; Skálová, L. Sesquiterpenes α-Humulene and β-Caryophyllene Oxide Enhance the Efficacy of 5-Fluorouracil and Oxaliplatin in Colon Cancer Cells. *Acta Pharm.* **2019**, *69*, 121–128. [CrossRef] [PubMed]
12. Yang, M.; Lv, Y.; Tian, X.; Lou, J.; An, R.; Zhang, Q.; Li, M.; Xu, L.; Dong, Z. Neuroprotective Effect of β-Caryophyllene on Cerebral Ischemia-Reperfusion Injury via Regulation of Necroptotic Neuronal Death and Inflammation: In Vivo and in Vitro. *Front. Neurosci.* **2017**, *11*. [CrossRef] [PubMed]
13. Viveros-Paredes, J.M.; González-Castañeda, R.E.; Gertsch, J.; Chaparro-Huerta, V.; López-Roa, R.I.; Vázquez-Valls, E.; Beas-Zarate, C.; Camins-Espuny, A.; Flores-Soto, M.E. Neuroprotective Effects of β-Caryophyllene against Dopaminergic Neuron Injury in a Murine Model of Parkinson's Disease Induced by MPTP. *Pharmaceuticals* **2017**, *10*, 60. [CrossRef] [PubMed]
14. Younis, N.S.; Mohamed, M.E. β-Caryophyllene as a Potential Protective Agent Against Myocardial Injury: The Role of Toll-Like Receptors. *Molecules* **2019**, *24*, 1929. [CrossRef] [PubMed]
15. Meeran, M.F.N.; Al Taee, H.; Azimullah, S.; Tariq, S.; Adeghate, E.; Ojha, S. β-Caryophyllene, a Natural Bicyclic Sesquiterpene Attenuates Doxorubicin-Induced Chronic Cardiotoxicity via Activation of Myocardial Cannabinoid Type-2 (CB2) Receptors in Rats. *Chem.-Biol. Interact.* **2019**, *304*, 158–167. [CrossRef] [PubMed]
16. Harb, A.A.; Bustanji, Y.K.; Abdalla, S.S. Hypocholesterolemic Effect of β-Caryophyllene in Rats Fed Cholesterol and Fat Enriched Diet. *J. Clin. Biochem. Nutr.* **2018**, *62*, 230–237. [CrossRef] [PubMed]
17. Youssef, D.A.; El-Fayoumi, H.M.; Mahmoud, M.F. Beta-Caryophyllene Protects against Diet-Induced Dyslipidemia and Vascular Inflammation in Rats: Involvement of CB2 and PPAR-γ Receptors. *Chem.-Biol. Interact.* **2019**, *297*, 16–24. [CrossRef]
18. Basha, R.H.; Sankaranarayanan, C. β-Caryophyllene, a Natural Sesquiterpene, Modulates Carbohydrate Metabolism in Streptozotocin-Induced Diabetic Rats. *Acta Histochem.* **2014**, *116*, 1469–1479. [CrossRef]
19. Basha, R.H.; Sankaranarayanan, C. β-Caryophyllene, a Natural Sesquiterpene Lactone Attenuates Hyperglycemia Mediated Oxidative and Inflammatory Stress in Experimental Diabetic Rats. *Chem. Biol. Interact.* **2016**, *245*, 50–58. [CrossRef]
20. Da Silva Oliveira, G.L.; Machado, K.C.; Machado, K.C.; da Silva, A.P.D.S.C.L.; Feitosa, C.M.; de Castro Almeida, F.R. Non-Clinical Toxicity of β-Caryophyllene, a Dietary Cannabinoid: Absence of Adverse Effects in Female Swiss Mice. *Regul. Toxicol. Pharmacol.* **2018**, *92*, 338–346. [CrossRef]
21. Gertsch, J.; Leonti, M.; Raduner, S.; Racz, I.; Chen, J.-Z.; Xie, X.-Q.; Altmann, K.-H.; Karsak, M.; Zimmer, A. Beta-Caryophyllene Is a Dietary Cannabinoid. *Proc. Natl. Acad. Sci. USA* **2008**, *105*, 9099–9104. [CrossRef] [PubMed]
22. Wu, C.; Jia, Y.; Lee, J.H.; Jun, H.-J.; Lee, H.-S.; Hwang, K.-Y.; Lee, S.-J. Trans-Caryophyllene Is a Natural Agonistic Ligand for Peroxisome Proliferator-Activated Receptor-α. *Bioorganic Med. Chem. Lett.* **2014**, *24*, 3168–3174. [CrossRef] [PubMed]
23. Youssef, D.A.; El-Fayoumi, H.M.; Mahmoud, M.F. Beta-Caryophyllene Alleviates Diet-Induced Neurobehavioral Changes in Rats: The Role of CB2 and PPAR-γ Receptors. *Biomed. Pharmacother.* **2019**, *110*, 145–154. [CrossRef]

24. Pomatto, V.; Cottone, E.; Cocci, P.; Mozzicafreddo, M.; Mosconi, G.; Nelson, E.R.; Palermo, F.A.; Bovolin, P. Plasticizers Used in Food-Contact Materials Affect Adipogenesis in 3T3-L1 Cells. *J. Steroid Biochem. Mol. Biol.* **2018**, *178*, 322–332. [CrossRef] [PubMed]
25. Gallo, M.P.; Femminò, S.; Antoniotti, S.; Querio, G.; Alloatti, G.; Levi, R. Catestatin Induces Glucose Uptake and GLUT4 Trafficking in Adult Rat Cardiomyocytes. Available online: https://www.hindawi.com/journals/bmri/2018/2086109/cta/ (accessed on 9 October 2019). [CrossRef]
26. Kim, N.-H.; Jegal, J.; Kim, Y.N.; Heo, J.-D.; Rho, J.-R.; Yang, M.H.; Jeong, E.J. Chokeberry Extract and Its Active Polyphenols Suppress Adipogenesis in 3T3-L1 Adipocytes and Modulates Fat Accumulation and Insulin Resistance in Diet-Induced Obese Mice. *Nutrients* **2018**, *10*, 1734. [CrossRef] [PubMed]
27. Nuutinen, T. Medicinal Properties of Terpenes Found in Cannabis Sativa and Humulus Lupulus. *Eur. J. Med. Chem.* **2018**, *157*, 198–228. [CrossRef] [PubMed]
28. Fidyt, K.; Fiedorowicz, A.; Strządała, L.; Szumny, A. β-Caryophyllene and β-Caryophyllene Oxide—Natural Compounds of Anticancer and Analgesic Properties. *Cancer Med.* **2016**, *5*, 3007–3017. [CrossRef] [PubMed]
29. Arizuka, N.; Murakami, T.; Suzuki, K. The Effect of β-Caryophyllene on Nonalcoholic Steatohepatitis. *J. Toxicol. Pathol.* **2017**, *30*, 263–273. [CrossRef]
30. Butt, M.S.; Pasha, I.; Sultan, M.T.; Randhawa, M.A.; Saeed, F.; Ahmed, W. Black Pepper and Health Claims: A Comprehensive Treatise. *Crit. Rev. Food Sci. Nutr.* **2013**, *53*, 875–886. [CrossRef]
31. Bagheri, H.; Abdul Manap, M.Y.B.; Solati, Z. Response Surface Methodology Applied to Supercritical Carbon Dioxide Extraction of *Piper Nigrum* L. Essential Oil. *LWT-Food Sci. Technol.* **2014**, *57*, 149–155. [CrossRef]
32. Hafidi, M.E.; Buelna-Chontal, M.; Sánchez-Muñoz, F.; Carbó, R. Adipogenesis: A Necessary but Harmful Strategy. *Int. J. Mol. Sci.* **2019**, *20*, 3657. [CrossRef] [PubMed]
33. Yamaguchi, M.; Levy, R.M. β-Caryophyllene Promotes Osteoblastic Mineralization, and Suppresses Osteoclastogenesis and Adipogenesis in Mouse Bone Marrow Cultures in Vitro. *Exp. Ther. Med.* **2016**, *12*, 3602–3606. [CrossRef] [PubMed]
34. Suijun, W.; Zhen, Y.; Ying, G.; Yanfang, W. A Role for Trans-Caryophyllene in the Moderation of Insulin Secretion. *Biochem. Biophys. Res. Commun.* **2014**, *444*, 451–454. [CrossRef] [PubMed]
35. Morgan, B.J.; Chai, S.Y.; Albiston, A.L. GLUT4 Associated Proteins as Therapeutic Targets for Diabetes. *Recent. Pat. Endocr. Metab. Immune. Drug Discov.* **2011**, *5*, 25–32. [CrossRef] [PubMed]
36. Gannon, N.P.; Conn, C.A.; Vaughan, R.A. Dietary Stimulators of GLUT4 Expression and Translocation in Skeletal Muscle: A Mini-Review. *Mol. Nutr. Food Res.* **2015**, *59*, 48–64. [CrossRef] [PubMed]

International Journal of
Molecular Sciences

MDPI

Article

Beta-Caryophyllene Modifies Intracellular Lipid Composition in a Cell Model of Hepatic Steatosis by Acting through CB2 and PPAR Receptors

Rosaria Scandiffio [1,2], Sara Bonzano [1,3], Erika Cottone [1], Sujata Shrestha [1], Simone Bossi [2], Silvia De Marchis [1,3], Massimo E. Maffei [2] and Patrizia Bovolin [1,*]

[1] Cell Biology Unit, Department of Life Sciences and Systems Biology, University of Turin, Via Accademia Albertina 13, 10123 Turin, Italy
[2] Plant Physiology Unit, Department of Life Sciences and Systems Biology, University of Turin, Via Quarello 15/a, 10135 Turin, Italy
[3] Neuroscience Institute Cavalieri Ottolenghi (NICO), Regione Gonzole 10, Orbassano, 10043 Turin, Italy
* Correspondence: patrizia.bovolin@unito.it

Abstract: Non-alcoholic fatty liver disease (NAFLD) is the most common cause of chronic liver disease; however, no specific pharmacological therapy has yet been approved for this condition. Plant-derived extracts can be an important source for the development of new drugs. The aim of this study was to investigate the effects of (E)-β-caryophyllene (BCP), a phytocannabinoid recently found to be beneficial against metabolic diseases, on HepG2 steatotic hepatocytes. Using a fluorescence-based lipid quantification assay and GC-MS analysis, we show that BCP is able to decrease lipid accumulation in steatotic conditions and to change the typical steatotic lipid profile by primarily reducing saturated fatty acids. By employing specific antagonists, we demonstrate that BCP action is mediated by multiple receptors: CB2 cannabinoid receptor, peroxisome proliferator-activated receptor α (PPARα) and γ (PPARγ). Interestingly, BCP was able to counteract the increase in CB2 and the reduction in PPARα receptor expression observed in steatotic conditions. Moreover, through immunofluorescence and confocal microscopy, we demonstrate that CB2 receptors are mainly intracellularly localized and that BCP is internalized in HepG2 cells with a maximum peak at 2 h, suggesting a direct interaction with intracellular receptors. The results obtained with BCP in normal and steatotic hepatocytes encourage future applications in the treatment of NAFLD.

Keywords: β-caryophyllene; NAFLD; steatosis; lipid profile; CB2 receptors; PPARγ; PPARα; HepG2 cell line

Citation: Scandiffio, R.; Bonzano, S.; Cottone, E.; Shrestha, S.; Bossi, S.; De Marchis, S.; Maffei, M.E.; Bovolin, P. Beta-Caryophyllene Modifies Intracellular Lipid Composition in a Cell Model of Hepatic Steatosis by Acting through CB2 and PPAR Receptors. *Int. J. Mol. Sci.* **2023**, *24*, 6060. https://doi.org/10.3390/ijms24076060

Academic Editors: Giuseppe Colucci, Andrea Ferrigno and Mariapia Vairetti

Received: 15 February 2023
Revised: 15 March 2023
Accepted: 20 March 2023
Published: 23 March 2023

1. Introduction

Non-alcoholic fatty liver disease (NAFLD) is the most common chronic liver disorder, with an average prevalence of 25%, ranging from 13% (adult African population) to 32% (Middle East population) [1]. This disease is characterized by the excessive accumulation of fats, due to overnutrition or an unbalanced diet and not to ethanol consumption, with an increase of visceral fats that results in macrophage infiltration and pro-inflammatory conditions [2]. In this context, insulin resistance occurs, causing dysregulated lipolysis of triglyceride in the adipose tissue and delivery of fats to the liver. This is accompanied by increased de novo lipogenesis, the process through which hepatocytes convert excess carbohydrates to free fatty acids (FFA). The disposal of FFA occurs through beta-oxidation or re-esterification, and when this process is overloaded the formation of lipotoxic lipids may occur. This causes oxidative stress, endoplasmic reticulum stress and hepatocellular damages. The exacerbation of this condition leads to nonalcoholic steatohepatitis (NASH) that can progress to cirrhosis and liver cancer [1,2]. No specific pharmacological treatments are currently approved for NAFLD and NASH. The therapeutic strategies are based on lifestyle

improvement (i.e., physical activity and healthy diet) associated with periodical checking of cardiometabolic risk factors to avoid advanced forms of NAFLD and the prevention of complications [3]. Nevertheless, numerous anti-hypertensive, lipid-lowering (statins) and glucose-lowering drugs (metformin) have been investigated because of NAFLD association with type 2 diabetes (T2DM), hypertension, obesity and dyslipidemia [3]. Other investigated drugs are those belonging to peroxisome proliferator-activated receptor (PPAR)γ agonists (e.g., pioglitazone, rosiglitazone). However, because of the side effects, the incomplete efficacy of these drugs and the variability of the conditions that exist among different patients, the suggested strategies remain those mentioned above [3].

In recent years, natural molecules have been demonstrated to ameliorate typical conditions of NAFLD, from steatosis to inflammation. Among them, the methyl brevifolincarboxylate, a polyphenolic compound, can reduce inflammation and oxidative stress in an hepatocarcinoma cell line [4] and berberine, a benzylisoquinoline alkaloid, can reduce triglyceride synthesis-related genes in in vitro and in vivo models [5]; nevertheless these molecules have not yet been approved by the FDA. Instead, (E)-β-caryophyllene (BCP) has been recognized by the FDA as a safe food or cosmetic additive. BCP is a bicyclic sesquiterpene hydrocarbon widely distributed in the plant kingdom, especially in floral volatiles, occurring in more than 50% of angiosperm families [6]. In plants, BCP acts as a chemoattractant for pollinators, defense against bacterial pathogens and has a pivotal role in the survival and evolution of higher plants as well as in contributing to the unique aroma of essential oils extracted from numerous species [7]. In addition to its role in plants, recent studies have highlighted that BCP plays a role in animal cells as anti-cancer [8], antioxidant [9], anti-inflammatory agent [10]. Although its mechanism of action is not yet fully understood, studies indicate that BCP could act in animal cells through the specific binding to the CB2 cannabinoid receptors [11,12], of which it is a full selective agonist, and possibly through the interaction with members of the family of peroxisome proliferator-activated receptor (PPAR), in particular the isoforms α and γ [13,14].

CB2 receptors belong to the endocannabinoid system (ECS), a complex endogenous system involved in several physiological and pathophysiological functions. The ECS exerts regulatory control on metabolism and food intake and for this reason it represents a potential target for numerous metabolic disorders such as obesity, eating disorders, dyslipidemia and steatosis [15,16]. The ECS is also involved in the regulation of inflammation and in the modulation of depression, schizophrenia and chronic pain [17,18]. The selectivity of BCP for CB2 receptors avoids potential psychotropic effects mediated by the neuronal CB1 cannabinoid receptor, being CB2 receptors mainly expressed in peripheral tissues and in central nervous system (CNS) immune cells [19]. This peculiarity makes BCP a safe phytocannabinoid, with countless beneficial and non-psychoactive effects.

PPAR nuclear receptors are transcriptional modulators, with each isoform having a specific location and role regarding energy homeostasis, lipid and glucose metabolism and inflammatory response [20]. PPARα is mainly expressed in the liver (but also in brown adipose tissue, heart, muscles and kidney) and acts as the master regulator of hepatic lipid metabolism, being involved especially in fatty acid (FA) beta-oxidation. PPARγ is characterized by three isoforms: PPARγ1, PPARγ2 and PPARγ3. PPARγ1 is ubiquitously expressed, PPARγ2 is mainly expressed in adipose tissue and in the liver, whereas PPARγ3 is expressed in the colon and adipose tissue [20]. The role of the three isoforms slightly changes based on cell type, but in the liver they are essentially involved in the regulation of glucose and lipid metabolism, protection against inflammation, oxidation and liver fibrosis [21].

The interaction between BCP and PPARα and PPARγ is not as well documented as it is for CB2 receptors; however, some studies have shown that there is a direct interaction between BCP and PPARα [13] and probably an indirect interaction with PPARγ. In fact, the triggering of PPARγ via BCP-mediated CB2 receptor activation has been hypothesized [22].

This study aimed to investigate the anti-steatotic effects of BCP in the immortalized human hepatoma cell line HepG2, one of the cell models mostly used to induce NAFLD

and to test the therapeutic effects of pharmacological and natural compounds [23]. To mimic the key NAFLD risk factor, increased fat intake, we added palmitic and oleic acid to cell culture media obtaining significant intracellular lipid accumulation in the absence of overt cytotoxicity. We first investigated the effect of BCP on the intracellular lipid accumulation and lipid profile, then we examined the involvement of different receptors in these processes. Our findings suggest that treatment with BCP induces a reduction in lipid accumulation and a modification in intracellular lipid composition mediated by CB2 and PPAR receptors and that these effects are accompanied by a modulation of their expression. We also observed that BCP is able to cross the plasma membrane and therefore to act on intracellular localized receptors.

2. Results

2.1. HepG2 Cell Viability Is Not Affected by Steatosis Induction and BCP Treatment

HepG2 hepatoma cells were induced to become steatotic by 24 h treatment with 0.5 mM FFA mixture, made of sodium palmitate and sodium oleate (1:2, *w*/*w*, referred hereafter as FFAm) along with BSA (1%, *w*/*v*).

To analyze BCP effect on cell viability, HepG2 cells were treated for 24 h with 0.5 mM FFAm alone or in the presence of different concentrations of BCP (50 nM, 500 nM, 1 μM, 5 μM, 10 μM and 50 μM). Untreated cells and cells treated with 1% BSA only were used as controls. The CellTiter-Glo® viability assay shows that neither FFAm nor FFAm + BCP affect HepG2 steatotic cell viability (Figure 1).

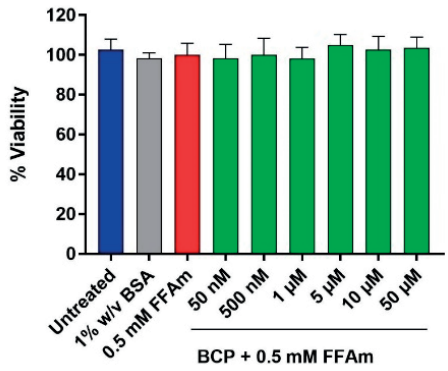

Figure 1. Cell viability assay of HepG2 cells based on ATP content. HepG2 cells were treated for 24 h with 0.5 mM FFAm and with increasing concentrations of BCP. Either BCP plus 0.5 mM FFAm, FFAm alone or 1% *w*/*v* BSA did not affect HepG2 cell viability. Control conditions (untreated) and treatments are represented as the mean ± SEM of three independent experiments.

2.2. BCP Reduces Intracellular Triglyceride Content in HepG2 Steatotic Cells

To study the effect of BCP on the induction of steatosis, HepG2 cells were co-treated with 0.5 mM FFAm and increasing concentrations of BCP (ranging from 50 nM to 50 μM). After 24 h treatment, lipid droplets and nuclei were visualized by AdipoRed™/NucBlue™ fluorescent staining (Figure 2A). Triglyceride accumulation and DNA content were quantified and expressed as a percentage change with respect to 0.5 mM FFAm-treated cells (positive control) (Figure 2B–D).

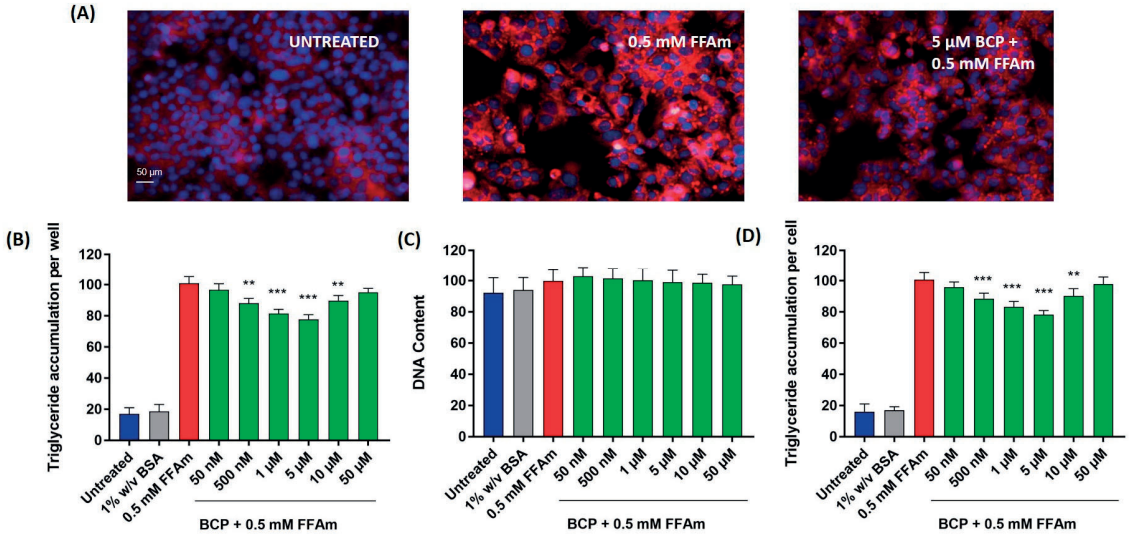

Figure 2. Lipid accumulation in HepG2 cells. BCP attenuates intracellular lipid accumulation in steatotic HepG2 cells without altering the cell number (DNA content). (**A**) Representative images of AdipoRed (red, triglycerides) and NucBlue (blue, nuclei) stainings; UNTREATED = untreated hepatocytes (control); 0.5 mM FFAm = palmitate and oleate-treated hepatocytes; 5 µM BCP + 0.5 mM FFAm = HepG2 cells co-treated for 24 h with BCP and FFAm. Scale bar: 50 µm. (**B**) Bar graph summarizing AdipoRed staining experiments to assess triglyceride accumulation per well in untreated cells, BSA-treated cells, 0.5 mM FFAm-treated positive control cells and HepG2 cells treated with 0.5 mM FFAm and various concentrations of BCP for 24 h. (**C**) Bar graph summarizing the DNA content per well (NucBlue staining). (**D**) Bar graph showing the triglyceride accumulation per cell, calculated as the ratio of AdipoRed and NucBlue stainings. Data are expressed as percentage change with respect to 0.5 mM FFA control condition (set equal to 100) and represent the mean ± SEM of five independent experiments. ** $p < 0.01$; *** $p < 0.001$ vs. positive control (0.5 mM FFAm-treated cells).

Triglyceride accumulation was highly increased by the treatment with FFAm, compared to untreated control cells, while the co-treatment with 500 nM, 1 µM, 5 µM and 10 µM BCP significantly ($p < 0.01$) reduced the amount of intracellular triglycerides (Figure 2B). This result was not due to cytotoxic effects or to a reduction in HepG2 cell proliferation, since the treatment with FFAm and BCP did not induce any significant change in the DNA content (Figure 2C), nor in the cell viability (Figure 1), in respect to untreated and FFAm-treated cells. No changes in triglyceride accumulation or the DNA content were observed in cells cultured in the presence of 1% w/v BSA alone.

The DNA content was used to normalize the total triglyceride values to obtain the triglyceride content per unit DNA (as a proxy for triglycerides accumulation per cell). Figure 2D shows that 500 nM, 1 µM, 5 µM and 10 µM BCP were able to induce a significant ($p < 0.01$) decrease in triglyceride accumulation/cell, with the maximum reduction at 5 µM (corresponding to a 22% reduction of the levels of the FFAm positive control).

2.3. BCP Modifies the Intracellular Lipid Profile of HepG2 Steatotic Cells

To evaluate whether the effect of BCP on total lipid content could be linked to changes in the intracellular lipid profile, GC-MS was employed to identify specific intracellular FFA, whereas GC-FID was used for the quantitative analysis. The FFA composition of steatotic HepG2 cells (0.5 mM FFAm-treated cells) was consistent with that of typical NAFLD models, including myristic acid (C14:0), palmitic acid (C16:0), palmitoleic acid

(*cis*-Δ^9-C16:1), stearic acid (C18:0), oleic acid (*cis*Δ^9-C18:1) and arachidonic acid (C20:4). Compared to untreated controls, steatotic HepG2 cells (Figure 3, red bars) showed a statistically significant ($p < 0.01$) increase of *cis*-Δ^9-C18:1 and C16:0 (Figure 3A), as well as C14:0, C18:0 and *cis*-Δ^9-C16:1 (Figure 3B); no significant ($p > 0.05$) changes were found for C20:4 (Figure 3B). Treatment of steatotic cells with BCP (Figure 3, green bars) caused a significant ($p < 0.01$) reduction (−22%) in the amount of *cis*-Δ^9-C18:1 and C16:0 (Figure 3A), compared to 0.5 mM FFAm-treated cells; the same reduction was found for C14:0, whereas a 19% reduction occurred for C18:0 (Figure 3B). Interestingly, a significant 37% increase was found for *cis*-Δ^9-C16:1. No changes were found for C20:4 ($p > 0.05$) (Figure 3B). These results indicate that BCP was able to reduce the amount of all the identified saturated FFA, while the unsaturated C20:4 was unaffected and the levels of the unsaturated *cis*-Δ^9-C16:1 were increased by BCP treatment.

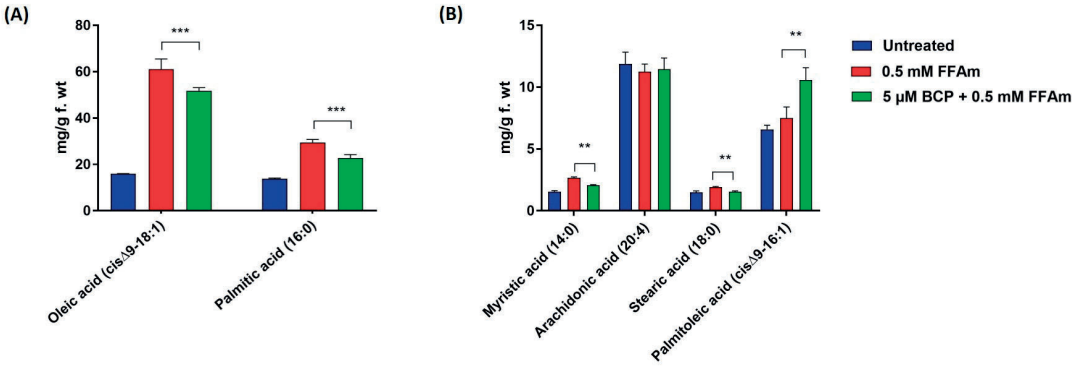

Figure 3. FFA composition of HepG2 cells after incubation for 24 h with 0.5 mM FFAm with or without BCP. Six fatty acids were identified and quantified. (**A**) BCP reduces the amount of oleic acid (cis-Δ9-C18:1) and palmitic acid (C:16) of steatotic cells. (**B**) BCP treatment significantly reduces the content of myristic acid (C14:0) and stearic acid (C18:0), while it increases palmitoleic acid (cis-Δ9-C16:1), in comparison to steatotic control cells. Data are represented as the mean ± SEM of three independent experiments and the values are expressed as mg g−1 fresh weight (f.wt). ** $p < 0.01$; *** $p < 0.001$ vs. positive control (0.5 mM FFAm-treated cells).

2.4. BCP Inhibits Lipid Accumulation through Interaction with Different Receptors: Effects of CB2 and PPAR Receptor Antagonists

In order to characterize the mechanism of action of BCP in the reduction of lipid accumulation in steatotic HepG2 cells, a receptor antagonist approach was employed. In particular, we focused on cannabinoid CB2 receptors and receptors involved in lipid metabolism, i.e., PPARα and PPARγ. The specific CB2 receptor antagonist AM630, the PPARα receptor antagonist GW6471 and the PPARγ antagonist GW9662 were used at concentrations obtained from literature data [11,24,25]. No effects on lipid accumulation (Figure 4A–C) nor on cell viability were observed when treating HepG2 cells with each of the different antagonists alone, AM630, GW6471 and GW9662.

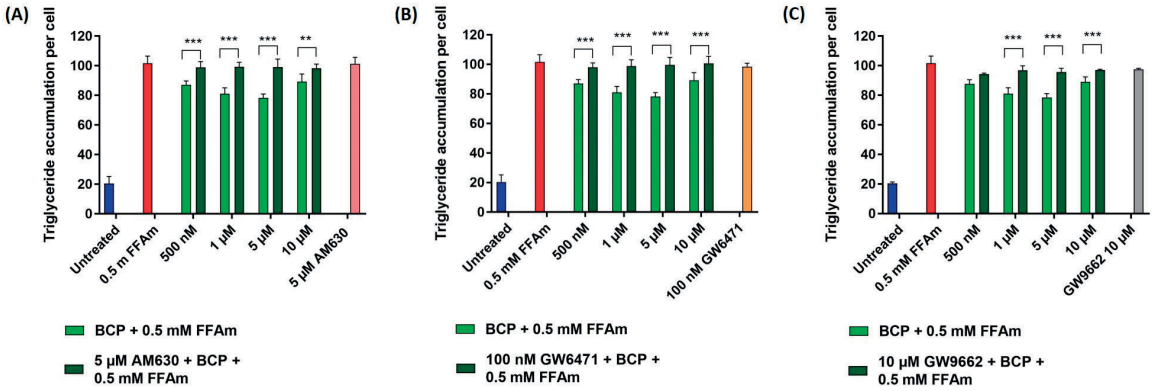

Figure 4. Effect of CB2, PPARα and PPARγ receptors antagonists on triglyceride accumulation per cell. Cells were incubated with different concentrations of BCP and 0.5 mM FFAm, in the presence or absence of specific receptor antagonists for 24 h. (**A**) Treatment of HepG2 cells with 5 µM CB2 antagonist AM630. (**B**) Treatment with 100 nM PPARα antagonist GW6471. (**C**) Treatment with 10 µM PPARγ antagonist GW9662. Data are expressed as a percentage change with respect to 0.5 mM FFA control condition (set equal to 100) and represent the mean ± SEM of five independent experiments. ** $p < 0.01$; *** $p < 0.001$ vs. BCP + 0.5 mM FFAm treated cells.

At the concentration range between 500 nM and 10 µM BCP (identified as the most effective doses in previous experiments), the co-treatment of HepG2 cells with the CB2 receptor antagonist AM630 (5 µM) completely reversed BCP-driven reduction of lipid accumulation, restoring values of intracellular triglycerides comparable to that of steatotic cells (Figure 4A). Similarly, treatment with the PPARα antagonist GW6471 (100 nM) completely reversed the anti-steatotic effect of BCP at all concentrations (Figure 4B). The treatment with the PPARγ-specific antagonist GW9662 (10 µM) partially reversed the lipid reduction induced by 1, 5 and 10 µM BCP (Figure 4C).

These results indicate that BCP is able to reduce lipid accumulation in steatotic HepG2 cells by interacting with CB2 and PPAR receptors.

2.5. CB2, PPARα and PPARγ mRNA Expression Is Affected by Steatosis and BCP Treatment

To investigate whether CB2, PPARα and PPARγ mRNA expression levels are modified by steatosis and the ability of BCP to revert these changes, qRT-PCR experiments were conducted. The expression level of the *CNR2* gene resulted in significantly upregulated steatotic cells, when compared to untreated cells. Interestingly, co-treatment with BCP significantly reduced ($p < 0.001$) CB2 mRNA levels in steatotic cells, bringing CB2 expression levels closer to those of the non-pathological condition (Figure 5A).

The expression of PPARs was significantly reduced in steatotic conditions compared to untreated cells (Figure 5B,C). Co-treatment of steatotic cells with BCP resulted in a significant ($p < 0.001$) increase in PPARα expression (Figure 5B), while no statistically significant change was observed in the expression of PPARγ (Figure 5C).

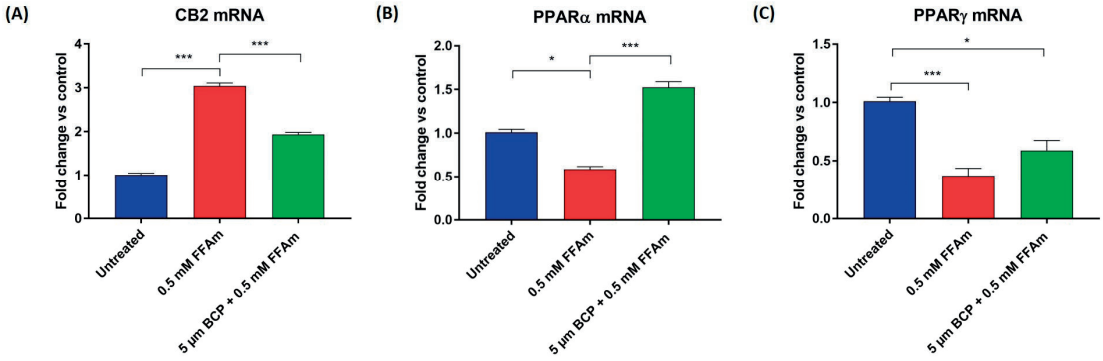

Figure 5. qRT-PCR analysis of CB2 (**A**), PPARα (**B**) and PPARγ (**C**) mRNAs normalized for the housekeeping gene β-actin. Data are represented as the mean ± SEM of three independent experiments. * $p < 0.05$, *** $p < 0.001$ vs. control (untreated cells, set equal to 1) or vs. 0.5 mM FFAm-treated cells.

2.6. CB2 Receptors Are Localized Intracellularly in HepG2 Cells

Since data on CB2 receptor localization are lacking in hepatocytes, we performed CB2 immunofluorescence experiments on HepG2 cells. Figure 6 shows a confocal image with punctate staining mainly located at intracellular sites. The staining level for CB2 in HepG2 cells appears quite heterogeneous, as evidenced by the presence of CB2high+ cells (arrows) and CB2low + (arrowheads) cells in the same clusters of cells (Figure 6, left panel). Single confocal planes show a prevalent perinuclear distribution of CB2 immunopositive puncta (Figure 6, right panels).

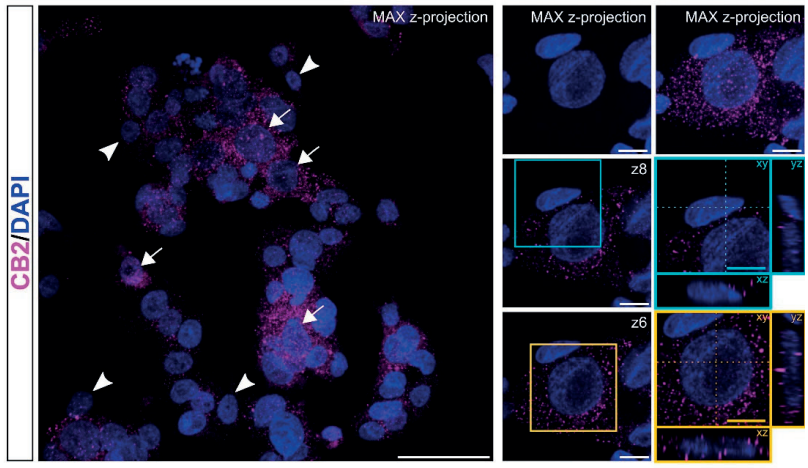

Figure 6. Localization of CB2 receptors. Representative confocal images showing CB2 immunostaining (magenta) in HepG2 cell line. Nuclei are stained with DAPI (blue). Pictures are shown as max z-projections (low magnification; **left**) with white arrows and arrowheads to highlight CB2high+ cells and CB2low+ cells, respectively, and a single confocal plane with reslicing (**right**) to better appreciate the intracellular distribution of CB2+ puncta in two of the cells present in the image. The cyan contoured image shows a cell positive for CB2 at low levels; the yellow contoured image identifies a cell with extensive immunolabelling for CB2. Scale bars: 50 µm (low magnification) and 10 µm (high magnification).

2.7. BCP Enters HepG2 Cells with a Maximum Uptake at 2 h from the Beginning of Treatment

Since we demonstrated that CB2 receptors are mostly intracellularly localized and PPAR receptors are well-known nuclear receptors, we decided to assess whether BCP is indeed able to enter HepG2 cells. The quantification of BCP intracellular uptake was evaluated by a time-course analysis in living cells by GC-MS. HepG2 cells were treated with 5 μM BCP for 24 h and samples were taken from time 0 to 24 h after treatment. By using GC-MS in the single ion monitoring (SIM) for BCP ions, we found that BCP was able to cross the cell membrane and enter HepG2 cells as soon as 1 h from the beginning of the treatment, with a maximum uptake measured at 2 h. After this period, the BCP intracellular concentration decreased linearly up to 24 h after treatment (Figure 7).

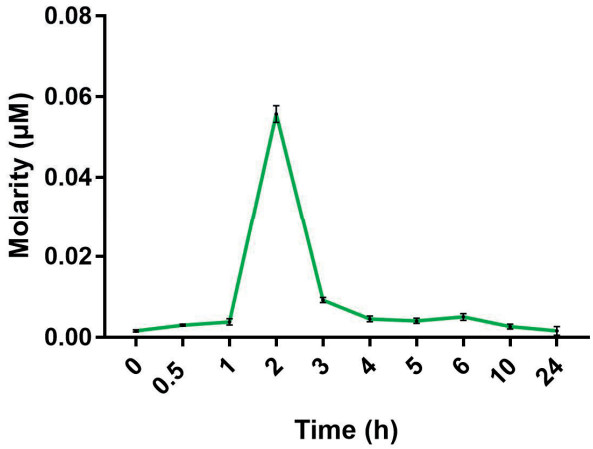

Figure 7. Time-course of BCP uptake by HepG2 cells measured with GC-MS. Maximum concentration of BCP was found 2 h after the beginning of the treatment. Data are represented as the mean ± SEM of three independent experiments.

3. Discussion

Despite recent progresses in understanding the various steps involved in the development and progression of NAFLD, no approved pharmacological treatments for this very common chronic disease are yet available [3]. Therefore, additional efforts are needed to find molecules able to interact with the molecular targets identified in NAFLD pathogenesis. Plant-derived molecules can be an important source for the development of new drugs [26]; in this work, we focused our attention on the anti-steatotic activity of BCP, a phytocannabinoid with promising therapeutic effects in metabolic disorders and inflammation.

In order to mimic NAFLD in vitro, we incubated HepG2 hepatocytes for 24 h with a mixture of oleate and palmitate, which are the most abundant monounsaturated and saturated FFA in human diet [23]. Our steatosis protocol differed from the one used by Kamikubo and colleagues [24], who incubated HepG2 cells with palmitic acid only, a treatment that generally induces higher toxicity and the release of pro-inflammatory chemokines, which are typical of NASH more than the NAFLD condition [23]. In line with the results obtained by Kamikubo et al. [24], we found that BCP co-incubation can reduce the total lipid accumulation in a dose-dependent manner, with maximal activity at 5 μM. BCP was able to reduce both oleic and palmitic acid, here used to induce steatosis in HepG2 cells and also significantly reduced stearic and myristic acid, both saturated fatty acids associated with cellular damage [27,28]. Noticeably, BCP was able to induce a 37% increase in palmitoleic acid, a monounsaturated fatty acid that has been widely studied in in vivo models of obesity because of its anti-inflammatory properties [29]. We argue that the increase in palmitoleic acid might represent a protective detoxifying strategy converting palmitic acid into an unsaturated FFA. There is a general agreement that NAFLD

progression occurs when mechanisms aimed at counteracting FFA-induced lipotoxicity are ineffective, leading to oxidative stress, ER stress, mitochondrial damage, immune-mediated cellular damage and apoptotic death [1]. Our data strongly suggest that BCP is able to reduce the amount of possibly toxic saturated fatty acids and increase selected monounsaturated fatty acids, thus representing a valuable agent in preventing cellular injuries associated with NASH.

Besides emphasizing BCP ability to modify intracellular lipid composition, our data suggest that BCP effects involve the activation of CB2 as well as PPAR receptors.

PPARα and PPARγ are ligand-activated transcription factors with pleiotropic actions in several tissues. They are critical regulators not only of fatty acid metabolism, but also of glucose metabolism, inflammation and fibrosis [20]. The role of PPARα in the liver has been widely investigated both in physiological and steatotic conditions. The activation of PPARα induces the transcription of a range of genes involved in mitochondrial and peroxisomal FA oxidation, ketogenesis and lipid transport, thereby reducing hepatic lipid levels [20]. A recent study demonstrated that the deletion of hepatic *Pparα* in mice results in enhanced liver steatosis because of the impaired oxidation of FFA [30], underscoring the relevance and potential of hepatocyte PPARα as a drug target for NAFLD.

PPARγ is involved in FFA uptake and lipogenesis and has significant anti-inflammatory properties. Early results demonstrated that its activation is steatogenic in the liver [31] while recent works showed that PPARγ ligands (such as thiazolidinediones) ameliorate fat accumulation by decreasing saturated fatty acids in a zebrafish model of NAFLD [32]. This last effect possibly depends on the enhanced release of adiponectin by the adipose tissue and a concomitant increase in FFA oxidation in hepatocytes by AMPK activation as demonstrated in in vivo studies [33]. There are also in vitro studies demonstrating the role of PPARγ agonists in ameliorating lipid accumulation and inflammation associated with NASH. This is the case of GVS-12, a synthetic PPARγ agonist that can reduce triglycerides, inflammatory interleukins and other biomarkers associated with NASH in HepG2 cells [34]. An interesting synthetic ligand is saroglitazar, a dual PPARα/γ agonist with prevalent PPARα agonist activity. The efficacy of saroglitazar in counteracting NAFLD/NASH has been compared to that of fenofibrate, a PPARα agonist, and pioglitazone, a PPARγ agonist, showing that the combined action of saroglitazar improves lipid-mediated oxidative stress, inflammation and impaired mitochondrial biogenesis more effectively than single agonists, both in vitro and in vivo [35]. Many PPAR agonists, such as saroglitazar, are currently tested in clinical trials or have already been approved for the treatment of other metabolic diseases, such as pioglitazone used for the treatment of T2DM [3,20]. Ongoing clinical trials indicate that dual PPAR agonists can have ameliorating effects on NASH by acting on interrelated mechanisms. Thus, combining PPARα and PPARγ activation may be a successful strategy in the therapy of NAFLD [36].

According to our data, BCP effects are mediated both through PPARα and PPARγ. The activation of PPARα likely occurs through a direct mechanism; in support of this view, an interesting study demonstrated through a surface plasmon resonance (SPR)-BIA core system that BCP directly binds the PPARα ligand binding domain (LBD) even if it is a hydrophobic molecule and has a relatively small molecular weight compared with conventional PPAR ligands [13]. For PPARγ, there are no studies demonstrating a direct interaction with BCP; however, there is evidence of an indirect activation, possibly through CB2 receptors [22,37]. BCP dual activation of PPARα and PPARγ, observed in our in vitro experiments and previously shown in cocaine addiction studies performed in vivo [38], highlights the possibility that BCP might behave as a dual PPARα/γ agonist like saroglitazar. It should also be noted that GW9662, the PPARγ antagonist used in our experiments, has an IC50 value of 3.3 nM for PPARγ and 32 nM for PPARα [39]. Therefore, it cannot be excluded that GW9662 partially blocks PPARα, contributing to the reversion of the anti-steatotic effect of BCP observed in our experiments. In accordance with recently published results [40], we found that both PPARα and γ are downregulated during the pathological condition of steatosis. Intriguingly, co-treatment with BCP induced

a marked upregulation of PPARα, bringing it back to even higher expression levels than in the untreated control. This latter result suggests that BCP might be able to enhance FA oxidation, therefore reducing hepatic steatosis.

The binding of BCP to the CB2 receptor has been well characterized [11], and the role of the endocannabinoid system (ECS) in the liver has been widely studied since it may be a therapeutic target for chronic liver disease [41], characterized by dysregulation of hepatic lipid metabolism and also perturbation of the hepatic endocannabinoid system [42]. Although CB2 expression in the liver is moderate, its role has been demonstrated in both physiological (regulating liver development in zebrafish embryos [43]) and pathological conditions. For example, recent studies showed that CB2, in contrast to CB1 [44], elicits anti-fibrogenic and anti-inflammatory effects [45]. However, the role of CB2 in the progression of NAFLD has been debated: on the one hand, studies on the activation of both CB1 and CB2 receptors have shown increased lipid accumulation [46] and potentiation of hepatic steatosis [47]; on the other hand, our results with a CB2 antagonist show that CB2 activation can counteract steatosis, in line with other works [24,48,49]. In agreement with in vivo data [50,51], we show that steatotic conditions upregulate CB2 expression in hepatocytes, and that concomitant exposure to BCP is able to revert the level of CB2 expression almost to control levels, thus facilitating return-to-normal conditions.

While PPARs are well known intracellular receptors, CB2 are seven-domain transmembrane receptors, whose localization is assumed to be on the plasma membrane. To verify this assumption, we performed immunolocalization studies. Unexpectedly, we found that CB2 receptors are located mainly intracellularly in HepG2 cells, often in a perinuclear position, most likely on the ER membrane or other intracellular organelles. Recent studies have suggested possible intracellular CB2 localization in specific cell types; for instance, Castaneda and colleagues [52] demonstrated that in peripheral blood B cells, CB2 receptor expression is regulated by different factors and these receptors are localized both on the cell membrane and on intracellular membranes. In line with this result, by kinetics studies, we showed for the first time that BCP can cross the hepatocyte plasma membrane and enter the cells with a maximum peak at 2 h, followed by a decrease, possibly due to BCP metabolism. Further studies are needed to determine the exact localization of intracellular CB2 receptors in hepatocytes and their involvement in the regulation of lipid metabolism.

4. Materials and Methods

4.1. Reagents

Chemicals used were: (E)-β-caryophyllene (BCP) purchased from Sigma-Aldrich (St. Louis, MO, USA), AdipoRed™ assay reagent from Lonza (Walkersville, MD, USA), NucBlue Live ReadyProbes Reagent from Invitrogen (Carlsbad, CA, USA), CellTiter-Glo® Luminescent Cell Viability from Promega (Madison, WI, USA), anti-CB2 primary antibody from Cayman chemical (Ann Arbor, MI, USA), anti-Rabbit IgG AlexaFluor647 secondary antibody from Jackson Immunoresearch (Ely, UK), AM630, GW9662 and GW6741 antagonists from Cayman chemical and sodium oleate, sodium palmitate and bovine serum albumin from Sigma-Aldrich. Unless otherwise specified, all other chemicals were purchased from Sigma-Aldrich.

4.2. Cell Cultures

HepG2 human hepatoma cell line (European Collection of Authenticated Cell Cultures ECACC catalogue number 85011430) was purchased from Sigma-Aldrich. Cells were cultured in Minimum Essential Medium Eagle (MEM) supplemented with 10% fetal bovine serum, 2 mM L-glutamine, 50 IU/mL penicillin, 50 μg/mL streptomycin and 1% non-essential amino acids (NEAA). For every experiment, cells were grown at sub-confluence.

4.3. Cell Viability

The viability of HepG2 cells was evaluated at the end of the steatosis induction experiments and treated with different concentrations of BCP, by CellTiter-Glo® Luminescent Cell

Viability Assay, based on the quantitation of ATP, which signals the presence of metabolically active cells. Cells were washed in phosphate-buffered saline (PBS), then CellTiter-Glo® reagent, diluted 1:1 in PBS, was added. Cells were incubated at room temperature in the dark for 10 min, then luminescence was detected and quantified with the FilterMax F5 Multi-Mode microplate reader (Molecular Devices, Sunnyvale, CA, USA). The values of luminescence are directly proportional to the number of viable cells.

4.4. In Vitro Steatosis Induction and Lipid Quantification

For steatosis induction experiments, 2×10^4 cells/well were seeded in 96-well black clear bottom plates (Greiner Bio-One, Frickenhausen, Germany). Prior to the experiments, cells were starved overnight with serum-free MEM, then cells were incubated for 12 h or 24 h in serum-free MEM containing 0.25 mM, 0.5 mM or 1 mM free fatty acid mixture (FFAm). The mixture was prepared by coupling sodium palmitate (Na^+-hexadecanoate) and sodium oleate (Na^+-(Z)-octadec-9-enoate) (1:2 ratio) with 1% w/v FFA-free BSA in serum free MEM, at 38 °C in agitation overnight, to allow FFA coupling with BSA; the mixture was then filtered and used immediately in subsequent experiments or frozen at 20 °C. Based on the preliminary results we obtained, for subsequent experiments, HepG2 cells were treated for 24 h with 0.5 mM FFAm alone or in the presence of scalar dilutions of BCP (50 nM−50 µM); control cells were grown with serum-free MEM containing 1% w/v BSA. At the end of the experiments, cells were washed in PBS, then a dye mixture containing AdipoRed and NucBlue reagents (25 µL and 1 drop, respectively, for each mL of PBS) was added. AdipoRed assay reagent quantifies intracellular triglycerides, while the DNA content was estimated by NucBlue staining. After 40 min of incubation at room temperature in the dark, fluorescence was measured with Filtermax F5 microplate reader (Molecular Devices, San Jose, CA, USA); for AdipoRed, quantification excitation was performed at 485 nm and emission read at 535 nm, while for NucBlue, excitation was at 360 nm and emission read at 460 nm.

4.5. Antagonists Treatment

For antagonists experiments, 2×10^4 cells/well were seeded in 96-well black clear bottom plates, starved and treated as above mentioned with FFA mixture, 5 µM BCP and the following antagonists: 5 µM AM630 (CB2 receptor antagonist), 100 nM GW6471 (PPARα receptor antagonist) or 10 µM GW9662 (PPARγ receptor antagonist).

4.6. Lipid Extraction, Identification and Quantification by Gas Chromatography

For lipid extraction and quantification experiments, 2×10^6 cells were grown on T-25 flasks. After cell starvation, HepG2 cells were treated with FFAm alone or FFAm and 5 µM BCP for 24 h. One ml of culture medium was then taken for gas chromatography–mass spectrometry (GC-MS) analysis of free fatty acids. The intracellular fatty acid content was also analyzed; cells were washed with PBS, detached with trypsin and centrifuged at 800 g, 5 min. Lipids were extracted from cell pellets using cyclohexane (1:10, w/v ratio) and then esterified with boron tri-fluoride (10% w/v in methanol). Fifty µg heptadecanoic acid (C17:0) was added as the internal standard. Fatty acid methyl esters (FAME) identification was performed by gas chromatography coupled with mass spectrometry (GC-MS) (5975T, Agilent Technologies, Santa Clara, CA, USA). FAME quantitative analyses were performed through GC coupled with a flame ionization detector (GC-FID) (GC-2010 Plus, SHIMADZU, Kyoto, Japan). The GC carrier gas was helium with a constant flux of 1 mL min^{-1}, and separation was obtained with a non-polar capillary column ZB5-MS (30 m length, 250 µm diameter and stationary phase thickness of 0.25 µm, 5% phenyl-arylene and 95% polydimethyl siloxane stationary phase) (Phenomenex, Torrance, CA, USA). GC-FID FAME separation was performed in the same conditions, by using a similar column. Mass spectrometer parameters were: ionization energy of the ion source set to 70 eV and the acquisition mode set to 50–350 *m/z*. Separated molecules were identified through the comparison of mass fragmentation spectra with reference spectra of the software NIST

v2.0 and libraries NIST 98, by comparison of Kovats indexes and the internal standard injection (C17,C20:4, C20:5—Sigma Aldrich, St Louis, MO, USA). The results are expressed as mg g^{-1} fresh weight (f.wt).

4.7. Intracellular Quantification of BCP in Time-Course Experiments

For BCP time-course uptake experiments, 1×10^6 cells were grown on 6-well plates and treated with 5 μM BCP. Starting from time zero and after 30 min, 1 h, 1.5 h, 2 h, 3 h, 4 h, 5 h, 6 h, 10 h and 24 h cells were washed in PBS, detached with trypsin, centrifuged and the pellets were transferred in glass vials where 1 mL of hexane was added. The identification of BCP amounts in cells at different times was performed with the Single Ion Monitoring (SIM) method by GC-MS. The following chromatographic conditions were used: column ZB5-MS (30 m length, 250 μm diameter and stationary phase thickness of 0.25 μm, 5% phenyl-arylene and 95% of poly-dimethyl siloxane stationary phase); splitless mode, oven program: 40° for 1 min, then a 5 °C min^{-1} ramp to 200 °C, a 10 °C min^{-1} ramp to 220 °C, and a 30 °C min^{-1} ramp to 260 °C, final temperature held for 3.6 min. Mass spectra were acquired within the 29–350 m/z interval operating the spectrometer at 70 eV and at scan speed mode. The identification of BCP was performed on the basis of both matches of the peak spectra with a library spectral database, and comparison with pure standards.

4.8. Immunofluorescence

For immunofluorescence experiments, 6×10^4 cell/cm^2 were seeded on glass coverslips and incubated for at least 3 h to allow adhesion. Then, cells were fixed for 30 min in 4% paraformaldehyde dissolved in 0.1 M phosphate buffer, pH 7.3. After three washes with PBS, cells were incubated for 15 min with PBS containing 0.01% Triton-X100 and then for 45 min with PBS containing 1% BSA and 10% normal donkey serum. Triton-X100, normal donkey serum and BSA concentrations were selected after several trials to avoid autofluorescence of HepG2. Cells were then incubated overnight at 4 °C with anti-CB2 (1:100 in PBS) primary polyclonal antibody. Coverslips were washed twice with PBS and incubated for 1 h at room temperature with the secondary antibody, anti-rabbit IgG Alexa Fluor 647 (1:600 in PBS containing 1% normal donkey serum). After two washes in PBS, cells were incubated for 20 min in DAPI (1:200 in PBS), washed again twice in PBS and then coverslips were mounted on standard slides with DABCO. Pictures of HepG2 cells immunolabeled for CB2 were taken with a TCS SP5 confocal microscope (Leica Microsystems, Wetzlar, Germany). Confocal image z-stacks were captured throughout the thickness of the cells and were performed with 0.7 μm optical step size using an objective 63X/1.4 NA oil immersion lens with a resolution of 8-bit, 1024/1024 pixels and 100-Hertz scan-speed (without additional zoom: 1 voxel, xyz = 240 nm × 240 nm × 692 nm; with 2.5× additional zoom: 1 voxel, xyz = 96 nm × 96 nm × 692 nm). Images are shown as maximum intensity projection or single plane with reslice.

4.9. RNA Extraction and qRT-PCR

For qRT-PCR experiments, 1×10^6 cells were grown on 6-well plates and treated to induce steatosis in the presence/absence of 5 μM BCP (see above). Total RNA extraction was performed using TRIZOL® Reagent (Invitrogen) following manufacturer's instructions. Chloroform was added and, after 5 min of centrifugation at 14,000 rpm, RNA was precipitated in isopropanol for 3 h at −20 °C. Samples were then centrifuged at 14,000 rpm for 15 min, the RNA was washed with 70% ethanol and centrifuged at 14,000 rpm for 5 min. The RNA pellet was briefly air-dried and resuspended in 30 μL sterile water. Samples were quantified using NanoDrop 8000 Spectrophotometer (Thermo Fisher Scientific, Waltham, MA, USA). qReal-time PCR was performed using SensiFast SYBR No-ROX One-Step Real-Time qPCR kit (Bioline, London, UK) in the thermal cycler Rotor Gene Q (Qiagen, Hilden, Germany). qRT-PCR conditions were: retrotranscription (55 °C, 15 min), initial denaturation (95 °C, 2 min), 50 cycles of denaturation (94 °C, 15 s), annealing (55 °C, 10 s), extension (68 °C, 24 s) and final melting (ramp from 56 °C to 99 °C). Each RNA sample was

analyzed in three technical replicates containing 50 ng of total RNA. Relative quantification of mRNA abundance in each sample was performed using a standard curve, built with several dilutions of the samples. The widely used housekeeping gene β-actin was used as an internal control to normalize target gene expression. The reliability of the housekeeping gene was confirmed by its consistency of expression across treatments. qRT-PCR starting from constant amounts (50 ng) of different RNA samples, accurately quantified by NanoDrop Spectrophotometer analysis, resulted in fact in comparable levels of amplification (Ct, cycle threshold values). Specific primers were designed with PrimerBlast software on the basis of human sequences (Table 1). The qPCR primer efficiencies were first assessed by the amplification of serial dilutions of RNA pools (three replicates for each dilution); the efficiency values were directly calculated by Rotor Gene Q software and were as follows: β-actin 98%, *CNR2* 103%, *PPARα* 95%, *PPARγ* 105%.

Table 1. Specific primers used in qRT-PCR.

Gene	Forward Sequence	Reverse Sequence	Amplicon Size	GenBank Accession Number
β-actin	5′ CCAACCGCGAGAAGATGA 3′	5′ CCAGAGGCGTACAGGGATAG 3′	97 bp	NM_001101.5
CNR2	5′ TGGCATAGAAGACGGAGCTG 3′	5′ CCCGGAGAGCCCCAAATG 3′	177 bp	NM_001841.3
PPARα	5′ ACACCGAGGACTCTTGCGA 3′	5′ GGAAAGGGCAAGTCCCGATG 3′	207 bp	NM_001393944.1
PPARγ	5′ TACTGTCGGTTTCAGAAATGCC 3′	5′ GTCAGCGGACTCTGGATTCAG 3′	141 bp	NM_138712.5

Primers sequences and amplicon size are reported in Table 1

4.10. Statistical Analysis

All experimental data are presented as means ± standard error of the mean (SEM) from at least three technical replicates of 3–5 independent biological experiments (the exact number of independent experiments is indicated in the figure legends). Statistical analysis was performed using the SPSS package version 28. Statistically significant differences between treatment and control groups were assessed by a one-way analysis of variance (ANOVA) followed by Bonferroni's multiple-comparison post hoc test. Differences were considered statistically significant at $p < 0.05$.

5. Conclusions

Taken together, our results suggest that BCP is a promising molecule for the treatment of NAFLD. This conclusion is based on several key aspects of this molecule. BCP may act on multiple targets, many of which are included in NAFLD and metabolic syndrome, since it is able to reduce lipid accumulation in hepatocytes but also in adipocytes [53], may improve muscle insulin resistance [12] and systemic inflammation, therefore resulting in a greater overall improvement compared with compounds with a more liver-restricted mode of action. It should also be considered that BCP is an approved dietary additive with a good safety profile and a safe phytocannabinoid, since it binds specifically to CB2 receptors, thus avoiding the psychotropic effects mediated by CB1 receptors [54]. There are, however, issues related to BCP bioavailability; in fact some studies have already focused on alternative formulations and vectorization techniques to allow better absorption, overcoming the limitations of BCP and making the most of all the properties of this phytocannabinoid [55,56].

Author Contributions: Conceptualization, R.S., S.D.M., M.E.M. and P.B.; methodology, R.S., S.B. (Sara Bonzano), E.C., S.S. and S.B. (Simone Bossi); validation, R.S., S.B. (Sara Bonzano), E.C. and S.B. (Simone Bossi); investigation, R.S., S.B. (Sara Bonzano), E.C., S.S. and S.B. (Simone Bossi); resources, P.B. and M.E.M.; data curation, R.S and E.C.; writing—original draft preparation, R.S.; writing—review and editing, R.S., S.B. (Sara Bonzano), E.C., S.S., S.B. (Simone Bossi), S.D.M., M.E.M. and P.B.; supervision, P.B. and M.E.M.; project administration, P.B. and M.E.M.; funding acquisition, P.B. and M.E.M. All authors have read and agreed to the published version of the manuscript.

Funding: This research was funded by Italian MUR, PRIN 20204YRYS5_004 to P.B., the University of Turin RILO_2022 to M.E.M., by the Doctorate School of Pharmaceutical and Molecular Sciences of the University of Turin.

Institutional Review Board Statement: Ethical review and approval were waived for this study.

Informed Consent Statement: Not applicable.

Data Availability Statement: Data are available upon request.

Acknowledgments: We thank Barbara Mognetti for reading and making useful suggestions to the manuscript.

Conflicts of Interest: The authors declare no conflict of interest.

References

1. Powell, E.E.; Wong, V.W.-S.; Rinella, M. Non-Alcoholic Fatty Liver Disease. *Lancet* **2021**, *397*, 2212–2224. [CrossRef]
2. Friedman, S.L.; Neuschwander-Tetri, B.A.; Rinella, M.; Sanyal, A.J. Mechanisms of NAFLD Development and Therapeutic Strategies. *Nat. Med.* **2018**, *24*, 908–922. [CrossRef] [PubMed]
3. Mantovani, A.; Dalbeni, A. Treatments for NAFLD: State of Art. *Int. J. Mol. Sci.* **2021**, *22*, 2350. [CrossRef] [PubMed]
4. Geethangili, M.; Lin, C.-W.; Mersmann, H.J.; Ding, S.-T. Methyl Brevifolincarboxylate Attenuates Free Fatty Acid-Induced Lipid Metabolism and Inflammation in Hepatocytes through AMPK/NF-KB Signaling Pathway. *Int. J. Mol. Sci.* **2021**, *22*, 10062. [CrossRef]
5. Zhu, X.; Bian, H.; Wang, L.; Sun, X.; Xu, X.; Yan, H.; Xia, M.; Chang, X.; Lu, Y.; Li, Y.; et al. Berberine Attenuates Nonalcoholic Hepatic Steatosis through the AMPK-SREBP-1c-SCD1 Pathway. *Free Radic. Biol. Med.* **2019**, *141*, 192–204. [CrossRef]
6. Maffei, M.E. Plant Natural Sources of the Endocannabinoid (E)-β-Caryophyllene: A Systematic Quantitative Analysis of Published Literature. *Int. J. Mol. Sci.* **2020**, *21*, 6540. [CrossRef] [PubMed]
7. Scandiffio, R.; Geddo, F.; Cottone, E.; Querio, G.; Antoniotti, S.; Gallo, M.P.; Maffei, M.E.; Bovolin, P. Protective Effects of (E)-β-Caryophyllene (BCP) in Chronic Inflammation. *Nutrients* **2020**, *12*, 3273. [CrossRef]
8. Mannino, F.; Pallio, G.; Corsaro, R.; Minutoli, L.; Altavilla, D.; Vermiglio, G.; Allegra, A.; Eid, A.H.; Bitto, A.; Squadrito, F.; et al. Beta-Caryophyllene Exhibits Anti-Proliferative Effects through Apoptosis Induction and Cell Cycle Modulation in Multiple Myeloma Cells. *Cancers* **2021**, *13*, 5741. [CrossRef] [PubMed]
9. Yovas, A.; Manjusha, W.A.; Ponnian, S.M.P. β-Caryophyllene Modulates B-Cell Lymphoma Gene-2 Family Genes and Inhibits the Intrinsic Pathway of Apoptosis in Isoproterenol-Induced Myocardial Infarcted Rats; A Molecular Mechanism. *Eur. J. Pharmacol.* **2022**, *932*, 175181. [CrossRef]
10. Picciolo, G.; Pallio, G.; Altavilla, D.; Vaccaro, M.; Oteri, G.; Irrera, N.; Squadrito, F. β-Caryophyllene Reduces the Inflammatory Phenotype of Periodontal Cells by Targeting CB2 Receptors. *Biomedicines* **2020**, *8*, 164. [CrossRef]
11. Gertsch, J.; Leonti, M.; Raduner, S.; Racz, I.; Chen, J.Z.; Xie, X.Q.; Altmann, K.H.; Karsak, M.; Zimmer, A. Beta-Caryophyllene Is a Dietary Cannabinoid. *Proc. Natl. Acad. Sci. USA* **2008**, *105*, 9099–9104. [CrossRef]
12. Geddo, F.; Antoniotti, S.; Querio, G.; Salaroglio, I.C.; Costamagna, C.; Riganti, C.; Gallo, M.P. Plant-Derived Trans-β-Caryophyllene Boosts Glucose Metabolism and ATP Synthesis in Skeletal Muscle Cells through Cannabinoid Type 2 Receptor Stimulation. *Nutrients* **2021**, *13*, 916. [CrossRef]
13. Wu, C.; Jia, Y.; Lee, J.H.; Jun, H.J.; Lee, H.S.; Hwang, K.Y.; Lee, S.J. Trans-Caryophyllene Is a Natural Agonistic Ligand for Peroxisome Proliferator-Activated Receptor-α. *Bioorganic Med. Chem. Lett.* **2014**, *24*, 3168–3174. [CrossRef] [PubMed]
14. Irrera, N.; D'ascola, A.; Pallio, G.; Bitto, A.; Mazzon, E.; Mannino, F.; Squadrito, V.; Arcoraci, V.; Minutoli, L.; Campo, G.M.; et al. β-Caryophyllene Mitigates Collagen Antibody Induced Arthritis (CAIA) in Mice Through a Cross-Talk between CB2 and PPAR-γ Receptors. *Biomolecules* **2019**, *9*, 326. [CrossRef]
15. Charytoniuk, T.; Zywno, H.; Berk, K.; Bzdega, W.; Kolakowski, A.; Chabowski, A.; Konstantynowicz-Nowicka, K. The Endocannabinoid System and Physical Activity—A Robust Duo in the Novel Therapeutic Approach against Metabolic Disorders. *Int. J. Mol. Sci.* **2022**, *23*, 3083. [CrossRef] [PubMed]
16. Lowe, H.; Toyang, N.; Steele, B.; Bryant, J.; Ngwa, W. The Endocannabinoid System: A Potential Target for the Treatment of Various Diseases. *Int. J. Mol. Sci.* **2021**, *22*, 9472. [CrossRef] [PubMed]

17. Machado, K.d.C.; Islam, M.T.; Ali, E.S.; Rouf, R.; Uddin, S.J.; Dev, S.; Shilpi, J.A.; Shill, M.C.; Reza, H.M.; Das, A.K.; et al. *A Systematic Review on the Neuroprotective Perspectives of Beta-Caryophyllene*; John Wiley and Sons Ltd.: Hoboken, NJ, USA, 2018; Volume 32.
18. Mlost, J.; Wąsik, A.; Starowicz, K. Role of Endocannabinoid System in Dopamine Signalling within the Reward Circuits Affected by Chronic Pain. *Pharmacol. Res.* **2019**, *143*, 40–47. [CrossRef]
19. Francomano, F.; Caruso, A.; Barbarossa, A.; Fazio, A.; La Torre, C.; Ceramella, J.; Mallamaci, R.; Saturnino, C.; Iacopetta, D.; Sinicropi, M.S. β-Caryophyllene: A Sesquiterpene with Countless Biological Properties. *Appl. Sci.* **2019**, *9*, 5420. [CrossRef]
20. Berthier, A.; Johanns, M.; Zummo, F.P.; Lefebvre, P.; Staels, B. PPARs in Liver Physiology. *Biochim. Biophys. Acta Mol. Basis Dis.* **2021**, *1867*, 166097. [CrossRef]
21. Wu, L.; Guo, C.; Wu, J. Therapeutic Potential of PPARγ Natural Agonists in Liver Diseases. *J. Cell. Mol. Med.* **2020**, *24*, 2736–2748. [CrossRef]
22. Youssef, D.A.; El-Fayoumi, H.M.; Mahmoud, M.F. Beta-Caryophyllene Protects against Diet-Induced Dyslipidemia and Vascular Inflammation in Rats: Involvement of CB2 and PPAR-γ Receptors. *Chem. -Biol. Interact.* **2019**, *297*, 16–24. [CrossRef]
23. Gómez-Lechón, M.J.; Donato, M.T.; Martínez-Romero, A.; Jiménez, N.; Castell, J.V.; O'Connor, J.-E. A Human Hepatocellular in Vitro Model to Investigate Steatosis. *Chem.-Biol. Interact.* **2007**, *165*, 106–116. [CrossRef] [PubMed]
24. Kamikubo, R.; Kai, K.; Tsuji-Naito, K.; Akagawa, M. β-Caryophyllene Attenuates Palmitate-Induced Lipid Accumulation through AMPK Signaling by Activating CB2 Receptor in Human HepG2 Hepatocytes. *Mol. Nutr. Food Res.* **2016**, *60*, 2228–2242. [CrossRef] [PubMed]
25. Ma, Z.-G.; Yuan, Y.-P.; Zhang, X.; Xu, S.-C.; Wang, S.-S.; Tang, Q.-Z. Piperine Attenuates Pathological Cardiac Fibrosis Via PPAR-γ/AKT Pathways. *EBioMedicine* **2017**, *18*, 179–187. [CrossRef]
26. Atanasov, A.G.; Zotchev, S.B.; Dirsch, V.M.; Supuran, C.T. Natural Products in Drug Discovery: Advances and Opportunities. *Nat. Rev. Drug Discov.* **2021**, *20*, 200–216. [CrossRef]
27. Saraswathi, V.; Kumar, N.; Ai, W.; Gopal, T.; Bhatt, S.; Harris, E.N.; Talmon, G.A.; Desouza, C.V. Myristic Acid Supplementation Aggravates High Fat Diet-Induced Adipose Inflammation and Systemic Insulin Resistance in Mice. *Biomolecules* **2022**, *12*, 739. [CrossRef]
28. Lu, H.; Guo, R.; Zhang, Y.; Su, S.; Zhao, Q.; Yu, Y.; Shi, H.; Sun, H.; Zhang, Y.; Li, S.; et al. Inhibition of LncRNA TCONS_00077866 Ameliorates the High Stearic Acid Diet-Induced Mouse Pancreatic β-Cell Inflammatory Response by Increasing MiR-297b-5p to Downregulate SAA3 Expression. *Diabetes* **2021**, *70*, 2275–2288. [CrossRef]
29. Simão, J.J.; Cruz, M.M.; Abdala, F.M.; Bolsoni-Lopes, A.; Armelin-Correa, L.; Alonso-Vale, M.I.C. Palmitoleic Acid Acts on Adipose-Derived Stromal Cells and Promotes Anti-Hypertrophic and Anti-Inflammatory Effects in Obese Mice. *Pharmaceuticals* **2022**, *15*, 1194. [CrossRef]
30. Montagner, A.; Polizzi, A.; Fouché, E.; Ducheix, S.; Lippi, Y.; Lasserre, F.; Barquissau, V.; Régnier, M.; Lukowicz, C.; Benhamed, F.; et al. Liver PPARα Is Crucial for Whole-Body Fatty Acid Homeostasis and Is Protective against NAFLD. *Gut* **2016**, *65*, 1202–1214. [CrossRef]
31. Yu, S.; Matsusue, K.; Kashireddy, P.; Cao, W.-Q.; Yeldandi, V.; Yeldandi, A.V.; Rao, M.S.; Gonzalez, F.J.; Reddy, J.K. Adipocyte-Specific Gene Expression and Adipogenic Steatosis in the Mouse Liver Due to Peroxisome Proliferator-Activated Receptor Gamma1 (PPARgamma1) Overexpression. *J. Biol. Chem.* **2003**, *278*, 498–505. [CrossRef] [PubMed]
32. Singh, M.K.; Yadav, R.; Bhaskar, A.K.; Sengupta, S.; Sachidanandan, C. A Diet-Independent Zebrafish Model for NAFLD Recapitulates Patient Lipid Profiles and Offers a System for Small Molecule Screening. *Biochim. et Biophys. Acta (BBA)—Mol. Cell. Biol. Lipids* **2023**, *1868*, 159246. [CrossRef]
33. Wang, Y.; Nakajima, T.; Gonzalez, F.J.; Tanaka, N. PPARs as Metabolic Regulators in the Liver: Lessons from Liver-Specific PPAR-Null Mice. *Int. J. Mol. Sci.* **2020**, *21*, 2061. [CrossRef] [PubMed]
34. Wang, Y.; Zhang, X.; Yuan, B.; Lu, X.; Zheng, D.; Zhang, K.; Zhong, M.; Xu, X.; Duan, X. GVS-12 Attenuates Non-Alcoholic Steatohepatitis by Suppressing Inflammatory Responses via PPARγ/STAT3 Signaling Pathways. *RSC Adv.* **2019**, *9*, 9555–9564. [CrossRef] [PubMed]
35. Jain, M.R.; Giri, S.R.; Bhoi, B.; Trivedi, C.; Rath, A.; Rathod, R.; Ranvir, R.; Kadam, S.; Patel, H.; Swain, P.; et al. Dual PPARα/γ Agonist Saroglitazar Improves Liver Histopathology and Biochemistry in Experimental NASH Models. *Liver Int.* **2018**, *38*, 1084–1094. [CrossRef] [PubMed]
36. Francque, S.; Szabo, G.; Abdelmalek, M.F.; Byrne, C.D.; Cusi, K.; Dufour, J.-F.; Roden, M.; Sacks, F.; Tacke, F. Nonalcoholic Steatohepatitis: The Role of Peroxisome Proliferator-Activated Receptors. *Nat. Rev. Gastroenterol. Hepatol.* **2021**, *18*, 24–39. [CrossRef] [PubMed]
37. Cheng, Y.; Dong, Z.; Liu, S. β-Caryophyllene Ameliorates the Alzheimer-like Phenotype in APP/PS1 Mice through CB2 Receptor Activation and the PPARγ Pathway. *Pharmacology* **2014**, *94*, 1–12. [CrossRef]
38. Galaj, E.; Bi, G.-H.; Moore, A.; Chen, K.; He, Y.; Gardner, E.; Xi, Z.-X. Beta-Caryophyllene Inhibits Cocaine Addiction-Related Behavior by Activation of PPARα and PPARγ: Repurposing a FDA-Approved Food Additive for Cocaine Use Disorder. *Neuropsychopharmacology* **2021**, *46*, 860–870. [CrossRef]
39. Indrayanto, G.; Putra, G.S.; Suhud, F. Chapter Six—Validation of in-Vitro Bioassay Methods: Application in Herbal Drug Research. In *Profiles of Drug Substances, Excipients and Related Methodology*; Al-Majed, A.A., Ed.; Academic Press: Cambridge, MA, USA, 2021; Volume 46, pp. 273–307.

40. Songtrai, S.; Pratchayasakul, W.; Arunsak, B.; Chunchai, T.; Kongkaew, A.; Chattipakorn, N.; Chattipakorn, S.C.; Kaewsuwan, S. Cyclosorus Terminans Extract Ameliorates Insulin Resistance and Non-Alcoholic Fatty Liver Disease (NAFLD) in High-Fat Diet (HFD)-Induced Obese Rats. *Nutrients* **2022**, *14*, 4895. [CrossRef]
41. Basu, P.P.; Aloysius, M.M.; Shah, N.J.; Brown, R.S., Jr. Review Article: The Endocannabinoid System in Liver Disease, a Potential Therapeutic Target. *Aliment. Pharmacol. Ther.* **2014**, *39*, 790–801. [CrossRef]
42. Mboumba Bouassa, R.-S.; Sebastiani, G.; Di Marzo, V.; Jenabian, M.-A.; Costiniuk, C.T. Cannabinoids and Chronic Liver Diseases. *Int. J. Mol. Sci.* **2022**, *23*, 9423. [CrossRef]
43. Liu, L.Y.; Alexa, K.; Cortes, M.; Schatzman-Bone, S.; Kim, A.J.; Mukhopadhyay, B.; Cinar, R.; Kunos, G.; North, T.E.; Goessling, W. Cannabinoid Receptor Signaling Regulates Liver Development and Metabolism. *Development* **2016**, *143*, 609–622. [CrossRef]
44. Jorgačević, B.; Vučević, D.; Samardžić, J.; Mladenović, D.; Vesković, M.; Vukićević, D.; Ješić, R.; Radosavljević, T. The Effect of CB1 Antagonism on Hepatic Oxidative/Nitrosative Stress and Inflammation in Nonalcoholic Fatty Liver Disease. *Curr. Med. Chem.* **2021**, *28*, 169–180. [CrossRef] [PubMed]
45. Julien, B.; Grenard, P.; Teixeira-Clerc, F.; Van Nhieu, J.T.; Li, L.; Karsak, M.; Zimmer, A.; Mallat, A.; Lotersztajn, S. Antifibrogenic Role of the Cannabinoid Receptor CB2 in the Liver. *Gastroenterology* **2005**, *128*, 742–755. [CrossRef] [PubMed]
46. De Gottardi, A.; Spahr, L.; Ravier-Dall'Antonia, F.; Hadengue, A. Cannabinoid Receptor 1 and 2 Agonists Increase Lipid Accumulation in Hepatocytes. *Liver Int.* **2010**, *30*, 1482–1489. [CrossRef] [PubMed]
47. Deveaux, V.; Cadoudal, T.; Ichigotani, Y.; Teixeira-Clerc, F.; Louvet, A.; Manin, S.; Nhieu, J.T.-V.; Belot, M.P.; Zimmer, A.; Even, P.; et al. Cannabinoid CB2 Receptor Potentiates Obesity-Associated Inflammation, Insulin Resistance and Hepatic Steatosis. *PLoS ONE* **2009**, *4*, e5844. [CrossRef] [PubMed]
48. Bazwinsky-Wutschke, I.; Zipprich, A.; Dehghani, F. Endocannabinoid System in Hepatic Glucose Metabolism, Fatty Liver Disease, and Cirrhosis. *Int. J. Mol. Sci.* **2019**, *20*, 2516. [CrossRef]
49. Baldassarre, M.; Giannone, F.A.; Napoli, L.; Tovoli, A.; Ricci, C.S.; Tufoni, M.; Caraceni, P. The Endocannabinoid System in Advanced Liver Cirrhosis: Pathophysiological Implication and Future Perspectives. *Liver Int.* **2013**, *33*, 1298–1308. [CrossRef]
50. Rivera, P.; Vargas, A.; Pastor, A.; Boronat, A.; López-Gambero, A.J.; Sánchez-Marín, L.; Medina-Vera, D.; Serrano, A.; Pavón, F.J.; de la Torre, R.; et al. Differential Hepatoprotective Role of the Cannabinoid CB1 and CB2 Receptors in Paracetamol-Induced Liver Injury. *Br. J. Pharmacol.* **2020**, *177*, 3309–3326. [CrossRef]
51. Mendez-Sanchez, N.; Zamora-Valdes, D.; Pichardo-Bahena, R.; Barredo-Prieto, B.; Ponciano-Rodriguez, G.; Bermejo-Martínez, L.; Chavez-Tapia, N.C.; Baptista-González, H.A.; Uribe, M. Endocannabinoid Receptor CB2 in Nonalcoholic Fatty Liver Disease. *Liver Int.* **2007**, *27*, 215–219. [CrossRef]
52. Castaneda, J.T.; Harui, A.; Roth, M.D. Regulation of Cell Surface CB2 Receptor during Human B Cell Activation and Differentiation. *J. Neuroimmune Pharm.* **2017**, *12*, 544–554. [CrossRef]
53. Geddo, F.; Scandiffio, R.; Antoniotti, S.; Cottone, E.; Querio, G.; Maffei, M.E.; Bovolin, P.; Gallo, M.P. Pipenig®-FL, a Fluid Extract of Black Pepper (*Piper Nigrum* L.) with a High Standardized Content of Trans-β-Caryophyllene, Reduces Lipid Accumulation in 3T3-L1 Preadipocytes and Improves Glucose Uptake in C2C12 Myotubes. *Nutrients* **2019**, *11*, 2788. [CrossRef] [PubMed]
54. Hempel, B.; Xi, Z.-X. Receptor Mechanisms Underlying the CNS Effects of Cannabinoids: CB1 Receptor and Beyond. *Adv. Pharm.* **2022**, *93*, 275–333. [CrossRef]
55. Santos, P.S.; Oliveira, T.C.; Júnior, L.M.R.; Figueiras, A.; Nunes, L.C.C. β-Caryophyllene Delivery Systems: Enhancing the Oral Pharmacokinetic and Stability. *Curr. Pharm. Des.* **2018**, *24*, 3440–3453. [CrossRef] [PubMed]
56. Mödinger, Y.; Knaub, K.; Dharsono, T.; Wacker, R.; Meyrat, R.; Land, M.H.; Petraglia, A.L.; Schön, C. Enhanced Oral Bioavailability of β-Caryophyllene in Healthy Subjects Using the VESIsorb® Formulation Technology, a Novel Self-Emulsifying Drug Delivery System (SEDDS). *Molecules* **2022**, *27*, 2860. [CrossRef] [PubMed]

molecules

MDPI

Article

Cannabinoid Receptor Modulation of Neurogenesis: ST14A Striatal Neural Progenitor Cells as a Simplified In Vitro Model

Erika Cottone [1], Valentina Pomatto [1], Stefania Rapelli [1], Rosaria Scandiffio [1], Ken Mackie [2] and Patrizia Bovolin [1,*]

[1] Department of Life Sciences and Systems Biology, University of Turin, 10123 Torino, Italy; erika.cottone@unito.it (E.C.); valentina.pomatto@gmail.com (V.P.); stefania.rapelli@unito.it (S.R.); rosaria.scandiffio@unito.it (R.S.)

[2] Department of Psychological and Brain Sciences, Gill Center for Biomolecular Science, Indiana University, Bloomington, IN 47405, USA; kmackie@indiana.edu

* Correspondence: patrizia.bovolin@unito.it; Tel.: +39-011-6704679

Abstract: The endocannabinoid system (ECS) is involved in the modulation of several basic biological processes, having widespread roles in neurodevelopment, neuromodulation, immune response, energy homeostasis and reproduction. In the adult central nervous system (CNS) the ECS mainly modulates neurotransmitter release, however, a substantial body of evidence has revealed a central role in regulating neurogenesis in developing and adult CNS, also under pathological conditions. Due to the complexity of investigating ECS functions in neural progenitors in vivo, we tested the suitability of the ST14A striatal neural progenitor cell line as a simplified in vitro model to dissect the role and the mechanisms of ECS-regulated neurogenesis, as well as to perform ECS-targeted pharmacological approaches. We report that ST14A cells express various ECS components, supporting the presence of an active ECS. While CB1 and CB2 receptor blockade did not affect ST14A cell number, exogenous administration of the endocannabinoid 2-AG and the synthetic CB2 agonist JWH133 increased ST14A cell proliferation. Phospholipase C (PLC), but not PI3K pharmacological blockade negatively modulated CB2-induced ST14A cell proliferation, suggesting that a PLC pathway is involved in the steps downstream to CB2 activation. On the basis of our results, we propose ST14A neural progenitor cells as a useful in vitro model for studying ECS modulation of neurogenesis, also in prospective in vivo pharmacological studies.

Keywords: endocannabinoid system; cannabinoid receptor; CB1; CB2; CB ligands; antagonists; neural progenitors; ST14A; proliferation; neurogenesis

Citation: Cottone, E.; Pomatto, V.; Rapelli, S.; Scandiffio, R.; Mackie, K.; Bovolin, P. Cannabinoid Receptor Modulation of Neurogenesis: ST14A Striatal Neural Progenitor Cells as a Simplified In Vitro Model. *Molecules* **2021**, *26*, 1448. https://doi.org/10.3390/molecules26051448

Academic Editors: Alessandra Bisi and Angela Rampa

Received: 24 January 2021
Accepted: 4 March 2021
Published: 7 March 2021

1. Introduction

The endocannabinoid system (ECS) is comprised of several different components: (a) the cannabinoid receptors, the best characterized being CB1 and CB2 receptors; (b) the endogenous cannabinoids, also called endocannabinoids (eCBs), among which anandamide (AEA) and 2-arachidonoylglycerol (2-AG); (c) the enzymes involved in eCB biosynthesis "on demand", e.g., *N*-acylphosphatidylethanolamine-specific phospholipase D-like hydrolase (NAPE-PLD) and diacylglycerol lipase (DAGL); (d) the enzymes involved in eCB degradation, e.g., fatty acid amide hydrolase (FAAH) and monoacylglycerol lipase (MAGL); (e) the molecules involved in eCB transport across the membrane [1–3]. Additionally, various natural exogenous cannabinoids do exist, the most potent of which is Δ^9-tetrahydrocannabinol (THC), the main psychoactive component of *Cannabis sativa* [4]. Considering that marijuana is one of the most abused substances in the world and it is becoming legal in many countries, a particular concern is on the fact that acute and chronic use of cannabis could lead to cognitive impairments; interestingly, not only chronic treatment with THC, but also the administration of a single ultra-low dose of THC was shown to lead to long-term cognitive impairments, possibly resulting from deficits in attention

or motivation [5]. A noteworthy finding is the fact that THC induces striatal dopamine release in animals and humans [6], thus explaining some of the adverse effects of cannabis consumption on neuropsychiatric disorders, such as schizophrenia, and also suggesting that THC could share addictive properties with other drugs of abuse.

The ECS shares mediators and overlaps with other metabolic processes, thus recently an "expanded endocannabinoid system" or "endocannabinoidome" has been defined [7].

CB1 and CB2 cannabinoid receptors are seven-transmembrane G protein-coupled receptors [8]; they primarily signal through $G_{i/o}$ proteins, leading to the inhibition of adenylyl cyclase and activation of Mitogen-activated protein kinases (MAPKs). In response to CB1 stimulation, MAPKs such as ERK1/2, c-Jun N-terminal kinase (JNK) and p38 are activated; CB1 was also shown to activate the Phosphoinositide 3-kinases (PI3K) pathway, thus leading to the regulation of neuronal survival. Similar to the CB1 receptor, the stimulation of CB2 has been demonstrated to promote neuronal survival through the activation of the PI3K/AKT/mTORC and JNK pathway; also, a Phospholipase C (PLC)-mediated intracellular calcium increase has been shown to activate MAPKs. Apart from these canonical signaling pathways, cannabinoid receptors are also able to signal through other non-canonical ways, such as activation of G_s and G_q proteins; also, complex crosstalk among cannabinoid receptors and other receptors, leading to heterodimerization and transactivation, has been shown [8]. Interestingly, different ligands can elicit different signaling pathways mediated by cannabinoid receptors [1].

CB1 is the most abundant G-protein coupled receptor in the mammalian brain; it is highly expressed by neurons in the cortex, amygdala, hippocampus, basal ganglia, and cerebellum, its activation leading to the modulation of neurotransmitter release [9]. The CB1 cannabinoid receptor has a pivotal role in neuroprotection, control of excitotoxicity, the survival of neural cells, as well as proliferation, differentiation and migration processes of neural progenitors (NPs) [10–12].

Different from CB1, the CB2 receptor is mostly distributed peripherally, especially in cells of the immune system [13], with a prevalent immunomodulatory role. However, recent studies showed CB2 expression also in the central nervous system [14], especially in association with neurodegenerative disorders [15]. In the adult brain, the CB2 receptor is localized in microglia, brain stem neurons, striatal neurons, hippocampal glutamatergic neurons, and dopaminergic neurons of the ventral tegmental area; CB2 mRNA levels are 100–200 times less abundant than CB1 mRNA, being however strongly upregulated in response to chronic pain, neuroinflammation and stroke [11]. Interestingly, the CB2 receptor is expressed in oligodendrocyte progenitors and neural progenitors [16–18] and it has been demonstrated that its activity is important in the control of adult neurogenesis under pathological conditions [12]. Indeed, the involvement of the CB2 receptor in neurodegenerative and neuroinflammatory disorders stimulated research toward CB2-targeted pharmacological approaches [2]. A substantial body of evidence suggests that the ECS modulates the proliferation, migration, specification and survival of neural progenitors in the developing and adult CNS [10]. During the different phases of neurogenesis in pre- and post-natal brain, all the ECS components are differentially expressed, e.g., 2-AG is prevalent in the prenatal period and dramatically decreases postnatally, while anandamide levels increase postnatally [19]. Interestingly, NPs commonly co-express CB1 and CB2 receptors; upon commitment to a neuronal fate, CB1 levels become up-regulated at the expense of CB2. CB2 seems more linked to a precursor undifferentiated proliferative state [16–18,20,21] and its involvement in axon guidance along the forming retino-thalamic pathway in vitro and in vivo has also been demonstrated [22]. Studies showed that 2-AG can act both on CB1 and CB2 receptors present in NPs derived from the subventricular zone, thus regulating cell proliferation and affecting neuroblast migration towards the olfactory bulbs [23–25].

Due to the complexity of the ECS, the full understanding of how its various components may contribute to control neurogenesis in developing and the adult brain is difficult to reach by in vivo approaches. A simplified in vitro model of neural progenitor cells could

therefore be a useful tool to better understand the role of ECS components and to identify the intracellular mechanisms involved, as well as to provide the basis for ECS-targeted pharmacological approaches.

In this paper, we used the ST14A cell line, immortalized neural precursor-derived primary cells, dissociated from the rat striatal primordia at embryonic day 14 and conditionally immortalized by retroviral transduction of the temperature-sensitive variant of the SV40 large T antigen [26]. At the permissive conditions of 33 °C and 10% serum-containing medium, ST14A cells show high proliferative activity, while switching to the non-permissive temperature of 39 °C or at low serum concentrations [26–28] the cells stop or slow down their proliferation and start differentiating into striatal medium-sized spiny neurons [26,28,29]. Due to their simplicity of in vitro culturing, the possibility to be easily transfected and to be transplanted into an adult and developing rodent brain, ST14A has been successfully used by many authors to investigate several processes correlated to neural progenitors development and migration [30–33], as well as a model for studying Huntington's disease [34,35].

In our research, we tested the suitability of ST14A cells as a simplified in vitro model for studying ECS modulation of neurogenesis. First of all, we assessed the expression of the ECS components necessary to a functional endocannabinoid system. Then, by using CB1/CB2 agonists and antagonists, we evaluated the effects of CB1 and CB2 receptor modulation on neural progenitor proliferation. Finally, we began to characterize the intracellular pathways involved in the CB2-regulated proliferation of striatal projection neuron progenitors.

2. Results

2.1. The Endocannabinoid System Is Expressed in ST14A Striatal Neural Progenitor Cells

The expression of ECS components was evaluated in the ST14A striatal neural progenitor cell line. Cells were cultured for 48 h under permissive, proliferating conditions (P; 10% serum-containing medium, incubation at 33 °C). By means of qualitative RT-PCR, ST14A cells were shown to express mRNAs encoding for CB1 and CB2 receptors; moreover, diacylglycerol lipase α (DAGLα) and monoacylglycerol lipase (MAGL), mainly involved respectively in the biosynthesis and degradation of 2-AG, were also expressed (Figure 1A). Focusing on cannabinoid receptors, CB1 and CB2 expression was also investigated at the protein level by Western blot analysis (Figure 1B). In the case of CB1, two bands with apparent molecular weights around 60 and 55 kDa, possibly corresponding to differently glycosylated forms, were observed. The Western blot for CB2 receptor revealed instead a major band of 45 kDa and a weaker band of about 40 kDa. CB receptor cellular localization was then assessed by means of immunofluorescence (Figure 1C); CB1 and CB2 immunoreactivities were abundantly found in the cytoplasm, especially around the nucleus.

The expression of the ECS was also evaluated in ST14A cells cultured for 72 h in differentiating conditions (D; 0.5% serum-containing medium, incubation at 33 °C), which favors a reduction of cell proliferation and allows the progenitors to start the differentiation toward striatal medium-sized spiny neurons. Differentiating ST14A cells were found to express the mRNAs encoding for both CB1 and CB2 receptors, as well as for DAGLα and MAGL (Figure 1A).

The detection of cannabinoid receptors mRNAs and proteins, as well as the expression of the mRNAs encoding endocannabinoid synthetic and degradative enzymes, strongly support the presence of an active ECS in ST14A neural progenitor cells.

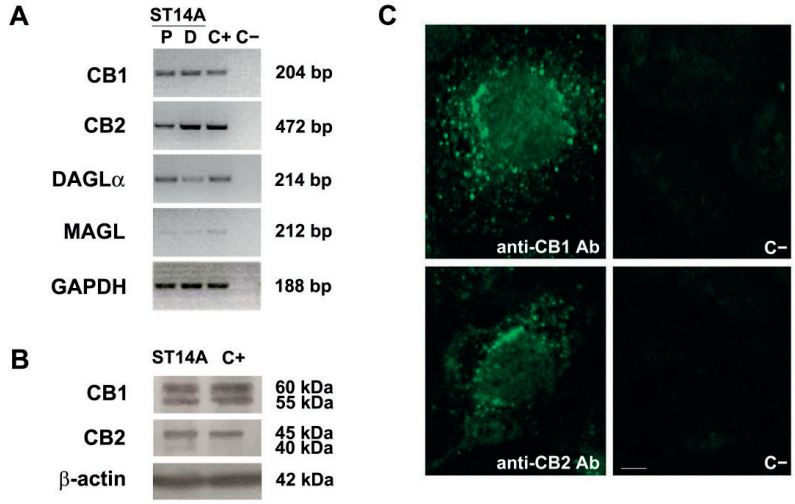

Figure 1. Endocannabinoid system expression in ST14A neural progenitor cells. (**A**) RT-PCR revealed specific bands corresponding to CB1 and CB2 receptors and to the enzymes DAGLα and MAGL in ST14A cells cultured 48 h under proliferating conditions (P). The same genes were also expressed in ST14A cells induced to differentiate toward a neuronal phenotype for 72 h (D, differentiating conditions). The housekeeping gene GAPDH was used as reference gene. The base pair (bp) length of the different amplicons is indicated. C+: positive controls, i.e., cDNA from rat brain or from rat spleen (for CB2 only); C−: negative control (no RT). (**B**) Western blot showing the expression of CB1 and CB2 receptors in ST14A neural progenitors (cells cultured 48 h under proliferating conditions); β-actin protein expression was used as a quality control of the protein extract. The apparent molecular weights of the bands are indicated (kDa). C+: positive controls, i.e., protein extracts from rat brain or spleen (for CB2 only). (**C**) Immunofluorescence for CB1 and CB2 receptors in ST14A cells neural progenitors (cells cultured 48 h under proliferating conditions). Single-cell magnification. Specific immunoreactivities are mainly distributed in the cytoplasm and in proximity to the nucleus. C−: negative controls, i.e., anti-CB1 or anti-CB2 pre-adsorbed antibodies. Calibration bar: 5 μm.

2.2. The Pharmacological Blockade of Cannabinoid Receptors Does Not Affect ST14A Cell Number

In order to determine if ST14A progenitor proliferation is under constitutive endocannabinoid regulation, we tested the effects of CB1 and CB2 pharmacological blockade.

Cells were cultured in proliferating conditions (at 33 °C, in 10% serum-containing medium) and treated for 24 h with alternatively one of the two selective CB1 antagonists AM251 and PF514273, and the CB2 antagonist AM630. A dose–response experiment (Figure S1) was conducted in order to verify different antagonist concentration effects on cell number, as well as to exclude cytotoxic effects and to select the best antagonist concentration to be used in subsequent experiments; based on previously unpublished experiments performed in our lab, a 24 h treatment was chosen. As shown in Figure 2 and Figure S1, neither CB1 nor CB2 blockade, at any antagonist concentration used, led to a change in ST14A cell number compared to untreated control cells, suggesting that constitutive cannabinoid signaling is not involved in ST14A cell proliferation/survival.

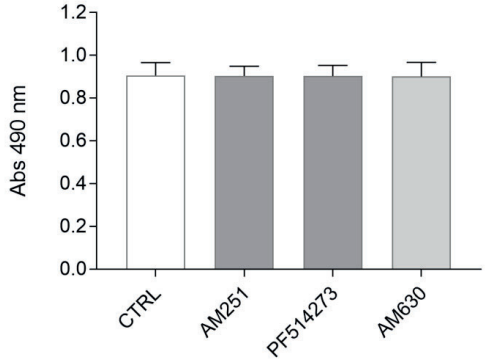

Figure 2. Evaluation of CB1/CB2 blockade effects on ST14A cell number. ST14A were treated for 24 h with 250 nM AM251 or 50 nM PF514273 (CB1 antagonists), or 300 nM AM630 (CB2 antagonist), then an MTS assay was performed. No effect on ST14A cell number was observed in treated cells, in respect to control (CTRL, medium plus 0.05% DMSO). Data from the MTS assay are expressed as mean ± standard deviation (SD) of the absorbance (λ = 490 nm); n = 8 replicates, 3 independent experiments.

2.3. Exogenous Administration of the Endocannabinoid 2-AG and the CB2 Agonist JWH133 Induces ST14A Cell Proliferation through CB2 Receptor Activation

We subsequently tested whether exogenous activation of CB1 and CB2 receptors by the administration of the CB1/CB2 agonist 2-AG could affect ST14A cell proliferation. Cells were stimulated for 24 h under proliferating conditions with 2-AG, then an MTS assay was performed. A preliminary dose–response experiment (Figure S2, panel A) allowed us to select the optimal agonist concentration to be used in this and subsequent experiments; based on previously unpublished experiments performed in our lab, a 24 h treatment was chosen.

As shown in Figure 3, 2-AG (5 μM) was able to induce a statistically significant increase in ST14A cell number, compared to control levels. To clarify the receptor subtype involved, CB1 and CB2 selective antagonists, used at the previously selected concentrations, were coadministered with 2-AG. 2-AG (5 μM) effects were not modified by co-treatment with the CB1 antagonists (250 nM AM251 or 50 nM PF514273), thus excluding a CB1-mediated effect. On the other hand, the 2-AG-mediated increase in ST14A cell number was specifically reverted by the coadministration of the CB2 selective antagonists AM630 (300 nM), indicating the involvement of CB2 receptor. This result was further confirmed by treatment for 24 h with a selective CB2 receptor agonist; indeed, JWH133 (300 nM; see Figure S2, panel B for preliminary dose–response experiment) induced an increase in cell number, in respect to control, and the effect was specifically reverted by coadministration of AM630 (300 nM) (Figure 3).

To confirm that the increase in ST14A cell number observed after 2-AG and JWH133 treatment was the result of an increase in cell proliferation and not in the survival rate, a BrdU-based proliferation assay was performed. Both the endocannabinoid 2-AG (5 μM) and the synthetic CB2 agonist JWH133 (300 nM) significantly increased BrdU incorporation in ST14A cells, thus indicating a proliferative effect (Figure 4). AM630 (300 nM) administration alone did not influence ST14A proliferation rate, while its coadministration with 2-AG and JWH133 specifically blocked the proliferative effect induced by the agonists (Figure 4).

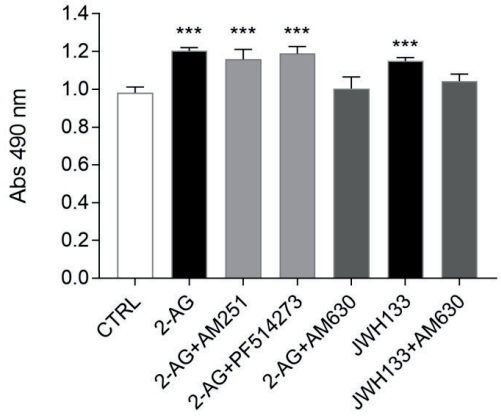

Figure 3. Evaluation of the effects of 2-AG and JWH133 alone or in the presence of specific CB1/CB2 antagonists on ST14A cell number. 2-AG (5 μM) induces an increase of ST14A cell number after 24 h, with respect to control cells (CTRL). The effect was not reverted by the coadministration of 2-AG with the CB1 selective antagonists AM251 (250 nM) and PF514273 (50 nM); on the other hand, cell number was comparable to control when 2-AG was coadministered with the selective CB2 antagonist AM630 (300 nM). Similarly, the selective CB2 receptor agonist JWH133 (300 nM) induced ST14A cell number increase, which was specifically reverted by the coadministration of AM630 (300 nM). Data from the MTS assay are expressed as means ± SD of the absorbance (λ = 490 nm); n = 5 replicates, 3 independent experiments. *** = $p \leq 0.001$ vs. control.

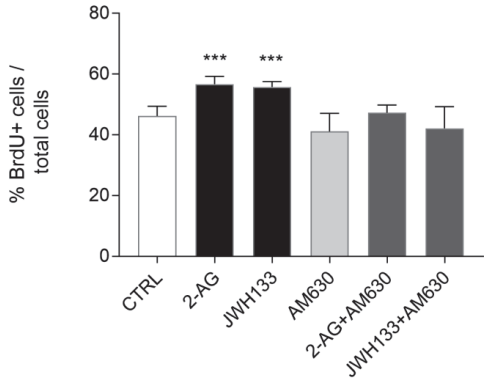

Figure 4. Evaluation of the effects of 2-AG and JWH133 alone or in the presence of the specific CB2 antagonist AM630 on ST14A cell proliferation rate. Results are shown as ratio (%) of the number of BrdU+ cells over the number of total cells, stained with DAPI fluorophore. After 24 h treatment with 2-AG (5 μM) and JWH133 (300 nM) an increase in BrdU incorporation was observed, with respect to untreated cells (CTRL); the effect was specifically reverted in both the cases by 300 nM AM630 coadministration. Data are expressed as mean ± standard deviation (SD); n = 3 replicates (5 random fields counted in each well), 3 independent experiments. *** = $p \leq 0.001$ vs. control.

BrdU-based experiments demonstrated therefore that exogenously administered endocannabinoid 2-AG induces ST14A neural progenitor proliferation via a CB2-mediated mechanism.

2.4. PLC Pharmacological Blockade Impairs CB2-Mediated ST14A Cell Proliferation

In order to identify the possible intracellular effectors involved in CB2-mediated ST14A cell proliferation, we evaluated the effects of pharmacological blockade of the signalling cascades involving PLC and PI3K activation.

The day after seeding, ST14A cells were pre-incubated for 30 min with the PLC inhibitor U73122 (2 μM) or the PI3K inhibitor wortmannin (150 nM), then inhibitors were removed and cells were cultured for 24 h in the presence of the agonists 2-AG or JWH133; cell counting was then performed with an MTS assay. The experiments were conducted in a medium containing 2% serum (instead of 10%) in order to reduce possible interference of serum components on the effects of PLC and PI3K inhibitors on cell proliferation.

As shown in Figure 5, at the concentrations used, the pre-treatment with the two inhibitors did not have any effect *per se* on ST14A viability/cell number, allowing further investigations. Interestingly, wortmannin pretreatment did not counteract the 2-AG- and JWH133-driven increase in cell number. On the opposite, the presence of the PLC inhibitor U73122 was able to revert the cell number increase induced by 2-AG- and JWH133 to control conditions.

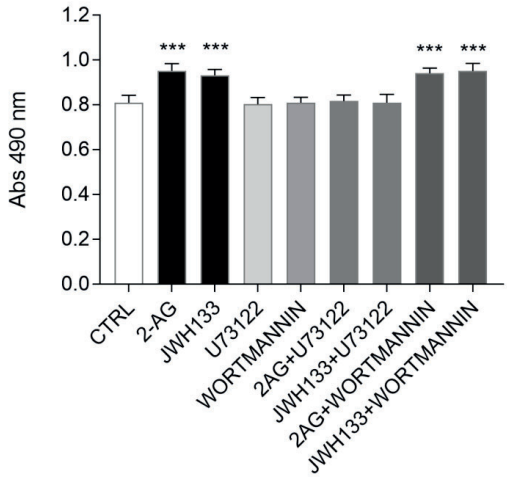

Figure 5. Evaluation of Phospholipase C (PLC) and PI3K pharmacological blockade on 2-AG- and JWH133-induced ST14A cell number increase. Cells were pretreated 30 min with U73122 (2 μM) or wortmannin (150 nM) prior to 2-AG (5 μM) or JWH133 (300 nM) incubation for 24 h in 2% serum-containing medium. U73122, but not wortmannin pretreatment, reverted 2-AG- and JWH133-driven ST14A cell number increase. Data from MTS assay are expressed as means ± standard deviation (SD) of the absorbance (λ = 490 nm); n = 8 replicates, 3 independent experiments. *** = $p \leq 0.001$ vs. control.

Overall, our findings indicate that exogenously administered 2-AG promote ST14A neural progenitor proliferation through CB2 receptor engagement and PLC pathway activation.

3. Discussion

The endocannabinoid system modulates several biological processes, including the generation and survival of neurons in the developing and adult CNS, also under pathological conditions [10]. Indeed, the involvement of CB2 receptor in neurogenesis, as well as neurodegenerative and neuroinflammatory disorders, open to new possible pharmacological strategies based on the use of CB2-specific therapeutic drugs, possibly overcoming the neuropsychiatric adverse effects of CB1-targeted therapies [2,8].

In this work, we propose ST14A striatal neural progenitor cells as a simplified in vitro model suitable for studying the role of the ECS in neurogenesis, as well as for ECS-targeted pharmacological approaches.

The ST14A cell line was established by immortalization of neural precursor-derived primary cells dissociated from the rat striatal primordia at embryonic day 14 [26]. Compared to neuroblast primary cultures, this experimental model is easier to handle and to maintain in culture, so it is more suitable when approaching initial studies on molecular interactions. Furthermore, ST14A cells have also been used extensively for genetic manipulation experiments and transplantation into an adult and developing rodent brain, making these cells an in vitro system with great potential for biochemical, molecular, and biological studies correlated to neural progenitors development and migration [26,30–33], as well as a model for studying neurological diseases [34,35].

In this paper we showed that ST14A neural progenitor cells display an active ECS, in agreement with the findings obtained by Bari and colleagues [34] on ST TetOn 12.7, a ST14A subclone able to express reverse tetracycline-controlled transactivator under the control of doxycycline; also, previous studies on primary cultures of neural progenitors demonstrated functional CB1 and CB2 receptor expression [17,24,36,37]. In particular, we found that several components of the system, such as the cannabinoid receptors CB1 and CB2, as well as the endocannabinoid synthetic and degradative enzymes DAGLα and MAGL, are expressed in ST14A neural progenitors (cultured under permissive, proliferating conditions). Consistent with previous results [34], Western blot analysis confirmed the expression of both CB1 and CB2 receptors; CB1 receptor appeared as two bands with an apparent molecular weight around 60 and 55 kDa, possibly corresponding to differently glycosylated forms, while in the case of CB2 receptor a major band of 45 kDa and a weaker band of about 40 kDa were seen. In ST TetOn 12.7, instead, CB1 and CB2 receptors were detected as single bands of 60 kDa and 45 kDa, respectively [34]; the discrepancy with our results could be either due to the different ST14A clone and/or the different primary antibodies used. Immunofluorescence analysis for CB1 and CB2 revealed, accordingly with [34], cytoplasmic localizations of both the receptors, rather than a membrane localization, probably due to their intense trafficking and internalization; a marked perinuclear localization was found for CB2, according to the observations reported by [38]. Actually, CB2 binding sites were demonstrated to be predominantly located intracellularly in prefrontal cortical pyramidal neurons [39] and functional CB2 receptors were demonstrated at the endo-lysosome level [40]; also, CB1 receptor localization is not exclusively on the plasma membrane, since active CB1 were localized also in the outer membrane of mitochondria [41] and a predominant intracellular localization have been observed in diverse cell types and also undifferentiated neuronal cells [42]. In our study, we also widened our analysis to ECS expression in ST14A cells induced to differentiate toward a medium-size spiny neuron phenotype; mRNAs encoding for CB1 and CB2 receptors, as well as for DAGLα and MAGL were detected, consistent with studies showing the presence of a functional ECS in the striatum [14,43].

We subsequently focused our attention on the possible modulation played by the ECS on ST14A neural progenitor proliferation [44,45].

First, we assessed the effects of a perturbation of the endogenous ECS by pharmacological blockade of the cannabinoid receptors. Under these conditions, neither CB1 nor CB2 blockade had significant effects on ST14A neural progenitor cell number. On the other hand, the stimulation of cannabinoid receptors with a non-selective CB1/CB2 ligand, the endocannabinoid 2-AG, induced ST14A cell number increase through the activation of the CB2 receptor, as indicated by the fact that the effect was reverted by the coadministration of 2-AG with the CB2 specific antagonist AM630, but not with the CB1 antagonists AM251 and PF514273. CB2 involvement was further supported by the finding that the CB2 specific synthetic agonist JWH133 increased ST14A cell number, an effect reversed by the coadministration of the CB2 antagonist. Interestingly, a BrdU assay allowed us to demonstrate that the increase in ST14A cell number was related to an enhancement of

neural precursor proliferation rate, rather than an increase in cell survival. In our study, we chose to use the endogenous ligand 2-AG to better mimic the ECS in an embryonic environment, since until birth 2-AG is much more abundant than AEA [19]. Our results about CB2-mediated proliferation are in agreement with the findings of [16,17,23,24], showing that endocannabinoids and synthetic cannabinoids can act on CB2 receptors present in NPs, regulating cell proliferation. The fact that we did not observe any effect on neural progenitor cell number following CB2 blockade, while CB2 agonist administration induced cell proliferation, could possibly be explained by the fact that only a few receptors might be activated in basal conditions; conversely, following exposure to exogenous ligands, CB2 receptors are massively activated and the effect of inhibition could be readily visible.

We aimed also to identify some of the possible intracellular effectors involved in CB2-mediated ST14A cell proliferation. CB1 and CB2 share several downstream signaling mechanisms in neural progenitors [21]; in particular, they are coupled to the activation of the ERK and the PI3K/Akt pathways. In cerebellar progenitor cells, CB1-induced cell proliferation was shown to be mediated by the PI3K/Akt/GSK3β and in cortical progenitors, CB1 drives mTORC1 signaling and cell proliferation. CB2 was shown to promote hippocampal neural progenitor proliferation through activation of the PI3K/Akt/mTORC axis [17,46]. In addition, previous studies demonstrated that 2-AG-mediated activation of CB2 leads to a PLC-IP_3R dependent intracellular calcium increase and subsequent massive activation of MAPK/ERK cascade [46]. By preincubation with the PI3K inhibitor wortmannin or the PLC inhibitor U73122, we observed that the inhibition of PI3K had no consequence on CB2 ligand-mediated proliferation, while the PLC inhibitor U73122 significantly impaired the process. The dissimilarity between our data and Palazuelos and colleagues' observations [17] could be possibly due to the different brain areas of cell origin (hippocampus vs. striatum). Furthermore, cells belonging to different brain areas and ages (embryonic and adult) could display diverse intracellular cascades related to their stage-specific enzymatic equipment. Interestingly, intracellularly located CB2 receptors were demonstrated to open IP_3R-dependent Ca^{2+}-activated Cl^- channels in prefrontal cortex pyramidal neurons [46].

In conclusion, our study indicates that ST14A cells express a functional endocannabinoid system that is actively involved in the regulation of neural progenitor proliferation. ST14A cells could therefore represent a useful, simplified in vitro model for studying ECS modulation of neurogenesis. Moreover, the model could be used to test new therapeutic drugs acting on the cannabinoid system, thus providing the basis for in vivo pharmacological studies.

4. Materials and Methods

4.1. Cell Culture

ST14A striatal neural progenitor cell line (kindly provided by Dr. Elena Cattaneo, University of Milan, Milan, Italy) was cultured on 100 mm Petri-dishes (BD Biosciences, San Jose, CA, USA) in Dulbecco's modified Eagle's medium (DMEM) supplemented with 100 units/mL penicillin, 0.1 mg/mL streptomycin, 1 mM sodium pyruvate, 2 mM L-glutamine (all supplied by Sigma-Aldrich, St. Louis, MO, USA), and 10% fetal bovine serum (FBS, GIBCO®, Gaithersburg, MD, USA) decomplemented at 56 °C for 30 min. Cells were grown as monolayers at 33 °C in a 5% CO_2 incubator.

4.2. RNA Extraction and RT-PCR

Cells were seeded and let grow under permissive, proliferating conditions at 33 °C for 48 h in DMEM containing 10% FBS. Only for gene expression studies, cells were also grown under non-permissive, differentiating conditions at 33 °C for 72 h in DMEM containing 0.5% FBS. Total RNA extraction was performed using TRIZOL® Reagent (Invitrogen, Carlsbad, CA, USA) following the manufacturer's instruction. DNA contaminants were eliminated using TURBO DNA-free kit (Applied Biosystems, San Francisco, CA, USA). cDNA was synthesized from total RNA by using Multiscribe RT (Applied Biosystems,

USA) and random nonamers, starting from 2 μg of total RNA for each sample. PCR (30 amplification cycles) was performed using 250 ng cDNAs. Negative controls (C−) were carried out replacing cDNA with an equal amount of total RNA (no RT); as positive controls (C+), cDNAs from rat brain or rat spleen (for CB2 amplification only) were used. The housekeeping gene GAPDH was used as reference gene. Specific primers (Table 1) were designed on the basis of rat sequences, using both Primer3 (http://frodo.wi.mit.edu/primer3/, accessed on 15 December 2020) and AnnHyb (http://www.bioinformatics.org/annhyb/, accessed on 15 December 2020) programs, paying attention to choose primers on different exons to avoid amplification of genomic DNA.

Table 1. List of the primers used for PCR analysis.

	PCR Primers	Annealing T (°C)
GAPDH	Fw: 5′-TGGCATTGTGGAAGGGCTCATGAC-3 Rev: 5′-ATGCCAGTGAGCTTCCCGTTCAGC-3′	60
CB1	Fw: 5′-GGGTTACAGCCTCCTTCACA-3′ Rev: 5′-CAGATTGCAGCTTCTTGCAG-3′	55
CB2	Fw: 5′-GGAGTACATGATCTTGAGTGAT-3′ Rev: 5′-AGAACAGGGACTAGGACAAC-3′	50
DAGLα	Fw: 5′-GGCAAGACCCTGTAGAGCTG-3′ Rev: 5′-TAAAACAGGTGGCCCTCATC-3′	60
MAGL	Fw: 5′-TAGCAGCTGCAGAGAGACCA-3′ Rev: 5′-GATGAGTGGGTCGGAGTTGT-3′	60

PCR reaction products were separated by 2% agarose gel electrophoresis in 1X TAE buffer. The correct length of the amplicons was confirmed by analysis with Gel Doc system and the software Quantity One (BioRad, Hercules, CA, USA), using Low DNA Mass Ladder (Invitrogen, USA) as molecular weight standards.

4.3. Western Blot

Cells were seeded and let grow under proliferating conditions at 33 °C for 48 h in DMEM containing 10% FBS, then total proteins were extracted by lysing cells in boiling Laemmli buffer (2.5% SDS, 0.125 M Tris-HCl, pH 6.8), followed by 3 min denaturation at 100 °C. Protein concentration was determined by BCA kit (Sigma-Aldrich, USA). As positive controls, rat brain or rat spleen (for CB2) total proteins were used. Protein extracts (20 μg/lane) were subjected to 10% SDS polyacrylamide gel electrophoresis (SDS-PAGE) and then blotted onto nitrocellulose membranes (BioRad, Hercules, CA, USA) according to the manufacturer's instructions. After blocking with 5% powder milk in TBS-T buffer (20 mM Tris, 150 mM NaCl, 0.1% Tween20, pH 7.4), filters were probed with anti-CB1 C-terminus (last 15 aa of CB1 rat receptor) or anti-CB2 N-terminus (first 39 aa of CB2 rat receptor) primary polyclonal antibodies (diluted 1:800 in TBS-T containing 1% no-fat milk); both the antibodies were produced in Ken Mackie's lab (Indiana University, Bloomington, IN, USA). Membranes were then washed in TBS-T and incubated with an anti-rabbit IgG HRP-conjugated secondary antibody (1:5000 dilution; Amersham Biosciences, Little Chalfont, UK). In order to check protein integrity, the expression of the housekeeping protein β-actin was revealed by means of anti-β-actin monoclonal primary antibody (diluted 1:10,000; Sigma-Aldrich, USA) and anti-mouse IgG HRP-conjugated secondary antibody (1:5000 dilution; Amersham Biosciences, USA). Specific bands were visualized by using enhanced chemiluminescence (ECL) detection system (Amersham Biosciences, USA). The apparent molecular weights of the stained proteins were determined by analysis with Gel Doc system and the software Quantity One, using prestained protein ladders (PageRuler Plus, Fermentas, Waltham, MA, USA) as reference.

4.4. Immunofluorescence

ST14A cells were seeded on poly-L-lysine-coated coverslips (3500 cells/cm^2). After 48 h of growth in DMEM containing 10% FBS, at 33 °C (proliferating conditions), cell

were first rinsed in PBS containing Ca^{2+} and Mg^{2+}, and then in 0.05% sucrose-PBS. Cells were subsequently fixed with 4% PAF in 0.1 M phosphate buffer (PB), pH 7.4 for 10 min. After 4 washings in PBS, cells were incubated in blocking serum (PBS containing 5% BSA, 10% normal serum, 0.1% TritonX-100) at RT for 1 h. Cells were then incubated O/N at 4 °C with the anti-CB1 or anti-CB2 primary antibody, diluted 1:400 or 1:200, respectively, in 0.01 M PBS plus 10% normal goat serum. Controls were set up by incubating cells with primary antibodies pre-adsorbed O/N with the specific immunogens. Cells were washed in PBS and incubated for 1 h with anti-rabbit IgG AlexaFluor 488-conjugated secondary antibody (1:250 dilution; Invitrogen, USA), washed again and mounted with 1,4-diazabicyclo [2.2.2]-octane (DABCO; Sigma-Aldrich, USA). Image analysis was performed with a Nikon fluorescent microscope coupled with a computer-assisted image analysis system (Neurolucida software, MicroBrightField, Williston, VT, USA).

4.5. Cell Count Assays

Cells were seeded at a density of 1500 cells/well in 96-well plates, in 200 μL DMEM containing 10% FBS and incubated at 33 °C. The following day, the medium was replaced with DMEM plus 10% FBS, containing alternatively or in combination (depending on the experiment) 5 μM 2-AG, 300 nM JWH133, 250 nM AM251, 50 nM PF514273, 300 nM AM630 (all purchased from Tocris Bioscience, Bristol, UK); for controls, medium plus 0.05% DMSO was used. Then, 24 h later, 20 μL of MTS Cell Titer 96 solution (Promega, Madison, WI, USA) was added and plates were incubated at 37 °C for 4 h. The absorbance was measured in a Microplate Reader (Bio-Rad, USA) at a wavelength (λ) of 490 nm. At least 5 replicates for each condition were set up and the experiment was repeated three times.

For PLC- and PI3K-blockade experiments, cells were seeded as before, then the medium was replaced with DMEM plus 2% FBS, containing 2 μM U73122 (PLC inhibitor, Sigma-Aldrich, USA), 150 nM wortmannin (PI3K inhibitor, Sigma-Aldrich, USA) or 0.05% DMSO (vehicle only) for 30 min. Then, all the wells were washed with PBS and the medium was replaced with DMEM plus 2% FBS, containing alternatively 5 μM 2-AG or 300 nM JWH133. Then, 24 h later, MTS assay was performed and cell density was measured following the protocol reported above.

4.6. Cell Proliferation Assay

Cells were seeded on poly-L-lysine coated coverslips in 10% FBS-DMEM at a density of 3500 cells/cm^2. The following day, the medium was replaced with 10% FBS-DMEM with or without 5 μM 2-AG, 300 nM JWH133, 300 nM AM630 and cells were cultured for another 24 h. Six hours before cell fixation, BrdU (10 μM) was added to the culture medium, then cells were fixed with 4% PAF in 0.1 M PB, pH 7.4, for 10 min and processed for BrdU-immunocytochemistry and DAPI staining. Briefly, cells were washed in PBS, then incubated at 37 °C with 2N HCl for 30 min and washed for 10 min with boric acid (0.1 M, pH = 8.5). Cells were washed and incubated in blocking serum (0.01 M PBS plus 10% normal serum) at RT for 1 h. Cells were incubated O/N at 4 °C with anti-BrdU mouse monoclonal antibody (Sigma-Aldrich, USA; dilution 1:3000 in 0.01 M PBS and 10% normal serum). Cells were washed and incubated for 1 h with anti-mouse IgG Cy3-conjugated secondary antibody (dilution 1:400; Jackson ImmunoResearch, West Grove, PA, USA). For nuclear staining, cells were labelled with 4′,6-diamidino-2-phenylindole (DAPI) for 10 min and mounted with DABCO. Cell counts and image analysis were performed with a Nikon fluorescent microscope coupled with a computer-assisted image analysis system (Neurolucida Software, MicroBrightField, USA). Five random fields were counted in each well and each treatment was done at least in triplicate; the experiment was repeated three times. The cell proliferation was determined for each sample as the ratio of the number of BrdU+ cells over the total cell number (cells stained with DAPI).

4.7. Statistical Analysis

All the data were analyzed using commercially available software (SPSS version 26 for Windows; SPSS Inc., Chicago, IL, USA). Statistical analysis was performed using one-way ANOVA followed by Tukey's and Bonferroni's post hoc tests. The level of significance was set at $p < 0.05$.

Supplementary Materials: The following are available online, Figure S1. Evaluation of the effect of different concentrations of AM251, PF514273 and AM630 on ST14A cell number. Figure S2. Evaluation of the effect of different concentrations of 2-AG and JWH133 on ST14A cell number.

Author Contributions: Conceptualization, P.B.; Data curation, E.C., V.P., S.R. and R.S.; Formal analysis, E.C. and V.P.; Funding acquisition, P.B.; Investigation, E.C., V.P., S.R. and R.S.; Project administration, P.B.; Resources, K.M.; Supervision, P.B.; Writing—Original draft, E.C., V.P and P.B.; Writing—Review and editing, E.C., R.S., K.M. and P.B. All authors have read and agreed to the published version of the manuscript.

Funding: This research was funded by Local grants from the University of Turin, Italy to P.B.

Institutional Review Board Statement: Not applicable.

Informed Consent Statement: Not applicable.

Data Availability Statement: The data presented in this study are available on request from the corresponding author.

Conflicts of Interest: The authors declare no conflict of interest.

Sample Availability: Anti-CB1 and anti-CB2 primary antibodies are available from Ken Mackie (Indiana University, Bloomington, IN, USA).

References

1. Lu, H.-C.; Mackie, K. Review of the Endocannabinoid System. *Biol. Psychiatry Cogn. Neurosci. Neuroimaging* **2020**. [CrossRef]
2. Di Marzo, V. New approaches and challenges to targeting the endocannabinoid system. *Nat. Rev. Drug Discov.* **2018**, *17*, 623–639. [CrossRef]
3. Shahbazi, F.; Grandi, V.; Banerjee, A.; Trant, J.F. Cannabinoids and Cannabinoid Receptors: The Story so Far. *iScience* **2020**. [CrossRef]
4. Mechoulam, R.; Gaoni, Y. A Total Synthesis of dl-Δ1-Tetrahydrocannabinol, the Active Constituent of Hashish1. *J. Am. Chem. Soc.* **1965**, *87*, 3273–3275. [CrossRef]
5. Amal, H.; Fridman-Rozevich, L.; Senn, R.; Strelnikov, A.; Gafni, M.; Keren, O.; Sarne, Y. Long-term consequences of a single treatment of mice with an ultra-low dose of Δ9-tetrahydrocannabinol (THC). *Behav. Brain Res.* **2010**, *206*, 245–253. [CrossRef]
6. Bossong, M.G.; Van Berckel, B.N.M.; Boellaard, R.; Zuurman, L.; Schuit, R.C.; Windhorst, A.D.; Van Gerven, J.M.A.; Ramsey, N.F.; Lammertsma, A.A.; Kahn, R.S. Δ9-Tetrahydrocannabinol Induces Dopamine Release in the Human Striatum. *Neuropsychopharmacology* **2008**, *34*, 759–766. [CrossRef]
7. Di Marzo, V.; Piscitelli, F. The Endocannabinoid System and its Modulation by Phytocannabinoids. *Neurotherapeutics* **2015**, *12*, 692–698. [CrossRef]
8. Haspula, D.; Clark, M.A. Cannabinoid Receptors: An Update on Cell Signaling, Pathophysiological Roles and Therapeutic Opportunities in Neurological, Cardiovascular, and Inflammatory Diseases. *Int. J. Mol. Sci.* **2020**, *21*, 7693. [CrossRef]
9. Pertwee, R.G. Endocannabinoids and their pharmacological actions. In *Endocannabinoids*; Pertwee, R.G., Ed.; Springer: Berlin, Germany, 2015; Volume 231, pp. 1–37. [CrossRef]
10. De Oliveira, R.W.; Oliveira, C.L.; Guimarães, F.S.; Campos, A.C. Cannabinoid signalling in embryonic and adult neurogenesis: Possible implications for psychiatric and neurological disorders. *Acta Neuropsychiatr.* **2018**, *31*, 1–16. [CrossRef]
11. Lutz, B. Neurobiology of cannabinoid receptor signaling. *Dialog Clin. Neurosci.* **2020**, *22*, 207–222. [CrossRef]
12. Oddi, S.; Scipioni, L.; Maccarrone, M. Endocannabinoid system and adult neurogenesis: A focused review. *Curr. Opin. Pharmacol.* **2020**, *50*, 25–32. [CrossRef]
13. Galiegue, S.; Mary, S.; Marchand, J.; Dussossoy, D.; Carriere, D.; Carayon, P.; Bouaboula, M.; Shire, D.; Fur, G.; Casellas, P. Expression of Central and Peripheral Cannabinoid Receptors in Human Immune Tissues and Leukocyte Subpopulations. *JBIC J. Biol. Inorg. Chem.* **1995**, *232*, 54–61. [CrossRef]
14. Gong, J.-P.; Onaivi, E.S.; Ishiguro, H.; Liu, Q.-R.; Tagliaferro, P.A.; Brusco, A.; Uhl, G.R. Cannabinoid CB2 receptors: Immunohistochemical localization in rat brain. *Brain Res.* **2006**, *1071*, 10–23. [CrossRef] [PubMed]

15. Aymerich, M.S.; Aso, E.; Abellanas, M.A.; Tolon, R.M.; Ramos, J.A.; Ferrer, I.; Romero, J.; Fernández-Ruiz, J. Cannabinoid pharmacology/therapeutics in chronic degenerative disorders affecting the central nervous system. *Biochem. Pharmacol.* **2018**, *157*, 67–84. [CrossRef]
16. Palazuelos, J.; Aguado, T.; Egia, A.; Mechoulam, R.; Guzmán, M.; Galve-Roperh, I. Non-psychoactive CB 2 cannabinoid agonists stimulate neural progenitor proliferation. *FASEB J.* **2006**, *20*, 2405–2407. [CrossRef] [PubMed]
17. Palazuelos, J.; Ortega, Z.; Díaz-Alonso, J.; Guzmán, M.; Galve-Roperh, I. CB2 Cannabinoid Receptors Promote Neural Progenitor Cell Proliferation via mTORC1 Signaling. *J. Biol. Chem.* **2012**, *287*, 1198–1209. [CrossRef] [PubMed]
18. Molina-Holgado, F.; Rubio-Araiz, A.; García-Ovejero, D.; Williams, R.J.; Moore, J.D.; Arévalo-Martín, Á.; Gómez-Torres, O. CB2 cannabinoid receptors promote mouse neural stem cell proliferation. *Eur. J. Neurosci.* **2007**, *25*, 629–634. [CrossRef] [PubMed]
19. Anavi-Goffer, S.; Mulder, J. The Polarised Life of the Endocannabinoid System in CNS Development. *ChemBioChem* **2009**, *10*, 1591–1598. [CrossRef]
20. Fernández-Ruiz, J.; Romero, J.; Velasco, G.; Tolón, R.M.; Ramos, J.A.; Guzmán, M. Cannabinoid CB2 receptor: A new target for controlling neural cell survival? *Trends Pharmacol. Sci.* **2007**, *28*, 39–45. [CrossRef]
21. Galve-Roperh, I.; Chiurchiù, V.; Díaz-Alonso, J.; Bari, M.; Guzmán, M.; Maccarrone, M. Cannabinoid receptor signaling in progenitor/stem cell proliferation and differentiation. *Prog. Lipid Res.* **2013**, *52*, 633–650. [CrossRef]
22. Duff, G.; Argaw, A.; Cecyre, B.; Cherif, H.; Tea, N.; Zabouri, N.; Casanova, C.; Ptito, M.; Bouchard, J.-F. Cannabinoid Receptor CB2 Modulates Axon Guidance. *PLoS ONE* **2013**, *8*, e70849. [CrossRef]
23. Goncalves, M.B.; Suetterlin, P.; Yip, P.; Molina-Holgado, F.; Walker, D.J.; Oudin, M.J.; Zentar, M.P.; Pollard, S.; Yáñez-Muñoz, R.J.; Williams, G.; et al. A diacylglycerol lipase-CB2 cannabinoid pathway regulates adult subventricular zone neurogenesis in an age-dependent manner. *Mol. Cell. Neurosci.* **2008**, *38*, 526–536. [CrossRef] [PubMed]
24. Oudin, M.J.; Gajendra, S.; Williams, G.; Hobbs, C.; Lalli, G.; Doherty, P. Endocannabinoids Regulate the Migration of Subventricular Zone-Derived Neuroblasts in the Postnatal Brain. *J. Neurosci.* **2011**, *31*, 4000–4011. [CrossRef] [PubMed]
25. Jin, K.; Xie, L.; Kim, S.H.; Parmentier-Batteur, S.; Sun, Y.; Mao, X.O.; Childs, J.; Greenberg, D.A. Defective Adult Neurogenesis in CB1 Cannabinoid Receptor Knockout Mice. *Mol. Pharmacol.* **2004**, *66*, 204–208. [CrossRef]
26. Cattaneo, E.; Conti, L. Generation and characterization of embryonic striatal conditionally immortalized ST14A cells. *J. Neurosci. Res.* **1998**, *53*, 223–234. [CrossRef]
27. Hovakimyan, M.; Weinreich, K.; Haas, S.J.-P.; Cattaneo, E.; Rolfs, A.; Wree, A. In Vitro Characterization of Embryionic ST14A-Cells. *Int. J. Neurosci.* **2008**, *118*, 1489–1501. [CrossRef]
28. Ehrlich, M.E.; Conti, L.; Tosellic, M.; Tagliettic, L.; Fiorilloc, E.; Tagliettic, V.; Ivkovica, S.; Guineaa, B.; Tranberga, A.; Sipioneb, S.; et al. ST14A Cells Have Properties of a Medium-Size Spiny Neuron. *Exp. Neurol.* **2001**, *167*, 215–226. [CrossRef]
29. Rigamonti, D.; Bauer, J.H.; De-Fraja, C.; Conti, L.; Sipione, S.; Sciorati, C.; Clementi, E.; Hackam, A.; Hayden, M.R.; Li, Y.; et al. Wild-Type Huntingtin Protects from Apoptosis Upstream of Caspase-3. *J. Neurosci.* **2000**, *20*, 3705–3713. [CrossRef]
30. Cacci, E.; Salani, M.; Anastasi, S.; Perroteau, I.; Poiana, G.; Biagioni, S.; Augusti-Tocco, G. Hepatocyte growth factor stimulates cell motility in cultures of the striatal progenitor cells ST14A. *J. Neurosci. Res.* **2003**, *74*, 760–768. [CrossRef]
31. Gambarotta, G.; Garzotto, D.; Destro, E.; Mautino, B.; Giampietro, C.; Cutrupi, S.; Dati, C.; Cattaneo, E.; Fasolo, A.; Perroteau, I. ErbB4 Expression in Neural Progenitor Cells (ST14A) Is Necessary to Mediate Neuregulin-1β1-induced Migration. *J. Biol. Chem.* **2004**, *279*, 48808–48816. [CrossRef]
32. Pregno, G.; Zamburlin, P.; Gambarotta, G.; Farcito, S.; Licheri, V.; Fregnan, F.; Perroteau, I.; Lovisolo, D.; Bovolin, P. Neuregulin1/ErbB4-induced migration in ST14A striatal progenitors: Calcium-dependent mechanisms and modulation by NMDA receptor activation. *BMC Neurosci.* **2011**, *12*, 103. [CrossRef]
33. Beyer, S.; Mix, E.; Hoffrogge, R.; Lünser, K.; Völker, U.; Rolfs, A. Neuroproteomics in stem cell differentiation. *Proteom. Clin. Appl.* **2007**, *1*, 1513–1523. [CrossRef]
34. Bari, M.; Battista, N.; Valenza, M.; Mastrangelo, N.; Malaponti, M.; Catanzaro, G.; Centonze, D.; Finazzi-Agrò, A.; Cattaneo, E.; Maccarrone, M. In vitro and in vivo models of Huntington's disease show alterations in the endocannabinoid system. *FEBS J.* **2013**, *280*, 3376–3388. [CrossRef]
35. Saba, J.; Couselo, F.L.; Turati, J.; Carniglia, L.; Durand, D.; De Laurentiis, A.; Lasaga, M.; Caruso, C. Astrocytes from cortex and striatum show differential responses to mitochondrial toxin and BDNF: Implications for protection of striatal neurons expressing mutant huntingtin. *J. Neuroinflam.* **2020**, *17*, 1–15. [CrossRef]
36. Avraham, H.K.; Jiang, S.; Fu, Y.; Rockenstein, E.; Makriyannis, A.; Zvonok, A.; Masliah, E.; Avraham, S. The cannabinoid CB2receptor agonist AM1241 enhances neurogenesis in GFAP/Gp120 transgenic mice displaying deficits in neurogenesis. *Br. J. Pharmacol.* **2014**, *171*, 468–479. [CrossRef] [PubMed]
37. Aguado, T.; Monory, K.; Palazuelos, J.; Stella‡, N.; Cravatt, B.; Lutz, B.; Marsicano, G.; Kokaia, Z.; Guzmán, M.; Galve-Roperh, I. The endocannabinoid system drives neural progenitor proliferation. *FASEB J.* **2005**, *19*, 1704–1706. [CrossRef]
38. Atwood, B.K.; Lee, D.; Straiker, A.; Widlanski, T.S.; Mackie, K. CP47,497-C8 and JWH073, commonly found in 'Spice' herbal blends, are potent and efficacious CB1 cannabinoid receptor agonists. *Eur. J. Pharmacol.* **2011**, *659*, 139–145. [CrossRef]
39. Boon, F.S.D.; Chameau, P.; Schaafsma-Zhao, Q.; Van Aken, W.; Bari, M.; Oddi, S.; Kruse, C.G.; Maccarrone, M.; Wadman, W.J.; Werkman, T.R. Excitability of prefrontal cortical pyramidal neurons is modulated by activation of intracellular type-2 cannabinoid receptors. *Proc. Natl. Acad. Sci. USA* **2012**, *109*, 3534–3539. [CrossRef] [PubMed]

40. Brailoiu, G.C.; Deliu, E.; Marcu, J.; Hoffman, N.E.; Console-Bram, L.; Zhao, P.; Madesh, M.; Abood, M.E.; Brailoiu, E. Differential Activation of Intracellular versus Plasmalemmal CB2Cannabinoid Receptors. *Biochem.* **2014**, *53*, 4990–4999. [CrossRef] [PubMed]
41. Bénard, G.; Massa, F.; Puente, N.; Lourenço, J.; Bellocchio, L.; Soria-Gómez, E.; Matias, I.; Delamarre, A.; Metna-Laurent, M.; Cannich, A.; et al. Mitochondrial CB1 receptors regulate neuronal energy metabolism. *Nat. Neurosci.* **2012**, *15*, 558–564. [CrossRef] [PubMed]
42. Rozenfeld, R. Type I Cannabinoid Receptor Trafficking: All Roads Lead to Lysosome. *Traffic* **2010**, *12*, 12–18. [CrossRef] [PubMed]
43. Augustin, S.M.; Lovinger, D.M. Functional Relevance of Endocannabinoid-Dependent Synaptic Plasticity in the Central Nervous System. *ACS Chem. Neurosci.* **2018**, *9*, 2146–2161. [CrossRef] [PubMed]
44. Soldati, C.; Biagioni, S.; Poiana, G.; Augusti-Tocco, G. β-Catenin and actin reorganization in HGF/SF response of ST14A cells. *J. Neurosci. Res.* **2008**, *86*, 1044–1052. [CrossRef]
45. Lange, C.; Mix, E.; Rateitschak, K.; Rolfs, A. Wnt Signal Pathways and Neural Stem Cell Differentiation. *Neurodegener. Dis.* **2006**, *3*, 76–86. [CrossRef] [PubMed]
46. Shoemaker, J.L.; Ruckle, M.B.; Mayeux, P.R.; Prather, P.L. Agonist-Directed Trafficking of Response by Endocannabinoids Acting at CB2 Receptors. *J. Pharmacol. Exp. Ther.* **2005**, *315*, 828–838. [CrossRef] [PubMed]

Chemosphere 263 (2021) 128090

Contents lists available at ScienceDirect

Chemosphere

journal homepage: www.elsevier.com/locate/chemosphere

Microplastics and their associated organic pollutants from the coastal waters of the central Adriatic Sea (Italy): Investigation of adipogenic effects *in vitro*

Martina Capriotti [a, b], Paolo Cocci [b], Luca Bracchetti [b], Erika Cottone [c], Rosaria Scandiffio [c], Giovanni Caprioli [d], Gianni Sagratini [d], Gilberto Mosconi [b], Patrizia Bovolin [d], Francesco Alessandro Palermo [b, *]

[a] Department of Marine Sciences, University of Connecticut, 1080 Shennecossett Rd, Groton, CT, USA
[b] School of Biosciences and Veterinary Medicine, University of Camerino, Via Gentile III da Varano, 62032, Camerino, MC, Italy
[c] Department of Life Sciences and Systems Biology, University of Turin, Via Accademia Albertina 13, 10123, Torino, TO, Italy
[d] School of Pharmacy, University of Camerino, Via Madonna Delle Carceri 9, 62032, Camerino, MC, Italy

HIGHLIGHTS

- Floating MPs were collected along the western coasts of the Central Adriatic Sea.
- MPs were found in all sampling stations showing the highest abundance in open waters.
- Chemical analysis showed relevant concentrations of pollutants onto MP surfaces.
- MP extracts induced triglyceride accumulation in 3T3-L1 preadipocytes.
- Our results provide further support for the eco-toxicological impact of MPs.

ARTICLE INFO

Article history:
Received 25 May 2020
Received in revised form
28 July 2020
Accepted 19 August 2020
Available online 22 August 2020

Handling Editor: Shane Snyder

Keywords:
Adriatic sea
Microplastic
Biomonitoring
Endocrine disruptors
Metabolic disruptors
Adipocytes

ABSTRACT

Even though microplastic (MP) pollution in aquatic environment is nowadays widely studied, a huge gap of knowledge exists on their actual biological effects. In this study we first reported environmental baseline data on the occurrence and characterization of floating MPs in Italian coastal waters of the Central Adriatic Sea by using a standardized monitoring protocol. Further, we analyzed the concentrations of MP-associated chemicals and evaluated their potential adipogenic effects using 3T3-L1 preadipocytes. MPs were found in each sampling stations showing the highest abundance (1.88 ± 1.78 items/m^3) in the sites more distant from the coast with fragments as the most common shape category. All targeted organic pollutants (*i.e.* polychlorinated biphenyls - PCBs, polycyclic aromatic hydrocarbons -PAHs, organophosphorus - OP, and organochlorine - OC pesticides) have been detected on the surface of the collected MPs. The highest concentrations of PAHs were found on MPs from inshore (*i.e.* <1.5 NM) surface waters with low-ring PAHs as dominant components. Similarly, MPs from inshore waters had higher ΣPCB concentrations (64.72 ng/g plastic) than those found in offshore (*i.e.* >6 NM) waters (10.37 ng/g plastic). Among pesticides, all measured OPs were detected in each sample analyzed with pirimiphos-methyl as the most representative compound. For OCs, the sum of all concentrations of congeners was higher in coastal with respect to offshore waters. Moreover, *in vitro* 3T3-L1 screening of MP extracts indicated potential metabolic effects resulting in both adipogenesis and lipid uptake/storage.

1. Introduction

Microplastics (MPs, ≥0.001 mm and<5 mm) (Shim et al., 2018) are a well known global issue for marine and coastal ecosystems (Browne et al., 2011; UNEP, 2016) due to their ubiquitous presence

* Corresponding author. School of Biosciences and Veterinary Medicine, University of Camerino, Via Gentile III Da Varano, I-62032, Camerino, MC, Italy.
E-mail address: francesco.palermo@unicam.it (F.A. Palermo).

https://doi.org/10.1016/j.chemosphere.2020.128090
0045-6535/

throughout the marine environment compartments, as surface and water column, sediments, and biota. In this regard, the Mediterranean Sea with a mean density of floating microplastics of about 100,000 items/km^2 represents one of the basin most affected by MP litter (Fossi et al., 2012). Within the Mediterranean Sea, however, very few studies have investigated the occurrence of floating plastic debris in the Adriatic Sea that, due to its features (*e.g.* semi-closed conformation, oceanographic conditions and heavy anthropogenic pressure), can be considered a plastic pollution hot spot (Gomiero et al., 2018). In this regard, recent data on the Mediterranean Sea (partially including the Adriatic area) reported a MP range of 0.4–1.8 items/m^3 with polyethylene (PE) as the most common polymer composition types (Suaria et al., 2016). Similarly, a clear prevalence of MPs (65.1% of sampled debris) was demonstrated in marine sediments from the Central Adriatic (Munari et al., 2017). MPs were also found in a wide range of marine species collected along the Adriatic Sea showing highest concentrations (*i.e.* 1.0–1.7 items/specimens) in fish (Avio et al., 2015; Pellini et al., 2018). These findings indicate that small size debris are available to marine vertebrates and invertebrates, resulting in both physical and chemical impacts (Fossi et al., 2012, 2014; Gall and Thompson, 2015). MPs can be translocated to the lymphatic and/or circulatory system, and accumulated in organs as the digestive and the respiratory tracts (Barnes et al., 2009; Cole and Galloway, 2015; Mazurais et al., 2015; Besley et al., 2017; Lusher et al., 2017a, 2017b).

Nowadays the research on the ecological impact of microplastics is not limited to evaluate their accumulation in the marine environment and consequently in living organisms, but is now moving on to investigate the role of MPs as potential vehicles of a wide range of toxic chemicals (Teuten et al., 2007; Engler, 2012). Recent data indicate that hydrophobic organic contaminants (HOCs), including endocrine disrupting chemicals (EDCs), have been detected on the surface of MPs (Mato et al., 2001; Ogata et al., 2009; Rios et al., 2010; Hirai et al., 2011; Rochman et al., 2014a). Indeed, due to the physical and chemical properties of plastic polymers, MPs can quickly accumulate and concentrate HOCs present in the surrounding water. It should also be taken into account that MP-associated HOCs have to be added to the chemicals already included as additives during plastic manufacturing (*e.g.* bisphenol A or nonylphenol) (Ogata et al., 2009; Hirai et al., 2011; Engler, 2012; Mai et al., 2018; Alimba and Faggio, 2019; Chen et al., 2019), making the potential of chemicals release from MPs to the marine environment and wildlife particularly harmful. In addition, ingestion of MPs by aquatic animals may result in increased bioavailability of HOCs, bioaccumulation and both potential toxicity and transfer along the trophic web (Avio et al., 2015; Batel et al., 2016).

It has been demonstrated that among HOCs, EDCs are commonly found on MPs, including abrasion beads, and easily released from plastic debris due to lower partition coefficients between plastic and water (Liu et al., 2016). EDCs accumulation in tissues of marine organisms, following their MP-mediated release, can thus exert adverse effects ranging from disruption of endocrine-based reproductive pathways to metabolic alterations (Franzellitti et al., 2019). In this last regard, a group of endocrine disruptors, named obesogens or metabolic disruptors, have been found to affect adipogenesis by perturbing peroxisome proliferator activated receptor (PPAR) signaling pathways (Grün and Blumberg, 2009). Recently, the obesogenic potential of these pollutants were assayed *in vitro* using 3T3-L1 adipocytes and primary cultures of sea bream hepatocytes (Cocci et al., 2017; Pomatto et al., 2018).

Thus, our first objective in this study was to collect environmental baseline data on the occurrence and characterization of floating MPs in Italian coastal waters of the Central Adriatic Sea by using a standardized monitoring protocol. Second, we aimed to examine the concentrations of chemicals adsorbed on MPs sampled from the same study area and to test their adverse effect by *in vitro* bioassays. In particular, we used 3T3-L1 preadipocytes to investigate the possible adipogenic effects of these plastic extracts in order to provide preliminary insights on potential ecotoxicological risk of MPs as vehicles of chemical pollutants.

2. Materials and methods

2.1. Sites and water surface sampling

Samples were collected inshore and offshore along the western (Italian) coasts of the Central Adriatic Sea (Province of Ascoli Piceno, Marche Region - Italy). The sampling operations were conducted during summer season 2018, following the microplastics monitoring methods applied by the Italian Ministry of the Environment and Land and Sea protection (Minambiente, 2018) and the requirements indicated by the ministerial protocol within the MSFD monitoring program (MSFD, 2013). Briefly, transects were outlined perpendicular to the coast line along the municipalities of San Benedetto del Tronto (SBT) and Grottammare (GRT), respectively (Fig. 1). Three sampling stations were located at different distance from the coast (0.5, 1.5 and 6 nautical Miles, NM) along each transect. An additional sampling station was located inside the San Benedetto del Tronto harbor. Floating samples were collected from surface sea water, using a manta trawl with mesh size of 300 μm (30 x 15 × 200 cm) equipped with a mechanical flow meter (Hydro-Bios). The manta net was towed on the water surface for 20 min at 2 knots and was kept at a distance far from the boat to avoid turbulence by the waking of the ship. Samples were rinsed from the outside to the end of the net, placed in glass containers and immediately stored at 4 °C until the sorting using a stereomicroscope. To prevent external contamination during the analysis, the laboratory procedures were performed according to Baini et al. (2018).

2.2. Microplastic identification and count

Samples where dried at room temperature and weighted in OHAUS Explorer analytical balance. For microplastics identification, samples were observed under a stereomicroscope (Carl Zeiss Stemi™) and images have been examined by a USB Camera (Optika B Series) using the Optika ProView software. Plastic particles were sorted based on their colour (blue, red, black, white, transparent,

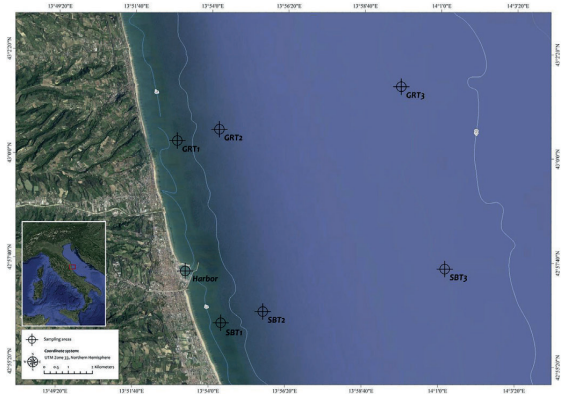

Fig. 1. Map of the study area. Sampling stations were located at different distance from the coast (0.5, 1.5 and 6 nautical Miles, NM) along each transect.

green, other colour), size (<5, 5–25, >25 mm) and shape (spherical, filament, fragment, sheet, other shape) according to the MSFD guidelines and Imhof et al. (2017). As reported by Baini et al. (2018), the number of microplastic was normalized to the total water volume filtered (V) and expressed as items/m^3.

2.3. Determination of PAHs, PCBs, organophosphorus and organochlorine pesticides

Due to limited amount of particles to be provided for both bioassay and chemical analysis, MPs collected within the study area were pooled according to distance from the coast in order to obtain 3 type of samples: offshore waters (*i.e.* 6 NM), inshore waters (*i.e.* <1.5 NM, corresponding to local areas of touristic and commercial traffics) and the harbor of San Benedetto del Tronto as expected polluted area.

Hydrophobic organic contaminants were isolated from marine debris following the protocol described by Chen et al. (2019) with slight modifications. Briefly, 4 mL of dichloromethane was added to each microplastic sample (400 mg) and incubated for 30 min at room temperature, vortexing every 10 min. The procedure was repeated for 3 times and finally the supernatant was evaporated to 500 μl using a Rotavapor R-300 (Buchi). The PCB mix standard (PCB 28, PCB 52, PCB 95, PCB 99, PCB 101, PCB 105, PCB 110, PCB 118, PCB 138, PCB 146, PCB 149, PCB 151, PCB 153, PCB 170, PCB 177, PCB 180, PCB 183, PCB 187) at a concentration of 10 mg/L in iso-octane, the organochlorine pesticides OC1 (six congeners, *i.e.* α-HCH, β-HCH, γ-HCH, HCB, heptachlor and heptachlor epoxide) mix standard at a concentration of 10 mg/L in cyclohexane and the organochlorine pesticides OC2 (six congeners, *i.e.* 2.4-DDT, 4.4-DDT, 2.4-DDE, 4.4-DDE, 2.4-DDD, 4.4-DDD) mix standard at a concentration of 10 mg/L in cyclohexane were supplied by Dr. Ehrenstorfer (Ausburg. Germany). Standard working solutions at various concentrations were prepared daily by appropriate dilution of the stock solutions with hexane. The organophosphorus pesticides (four congeners, *i.e.* chlorfenvinphos. chlorpyrifos. malathion. pirimiphos-methyl) mix standard were supplied by Fluka (Milano. Italy). Individual stock solutions of organophosphorus pesticides at concentrations of 1000 mg/L were prepared by dissolving pure standard compounds in HPLC grade methanol and then stored in glass-stoppered bottles at 4 °C. Afterwards standard working solutions at various concentrations were prepared daily by appropriate dilution of the stock solution with methanol. A gas chromatograph/mass selective detector (GC/MSD) (Hewlett Packard. Palo Alto. CA. USA; HP-6890 with HP 5973) was used. Separation was performed on an HP 5 MSI column (30 m × 0.25 mm X 0.25 μm film thickness). An HP Chem workstation was used with the GC/MS system. All injections were splitless and the volume was 1 μl. The flow rate (He) was 0.8 mL/min. The injector temperature was 270 °C. The column temperature program used for PCB and for the second group of organochlorine pesticides, *i.e.* dichlorodiphenyltrichloroethane (DDT) and its metabolites (OC 2 subgroup) analyses was from 60 °C (3 min) to 190 °C at 8 °C min^{-1}, from 190 °C (18 min) to 300 °C at 15 °C min^{-1}, then at 300 °C for 1 min. The column temperature programme used for the first group of organochlorine pesticides, *i.e.* α-HCH, β-HCH, γ-HCH, HCB, heptachlor and heptachlor epoxide (all included in the OC 1 subgroup) was from 60 °C (3 min) to 190 °C at 8 °C min^{-1}, from 190 °C (13 min) to 300 °C at 15 °C min^{-1}, then at 300 °C for 1 min. The column temperature programme used for organophosphorus pesticides analyses (chlorfenvinphos, chlorpyrifos, malathion, pirimiphos-methyl) was from 50 °C (5 min) to 320 °C at 15 °C min^{-1}, then at 320 °C for 4 min. Data were acquired in the electron impact (EI) mode (70 eV) using the selected ion monitoring (SIM) mode. For this purpose, a gas chromatograph/mass selective detector (GC/MSD) (Hewlett Packard. Palo Alto. CA. USA; HP-6890 with HP 5973) was used. Extracts were analyzed for concentrations of 15 of the most environmentally relevant PAHs (Naphthalene, Acenaphthene, Fluorene, Chrysene, Phenanthrene, Fluoranthene, Anthracene, Pyrene, Benzo[a]anthracene, Benzo[b]fluoranthene, Benzo[k]fluoranthene, Benzo[a]pyrene, Dibenz[a,h]anthracene, Benzo[g,h,i] perylene and Indeno[1,2,3-c,d]pyrene). The detailed methodology for separation and quantification of target analytes was published previously (see "Supplementary data" of Cocci et al., 2017).

2.4. 3T3-L1 cell culture and quantification of adipocyte lipid accumulation

3T3-L1 preadipocytes (ATCC® CL-173™; Lot No 70009858, ATCC, Manassas, VA, USA) were cultured in high-glucose (4.5 g/L) Dulbecco's modified Eagle's medium (DMEM) supplemented with 10% bovine calf serum, 2 mM L-glutamine, 50 IU/mL penicillin, and 50 μg/mL streptomycin (Sigma Aldrich, St. Louis, MO, USA).

For experiments, 5×10^3 cells/well were seeded in 96-black well clear bottom plates (Greiner Bio-One, Frickenhausen, Germany). Two days after reaching confluence (day 0), cells were incubated with differentiation medium (MDI; DMEM containing 10% fetal bovine serum, 1 μg/mL insulin, 0.5 mM isobutylmethylxanthine), containing different concentrations of the various microplastic organic extracts. In particular, inshore, offshore and harbor microplastic extracts were dried and redissolved in 30 μl DMSO; then scalar dilutions, ranging from 10^{-3} to 10^{-6}, were added to the MDI used for adipocyte differentiation. Two days later (day 2), MDI medium was replaced with maintenance medium (MM; DMEM 10% FBS, 1 μg/mL insulin), always containing the various dilutions of microplastic extracts. Negative controls (solvent only) were set up using MDI and MM added with 0.1% DMSO, corresponding to the maximum solvent concentration present in microplastic extract dilutions; as a positive control, 100 nM Rosiglitazone (Sigma Aldrich) was added to MDI and MM. Fresh medium was provided every two days; experiments ended after 9 days from the beginning of the differentiation (day 9). Lipid accumulation was quantified by using AdipoRed™ assay reagent (Lonza, Walkersville, MD, USA), while the DNA content (that correlates with cell number) was estimated by NucBlue™ staining (Invitrogen, Carlsbad, CA, USA). Briefly, medium was removed from 3T3-L1 cultures and cells were rinsed with PBS, subsequently replaced with a dye mixture containing AdipoRed™ and NucBlue™ assay reagents diluted in PBS (25 μl and 1 drop, respectively, per mL of PBS). After 40 min of incubation at room temperature in the dark, fluorescence was measured with Filtermax F5 microplate reader (Molecular Devices, Sunnyvale, CA, USA) with excitation at 485 nm and emission at 535 nm for AdipoRed™ and excitation at 360 nm and emission at 460 nm for NucBlue™ quantification. Experiments were repeated three times (four wells for each condition), using cells at different passage numbers (p3-p5). Data were referred as % of the control (0.1% DMSO) condition (set = 100%).

2.5. Statistical analysis

Data are expressed as mean ± standard error of the mean (SEM). Statistical analysis was performed using ANOVA (one-way analysis of variance) followed by Bonferroni's multiple comparison test. Differences with $p < 0.05$ were considered statistically significant.

3. Results

3.1. Microplastics in water surface samples

Particles isolated from surface seawater were visually counted

and sorted based on their dimension, shape and color (Table 1). Among the total particles sampled, microplastics (<5 mm) constituted the most representative size class (n = 401.08, 95%), and were detected in each transect representing the totality of plastic litter (100%) in GRT1, GRT2 and SBT2 stations and showing the highest abundance in the sites more distant from the coast (SBT3: 1.88 ± 1.78 and GTR3: 3.42 ± 2.28 items/m^3) or inside the San Benedetto del Tronto harbor (0.91 ± 0.58 items/m^3). Marine debris larger than 5 mm were recorded in harbor (16%), open waters (SBT3, 6% and GRT3, 12%), and also at 0.5 NM along the SBT transect (2%).

Analyzing the overall study area by combining the values measured at two sampling stations at the same distance (along both transects), 75% of the total MPs were collected from sampling sites at 6 NM, 3% at 1.5 NM, 8% at 0.5 NM from the coastline and finally the 13% inside the harbor. Fragments were the most common shape category observed in each sampling station (Fig. 2a), reaching the 74.7% (n = 28.4) of all the MP types sampled in coastal sites (<1.5 NM). Films were the second most abundant group of the plastic items collected with the highest number (n = 23.3, 42.9%) recorded in SBT harbor. On the other hand, spherical particles were commonly found in offshore waters (6 NM) showing a total number of 54 (25%, Fig. 2a).

Analysis of MP color pattern revealed that transparent and white items accounted for 37% and 44% of the particles collected respectively (Fig. 2b).

3.2. Concentrations of pollutants on inshore and offshore microplastic samples

MP extracts were analyzed for PCBs, PAHs, OPs, and OCs (Table 2).

The highest concentrations of PAHs were found in microplastics collected from both inshore and harbor surface waters (Fig. 3) with low-ring PAHs as dominant components (Table 2). On the contrary, high-ring PAHs were most abundant in offshore samples (Table 2).

Among the sixteen PCB congeners analyzed, only seven, namely PCB 52, PCB 95, PCB 99, PCB 101, PCB 110, PCB 138 and PCB 149, were detected in the different samples (Table 2). The congeners 52, 95, 138 and 149 were found in MPs from each sampling area. If congeners were considered altogether, inshore waters had the highest ΣPCB concentrations (64.72 ng/g plastic) followed by SBT harbor (37.86 ng/g plastic). On the contrary, the lowest ΣPCBs was found in MPs from offshore waters (10.37 ng/g plastic) (Fig. 3).

All measured OPs were detected in each sample analyzed with pirimiphos-methyl as the most representative compound. Generally, the highest ΣOP concentrations were found in samples from inshore waters (Fig. 3). For OC1 and OC2, the sum of all concentrations of congeners were higher in coastal waters with respect to offshore waters (Fig. 3).

3.3. Effects of microplastic extracts on 3T3-L1 adipocyte differentiation

The effect of MP extracts was assayed on the murine 3T3-L1 preadipocyte cell line, a commonly used cell model for adipose cell biology research. Since adipogenic effects can be exerted by increasing intracellular lipids (adipocytes hypertrophy) and/or adipocytes number (adipocytes hyperplasia), we assayed both triglyceride accumulation (AdipoRed™ assay) and total cell number (NucBlue™ staining, measuring DNA content). Confluent preadipocytes, cultured in 96-well plates, were induced to start adipogenic differentiation and were treated throughout the differentiation period (9 days) with solvent only (0.1% DMSO; negative control) or with different concentrations of microplastic extracts (serial dilutions ranging from 10^{-3} to 10^{-6}); Rosiglitazone, a well-known agonist of the adipogenesis master regulator PPARγ, was used as a positive control. All the tested concentrations of microplastic extracts did not exert cytotoxic effects, as demonstrated by cell evaluation under the microscope and by NucBlue staining quantification, showing no difference in DNA content, and thus in cell number, in microplastic extract-exposed cells versus control adipocytes (Fig. 4c). Interestingly, harbor, inshore and offshore microplastic extracts, at all the concentrations used, induced an increase in triglyceride accumulation, in respect to control cells (Fig. 4a and b). Differently from Rosiglitazone treatment, exposure to microplastic extracts induced no changes in total cell number (Fig. 4c), thus indicating that microplastic extracts did not induce adipocytes hyperplasia. On the other hand, triglyceride accumulation per cell (i.e. triglyceride accumulation normalized for DNA content) resulted statistically increased after microplastic extracts exposure (Fig. 4d), thus suggesting an induction of adipocytes hypertrophy.

4. Discussion

Despite the growing monitoring of MP presence in the Mediterranean Sea, there is still a substantial lack of information on amount and distribution of MPs in the Adriatic Sea (de Lucia et al., 2014; Gomiero et al., 2018). In this respect, the present study was aimed to provide new insight on the occurrence of MPs in Italian coastal waters of the Central Adriatic Sea and on their capability to adsorb organic pollutants.

Our results revealed that the average amount of MPs (2.65 items/m^3) estimated in surface offshore waters was similar to that recorded within the Tremiti island Marine Protected Area (Central Adriatic Sea, Italy) in 2017 (2.2 items/m^3; Mezzelani et al., 2018). Interestingly, this last data was considerably increased with respect to the amount of 0.165 items/m^3 found by (De Lucia et al., 2018) in the same area during 2015. These findings suggest how the Adriatic Sea basin has been characterized by an exponential increase in plastic pollution over the last years. Recently, a range of 0.05–4.90 particles/m^3 was reported for quantification of floating plastics (<700 μm) in the southern Adriatic Sea by a large scale monitoring

Table 1
Particles abundance (items/m^3) and size (mm) in water surface samples collected in three different sampling sites; mean values ± s.d. for each transect have been reported.

Sampling site	Distance (nM)	Items/m^3	Micro-(<5 mm)	Meso-(5–25 mm)	Macro-(>25 mm)
GRT1	0.5	0.17 ± 0.02	12.33 ± 2.51 (100%)	–	–
GRT2	1.5	0.11 ± 0.05	9.34 ± 4.01 (100%)	–	–
GRT3	6	3.42 ± 2.28	240.33 ± 160.55 (88%)	38.33 ± 33.29 (10%)	1.67 ± 1.53 (2%)
SBT1	0.5	0.17 ± 0.11	15.75 ± 10.59 (98%)	0.50 ± 1.00 (2%)	–
SBT2	1.5	0.04 ± 0.01	3.00 ± 0.00 (100%)	–	–
SBT3	6	1.88 ± 1.78	66.00 ± 8.54 (94%)	3.33 ± 0.58 (5%)	1.0 ± 1.00 (1%)
Harbor		0.91 ± 0.57	54.33 ± 24.11 (84%)	11.67 ± 15.30 (11%)	4.33 ± 4.51 (5%)

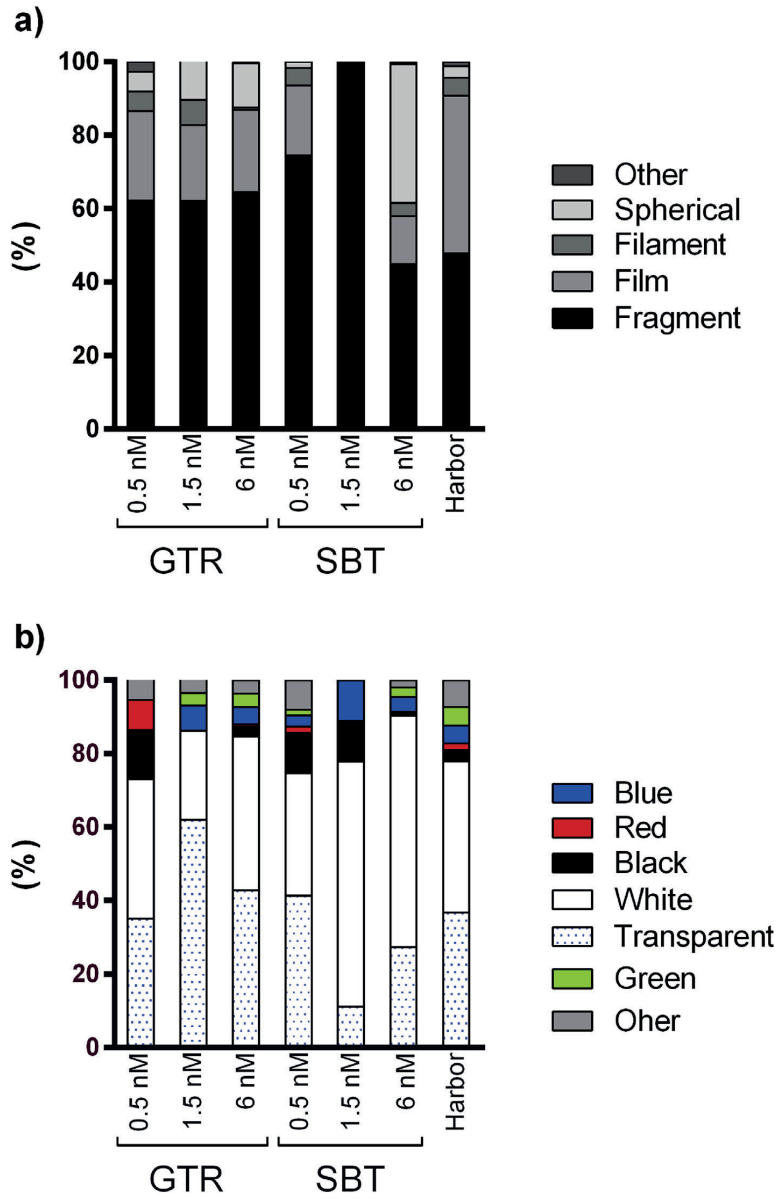

Fig. 2. Sampling station-related abundance % of microplastics isolated from water surface samples in relation to shape (a) and color (b). (For interpretation of the references to color in this figure legend, the reader is referred to the Web version of this article.)

study (Suaria et al., 2018). The results of this study also showed that about 51% of the total recorded particles were smaller than 500 μm (Gomiero et al., 2018) thus supporting the key role of this size fraction within the plastic pollution affecting the Adriatic Sea (Mezzelani et al., 2018; Zeri et al., 2018). In addition, the high abundance of fragments, as previously observed in other studies (Isobe et al., 2014; Baini et al., 2018), suggests that fragmentation of large plastic objects could represent the main source of MPs in our study area.

In the present work, we observed that higher MP abundances were detected in offshore (6 nM) rather than in inshore (<1.5 nM) sampling sites. These findings are consistent with the results of some previous studies which observed prevalence of plastic debris in areas 10–100 Km far from the coastline, indicating a progressive decrease in the number of plastic items from open sea to coastal waters (Pedrotti et al., 2016; Baini et al., 2018). In contrast, Zeri et al. (2018) have recently found a statistically significant increases in nearshore (≤4 km) microplastic concentration with respect to that

Table 2
Concentration (ng/g plastic) of Polychlorinated biphenyls (PCBs), organophosphorus (OPs), organochlorine pesticides (OCs), and polycyclic aromatic hydrocarbon (PAH) congeners measured on microplastics from inshore (i.e. <1.5 NM), offshore waters (i.e. 6 NM), and harbor.

POPs	Inshore (ng/g plastic)	Offshore (ng/g plastic)	Harbor (ng/g plastic)
PCB 28	n.d.	n.d.	n.d.
PCB 52	27.91	0.70	12.22
PCB 95	3.58	0.17	5.85
PCB 99	0.60.	n.d.	n.d.
PCB 101	n.d.	0.08	0.52
PCB 105	n.d.	n.d.	n.d.
PCB 110	n.d.	0.08	0.34
PCB 118	n.d.	n.d.	n.d.
PCB 138	28.51	0.54	16.01
PCB 146	n.d.	n.d.	n.d
PCB 149	5.07	0.29	2.84
PCB 151	n.d.	n.d.	n.d.
PCB 153	n.d.	n.d.	n.d.
PCB 170	n.d.	n.d.	n.d.
PCB 177	n.d.	n.d.	n.d.
PCB 180	n.d.	n.d.	n.d.
PCB 183	n.d.	n.d.	n.d.
PCB 187	n.d.	n.d.	n.d.
∑PCBs	65.67	1.86	37.78
Chlorfenvinphos	6.57	0.14	1.98
Chlorpyrifos	45.37	0.77	32.19
Malathion	17.31	0.22	7.23
Pirimiphos-methyl	78.36	3.59	32.70
∑OPs	147.61	4.72	74.10
α-HCH	95.22	0.84	27.02
β-HCH	0.37	0.02	0.86
γ-HCH	3.58	0.07	1.98
HCB	2.09	0.10	10.84
Heptachlor	n.d.	n.d.	n.d.
Heptachlor epoxide	n.d.	n.d.	n.d.
∑OC1s	101.26	1.03	40.70
2.4-DDE	10.15	0.16	2.41
4.4-DDE	8.66	0.19	n.d.
2.4-DDD	n.d.	1.32	8.00
4.4-DDD	15.52	n.d.	67.38
2.4-DDT	n.d.	0.59	n.d.
4.4-DDT	n.d.	2.79	n.d.
∑OC2s	34.33	5.05	77.79
Naphthalene	9.55	n.d.	6.71
Acenaphthene	n.d.	n.d.	n.d.
2-Bromonaphthalene	46.27	2.46	40.36
Acenaphthylene	109.40	1.27	100.00
Fluorene	n.d.	n.d.	n.d.
Phenanthrene	n.d.	n.d.	2.58
Anthracene	64.18	1.54	25.04
Fluoranthene	16.87	0.57	n.d.
Pyrene	n.d.	1.48	35.13
Benzo(a)Anthracene	67.31	2.64	40.36
Chrysene	81.64	2.28	47.93
Benzo(bFluoranthene	n.d.	n.d.	n.d.
Benzo(a)Pyrene	n.d.	n.d.	7.66
Indeno(1,2,3-cd)Pyrene	n.d.	n.d.	n.d.
DiBenz(a,h)Anthracene	n.d.	4.40	12.91
Benzo(g,h,i)Perylene	12.84	2.34	41.48
∑low-ring PAHs	229.40	5.27	174.69
∑high-ring PAHs	178.66	13.71	185.47
∑Total PAHs	408.06	18.98	360.16

n.d.: not detectable.

of offshore (>4 km) Adriatic waters. These contrasting results could be attributed to the variability in observational conditions which are severely affected by the complexity of the study area circulation patterns, weather conditions and the heterogeneity in sources of marine litter.

A great body of studies is nowadays starting to focus on the potential toxicity of MPs and to investigate their role as vector of HOCs (Endo et al., 2005; Teuten et al., 2007; Bakir et al., 2014; Chen et al., 2019; Tang et al., 2020). In this study, the overall evaluation of pollutants carried on MPs provided a clear separation between in- and offshore waters, highlighting the highest abundance of these chemicals in the former. This finding is likely due to adsorption mechanisms from the surrounding environment, because these chemicals, especially PAHs and PCBs, show affinity with plastic particles (Teuten et al., 2009) and the tendency to accumulate in the organic phase of sediments (Leggett and Parker, 1994).

Among the great variety of organic pollutants which have been isolated on the surface of microplastics, PHAs (Teuten et al., 2007), PCBs (Endo et al., 2005) and pesticides (Bakir et al., 2014) represent the most common categories of contaminants. Indeed, PAHs are ubiquitous pollutants in waters, sediments and marine organisms from the Italian coasts of the Adriatic Sea (Cocci et al., 2017, 2018;

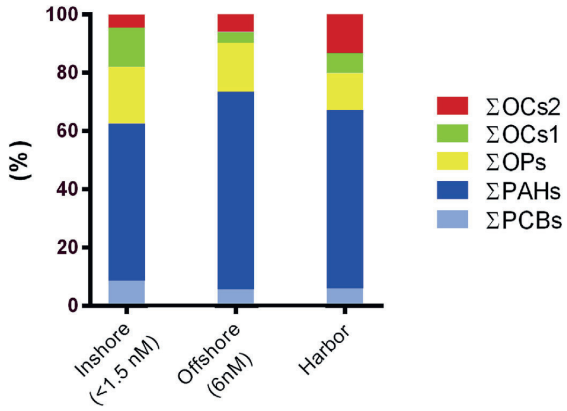

Fig. 3. Microplastic-associated PAH, PCB, OP, OC1 and OC2 patterns across sampling sites.

Frapiccini et al., 2018; Bajt et al., 2019). Due to their strong ability to bind to plastic particles (Liu et al., 2016), it's not surprising that PAHs are the most abundant contaminants found on the surface of MPs collected from our study area. The measured concentration of ∑PAHs is consistent with that found on plastic pellets (166.3–2781 ng/g plastic) or fragments (85.9–2841 ng/g plastic) beached along Crete shore (Karkanorachaki et al., 2018). Additionally, the levels of PAHs were found to range from 35.1 to 17,023.6 ng/g in marine plastic debris from Canary Island beaches (Camacho et al., 2019) and from 3400 to 120,000 ng/g in microplastics from Chinese surface waters (Mai et al., 2018). Our findings are also comparable to the PAH concentrations (*i.e.* 136.3–1586.9 μg/kg plastic and of 397.6–2384.2 μg/kg plastic) recently found in microplastics from two beaches in China (Zhang et al., 2015). Low-ring PAHs were the most prominent components especially in inshore MPs thus suggesting that petroleum-derived contaminants are likely to be the main sources of MP contamination. Of the sixteen PAHs, Acenaphthylene (Acl) showed the highest abundance in each analyzed samples; interestingly, this finding parallels the highest Acl concentration found in surface coastal waters by our previous survey (Cocci et al., 2017).

PCBs were one of the most abundant group observed in our study showing higher concentrations in microplastics sampled from coastal areas than in those from offshore waters. These levels are substantially in line with the measures (*i.e.* 0.9–2285.8 ng/g plastic particles) recorded in plastic pellets and micro fragments beached along the coasts of Canary Islands (Camacho et al., 2019). PCB concentrations in coastal surface waters of the central Western Adriatic Sea were found to vary from 6260 ng/L in areas interested by an intense maritime traffic to 10,650 ng/L in sea basin affected by riverine runoffs (Cocci et al., 2017). Interestingly, we observed similar patterns in PCB congener distribution between waters and plastics with highest levels of PCB 52 and 138 (Cocci et al., 2017). On the other hand, PCB congener 101 and 110 were exclusively identified in microplastics from the offshore sites or from the harbor, and no detectable concentrations were found in inshore samples.

Total concentrations of OCs (OCs1 and OCs2) were 130.62 ng/g plastic, 19.20 and 59.25 ng/g plastic in MP from coastal-, offshore

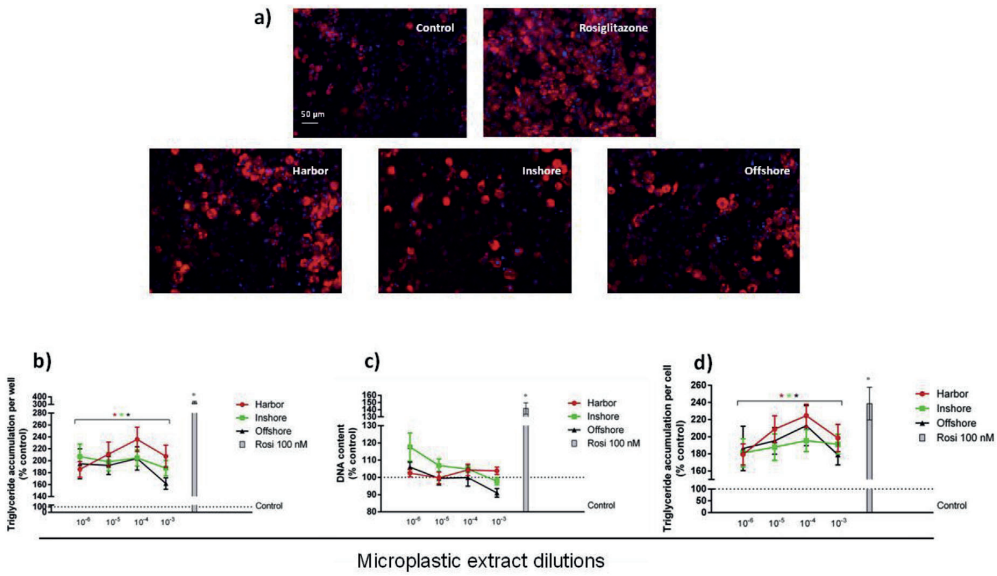

Fig. 4. (a) Representative micrographs of AdipoRed (red) and NucBlue (blue) staining of undifferentiated 3T3-L1 preadipocytes (Undiff.) and adipocytes after 9 days of differentiation in the presence of vehicle only (0.1% DMSO; Control), Rosiglitazone, or extracts obtained from microplastics collected at the different sampling stations (Harbor, Inshore, Offshore). Scale bar: 50 μm. (b) Graph summarizing AdipoRed staining experiments to assess lipid accumulation in differentiated 3T3-L1 adipocytes treated with 0.1% DMSO solvent (control) or cells treated with 100 nM Rosiglitazone (positive control) or serial dilutions (ranging from 10^{-3} to 10^{-6}) of the different microplastic extracts, showing triglyceride accumulation per well. (c) Graph summarizing NucBlue staining experiments to assess variations in the number of cells, showing DNA content per well. (d) Graph showing triglyceride accumulation per cell (triglyceride accumulation normalized to DNA content), calculated as the ratio of AdipoRed and NucBlue staining. In b,c,d data are reported as % of control condition (solvent control values were set equal to 100%; horizontal dotted line) and represent the mean ± SEM of three independent experiments. *Indicates dilutions with significant increase over solvent control, $p < 0.05$, within each sampling site. (For interpretation of the references to color in this figure legend, the reader is referred to the Web version of this article.)

waters and harbor, respectively. In the context of pesticides, there is considerable evidence that OCs are chemically stable under environmental condition, and their residues can be found in the water even years later then their ban (Breivik et al., 2004). Among OCs1, we observed that four of them (α-HCH, β-HCH, γ-HCH and HCB) were found in the analyzed samples with α-HCH and β-HCH present in each sampling site. The detected concentration of OC1s (*e.g.* HCB) is consistent with levels found in pellets and plastic fragments from Camacho et al. (2018) but higher (*e.g.* α-HCH) than values measured in pellets sampled from beaches in China (Zhang et al., 2015). The α-HCH/γ-HCH ratio was higher than 1, which means that there has been no major recent input of HCHs and that the observed values are due to their persistence in the marine environment. After all, isomeric mixture of HCHs has been used as pesticides for a long time. Recent studies have shown higher concentrations of β-HCH with respect to the other isomers in tissues of mollusks collected at different areas including the Eastern Adriatic (Wang et al., 2008; Kljakovic-Gaspic et al., 2010). These findings are interesting because support the role of environmental conditions in determining the different behaviors of HCH contaminations in different matrices.

Regarding OCs2, 2.4-DDE was found at each sampling site while very high concentration of 4.4-DDD were detected exclusively in the harbor. In addition, high levels of 4.4-DDT were measured in pooled samples from offshore waters. The overall analysis of DDT input in terms of ratio of (DDD + DDE)/DDT (Hitch and Day, 1992) shows a value of >0.5 suggesting presence of DDT residues in the environment. It is not surprising that we found similar values since DDT in the environment is mostly a result of both past production and use (ATSDR, 2002).

OPs are the major representative groups of pesticides found on MPs. In particular, the Chlorpyrifos pesticide was carried by MPs sampled at each site and was found to show the highest concentration among OPs. This is an innovative finding due to the classification of chlorpyrifos as emerging contaminant but, at the same time, it is not surprising because Camacho and coworkers (2019) have recently found this pesticide bound to microplastics collected along the Canary Islands beaches. Chlorpyrifos, malathion and pirimiphos-methyl have been extensively used in agriculture during the last decade and therefore have been detected in biotic and abiotic marine compartments (Henriquez-Hernandez et al., 2017; Moreno-Gonzalez and Leon, 2017). In Italy, chlorpyrifos is largely employed on vineyards and despite the low persistence in the environment occasional contamination of surface water can be related to point-source pollution (Carter and Capri, 2004; Capri et al., 2005). In addition to these findings, starting in 2007, a particularly interesting massive use of chlorpyrifos was made as part of the integrated pest management (IPM) strategy for *R. ferrugineus* control in the Marche region (Central-Eastern Italy) (Nardi et al., 2011).

Several recent reports have provided evidences that marine microplastics can work as contaminants vectors and that their leachates of chemical pollutants exert possible adverse effects on health (Franzellitti et al., 2019). Although these studies have investigated the activation of both aryl hydrocarbon-receptor (AhR)- and estrogen receptor (ER)-signal transduction pathways, little research has been carried out to investigate the role of MP-associated micropollutants in altering metabolic functions. In this regard, recent evidence proves that environmental pollutants can affect lipid homeostasis promoting obesogenic effects (Cocci et al., 2015, 2017, 2019; Palermo et al., 2016). The present study thus aimed to investigate the potential adipogenic properties of MP extracts by using 3T3-L1 adipocytes, a long-established *in vitro* model to assess adipocyte differentiation. Indeed, our results revealed that the pollutants extracted from microplastics recovered in different sites of the Central Adriatic Sea are able to trigger obesogenic effects *in vitro*. Comparatively, it is not possible to define the contribution of each toxicant to the observed effect, because not all components present in the extract may induce the effect chosen for analysis. We can, however, suggest a modulatory influence of pollutants on the effects of other chemicals (found in the extract) that cannot be predicted by adopting the concept of additivity (Kortenkamp, 2007). Our findings are in line with previous observations reporting obesogenic effects of persistent organic pollutants including PCBs, PAHs and OC pesticides (Lee et al., 2012; Rundle et al., 2012; Ferrante et al., 2014). *In vitro* data have demonstrated the obesogenic nature of some PCBs which are likely to modulate adipogenesis via AhR-mediated mechanisms (Arsenescu et al., 2008). Interestingly, two of the PCBs found in our plastic extracts, PCB101 and 138, were able to promote adipogenesis in 3T3-L1 cells (Ferrante et al., 2014; Kim et al., 2017). In particular, these studies suggest that the obesogenicity of PCBs seems to be congener specific.

It has also been reported that prenatal exposure to PAH mixture can be associated to obesity (Rundle et al., 2012). This finding was further confirmed following postnatal exposure to benzo(a)pyrene that was found to induce similar increases in fat mass (Irigaray et al., 2006). Also OC pesticides have been suggested as a possible causative agents of obesity due their role in modulating adipogenesis and lipid metabolism (Lee et al., 2012; Rosenbaum et al., 2017). Previous *in vitro* data found that both p,p′-DDT and DDE significantly enhanced differentiation of 3T3-L1 preadipocytes (Moreno-Aliaga and Matsumura, 2002; Mangum et al., 2015). For β-HCH, one of the most common OCs2 found in our plastic extracts, epidemiological data indicate the presence of a positive correlation between its serum levels and BMI (Jakszyn et al., 2009; Dirinck et al., 2011).

It is clear from the previous findings and the results presented here that the metabolic effects induced by MP-associated contaminants are due to altered expression of key lipogenic transcriptional factors such as the PPARγ. Indeed, the signaling cascades that provoke adipogenesis and lipid accumulation in adipocytes is mediated by the induction of PPARγ (Tontonoz and Spiegelman, 2008). Most of the chemicals found in the present work have demonstrated the ability to interact with nuclear receptors acting as agonist of the different PPAR isoforms in both *in vitro* and *in vivo* models. Previous data from our lab found that exposure to environmentally relevant doses of several plasticizers induce PPARγ-mediated lipid accumulation in 3T3-L1 adipocytes (Pomatto et al., 2018). Besides PPARγ, the other PPARs play also a role in tissue fatty acid metabolism. For example, Cocci et al. (2017) observed an upregulation of PPARα in fish hepatocytes exposed to seawater organic extracts from PAHs and PCBs contaminated areas of Adriatic Sea. Adeogun et al. (2016) found similar effects demonstrating a correlation between the chemical levels of PAHs and PCBs detected in Tilapia ssp sampled from African polluted rivers and the expression levels of PPARs genes. Therefore, PPARγ seems to be the principal driver of environmental pollutant-induced adipogenic effects and epigenetic mechanisms are most likely to be responsible for this action.

Although the present work doesn't investigate the potential transfer of MP-associated contaminants to marine organisms, our results provide further indication of the risk related to litter pollution. Ecotoxicological effects of microplastics have been demonstrated by Avio et al. (2015) showing bioaccumulation of PAHs in mussels exposed to pyrene-coated plastic. Similarly, ingestion of PVC with sorbed tricolosan was found to affect feeding behavior or cause mortality in lungworms (Browne et al., 2013). In fish, Rochman et al. (2013, 2014b) showed that long term exposure to plastics coated with a complex mixture of POPs and metals,

caused liver toxicity, glycogen depletion, lipidosis, cellular death, tumor promotion, abnormal growth of germ cells in gonads. Overall these findings highlight the importance of combined chemical and physical impacts of microplastics to marine ecosystem.

5. Conclusions

In conclusion, this paper reports new preliminary monitoring data, obtained by a standardized sampling protocol, on the quantification of floating microplastics along the coastline in the southern Marche (middle Adriatic). We found a higher abundance of items in the offshore waters (3–10 km to the coast) and a general prevalence of fragments as shape category. Land-based sources and riverine inputs are most likely to influence the presence of microplastics, whose distribution depends on the complexity of the study area circulation patterns. There is overall consistency between our findings and those already published for the Adriatic basin. Chemical analysis showed that microplastics, mainly from inshore coastal surface waters, possessed relevant hydrophobic organic contaminants concentrations, including PAHs and pesticides. These findings clearly support the greater sorption ability of marine microplastics. Moreover, *in vitro* 3T3-L1 screening of MP extracts indicated potential metabolic effects resulting in both adipogenesis and lipid uptake/storage. Although our results cannot represent a long-term weather exposure scenario, it is clear from this study and other works that special attention should be paid to the ecotoxicological impact of microplastics, including potential obesogenic effects. It is now evident that combined chemical and physical effects of microplastics may pose health risks to marine organisms, especially when considering long term exposure in low-flow ecosystems. However, further investigations are needed to elucidate ecotoxicological models in order to ensure a suitable and detailed risk assessment.

Author statement

Martina Capriotti: Investigation, Resources, Writing- Original draft; Paolo Cocci: Methodology, Investigation, Writing- Original draft; Luca Bracchetti: Investigation; Erika Cottone: Methodology, Writing- Original draft; Rosaria Scandiffio: Investigation, Data curation; Giovanni Caprioli: Investigation, Methodology; Gianni Sagratini: Investigation, Methodology; Gilberto Mosconi: Data curation; Patrizia Bovolin: Formal analysis, Writing- Original draft; Francesco Alessandro Palermo: Conceptualization, Data curation, Supervision, Writing - original draft, Writing- Reviewing and Editing.

Declaration of competing interest

The authors declare that they have no known competing financial interests or personal relationships that could have appeared to influence the work reported in this paper. On behalf of all authors, the corresponding author states that there is no conflict of interest.

Acknowledgement

This work was partially supported by the grant n°EC-172R-18 from the National Geographic Society and by Sky Ocean Rescue.

References

Adeogun, A.O., Ibor, O.R., Regoli, F., Arukwe, A., 2016. Peroxisome proliferator-activated receptors and biotransformation responses in relation to condition factor and contaminant burden in tilapia species from Ogun River, Nigeria. Comparative biochemistry and physiology. Toxicology & pharmacology : CB (Curr. Biol.) 183–184, 7–19.

Alimba, C.G., Faggio, C., 2019. Microplastics in the marine environment: current trends in environmental pollution and mechanisms of toxicological profile. Environ. Toxicol. Pharmacol. 68, 61–74.

Arsenescu, V., Arsenescu, R.I., King, V., Swanson, H., Cassis, L.A., 2008. Polychlorinated biphenyl-77 induces adipocyte differentiation and proinflammatory adipokines and promotes obesity and atherosclerosis. Environ. Health Perspect. 116, 761–768.

ATSDR, 2002. Agency for toxic substances and disease registry. Toxicological Profile for DDT, DDE, and DDD. U.S. Department of Health and Human Services, Public Health Service, Atlanta, GA.

Avio, C.G., Gorbi, S., Milan, M., Benedetti, M., Fattorini, D., d'Errico, G., Pauletto, M., Bargelloni, L., Regoli, F., 2015. Pollutants bioavailability and toxicological risk from microplastics to marine mussels. Environ. Pollut. 198, 211–222.

Baini, M., Fossi, M.C., Galli, M., Caliani, I., Campani, T., Finoia, M.G., Panti, C., 2018. Abundance and characterization of microplastics in the coastal waters of Tuscany (Italy): the application of the MSFD monitoring protocol in the Mediterranean Sea. Mar. Pollut. Bull. 133, 543–552.

Bajt, O., Ramsak, A., Milun, V., Andral, B., Romanelli, G., Scarpato, A., Mitric, M., Kupusovic, T., Kljajic, Z., Angelidis, M., ullaj, A., Galgani, F., 2019. Assessing chemical contamination in the coastal waters of the Adriatic Sea using active mussel biomonitoring with *Mytilus galloprovincialis*. Mar. Pollut. Bull. 141, 283–298.

Bakir, A., Rowland, S.J., Thompson, R.C., 2014. Transport of persistent organic pollutants by microplastics in estuarine conditions. Estuar. Coast Shelf Sci. 140, 14–21.

Barnes, D.K., Galgani, F., Thompson, R.C., Barlaz, M., 2009. Accumulation and fragmentation of plastic debris in global environments. Philos. Trans. R. Soc. Lond. Ser. B Biol. Sci. 364, 1985–1998.

Batel, A., Linti, F., Scherer, M., Erdinger, L., Braunbeck, T., 2016. Transfer of benzo[a]pyrene from microplastics to *Artemia* nauplii and further to zebrafish via a trophic food web experiment: CYP1A induction and visual tracking of persistent organic pollutants. Environ. Toxicol. Chem. 35, 1656–1666.

Besley, A., Vijver, M.G., Behrens, P., Bosker, T., 2017. A standardized method for sampling and extraction methods for quantifying microplastics in beach sand. Mar. Pollut. Bull. 114, 77–83.

Breivik, K., Alcock, R., Li, Y.F., Bailey, R.E., Fiedler, H., Pacyna, J.M., 2004. Primary sources of selected POPs: regional and global scale emission inventories. Environ. Pollut. 128, 3–16.

Browne, M.A., Crump, P., Niven, S.J., Teuten, E., Tonkin, A., Galloway, T., Thompson, R., 2011. Accumulation of microplastic on shorelines woldwide: sources and sinks. Environ. Sci. Technol. 45, 9175–9179.

Browne, M.A., Niven, S.J., Galloway, T.S., Rowland, S.J., Thompson, R.C., 2013. Microplastic moves pollutants and additives to worms, reducing functions linked to health and biodiversity. Curr. Biol. : CB 23, 2388–2392.

Camacho, M., Herrera, A., Gomez, M., Acosta-Dacal, A., Martinez, I., Henriquez-Hernandez, L.A., Luzardo, O.P., 2019. Organic pollutants in marine plastic debris from Canary Islands beaches. Sci. Total Environ. 662, 22–31.

Capri, E., Balderacchi, M., Yon, D., Reeves, G., 2005. Deposition and dissipation of chlorpyrifos in surface water following vineyard applications in northern Italy. Environ. Toxicol. Chem. 24, 852–860.

Carter, A., Capri, E., 2004. Exposure and effect of chlorphyrifos following use under southern European conditions. Pestic. Outlook 15, 24–28.

Chen, Q., Zhang, H., Allgeier, A., Zhou, Q., Ouellet, J.D., Crawford, S.E., Luo, Y., Yang, Y., Shi, H., Hollert, H., 2019. Marine microplastics bound dioxin-like chemicals: model explanation and risk assessment. J. Hazard Mater. 364, 82–90.

Cocci, P., Capriotti, M., Mosconi, G., Campanelli, A., Frapiccini, E., Marini, M., Caprioli, G., Sagratini, G., Aretusi, G., Palermo, F.A., 2017. Alterations of gene expression indicating effects on estrogen signaling and lipid homeostasis in seabream hepatocytes exposed to extracts of seawater sampled from a coastal area of the central Adriatic Sea (Italy). Mar. Environ. Res. 123, 25–37.

Cocci, P., Mosconi, G., Arukwe, A., Mozzicafreddo, M., Angeletti, M., Aretusi, G., Palermo, F.A., 2015. Effects of diisodecyl phthalate on PPAR:RXR-Dependent gene expression pathways in sea bream hepatocytes. Chem. Res. Toxicol. 28, 935–947.

Cocci, P., Mosconi, G., Bracchetti, L., Nalocca, J.M., Frapiccini, E., Marini, M., Caprioli, G., Sagratini, G., Palermo, F.A., 2018. Investigating the potential impact of polycyclic aromatic hydrocarbons (PAHs) and polychlorinated biphenyls (PCBs) on gene biomarker expression and global DNA methylation in loggerhead sea turtles (*Caretta caretta*) from the Adriatic Sea. Sci. Total Environ. 619–620, 49–57.

Cocci, P., Mosconi, G., Palermo, F.A., 2019. Changes in expression of microRNA potentially targeting key regulators of lipid metabolism in primary gilthead sea bream hepatocytes exposed to phthalates or flame retardants. Aquat. Toxicol. 209, 81–90.

Cole, M., Galloway, T.S., 2015. Ingestion of nanoplastics and microplastics by pacific oyster larvae. Environ. Sci. Technol. 49, 14625–14632.

De Lucia, G., Vianello, A., Camedda, A., Vani, D., Tomassetti, P., Coppa, S., Palazzo, L., Amici, M., Romanelli, G., Zampetti, G., Cicero, A., Carpentieri, S., Di Vito, S., Matiddi, M., 2018. sea water contamination in the vicinity of the Italian minor islands caused by microplastic pollution. Water 10, 1108.

de Lucia, G.A., Caliani, I., Marra, S., Camedda, A., Coppa, S., Alcaro, L., Campani, T., Giannetti, M., Coppola, D., Cicero, A.M., Panti, C., Baini, M., Guerranti, C., Marsili, L., Massaro, G., Fossi, M.C., Matiddi, M., 2014. Amount and distribution

of neustonic micro-plastic off the western Sardinian coast (Central-Western Mediterranean Sea). Mar. Environ. Res. 100, 10–16.
Dirinck, E., Jorens, P.G., Covaci, A., Geens, T., Roosens, L., Neels, H., Mertens, I., Van Gaal, L., 2011. Obesity and persistent organic pollutants: possible obesogenic effect of organochlorine pesticides and polychlorinated biphenyls. Obesity 19, 709–714.
Endo, S., Takizawa, R., Okuda, K., Takada, H., Chiba, K., Kanehiro, H., Ogi, H., Yamashita, R., Date, T., 2005. Concentration of polychlorinated biphenyls (PCBs) in beached resin pellets: variability among individual particles and regional differences. Mar. Pollut. Bull. 50, 1103–1114.
Engler, R.E., 2012. The complex interaction between marine debris and toxic chemicals in the ocean. Environ. Sci. Technol. 46, 12302–12315.
Ferrante, M.C., Amero, P., Santoro, A., Monnolo, A., Simeoli, R., Di Guida, F., Mattace Raso, G., Meli, R., 2014. Polychlorinated biphenyls (PCB 101, PCB 153 and PCB 180) alter leptin signaling and lipid metabolism in differentiated 3T3-L1 adipocytes. Toxicol. Appl. Pharmacol. 279, 401–408.
Fossi, M.C., Coppola, D., Baini, M., Giannetti, M., Guerranti, C., Marsili, L., Panti, C., de Sabata, E., Clo, S., 2014. Large filter feeding marine organisms as indicators of microplastic in the pelagic environment: the case studies of the Mediterranean basking shark (*Cetorhinus maximus*) and fin whale (*Balaenoptera physalus*). Mar. Environ. Res. 100, 17–24.
Fossi, M.C., Panti, C., Guerranti, C., Coppola, D., Giannetti, M., Marsili, L., Minutoli, R., 2012. Are baleen whales exposed to the threat of microplastics? A case study of the Mediterranean fin whale (*Balaenoptera physalus*). Mar. Pollut. Bull. 64, 2374–2379.
Franzellitti, S., Canesi, L., Auguste, M., Wathsala, R., Fabbri, E., 2019. Microplastic exposure and effects in aquatic organisms: a physiological perspective. Environ. Toxicol. Pharmacol. 68, 37–51.
Frapiccini, E., Annibaldi, A., Betti, M., Polidori, P., Truzzi, C., Marini, M., 2018. Polycyclic aromatic hydrocarbon (PAH) accumulation in different common sole (*Solea solea*) tissues from the North Adriatic Sea peculiar impacted area. Mar. Pollut. Bull. 137, 61–68.
Gall, S.C., Thompson, R.C., 2015. The impact of debris on marine life. Mar. Pollut. Bull. 92, 170–179.
Gomiero, A., Strafella, P., Fabi, G., 2018. From macroplastic to microplastic litter: occurrence, composition, source identification and interaction with aquatic organisms. Experiences from the Adriatic Sea. Plastics in the Environment. Alessio Gomiero, IntechOpen. https://doi.org/10.5772/intechopen.81534.
Grün, F., Blumberg, B., 2009. Endocrine disrupters as obesogens. Mol. Cell. Endocrinol. 304 (1–2), 19–29.
Henriquez-Hernandez, L.A., Carreton, E., Camacho, M., Montoya-Alonso, J.A., Boada, L.D., Valeron, P.F., Falcon-Cordon, Y., Falcon-Cordon, S., Almeida-Gonzalez, M., Zumbado, M., Luzardo, O.P., 2017. The heartworm (*Dirofilaria immitis*) seems to be able to metabolize organochlorine pesticides and polychlorinated biphenyls: a case-control study in dogs. Sci. Total Environ. 575, 1445–1452.
Hirai, H., Takada, H., Ogata, Y., Yamashita, R., Mizukawa, K., Saha, M., Kwan, C., Moore, C., Gray, H., Laursen, D., Zettler, E.R., Farrington, J.W., Reddy, C.M., Peacock, E.E., Ward, M.W., 2011. Organic micropollutants in marine plastics debris from the open ocean and remote and urban beaches. Mar. Pollut. Bull. 62, 1683–1692.
Hitch, R.K., Day, H.R., 1992. Unusual persistence of DDT in some Western USA soils. Bull. Environ. Contam. Toxicol. 48, 259–264.
Imhof, H.K., Sigl, R., Brauer, E., Feyl, S., Giesemann, P., Klink, S., Leupolz, K., Loder, M.G., Loschel, L.A., Missun, J., Muszynski, S., Ramsperger, A.F., Schrank, I., Speck, S., Steibl, S., Trotter, B., Winter, I., Laforsch, C., 2017. Spatial and temporal variation of macro-, meso- and microplastic abundance on a remote coral island of the Maldives, Indian Ocean. Mar. Pollut. Bull. 116, 340–347.
Irigaray, P., Ogier, V., Jacquenet, S., Notet, V., Sibille, P., Mejean, L., Bihain, B.E., Yen, F.T., 2006. Benzo[a]pyrene impairs beta-adrenergic stimulation of adipose tissue lipolysis and causes weight gain in mice. A novel molecular mechanism of toxicity for a common food pollutant. FEBS J. 273, 1362–1372.
Isobe, A., Kubo, K., Tamura, Y., Kako, S., Nakashima, E., Fujii, N., 2014. Selective transport of microplastics and mesoplastics by drifting in coastal waters. Mar. Pollut. Bull. 89, 324–330.
Jakszyn, P., Goni, F., Etxeandia, A., Vives, A., Millan, E., Lopez, R., Amiano, P., Ardanaz, E., Barricarte, A., Chirlaque, M.D., Dorronsoro, M., Larranaga, N., Martinez, C., Navarro, C., Rodriguez, L., Sanchez, M.J., Tormo, M.J., Gonzalez, C.A., Agudo, A., 2009. Serum levels of organochlorine pesticides in healthy adults from five regions of Spain. Chemosphere 76, 1518–1524.
Karkanorachaki, K., Kiparissis, S., Kalogerakis, G.C., Yiantzi, E., Psillakis, E., Kalogerakis, N., 2018. Plastic pellets, meso- and microplastics on the coastline of Northern Crete: distribution and organic pollution. Mar. Pollut. Bull. 133, 578–589.
Kim, H.Y., Kwon, W.Y., Kim, Y.A., Oh, Y.J., Yoo, S.H., Lee, M.H., Bae, J.Y., Kim, J.M., Yoo, Y.H., 2017. Polychlorinated biphenyls exposure-induced insulin resistance is mediated by lipid droplet enlargement through Fsp27. Arch. Toxicol. 91, 2353–2363.
Kljakovic-Gaspic, Z., Herceg-Romanic, S., Kozul, D., Veza, J., 2010. Biomonitoring of organochlorine compounds and trace metals along the Eastern Adriatic coast (Croatia) using Mytilus galloprovincialis. Mar. Pollut. Bull. 60, 1879–1889.
Kortenkamp, A., 2007. Ten years of mixing cocktails: a review of combination effects of endocrine-disrupting chemicals. Environ. Health Perspect. 115 (Suppl. 1), 98–105.
Lee, D.H., Lind, L., Jacobs Jr., D.R., Salihovic, S., van Bavel, B., Lind, P.M., 2012. Associations of persistent organic pollutants with abdominal obesity in the elderly: the Prospective Investigation of the Vasculature in Uppsala Seniors (PIVUS) study. Environ. Int. 40, 170–178.
Leggett, D.C., Parker, L.V., 1994. Modeling the equilibrium partitioning of organic contaminants between PTFE, PVC, and groundwater. Environ. Sci. Technol. 28, 1229–1233.
Liu, L., Fokkink, R., Koelmans, A.A., 2016. Sorption of polycyclic aromatic hydrocarbons to polystyrene nanoplastic. Environ. Toxicol. Chem. 35, 1650–1655.
Lusher, A.L., Hollman, P.C.H., Mendoza-Hill, J.J., 2017a. Microplastics in Fisheries and Aquaculture: Status of Knowledge on Their Occurrence and Implications for Aquatic Organisms and Food Safety. FAO Fisheries and Aquaculture Technical Paper. No. 615. Rome, Italy.
Lusher, A.L., Welden, N.A., Sobral, P., Cole, M., 2017b. Sampling, isolating and identifying microplastics ingested by fish and invertebrates. Analytical Methods 9 (9), 1346–1360.
Mai, L., Bao, L.J., Shi, L., Liu, L.Y., Zeng, E.Y., 2018. Polycyclic aromatic hydrocarbons affiliated with microplastics in surface waters of Bohai and Huanghai Seas, China. Environ. Pollut. 241, 834–840.
Mangum, L.H., Howell 3rd, G.E., Chambers, J.E., 2015. Exposure to p,p'-DDE enhances differentiation of 3T3-L1 preadipocytes in a model of sub-optimal differentiation. Toxicol. Lett. 238, 65–71.
Mato, Y., Isobe, T., Takada, H., Kanehiro, H., Ohtake, C., Kaminuma, T., 2001. Plastic resin pellets as a transport medium for toxic chemicals in the marine environment. Environ. Sci. Technol. 35, 318–324.
Mazurais, D., Ernande, B., Quazuguel, P., Severe, A., Huelvan, C., Madec, L., Mouchel, O., Soudant, P., Robbens, J., Huvet, A., Zambonino-Infante, J., 2015. Evaluation of the impact of polyethylene microbeads ingestion in European sea bass (*Dicentrarchus labrax*) larvae. Mar. Environ. Res. 112, 78–85.
Mezzelani, M., Avio, C.G., Nardi, A., Regoli, F., 2018. Microplastic investigation in water and trophic chain along the Italian coast 06/24/2017-07/15/2017.
Minambiente, 2018. Programmi di Monitoraggio per la Strategia Marina (Art. 11, D.lgs. 190/2010). Schede metodologiche per l'attuazione delle Convenzioni stipulate tra Ministero dell'Ambiente e della Tutela del Territorio e del Mare e Agenzie Regionali per la protezione dell'Ambiente nel dicembre 2017. Modulo 2: Analisi delle microplastiche, macroplastiche e altri rifiuti flottanti.
Moreno-Aliaga, M.J., Matsumura, F., 2002. Effects of 1,1,1-trichloro-2,2-bis(p-chlorophenyl)-ethane (p,p'-DDT) on 3T3-L1 and 3T3-F442A adipocyte differentiation. Biochem. Pharmacol. 63, 997–1007.
Moreno-Gonzalez, R., Leon, V.M., 2017. Presence and distribution of current-use pesticides in surface marine sediments from a Mediterranean coastal lagoon (SE Spain). Environ. Sci. Pollut. Res. Int. 24, 8033–8048.
MSFD, 2013. Technical subgroup on marine litter. Guidance on Monitoring of Marine Litter in European Seas. Joint Research Centre of the European Commission. Scientific and Policy Reports Report EUR 26113 EN.
Munari, C., Scoponi, M., Mistri, M., 2017. Plastic debris in the Mediterranean Sea: types, occurrence and distribution along adriatic shorelines. Waste Manag. 67, 385–391.
Nardi, S., Ricci, E., Lozzi, R., Marozzi, F., Ladurner, E., Chiabrando, F., Granchelli, L., Verdolini, E., Isidoro, N., Riolo, P., 2011. Control of *Rhynchophorus ferrugineus* (olivier, 1790) according to EU decision 2007/ 365/EC in the Marche region (Central-Eastern Italy). Bulletin OEPP/EPPO Bulletin 41, 103–115.
Ogata, Y., Takada, H., Mizukawa, K., Hirai, H., Iwasa, S., Endo, S., Mato, Y., Saha, M., Okuda, K., Nakashima, A., Murakami, M., Zurcher, N., Booyatumanondo, R., Zakaria, M.P., Dung le, Q., Gordon, M., Miguez, C., Suzuki, S., Moore, C., Karapanagioti, H.K., Weerts, S., McClurg, T., Burres, E., Smith, W., Van Velkenburg, M., Lang, J.S., Lang, R.C., Laursen, D., Danner, B., Stewardson, N., Thompson, R.C., 2009. International Pellet Watch: global monitoring of persistent organic pollutants (POPs) in coastal waters. 1. Initial phase data on PCBs, DDTs, and HCHs. Mar. Pollut. Bull. 58, 1437–1446.
Palermo, F.A., Cocci, P., Mozzicafreddo, M., Arukwe, A., Angeletti, M., Aretusi, G., Mosconi, G., 2016. Tri-m-cresyl phosphate and PPAR/LXR interactions in seabream hepatocytes: revealed by computational modeling (docking) and transcriptional regulation of signaling pathways. Toxicology research 5, 471–481.
Pedrotti, M.L., Petit, S., Elineau, A., Bruzaud, S., Crebassa, J.C., Dumontet, B., Marti, E., Gorsky, G., Cozar, A., 2016. Changes in the floating plastic pollution of the Mediterranean Sea in relation to the distance to Land. PloS One 11, e0161581.
Pellini, G., Gomiero, A., Fortibuoni, T., Ferra, C., Grati, F., Tassetti, A.N., Polidori, P., Fabi, G., Scarcella, G., 2018. Characterization of microplastic litter in the gastrointestinal tract of *Solea solea* from the Adriatic Sea. Environ. Pollut. 234, 943–952.
Pomatto, V., Cottone, E., Cocci, P., Mozzicafreddo, M., Mosconi, G., Nelson, E.R., Palermo, F.A., Bovolin, P., 2018. Plasticizers used in food-contact materials affect adipogenesis in 3T3-L1 cells. J. Steroid Biochem. Mol. Biol. 178, 322–332.
Rios, L.M., Jones, P.R., Moore, C., Narayan, U.V., 2010. Quantitation of persistent organic pollutants adsorbed on plastic debris from the Northern Pacific Gyre's "eastern garbage patch. J. Environ. Monit. : JEM 12, 2226–2236.
Rochman, C.M., Hentschel, B.T., Teh, S.J., 2014a. Long-term sorption of metals is similar among plastic types: implications for plastic debris in aquatic environments. PloS One 9, e85433.
Rochman, C.M., Hoh, E., Kurobe, T., Teh, S.J., 2013. Ingested plastic transfers hazardous chemicals to fish and induces hepatic stress. Sci. Rep. 3, 3263.
Rochman, C.M., Kurobe, T., Flores, I., Teh, S.J., 2014b. Early warning signs of endocrine disruption in adult fish from the ingestion of polyethylene with and without sorbed chemical pollutants from the marine environment. Sci. Total Environ. 493, 656–661.

Rosenbaum, P.F., Weinstock, R.S., Silverstone, A.E., Sjodin, A., Pavuk, M., 2017. Metabolic syndrome is associated with exposure to organochlorine pesticides in Anniston, AL, United States. Environ. Int. 108, 11–21.

Rundle, A., Hoepner, L., Hassoun, A., Oberfield, S., Freyer, G., Holmes, D., Reyes, M., Quinn, J., Camann, D., Perera, F., Whyatt, R., 2012. Association of childhood obesity with maternal exposure to ambient air polycyclic aromatic hydrocarbons during pregnancy. Am. J. Epidemiol. 175, 1163–1172.

Shim, W.J., Hong, S.H., Eo, S., 2018. Marine microplastics: abundance, distribution, and composition.. In: Microplastic contamination in aquatic environments. An Emerging Matter of Environmental Urgency, pp. 1–26. https://doi.org/10.1016/B978-0-12-813747-5.00001-1.

Suaria, G., Avio, C.G., Mineo, A., Lattin, G.L., Magaldi, M.G., Belmonte, G., Moore, C.J., Regoli, F., Aliani, S., 2016. The Mediterranean Plastic Soup: synthetic polymers in Mediterranean surface waters. Sci. Rep. 6, 37551.

Suaria, G., Avio, C.G., Regoli, F., Aliani, S., 2018. Sub-basin scale heterogeneity in the polymeric composition of floating microplastics in the Mediterranean Sea. Proceedings of the International Conference on Microplastic Pollution in the Mediterranean Sea, pp. 1–7.

Tang, Y., Rong, J., Guan, X., Zha, S., Shi, W., Han, Y., Du, X., Wu, F., Huang, W., Liu, G., 2020. Immunotoxicity of microplastics and two persistent organic pollutants alone or in combination to a bivalve species. Environ. Pollut. 258, 113845.

Teuten, E.L., Rowland, S.J., Galloway, T.S., Thompson, R.C., 2007. Potential for plastics to transport hydrophobic contaminants. Environ. Sci. Technol. 41, 7759–7764.

Teuten, E.L., Saquing, J.M., Knappe, D.R., Barlaz, M.A., Jonsson, S., Bjorn, A., Rowland, S.J., Thompson, R.C., Galloway, T.S., Yamashita, R., Ochi, D., Watanuki, Y., Moore, C., Viet, P.H., Tana, T.S., Prudente, M., Boonyatumanond, R., Zakaria, M.P., Akkhavong, K., Ogata, Y., Hirai, H., Iwasa, S., Mizukawa, K., Hagino, Y., Imamura, A., Saha, M., Takada, H., 2009. Transport and release of chemicals from plastics to the environment and to wildlife. Philos. Trans. R. Soc. Lond. Ser. B Biol. Sci. 364, 2027–2045.

Tontonoz, P., Spiegelman, B.M., 2008. Fat and beyond: the diverse biology of PPARgamma. Annu. Rev. Biochem. 77, 289–312.

UNEP, 2016. Marine Plastic Debris and Microplastics - Global Lessons and Research to Inspire Action and Guide Policy Change. United Nations Environment Programme, Nairobi.

Wang, Y., Wang, T., Li, A., Fu, J., Wang, P., Zhang, Q., Jiang, G., 2008. Selection of bioindicators of polybrominated diphenyl ethers, polychlorinated biphenyls, and organochlorine pesticides in mollusks in the Chinese Bohai Sea. Environ. Sci. Technol. 42, 7159–7165.

Zeri, C., Adamopoulou, A., Bojanic Varezic, D., Fortibuoni, T., Kovac Virsek, M., Krzan, A., Mandic, M., Mazziotti, C., Palatinus, A., Peterlin, M., Prvan, M., Ronchi, F., Siljic, J., Tutman, P., Vlachogianni, T., 2018. Floating plastics in Adriatic waters (Mediterranean Sea): from the macro- to the micro-scale. Mar. Pollut. Bull. 136, 341–350.

Zhang, W., Ma, X., Zhang, Z., Wang, Y., Wang, J., Wang, J., Ma, D., 2015. Persistent organic pollutants carried on plastic resin pellets from two beaches in China. Mar. Pollut. Bull. 99, 28–34.

Toxicology 461 (2021) 152900

Contents lists available at ScienceDirect

Toxicology

journal homepage: www.elsevier.com/locate/toxicol

Reproducibility of adipogenic responses to metabolism disrupting chemicals in the 3T3-L1 pre-adipocyte model system: An interlaboratory study

Christopher D. Kassotis [a,b,*], Kate Hoffman [b], Johannes Völker [c], Yong Pu [d], Almudena Veiga-Lopez [d], Stephanie M. Kim [e], Jennifer J. Schlezinger [e], Patrizia Bovolin [f], Erika Cottone [f], Astrid Saraceni [f], Rosaria Scandiffio [f], Ella Atlas [g], Karen Leingartner [g], Stacey Krager [h], Shelley A. Tischkau [h], Sibylle Ermler [i], Juliette Legler [i,j], Vesna A. Chappell [k], Suzanne E. Fenton [k], Fahmi Mesmar [l], Maria Bondesson [l], Mariana F. Fernández [m], Heather M. Stapleton [b]

[a] Institute of Environmental Health Sciences and Department of Pharmacology, Wayne State University, Detroit, MI, 48236, USA
[b] Nicholas School of the Environment, Duke University, Durham, NC, 27708, USA
[c] Department of Biology, Norwegian University of Science and Technology (NTNU), Trondheim, 7491, Norway
[d] Department of Pathology, University of Illinois at Chicago, Chicago, IL, 60612, USA
[e] School of Public Health, Boston University, Boston, MA, 02118, USA
[f] Department of Life Sciences and Systems Biology, University of Torino, 10123, Torino, Italy
[g] Environmental Health Science and Research Bureau, Health Canada, 251 Sir Frederick Banting Drive, Ottawa, Canada
[h] Department of Pharmacology, Southern Illinois University School of Medicine, Springfield, IL, USA
[i] Department of Life Sciences, College of Health and Life Sciences, Brunel University London, Uxbridge, UB8 3PH, UK
[j] Institute for Risk Assessment Sciences, Department of Population Health Sciences, Faculty of Veterinary Medicine, Utrecht University, 3508 TD, Utrecht, Netherlands
[k] National Toxicology Program Laboratory, Division of the National Toxicology Program, National Institutes of Environmental Health Sciences, National Institutes of Health, Research Triangle Park, NC, USA
[l] Department of Intelligent Systems Engineering, Indiana University, Bloomington, IN, 47408, USA
[m] University of Granada, Center for Biomedical Research (CIBM), Granada, Spain

ARTICLE INFO

Handling Editor: Matthew Wright

Keywords:
Endocrine disrupting chemicals
Adipogenesis
Obesogen
Triglyceride accumulation
Metabolic disruption
Reproducibility
3T3-L1

ABSTRACT

The 3T3-L1 murine pre-adipocyte line is an established cell culture model for screening Metabolism Disrupting Chemicals (MDCs). Despite a need to accurately identify MDCs for further evaluation, relatively little research has been performed to comprehensively evaluate reproducibility across laboratories, assess factors that might contribute to varying degrees of differentiation between laboratories (media additives, plastics, cell source, etc.), or to standardize protocols. As such, the goals of this study were to assess interlaboratory variability of efficacy and potency outcomes for triglyceride accumulation and pre-adipocyte proliferation using the mouse 3T3-L1 pre-adipocyte cell assay to test chemicals. Ten laboratories from five different countries participated. Each laboratory evaluated one reference chemical (rosiglitazone) and three blinded test chemicals (tributyltin chloride, pyraclostrobin, and bisphenol A) using: 1) their Laboratory-specific 3T3-L1 Cells (LC) and their Laboratory-specific differentiation Protocol (LP), 2) Shared 3T3-L1 Cells (SC) with LP, 3) LC with a Shared differentiation Protocol (SP), and 4) SC with SP. Blinded test chemical responses were analyzed by the coordinating laboratory. The magnitude and range of bioactivities reported varied considerably across laboratories and test conditions, though the presence or absence of activity for each tested chemical was more consistent. Triglyceride accumulation activity determinations for rosiglitazone ranged from 90 to 100% across test conditions, but 30–70 % for pre-adipocyte proliferation; this was 40–80 % for triglyceride accumulation induced by pyraclostrobin, 80–100 % for tributyltin, and 80–100 % for bisphenol A. Consistency was much lower for pre-adipocyte proliferation, with 30–70 % active determinations for pyraclostrobin, 30–50 % for tributyltin, and 20–40 % for bisphenol A. Greater

* Corresponding author at: Wayne State University, Institute of Environmental Health Sciences and Department of Pharmacology, 2111 Integrative Biosciences Center, 6135 Woodward Avenue, Detroit, MI, 48202, USA.
E-mail address: christopher.kassotis@wayne.edu (C.D. Kassotis).

https://doi.org/10.1016/j.tox.2021.152900
Received 11 June 2021; Received in revised form 2 August 2021; Accepted 13 August 2021
Available online 17 August 2021

consistency was observed for the SC/SP assessment. As such, working to develop a standardized adipogenic differentiation protocol represents the best strategy for improving consistency of adipogenic responses using the 3T3-L1 model to reproducibly identify MDCs and increase confidence in reported outcomes.

1. Introduction

The 3T3-L1 murine pre-adipocyte cell line is an established model for *in vitro* screening of metabolism disrupting chemicals (MDCs) (Heindel et al., 2015, 2017). When exposed to adipogenic stimuli, pre-adipocytes will differentiate into mature adipocytes, undergo morphological changes, accumulate triglycerides, and eventually develop into a rounded white fat cell with a number of large lipid droplets often displacing the nucleus (Green and Meuth, 1974; Green and Kehinde, 1975). Adipocyte differentiation requires eventual activation of the peroxisome proliferator-activated receptor-gamma (PPARγ), often considered the "master regulator" of adipocyte differentiation (Rosen et al., 1999). Molecular pathways upstream that contribute to this activation are diverse and include modulation of thyroid receptor-beta (TRβ), glucocorticoid receptor (GR), estrogen receptor (ER), androgen receptor (AR), liver X receptor (LXR), retinoid X receptor (RXR), and others (Niemelä et al., 2008), including non-receptor mediated mechanisms (Bournat and Brown, 2010; Kassotis and Stapleton, 2019; Luz et al., 2018). These receptor pathways are highly conserved across vertebrate species (Fu et al., 2005; Zhao et al., 2015), suggesting that mechanisms of adipogenesis are highly translatable. Indeed, active MDCs identified using 3T3-L1 cells and other *in vitro* models (increased triglyceride accumulation/differentiation, pre-adipocyte proliferation, etc.) have been routinely shown to be active *in vivo*, such as bisphenol A and tributyltin chloride, among others (Angle et al., 2013; Chamorro-Garcia et al., 2013; Li et al., 2011; Masuno et al., 2005). Compounds that modulate these receptors belong to diverse chemical classes (Fang et al., 2015; Hamers et al., 2006; Orton et al., 2011), and many are frequently detected in indoor environments and in human tissues (Hoffman et al., 2015; Kitamura et al., 2005; Meerts et al., 2000; Shen et al., 2009; Stapleton et al., 2009, 2011; Takeuchi et al., 2005). A number of these chemicals have been associated with adiposity, obesity, type 2 diabetes, and other chronic metabolic health conditions in humans (Gore et al., 2015; Heindel et al., 2015, 2017; Ruiz et al., 2018). As such, there is a critical need to ensure robust and validated models that promote highly reproducible toxicological outcomes across laboratories.

Despite a need to accurately identify MDCs, relatively little research has been performed to comprehensively evaluate reproducibility across laboratories, and comprehensively assess factors that might contribute to varying degrees of differentiation among laboratories. Previous research has described diverse differentiation success and declining performance over time with various cell bank stocks of 3T3-L1 cells (Zebisch et al., 2012). Cell culture vessel size and proprietary tissue culture coatings have also been demonstrated to influence differentiation success of 3T3-L1 cells (Mehra et al., 2007), and various cell line suppliers provide disparate protocols and techniques for eliciting maximal differentiation success (American Type Culture Collection (ATCC) ATTC, 2011; Zenbio Inc, 2015). Other providers suggest an inability to differentiate their 3T3-L1 cell stocks, with timelines of 2–5 weeks and very limited differentiation (European Collection of Authenticated Cell Cultures (ECACC), 2020). Despite these notable gaps, reproducibility studies across toxicological studies are limited, and often conducted only within the establishment of guideline assays such as Organisation for Economic Co-operation and Development (OECD) test guidelines. Chemists, in contrast, have demonstrated robust success in improving methodology and laboratory-specific measurement reliability through participation in interlaboratory reproducibility programs (Boyer et al., 1985; Ikonomou et al., 2012; M.Weiss et al., 2013; Voet et al., 1999; Wong et al., 2010). For example, recent initiatives to improve measurements for novel brominated and organophosphate flame retardants have demonstrated high precision between technical replicates within laboratories but not as strong accuracy for measuring the provided values across laboratories (Melymuk et al., 2015, 2018). Importantly, analytical reproducibility studies benefit from the concrete nature of the outcome: chemicals can be included at specific, known concentrations, making the determination of the "correct" result more straightforward than possible in toxicological studies. A limited number of studies have attempted this with endocrine outcomes such as measurement of nuclear receptor activation (Hettwer et al., 2018; Mehinto et al., 2015; Zava et al., 1982), reporting variable consistency across trials and pathways, with variances often seemingly resulting from non-harmonized protocols.

We previously published an assessment of some disparities in adipogenic cell culture systems under various conditions (Kassotis et al., 2017b). Specifically, both cell line (3T3-L1 vs. OP9) and source (ATCC vs. Zenbio 3T3-L1) had a significant impact on the responses to various chemicals. Ligands for LXR, RXR, GR, and TR promoted disparate responses between cell sources (Kassotis et al., 2017b), in some cases apparently mediated through gene expression differences. We also noted significant differences based on the cell culture plastic utilized, with different 96-well plates contributing to <50 % reduction in maximal fold induction differences and appreciably altering chemical potencies (Kassotis et al., 2017b). Cytotoxicity and proliferative response differences were also observed among plates, in some cases negatively impacting the ability to even detect chemicals acting via pre-adipocyte proliferation (Kassotis et al., 2017b). Significant differences were also noted in both triglyceride accumulation and DNA content among different differentiation induction times (7, 10, 14 days) (Kassotis et al., 2017b), and it is still unclear what differences might stem from the wide degree of heterogeneity in media additives across varying differentiation protocols. For example, while many researchers do not include dexamethasone in the differentiation cocktail (Boucher et al., 2015; Kassotis et al., 2017a, 2018; Kassotis et al., 2019; Sargis et al., 2010), others use a 1000-fold range of concentrations (Li et al., 2011; Masuno et al., 2002; Temkin et al., 2016; Zebisch et al., 2012). Differing protocols and cell culture supplies utilized may contribute to a lack of reproducibility and bias in measuring adipogenic potency and efficacy of chemicals between laboratories. Importantly, while reported previously, these factors have never been assessed in a systematic manner across laboratories.

As such, the objectives of this study were to evaluate the interlaboratory variability in the response of 3T3-L1 cells to the exposures of several chemical compounds. Given previous reports of inconsistencies in responses using this model, we sought to comprehensively evaluate the underlying factors and how they might influence differences in efficacy (magnitude of effects) and/or potency (concentration of effects) for both triglyceride accumulation (marker of differentiation success) and pre-adipocyte proliferation (marker of cell number). To accomplish this, we assessed three blinded test chemicals (bisphenol A, BPA; tributyltin chloride, TBT; pyraclostrobin) between ten laboratories in the United States, Canada, Italy, Norway, and the United Kingdom. These data should provide comprehensive insight into the most important factors that influence the assay's responses and to inform strategies to increase interlaboratory reproducibility.

2. Materials and methods

2.1. Chemicals

Chemicals for use in bioassays were purchased as follows:

rosiglitazone (Sigma cat # R2408, ≥ 98 %), pyraclostrobin (Sigma cat # 33696, 99.9 %), tributyltin chloride (TBT; Aldrich cat # T50202, 96 %), and bisphenol A (BPA; Sigma cat # 239658, >99 %). Stock solutions were prepared in 100 % cell-culture grade DMSO (Sigma cat # D2650) and stored at − 20 °C between uses. Laboratories were recruited via a scientific conference discussion and coordination via a metabolism disruption research listserv. Rosiglitazone (1 mM) was provided as a labeled amber glass vial, and laboratories were instructed to dilute the solution 1000-fold and then perform four 10-fold dilutions (0.1 nM – 1 μM in contact with cells). Pyraclostrobin, TBT, and BPA (10 mM) were provided as blinded chemicals (Chemicals A, B, and C, respectively) in amber glass vials, and laboratories were instructed to perform the same 1000-fold dilution and four 10-fold dilution scheme (1 nM – 10 μM).

2.2. Sample shipments

Packages were shipped to participating laboratories in insulated Styrofoam shipping boxes with between one and five kilograms of dry ice, depending on distance of shipment. All packages were shipped priority overnight, generally resulting in next day domestic delivery; however, international shipments often took as long as ten days to clear customs and be delivered by local couriers. Additional dry ice was added by Fedex as necessary to ensure packages arrived frozen, and this was confirmed by receiving laboratories upon receipt. Given the long length of delivery for certain participating international laboratories, a cryo-shipper was utilized (Chart MVE BL-7) to allow for improved assurance on the frozen cell stock.

2.3. Testing, differentiation, and evaluation protocol

The following materials were provided to each laboratory (Fig. 1). One vial of murine 3T3-L1 cells (Zenbio cat# SP-L1-F, lot# 3T3062104; Research Triangle Park, NC), one vial NucBlue® Live ReadyProbes® Reagent (Thermo cat # R37605), one vial of laboratory prepared Nile Red reagent (40 μg/mL Nile Red in acetone; Sigma 72485−100MG), one sleeve containing six black clear-bottom 96-well tissue culture plates (Greiner cat # 655090; four for assays and two replacements), one vial of DMSO for use as a solvent control, one vial of rosiglitazone for use as a positive control, and three vials containing the blinded test chemicals. A shared differentiation protocol, differentiation data sheet, and test instructions were emailed to each participating laboratory. Differentiation data sheets included spaces to include raw fluorescence values from Nile Red and NucBlue outputs, a plate map to denote placement of all test chemicals and replicates, and spaces to specify differentiation details, media constituents, and other assay details. The shared differentiation protocol was adapted based on a previously published protocol (Zebisch et al., 2012) and has been described in detail previously (Kassotis et al., 2017a, b). A short protocol was provided to detail the desired test conditions. Laboratories were requested to prepare media according to the shared differentiation protocol and according to their own protocols and then test blinded test chemicals under four sets of conditions: 1) using their laboratory-specific differentiation protocol, media, and supplies along with laboratory-specific stock of 3T3-L1 cells (LC/LP), 2) using their laboratory-specific differentiation protocol, media, and supplies along with the provided stock of 3T3-L1 cells (SC/LP), 3) using the provided differential protocol, media prepared according to the shared protocol, and using the included cell culture plates along with laboratory-specific stock of 3T3-L1 cells (LC/SP, and 4) using the provided differential protocol, media prepared according to the shared protocol, and using the included cell culture plates along with the provided stock of 3T3-L1 cells (SC/SP, Fig. 1).

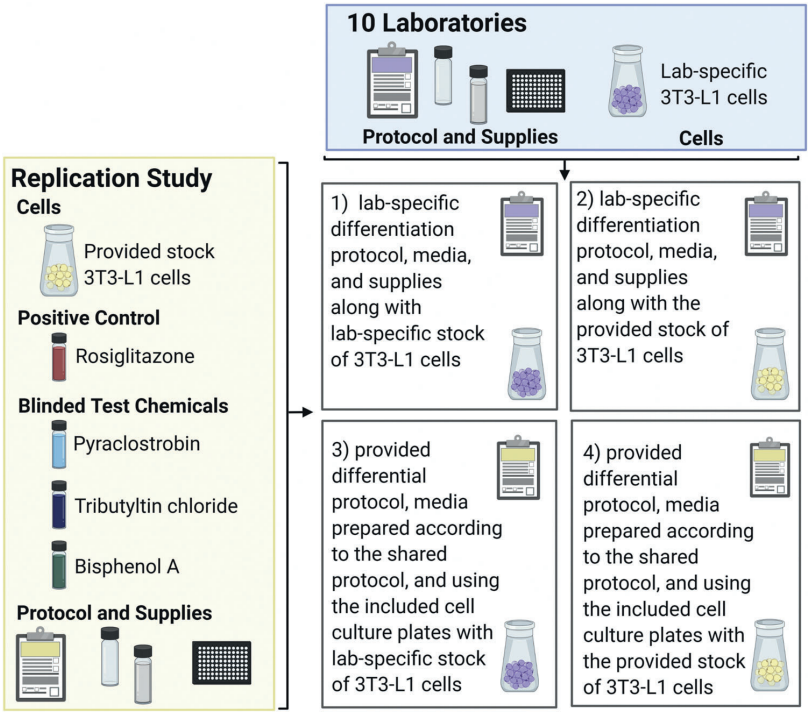

Fig. 1. Study Design and Test Conditions. Schematic of the study design and test conditions. Ten laboratories were recruited from the United States and other countries. The following materials were provided to each laboratory: one vial of 3T3-L1 cells, one vial NucBlue® Live ReadyProbes® Reagent, one vial of laboratory prepared Nile Red reagent, black clear-bottom 96-well tissue culture plates, DMSO, rosiglitazone, and three vials containing the blinded test chemicals. A shared differentiation protocol, differentiation data sheet, and test instructions were emailed to each participating laboratory. A short protocol was provided to detail the desired test conditions. Laboratories were requested to prepare media according to the shared differentiation protocol and according to their own protocols and then test blinded test chemicals under four sets of conditions: 1) using their laboratory-specific differentiation protocol, media, and supplies along with laboratory-specific stock of 3T3-L1 cells, 2) using their laboratory-specific differentiation protocol, media, and supplies along with the provided stock of 3T3-L1 cells, 3) using the provided differential protocol, media prepared according to the shared protocol, and using the included cell culture plates along with laboratory-specific stock of 3T3-L1 cells, and 4) using the provided differential protocol, media prepared according to the shared protocol, and using the included cell culture plates along with the provided stock of 3T3-L1 cells (For interpretation of the references to colour in this figure legend, the reader is referred to the web version of this article).

2.4. 3T3-L1 cell care and differentiation assays

Zenbio 3T3-L1 cells were provided to all laboratories and were used for SC test conditions. Laboratory-specific cell sources of 3T3-L1 cells (LC) varied depending on the laboratory and are detailed within Table 1. The shared protocol called for cells to be maintained in pre-adipocyte media (Dulbecco's Modified Eagle Medium – High Glucose; DMEM-HG; Gibco cat# 11995, supplemented with 10 % bovine calf serum and 1% penicillin and streptomycin; Gibco cat# 15140). These cells were seeded in pre-adipocyte media into 96-well tissue culture plates (Greiner cat # 655090) at approximately 30,000 cells/well and grown to confluency; after confluency, cells were allowed 48 h to undergo growth arrest and initiate clonal expansion. Media was then replaced with controls, and/or blinded test chemicals using a DMSO vehicle (at 0.1 %) in differentiation media (DMEM-HG with 10 % fetal bovine serum, 1% penicillin/streptomycin, 1.0 μg/mL human insulin, and 0.5 mM 3-isobutyl-1-methylxanthine, IBMX). After 48 h of differentiation induction, media was replaced with fresh dilutions of test chemicals in adipocyte maintenance media (differentiation media without IBMX), and this media was refreshed every 2–3 days until assay, ten days after induction. Laboratory-specific protocols varied among laboratories, with variations to this general protocol specified within Table 1. 3T3-L1 cells were utilized between passages 8 (at shipment) and 12 (provided Zenbio cells) or as noted in Table 1 for laboratory-specific cells, and were maintained in a sub-confluent state until differentiation.

2.5. 3T3-L1 triglyceride accumulation, cell proliferation, and cell viability measurements

Fluorescence endpoint measurements were measured using a plate reader for the shared protocol tests and using standard laboratory practice for laboratory-specific protocol tests. For shared protocol experiments, media was removed from plates, and cells were rinsed with Dulbecco's phosphate-buffered saline (DPBS; Gibco cat # 14040) before replacing with 200 μL of a live-cell dye mixture (19 mL DPBS, 1 drop/mL NucBlue® Live ReadyProbes® Reagent (cell proliferation/cytotoxicity measure of DNA content; Thermo cat # R37605) and 500 μL Nile Red (intracellular lipid measure of triglyceride accumulation; 40 μg/mL in acetone; Sigma 72485−100MG) per plate). Plates were protected from light and incubated at room temperature for approximately forty minutes; fluorescence was then measured on plate readers with excitation 485 nm/emission 572 nm (previously demonstrated to be ideal wavelengths for intracellular neutral lipids (Greenspan et al., 1985)) and/or 485/535 (more accessible, generally used) for Nile Red and 360/460 for NucBlue®. Measurement wavelengths varied for laboratory-specific protocols, with most laboratories also providing their data from plate readers using these wavelengths.

All laboratories provided raw data, and as such, normalizations and activity calculations and determinations were made in a uniform manner for all data. For triglyceride accumulation data, percent activities were calculated relative to the maximal rosiglitazone-induced fold induction over intra-assay differentiated vehicle control (0.1 % dimethylsulfoxide, DMSO) responses, after correcting for background fluorescence. Rosiglitazone was utilized as the positive control herein (provided as an unblinded chemical stock to all laboratories) due to selective, robust, and potent activation of PPARγ (Lehmann et al., 1995; Seimandi et al., 2005; Spiegelman, 1998) and in order to provide ease of comparisons across laboratories and experiments. DNA content was calculated as percent change from differentiated vehicle control (0.1 % DMSO) responses for each chemical at each concentration and was then used to normalize total triglyceride values to obtain triglyceride content per unit DNA (proxy for triglyceride accumulation per cell). Four technical (replicates within each assay plate) and two biological replicates (separate cell passages/assays) were requested for every test chemical and concentration herein.

2.6. Statistical analysis

Data for adipogenic activities (triglyceride accumulation and pre-adipocyte proliferation) are presented as means ± standard error of the mean (SEM) from replicates. First, the median of four technical replicates (within plates) was determined and then medians of two or three (depending on laboratory) biological replicates (separate experimental plates) were averaged to provide a final value for each chemical for each laboratory under each test condition. Efficacy values were defined as the percent maximal activity relative to the rosiglitazone-induced maximal response for each laboratory and test condition. Relative potency values (effective concentration, EC_{20}; concentration of each chemical that exhibits 20 % of assay maximal activity, respectively) values were estimated from raw fluorescence data, setting the axis to 20 % of response and estimating the concentration at which the response curve passes this activation value. Values were extrapolated as necessary for efficacy and potency values for samples approaching the cut-off; potency values were not extrapolated when there was no apparent activity (samples not approaching 20 % activity), as potencies cannot be calculated for inactive chemicals/samples. Sensitivity was defined as the lowest concentration that exhibited a significant effect for each chemical above its own solvent control under each set of test conditions for each laboratory. To ease comparisons among laboratories, a uniform limit of quantification was set between laboratories as follows: a biological activation threshold approach was utilized, where the variation in the differentiated solvent (0.1 % DMSO) control was calculated as the average differentiated solvent value plus three times the standard deviation of the differentiated solvent control response. All reproducibility metrics were based on the raw, unadjusted data to assess variance within experimental groups and across laboratories; they were calculated by subtracting the average experimental group response from each individual laboratory response and dividing by the standard deviation. Values further from zero in either direction represent greater variation from the average experimental group response. Responses were analyzed using a one-way ANOVA and Dunnett's post-hoc test. Differences between treatment and control groups were considered statistically significant at $p < 0.05$.

3. Results

Ten participating laboratories were asked to test three blinded test chemicals and one standard positive control chemical (rosiglitazone) under a defined concentration range and four defined sets of conditions (Fig. 1). Laboratories were asked to test using a shared differentiation protocol to assess the potential differences contributed by differentiation protocol variations and using a shared source of 3T3-L1 cells to assess potential differences contributed by variations in cell sources. Activity determinations were assessed as presence of significant activity above the biological activation threshold as described in the methods, and were based on triglyceride accumulation (standard marker for extent of differentiation) and pre-adipocyte proliferation (increase in DNA content relative to differentiated solvent controls).

3.1. Rosiglitazone responses across laboratories and test conditions

Rosiglitazone was tested under four sets of conditions within each laboratory (Fig. 2). Given that triglyceride accumulation efficacies for rosiglitazone were normalized to the maximal intra-assay rosiglitazone-induced response, maximal efficacies (percent activation) could not be compared and fold induction responses relative to the differentiated solvent control were used instead. Maximal triglyceride accumulation fold inductions for rosiglitazone did not vary considerably across the four test conditions (2.5–3.2-fold), with the highest fold induction responses observed in the shared protocol groups (Table S1, Fig. 2). More variation was observed among laboratories relative to among test conditions, with fold inductions ranging from 1.3–6.0 (agnostic of test

Table 1
Descriptive Statistics for Laboratory-Specific Differentiation Protocols.

	Laboratory cells/laboratory protocol													
Participating Laboratory	Cell Source	Cell Lot #	Passage	Test Chem Length (d)	Diff. Length (d)	Cocktail Length (d)	TC Plate	TC plate #	Base Media	IBMX	Insulin	Dexamethasone	Biotin	Ca Pantothenate	FBS
Lab 1	ATCC	Batch 6	u + 3	10	10	2	Falcon	353219	DMEM-LG	0.5 mM	0.6 mg/mL	250 nM	–	–	Wisent #090150, Lot#115680
Lab 2	ATCC	700009858	u + 3, 9	10	10	2	Greiner BioOne	82050–748	DMEM-HG	0.5 mM	1 mg/mL	250 nM	–	–	Euroclone, ECS0180 L, lot # EUS0040912
Lab 3	ATCC	63343749	u + 3	10	10	2	Corning	07–200-565	DMEM-HG	0.5 mM	1 mg/mL	250 nM	–	–	Sigma F6178, Lot #013K8411
Lab 4	ATCC	MBX clone[1]	u + 5	10	10	2	Greiner BioOne	82050–748	DMEM/F12	0.5 mM	1 mg/mL	–	33 mM	17 mM	Fisher Scientific (Gibco) 10437–028
Lab 5	ATCC	2268173	u + 9	14	14	2	Greiner BioOne	82050–748	DMEM-HG	0.5 mM	1 mg/mL	20 nM	–	–	Sigma #F2442, lot 1982183
Lab 6	ATCC	–	u + 3, 8	10	10	2	Greiner BioOne	82050–748	DMEM-HG	0.5 mM	10 mg/mL	1 mM	–	–	GE Healthcare life sciences, SH30910.03HI
Lab 7	ATCC	63891946	u + 3	10	10	2	Greiner CellStar	655090	DMEM-HG	0.5 mM	10 mg/mL	–	–	–	GIBCO; Ref: 10270–106; Lot: 41G1780K
Lab 8	Green[2]	–	11	8	8	2	Falcon	353219	DMEM-HG	125 mM	2.5 ug/mL	1.25 mM	2 mg/L	1 mg/L	Gemini #100–106
Lab 9	Zenbio	3T3L1062104	10	10	10	2	Greiner CellStar	M0562–32EA	DMEM-HG	0.5 mM	1 mg/mL	–	–	–	Sigma F9665
Lab 10	ATCC	–	u + 4	11	11	2	USA Scientific	5665–5087	DMEM-HG	0.5 mM	10 mg/mL	1 mM	–	–	Hyclone SH30541.03
Shared	Zenbio	3T3L1062104	8	10	10	2	Greiner BioOne	82050–748	DMEM-HG	0.5 mM	1 mg/mL	–	–	–	

Descriptive statistics for laboratory-specific differentiation protocols provided by each participating laboratory. These cells and differentiation details were utilized for the LC and LP conditions only. The "Shared" cell source was utilized for all SC conditions, and the shared protocol (Supplemental information) for all SP conditions. All laboratories completed tests using each of the four defined test conditions.
u = unknown passage number.
Differentiation length specifies the total duration of adipocyte differentiation and adipocyte maintenance media treatment, whereas cocktail length specifies just the duration of the differentiation induction media treatment.
[1] 3T3-L1 MBX clone utilized for these experiments: designed to ensure more complete adipocyte differentiation and insulin sensitivity; unknown lot #.
[2] Green H (isolating laboratory) source as gift from Philip Pekala (same apparent source as commercial Zenbio cells); no reported lot #.

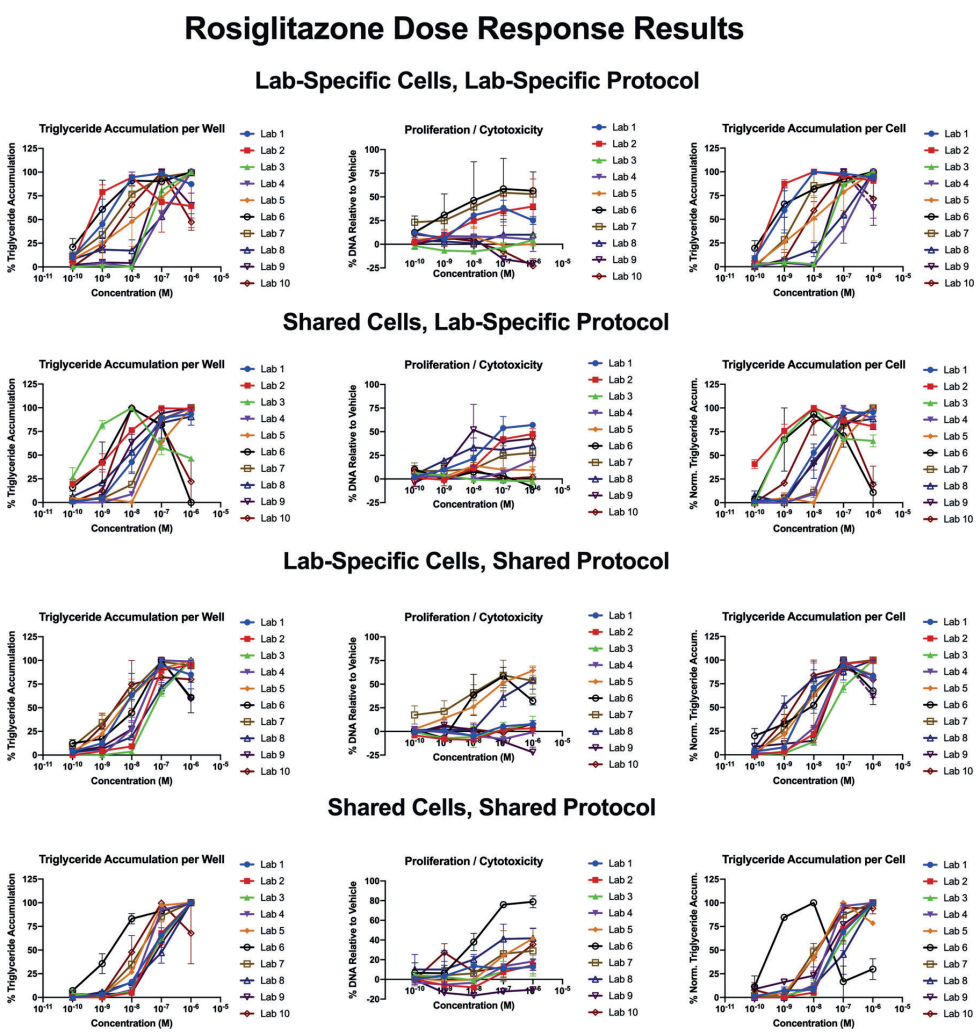

Fig. 2. Rosiglitazone Responses Across Laboratories and Conditions. Comparison of dose responses for rosiglitazone (provided, not blinded) across the ten participating laboratories. Responses are provided as raw triglyceride accumulation per well of tissue culture plate, normalized to maximal rosiglitazone-induced response using those test conditions (left column); cell proliferation and/or cytotoxicity as per Hoechst DNA dye (middle column); and normalized triglyceride accumulation per cell, normalized to DNA content of that treatment (right column). Laboratories were asked to test equivalent concentrations using their laboratory stock of 3T3-L1 cells and their laboratory differentiation protocol (top row), using the provided stock of 3T3-L1 cells and their laboratory protocol (second row), using their laboratory stock of 3T3-L1 cells and the provided protocol (third row), and using the provided 3T3-L1 cells and provided protocol (bottom row).

conditions; Table S2) and Z-scores exceeding ± 1.0. Lower variances were again observed in the shared protocol groups. With some exceptions, most laboratories reported the highest fold induction responses using the shared cell/shared protocol (SC/SP) test conditions. Dose responses were varied when laboratories utilized laboratory-specific cells and laboratory-specific protocols (LC/LP), with more than two orders of magnitude difference in potencies, three orders of magnitude difference in lowest observed effect level (LOEL; lowest tested concentration with significant increase above baseline), two orders of magnitude in maximal effective concentration, and a wide range of fold inductions relative to differentiated solvent controls (0.1 % DMSO; Fig. 2, Table S2). Similar variances were observed when all laboratories used the SC, with no apparent improvement in responses across laboratories, though variances improved slightly in the SP conditions (e.g. maximal concentrations demonstrated much greater consistency). Mean potencies (EC_{20}) for triglyceride accumulation were very similar, with values ranging from 0.009 μM for SC/SP, 0.004 for LC/SP, 0.006 for SC/LP, and 0.008 for LC/LP, though these trends were not evidence for pre-adipocyte proliferation (mean potencies of 18.45 μM for SC/SP, 146.72 for LC/SP, 0.17 for SC/LP, and 6.00 for LC/LP). For most laboratories, fold induction increased when using the shared protocol (with or without shared cells). Mean SC/SP metrics for rosiglitazone performance (triglyceride accumulation) were 0.04 ± 0.01 μM for LOEL, 0.72 ± 0.14 μM for maximal response concentration, 3.2 ± 0.4 for fold induction of response, and 0.02 ± 0.01 μM for potency (Table S2).

Pre-adipocyte proliferation means/deviations did not appreciably change across the test groups, though a greater proportion of laboratories reported significant adipogenic activity when using SC (with the most consistency using SC/SP; Fig. 1, Table S1, Table S2). Only one laboratory reported inactivity for pre-adipocyte proliferation using the

SC/SP, while 30–60 % of laboratories reported inactivity when assessed under the other test conditions. Efficacy ranged from < limit of detection (LOD) to ~80 % increased DNA content relative to the differentiated solvent control, and the magnitude of proliferation seemed to be highest in the SC/SP group (Table S1, Table S2). Average reproducibility metrics for the SC/SP conditions included LOEL (mean: 0.26 ± 0.13 μM), maximal efficacy (mean: 32.1 % ± 6.7 %), concentration at which maximal response was induced (mean: 0.9 ± 0.1 μM), and potency (18.45 ± 15.63 μM; Table S2). Maximal response concentration was nearly unanimous using the SC/SP, but large variances and potency shifts were observed in the other test groups (Fig. 1, Table S2). Some low-level cytotoxicity was observed for certain laboratories under certain test conditions, only at 10 mM, and all using the LC test conditions.

3.2. Pyraclostrobin responses across laboratories and conditions

Pyraclostrobin is a fungicide that has been reported previously to exhibit adipogenic effects (Kassotis et al., 2017a; Luz et al., 2018), though reportedly not through PPARγ activation (Luz et al., 2018). Maximal triglyceride accumulation efficacies for pyraclostrobin varied considerably across test conditions (<LOD – 400 %), with generally lower variances observed in the SP groups (Table S3, Table S4, Figure S1). Under each set of test conditions, there was at least one laboratory below or near the LOD for triglyceride accumulation. There appeared to be two groupings among laboratories for maximal efficacy

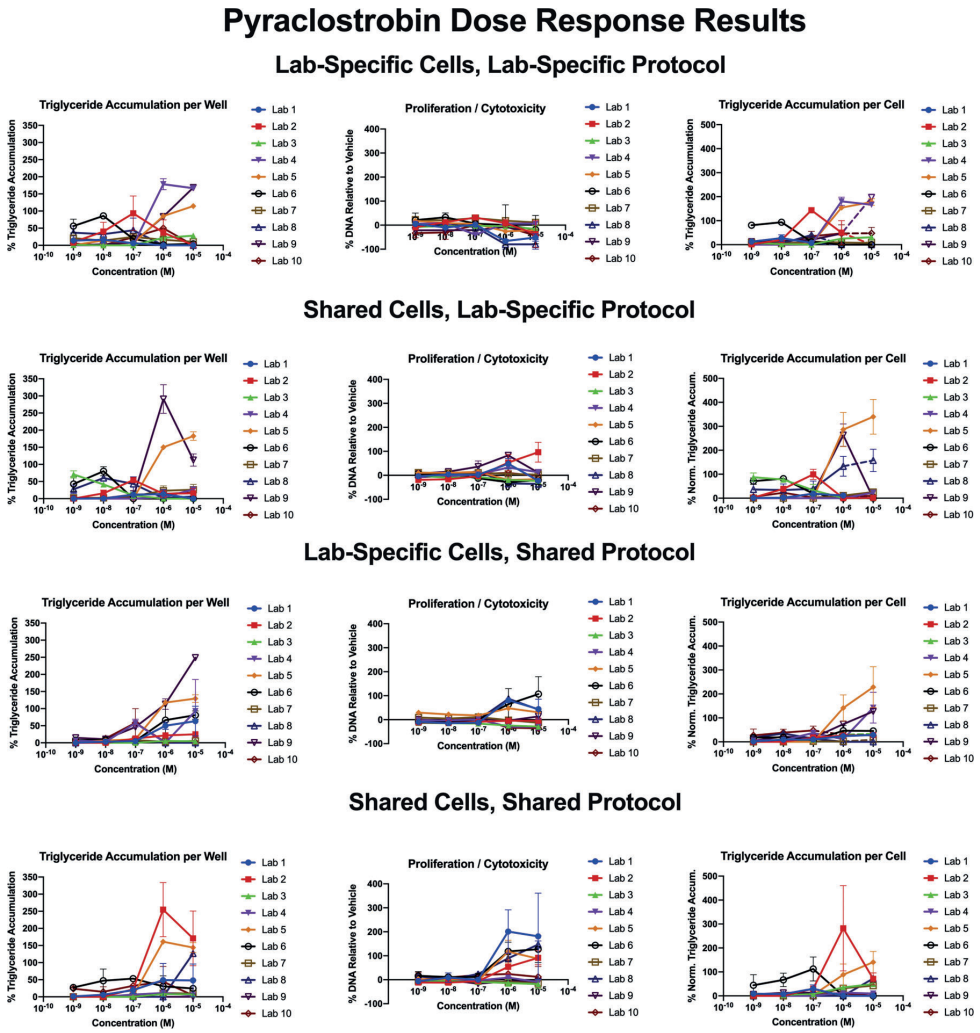

Fig. 3. Pyraclostrobin Responses Across Labs and Conditions. Comparison of dose responses for pyraclostrobin across the ten participating laboratories. Mean responses ± standard error of the mean (SEM) are provided as raw triglyceride accumulation per well of tissue culture plate, normalized to maximal rosiglitazone-induced response using those test conditions (left column); cell proliferation and/or cytotoxicity as per Hoechst DNA dye (middle column); and normalized triglyceride accumulation per cell, normalized to DNA content of that treatment (right column). Laboratories were asked to test equivalent concentrations using their lab stock of 3T3-L1 cells and their laboratory differentiation protocol (top row), using the provided stock of 3T3-L1 cells and their laboratory protocol (second row), using their lab stock of 3T3-L1 cells and the provided protocol (third row), and using the provided 3T3-L1 cells and provided protocol (bottom row). Dashed lines represent concentrations at which cytotoxicity was observed (significant decreased DNA content at that concentration).

results (low/no activity responders and high activity responders; Fig. 3). Three laboratories were consistently low responders, one was consistently a high responder, four laboratories were high responders in three of the four test conditions (test condition varied by laboratory), and two laboratories were split in responses across test conditions. The LOEL and maximal response concentrations appeared to be more consistent when using the SP, albeit with slightly lower potencies (particularly for the SC/SP condition; Fig. 3, Table S4). Almost all laboratories identified this chemical as active for inducing triglyceride accumulation with the exception of one each using LC/SP and SC/SP (blue boxes denote active determinations, whereas red denote inactive; Fig. 3, Table S3, Table S4).

For pre-adipocyte proliferation, maximal efficacies also varied widely (<LOD – 201 %; Fig. S1, Fig. 3, Table S4). A greater proportion of laboratories reported significant proliferative activity using the SC: 30 % using LC/LP, 40 % using LC/SP, 70 % using SC/LP, and 60 % using SC/SP. In most cases, greater efficacies for proliferation were observed when in SP groups. Greater consistency but lower sensitivity/potency were observed for the SC/SP group. At the level of activity determination, there was an almost even split in responses (Fig. 3D). Only five laboratories reported pyraclostrobin as active for proliferation in three or more four conditions (generally reported as inactive using LC/LP). Significant toxicity was observed for some laboratories under certain test conditions. No toxicity was observed for any laboratory in the SC/SP condition, but 40 % of laboratories reported significant toxicity in both the SC/LP (one at 1 and 10 mM and three at 10 mM only) and LC/SP (three at 1 and 10 mM and one at 10 mM only) conditions, and 50 %

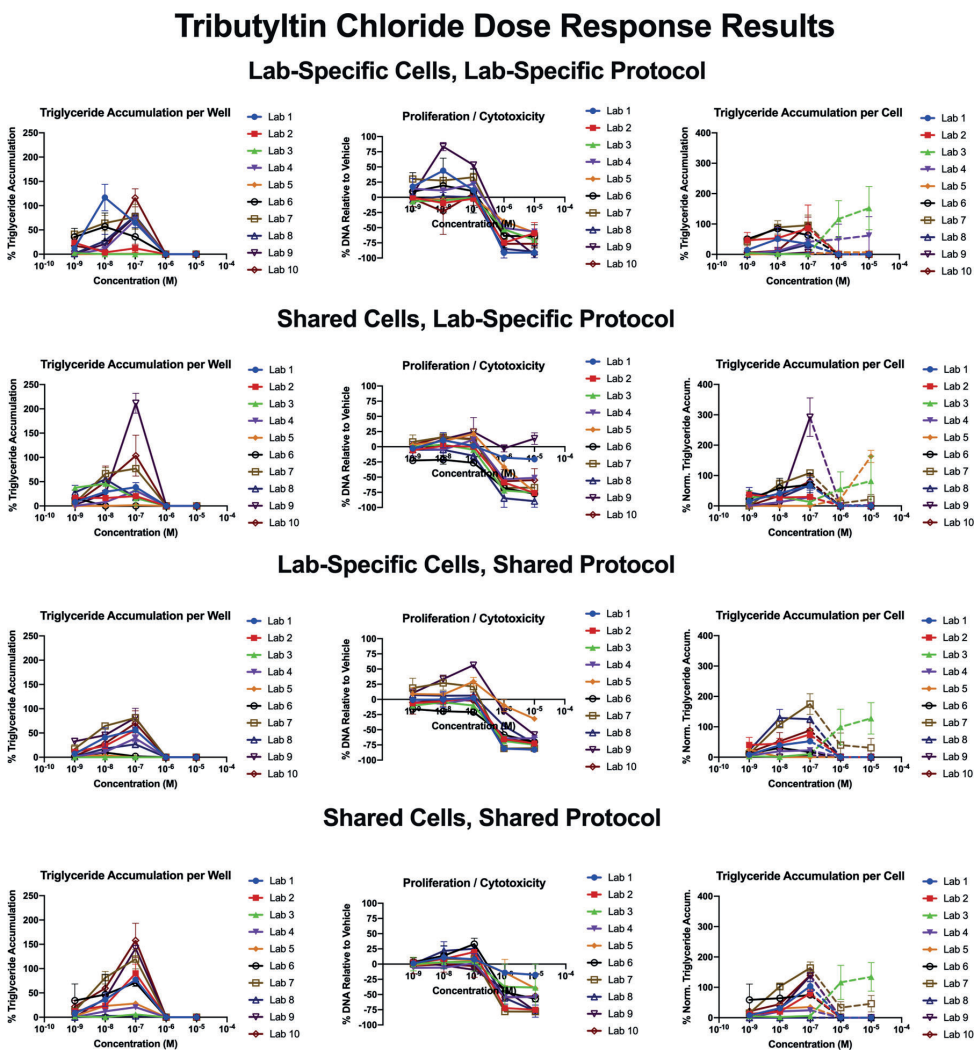

Fig. 4. Tributyltin Chloride Responses Across Labs and Conditions. Comparison of dose responses for tributyltin chloride across the ten participating laboratories. Mean responses ± standard error of the mean (SEM) are provided as raw triglyceride accumulation per well of tissue culture plate, normalized to maximal rosiglitazone-induced response using those test conditions (left column); cell proliferation and/or cytotoxicity as per Hoechst DNA dye (middle column); and normalized triglyceride accumulation per cell, normalized to DNA content of that treatment (right column). Laboratories were asked to test equivalent concentrations using their lab stock of 3T3-L1 cells and their laboratory differentiation protocol (top row), using the provided stock of 3T3-L1 cells and their laboratory protocol (second row), using their lab stock of 3T3-L1 cells and the provided protocol (third row), and using the provided 3T3-L1 cells and provided protocol (bottom row). Dashed lines represent concentrations at which cytotoxicity was observed (significant decreased DNA content at that concentration).

reported significant toxicity using LC/LP (two at 0.1, 1, and 10 mM; two at 1 and 10 mM; and one at 10 mM only).

3.3. Tributyltin chloride (TBT) responses across laboratories and conditions

TBT is a biocide that has been reported previously to exhibit robust adipogenic effects *in vitro* (Grun et al., 2006; Li et al., 2011; Pereira-Fernandes et al., 2013) and *in vivo* (Chamorro-Garcia et al., 2013; Penza et al., 2011). Maximal triglyceride accumulation efficacies for TBT varied considerably across test conditions (<LOD – 429 %), with lower variances in the LC/LP and SC/SP groups (Fig. 4, Fig. S2, Table S5, Table S6). Relative to pyraclostrobin, wide variances were observed even within laboratories, and two response groupings (high and low consistency) were observed. Five laboratories ranged widely in triglyceride accumulation responses across test conditions, and five laboratories were more consistent (moderate to high triglyceride accumulation). No differences were observed in LOELs, though maximum response concentrations and potencies appeared more consistent in the SC/SP group, albeit with slightly lower potencies (Fig. 4, Table S6). Almost all laboratories identified this chemical as active for inducing triglyceride accumulation, with the exception of two laboratories using the LC and one using the SC/SP (Fig. 4D).

For pre-adipocyte proliferation, maximal efficacies had low consistency (<LOD – 84 %; Fig. S2, Fig. 4, Table S6), but the highest consistencies for efficacy, LOEL, and potencies were observed in the SC/SP group. At the level of activity determination, 50–70 % of laboratories reported TBT as inactive for proliferation across all test conditions

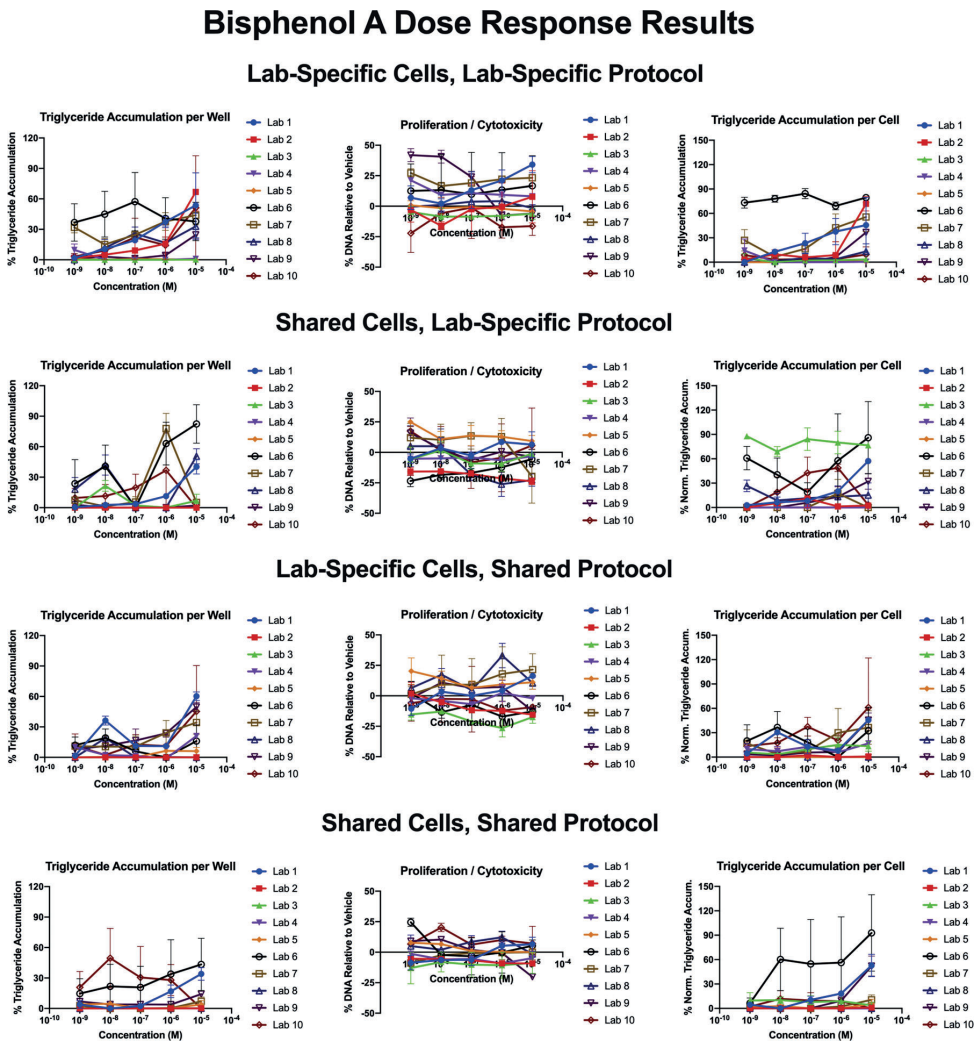

Fig. 5. Bisphenol A Responses Across Labs and Conditions. Comparison of dose responses for bisphenol A across the ten participating laboratories. Mean responses ± standard error of the mean (SEM) are provided as raw triglyceride accumulation per well of tissue culture plate, normalized to maximal rosiglitazone-induced response using those test conditions (left column); cell proliferation and/or cytotoxicity as per Hoechst DNA dye (middle column); and normalized triglyceride accumulation per cell, normalized to DNA content of that treatment (right column). Laboratories were asked to test equivalent concentrations using their lab stock of 3T3-L1 cells and their laboratory differentiation protocol (top row), using the provided stock of 3T3-L1 cells and their laboratory protocol (second row), using their lab stock of 3T3-L1 cells and the provided protocol (third row), and using the provided 3T3-L1 cells and provided protocol (bottom row).

(Fig. 4D), with no laboratory reporting consistent activity across test conditions. Two laboratories identified TBT as inactive for proliferation for all conditions and two as inactive in three of four conditions. Clear cytotoxicity was observed for TBT at 1 and 10 mM, with high consistency across laboratories and conditions (Fig. S2).

3.4. Bisphenol A responses across laboratories and conditions

BPA is a synthetic chemical used often as a cross-linker in the synthesis of some plastics and can be found in some consumer products. (vom Saal et al., 2007; Welshons et al., 2006) BPA has been extensively described to disrupt metabolic health *in vitro* (Masuno et al., 2002; Sargis et al., 2010; Taxvig et al., 2012), *in vivo* (Angle et al., 2013; Somm et al., 2009; Vom Saal et al., 2012), and in epidemiological studies (Carwile and Michels, 2011; Rochester, 2013; Trasande et al., 2012). Maximal triglyceride accumulation efficacies for BPA varied across test conditions (<LOD – 93 %), with apparent lower variances in the SP groups (Table S7, Table S8, Fig. S3, Fig. 5). Relatively wide variances were observed even within laboratories, and three response groupings (inactive, low/moderate and moderate/high activity) were observed. Given lower reported activity, potency and LOEL comparisons were difficult to ascertain (Fig. 5, Table S8). Nearly all laboratories identified this chemical as active for triglyceride accumulation, though with considerable variation across test conditions and no apparent difference between groups (Fig. 5).

For pre-adipocyte proliferation, maximal efficacies were again less consistent but with a smaller dynamic range (<LOD – 42 %; Fig. S3, Fig. 5, Table S8) that hindered evaluation of several reproducibility metrics. Greater agreement was observed for inactivity of BPA on the proliferation metric (Fig. 5D). Three laboratories reported BPA as inactive for proliferation across test conditions, three laboratories as inactive in three of four test conditions, and the remaining laboratories reported higher rates of activity. Within test conditions, the greatest consistency was observed using the SC/LP and SC/SP conditions, with 80 % of laboratories reporting BPA as inactive for proliferation. No significant toxicity was reported for BPA at any test concentration by any laboratory and in any test condition.

4. Discussion

These results confirm that repeatability of adipogenic (pre-adipocyte proliferation) and lipogenic (triglyceride accumulation) responses utilizing 3T3-L1 cells are highly variable across laboratories, which can be problematic for reproducibility and data comparability. There have been previous reports of inconsistencies in adipogenic determinations for specific chemicals (Kassotis et al., 2017b), but this has not previously been evaluated in a blinded, systematic manner. While standard in most areas, reproducibility studies are relatively uncommon for toxicological outcomes, and as a consequence, reproducibility across laboratories is not well-appreciated. While bioactivities (efficacies/potencies) varied considerably across laboratories and test conditions, activity determinations (active/inactive) were more consistent, which suggests that most laboratories can accurately identify MDCs. Though importantly, even these determinations were less consistent when using LC/LP, suggesting that standardization may greatly improve reproducibility between laboratories (at least for triglyceride accumulation) and thus confidence in reported outcomes. The most consistent results across test conditions and chemicals tested were generally observed in the LC/SP and SC/SP groups. While potencies were lower for rosiglitazone-induced triglyceride accumulation in the SC/SP group, this pattern did not carry over to other test chemicals or the pre-adipocyte proliferation metric, and this group had the most potent responses for other test chemicals.

Pyraclostrobin was selected for screening given the previously reported non-traditional mechanism(s) of action (antagonism of TRb and/or mitochondrial dysfunction) and robust adipogenic response (Kassotis et al., 2017a; Luz et al., 2018). A high degree of consistency was observed for triglyceride accumulation activity determination between laboratories and test conditions for this chemical, though magnitude and potency of responses were much more variable. Efficacy did not seem to vary based on test conditions, but instead was more laboratory-specific, with laboratories reporting more consistent responses regardless of test condition. These responses appeared independent of cell source and protocol, which could suggest more overarching variables such as fetal bovine serum source/consistency that may impact results across these conditions. Maximal response concentrations and LOELs were more consistent when using the SP, albeit with slightly lower potencies. Pre-adipocyte proliferation was much more variable (50 % of laboratories and test conditions reported active), though twice the laboratories reported significant proliferative activity using the SP. In most cases, greater proliferative responses were observed when using the SP, for which laboratories were provided tissue culture plates; it has been previously reported that the tissue culture plates used could drastically impact the proliferative response (Kassotis et al., 2017b; Mehra et al., 2007). Overall, greater consistency but lower sensitivity/potency were observed for the SC/SP group. It is worth noting that pyraclostrobin exhibited much greater activity

TBT was selected due to well-reported adipogenic effects via activation of PPAR and RXR (Chamorro-Garcia et al., 2013; Grun et al., 2006; le Maire et al., 2009; Li et al., 2011; Penza et al., 2011; Pereira-Fernandes et al., 2013). We previously demonstrated consistent expression for PPAR isoforms and RXRα in ATCC and Zenbio-sourced 3T3-L1 cells (Kassotis et al., 2017b), suggesting this chemical might have greater consistency across laboratories and test conditions. However, while nearly all laboratories and test conditions successfully identified TBT as active for promoting significant triglyceride accumulation, the broad range of efficacies, potencies, and sensitivities reported here would suggest that these methods may not be sensitive enough to accurately characterize less active chemicals. This could be due to small differences in cytotoxicity impacting our broad concentration response curves. Pre-adipocyte proliferation is a less frequently examined and/or reported endpoint in 3T3-L1 cells, with explicit reporting only becoming more standard in the last several years. Accounting for varying cell densities across wells and replicates can be achieved by normalizing the triglyceride content with the DNA content. Indeed, when examining the total triglyceride content per well only (Table S5), the number of laboratories and conditions reporting TBT inactive would increase from five to nine. Thus, the normalization to DNA content is important to accurately defining adipogenic activity, particularly given that varying cell densities across plates are common and since mature adipocytes detach easily from the plate bottom during media changes and rinses. Pre-adipocyte proliferation as its own metric, however, was considerably less consistent. Approximately half of the laboratories and test conditions reported TBT as inactive for proliferation (17/40) and half as active, demonstrating no clear correct determination for this endpoint. Greater consistency was observed when using SC/SP, however, demonstrating that greater concordance in testing may be possible if protocols were standardized.

BPA was selected due to the non-canonical mechanism of action and the less reproducible outcomes reported previously *in vitro* (Kassotis et al., 2017b). BPA has been reported to increase adipogenic gene expression (aP2) through an estrogen receptor-mediated mechanism (Boucher et al., 2014), which we reported to have differential expression between 3T3-L1 cell sources (Kassotis et al., 2017b). As expected, lower consistency was observed for BPA-induced triglyceride accumulation (65 % of laboratories/conditions reported as active). Lower variance was observed for DNA content measurements, with only 30 % of labs and test conditions reporting BPA as active for this metric. While test condition did not appreciably influence activity determinations for triglyceride accumulation, improved consistency was observed for the pre-adipocyte proliferation metric using the LC/SP and SC/SP conditions, suggesting that protocol and not cell differences were the primary

factors in these disparities.

Overall, cell source appeared to be a significant factor in variation observed between laboratories and test conditions. Zenbio-sourced cells often had lower variation than ATCC-sourced cells for chemicals, which we reported previously (Kassotis et al., 2017b). It is perhaps unsurprising that 3T3-L1 cells sourced from different companies had high variation in responses between them, though it is notable that considerable variation was observed even when comparing cells obtained from the same provider (Table 1, Figs. 2–5); cells sourced from the Green Lab were unsurprisingly more similar to the Zenbio-sourced cells. It has been previously established that ATCC maintains a variety of 3T3-L1 cell lots, which are described in ATCC protocols to differentiate to different extents (Kassotis et al., 2017b). This appears to be a common problem, as noted above, as the European Collection of Authenticated Cell Culture (ECACC) currently reports that their 3T3-L1 cells will not differentiate. It is likely, based on the varied responses reported herein and the differentiation issues noted by the providers, that continuity of this cell line has not been properly controlled across sources. This may be contributing to a portion of the divergent responses observed across laboratories. As observed here, this contributes to considerable variance even for laboratories ordering presumably the same cell line from the same supplier. This has been reported previously for MCF-7 cells obtained by two laboratories that ordered the same lot of MCF-7 cells from ATCC (Kleensang et al., 2016). Phenotypic, gene expression, metabolomic, and hormone-responsiveness were all demonstrated to clearly vary between these sub-clones even of the same lot of cells and were eventually linked to genetic variability in a single frozen lot of ATCC MCF-7 cells (Kleensang et al., 2016). As these authors recommended, future research should investigate these 3T3-L1 cell sources and lots through Direct Compararative Genome Hybridization and/or deep sequencing approaches to determine shifts in frozen cell line stocks that may be contributing to disparate responses. This should be pursued to improve response consistency and to increase confidence and transparency of results.

For a number of chemicals and laboratories, the most reproducible and least variable outcomes (lower Z-score ranges; Supplemental Tables) based on the performance metrics examined here were observed in the SC/SP group. Often, we observed reduced variance in the LC/SP group as well, suggesting that while cell source should be considered as a contributory factor in improving reproducibility, improvements can be made more readily through taking steps to harmonize differentiation protocols across laboratories. Numerous factors varied widely across laboratories (Table 1). While the differentiation timeline was often consistent, a variety of cell culture plastics were used, concentrations and presence of media additives varied considerably. The source of additives such as fetal bovine serum have been reported to vary substantially and may have contributed to varying degrees of differentiation. While isobutylmethylxanthine (IBMX) concentrations were quite consistent, insulin concentrations varied >1000-fold, and seven laboratories used dexamethasone (10-fold variation in concentrations). Even 10-fold variations in insulin concentration have been described to promote robust impacts on adipogenesis via both triglyceride accumulation and pre-adipocyte proliferation (Green and Kehinde, 1975). Additionally, dexamethasone has been demonstrated to promote potent and efficacious effects on triglyceride accumulation (Kassotis et al., 2017b). Taken together, the concentrations of these additives are likely contributory factors, though no clear trends in media additive use could be associated with specific patterns of activity (Fig. S4). While the SP groups utilized consistent detection and staining protocols, these were not consistent in the LP groups and may have contributed to some of the protocol-specific variances. Despite these factors, particularly variation likely contributed by fetal bovine serum sourcing, we need to utilize models such as this to evaluate the tens of thousands of chemicals requiring toxicological characterization. Appreciating these factors, and understanding the inherent variability, is key to making proper determinations based on studies utilizing these and similar models.

In summary, we report poor reproducibility (efficacies, potencies, and sensitivities) for several blinded test chemicals across laboratories, though this largely did not impact determination of chemical activity classification (e.g. categorized as “active” or “inactive”). While activity determinations for triglyceride accumulation were quite consistent, even this gross level of bioactivity measurement was not consistent for pre-adipocyte proliferation. These results suggest that toxicologic reproducibility assessments are warranted for other endpoints (for other assays and other metrics of differentiation success such as percent of differentiated cells, etc.) and suggests some avenues for improvements through harmonization of cell sourcing and differentiation protocols. It is also important to note that analytical reproducibility efforts have also reported high variance across laboratories (Melymuk et al., 2015, 2018); we do not believe this should reduce confidence in bioassay findings, but should be acknowledged to support accurate determinations of activity for unknown test chemicals when considering regulatory next steps. We report that the differentiation protocol and the source of the 3T3-L1 cells both contributed to variance in responses and even some dissimilar determinations of activity, suggesting that these factors may provide opportunity for reducing inter-laboratory variability. While we did not detect specific differences that we could associate with individual media additives, further research should evaluate this more explicitly. It should be noted that pyraclostrobin exhibited much greater activities than BPA, though has received as of yet very limited relative research attention.

While human mesenchymal stem cell and human pre-adipocyte cell lines are increasingly available commercially, there are wide reported variations based on sex, race and ethnicity, as well as physiological status of the donor. These models should see increased use, and direct comparisons to 3T3-L1 results, in future research; however, the decades of research on 3T3-L1 cells support continued use of this model at least until there are clearly superior models and/or clear translation of prior findings to human models.

Given the increasing need for accurate and reliable metabolic health assays and the difficulty of policing cell line providers, we suggest that future efforts focus on establishing best practices and consistency in differentiation protocols to improve translation across laboratories. There are also notable efforts ongoing through the Horizon 2020 program in the European Union to develop and validate new and diverse metabolism disrupting chemical assays *in silico*, *in vitro,* and *in vivo* (Audouze et al., 2020; Legler et al., 2020). Towards that end, we have provided the detailed shared differentiation protocol used in this study (Supplemental File 1), though further efforts towards harmonization should be undertaken with experts to weigh inclusion or exclusion of specific factors in the protocol and to consider the issues inherent with specific sources of 3T3-L1 cells.

Funding

Over-arching project supported by grants [R01 ES016099 to HMS; R00 ES030405 to CDK] from the National Institute of Environmental Health Sciences (NIEHS). Laboratory-specific funding includes local funding 2018-19 from the University of Turin to PB. SE and JL received funding from the European Union’s Horizon 2020 research and innovation program under grant agreement GOLIATH No. 825489 and from Brunel University London. 1K22ES026208 and R01ES027863 to AV-L from NIEHS and NIEHS Z0ES102785 to SEF. MFF received funding from the Spanish Institute of Health Carlos III (grant FIS-PI16/01812).

Declaration of Competing Interest

The authors declare that they have no known competing financial interests or personal relationships that could have appeared to influence the work reported in this paper.

Appendix A. Supplementary data

Supplementary material related to this article can be found, in the online version, at doi:https://doi.org/10.1016/j.tox.2021.152900.

References

American Type Culture Collection (ATCC) ATTC, 2011. Chemically-induced Differentiation of ATCC CL-173 (3T3-L1) Using Single-component Commercially-available Reagents. Available: http://www.atcc.org//media/6124AF1E4C2A47CF904435117909AC25.ashx [accessed 17 May 2016.

Angle, B.M., Do RP, Ponzi D., Stahlhut, R.W., Drury, B.E., Nagel, S.C., et al., 2013. Metabolic disruption in male mice due to fetal exposure to low but not high doses of bisphenol A (BPA): evidence for effects on body weight, food intake, adipocytes, leptin, adiponectin, insulin and glucose regulation. Reprod. Toxicol. 42, 13.

Audouze, K., Sarigiannis, D., Alonso-Magdalena, P., Brochot, C., Casas, M., Vrijheid, M., et al., 2020. Integrative strategy of testing systems for identification of endocrine disruptors inducing metabolic disorders-an introduction to the Oberon project. Int. J. Mol. Sci. 21.

Boucher, J.G., Boudreau, A., Atlas, E., 2014. Bisphenol A induces differentiation of human preadipocytes in the absence of glucocorticoid and is inhibited by an estrogen-receptor antagonist. Nutr. Diabetes 4, e102.

Boucher, J.G., Boudreau, A., Ahmed, S., Atlas, E., 2015. In vitro effects of bisphenol A beta-d-glucuronide (BPA-G) on adipogenesis in human and murine preadipocytes. Environ. Health Perspect. 123, 1287–1293.

Bournat, J.C., Brown, C.W., 2010. Mitochondrial dysfunction in obesity. Curr. Opin. Endocrinol. Diabetes Obes. 17, 446–452.

Boyer, K.W., Horwitz, W., Albert, R., 1985. Interlaboratory variability in trace element analysis. Anal. Chem. 57, 454–459.

Carwile, J.L., Michels, K.B., 2011. Urinary bisphenol A and obesity: nhanes 2003-2006. Environ. Res. 111, 825–830.

Chamorro-Garcia, R., Sahu, M., Abbey, R.J., Laude, J., Pham, N., Blumberg, B., 2013. Transgenerational inheritance of increased fat depot size, stem cell reprogramming, and hepatic steatosis elicited by prenatal exposure to the obesogen tributyltin in mice. Environ. Health Perspect. 121, 359–366.

European Collection of Authenticated Cell Cultures (ECACC), 2020. ECACC General Cell Collection: 3T3-L1. Available: https://www.phe-culturecollections.org.uk/products/celllines/generalcell/detail.jsp?refId=86052701&collection=ecacc_gc#medDoc [accessed 4 February 2021].

Fang, M., Webster, T.F., Stapleton, H.M., 2015. Activation of human peroxisome proliferator-activated nuclear receptors (PPARgamma1) by semi-volatile compounds (SVOCs) and chemical mixtures in indoor dust. Environ. Sci. Technol. 49, 10057–10064.

Fu, M., Sun, T., Bookout, A.L., Downes, M., Yu, R.T., Evans, R.M., et al., 2005. A nuclear receptor atlas: 3T3-L1 adipogenesis. Mol. Endocrinol. 19, 2437–2450.

Gore, A.C., Chappell, V.A., Fenton, S.E., Flaws, J.A., Nadal, A., Prins, G.S., et al., 2015. Edc-2: the Endocrine Society's second scientific statement on endocrine-disrupting chemicals. Endocr. Rev. 36, E1–E150.

Green, H., Kehinde, O., 1975. An established preadipose cell line and its differentiation in culture. II. Factors affecting the adipose conversion. Cell 5, 19–27.

Green, H., Meuth, M., 1974. An established pre-adipose cell line and its differentiation in culture. Cell 3, 127–133.

Greenspan, P., Mayer, E.P., Fowler, S.D., 1985. Nile red: a selective fluorescent stain for intracellular lipid droplets. J. Cell Biol. 100, 965–973.

Grun, F., Watanabe, H., Zamanian, Z., Maeda, L., Arima, K., Cubacha, R., et al., 2006. Endocrine-disrupting organotin compounds are potent inducers of adipogenesis in vertebrates. Mol. Endocrinol. 20, 2141–2155.

Hamers, T., Kamstra, J.H., Sonneveld, E., Murk, A.J., Kester, M.H., Andersson, P.L., et al., 2006. In vitro profiling of the endocrine-disrupting potency of brominated flame retardants. Toxicol. Sci. 92, 157–173.

Heindel, J.J., vom Saal, F.S., Blumberg, B., Bovolin, P., Calamandrei, G., Ceresini, G., et al., 2015. Parma consensus statement on metabolic disruptors. Environ. Health 14, 54.

Heindel, J.J., Blumberg, B., Cave, M., Machtinger, R., Mantovani, A., Mendez, M.A., et al., 2017. Metabolism disrupting chemicals and metabolic disorders. Reprod. Toxicol. 68, 3–33.

Hettwer, K., Jahne, M., Frost, K., Giersberg, M., Kunze, G., Trimborn, M., et al., 2018. Validation of arxula yeast estrogen screen assay for detection of estrogenic activity in water samples: results of an international interlaboratory study. Sci. Total Environ. 621, 612–625.

Hoffman, K., Butt, C.M., Chen, A., Limkakeng, A.T., Stapleton, H.M., 2015. High exposure to organophosphate flame retardants in infants: associations with baby products. Environ. Sci. Technol. 49, 14554–14559.

Ikonomou, M.G., Kelly, B.C., Blair, J.D., Gobas, F.A., 2012. An interlaboratory comparison study for the determination of dialkyl phthalate esters in environmental and biological samples. Environ. Toxicol. Chem. 31, 1948–1956.

Kassotis, C.D., Stapleton, H.M., 2019. Endocrine-mediated mechanisms of metabolic disruption and new approaches to examine the public health threat. Front. Endocrinol. (Lausanne) 10, 39.

Kassotis, C.D., Hoffman, K., Stapleton, H.M., 2017a. Characterization of adipogenic activity of semi-volatile indoor contaminants and house dust. Environ Sci Technol In 51, 8735–8745.

Kassotis, C.D., Masse, L., Kim, S., Schlezinger, J.J., Webster, T.F., Stapleton, H.M., 2017b. Characterization of adipogenic chemicals in three different cell culture systems: implications for reproducibility based on cell source and handling. Sci. Rep. 7, 42104.

Kassotis, C.D., Kollitz, E.M., Ferguson, P.L., Stapleton, H.M., 2018. Nonionic ethoxylated surfactants induce adipogenesis in 3T3-L1 cells. Toxicol. Sci. 162, 124–136.

Kassotis, C.D., Kollitz, E.M., Hoffman, K., Sosa, J.A., Stapleton, H.M., 2019. Thyroid receptor antagonism as a contributory mechanism for adipogenesis induced by environmental mixtures in 3T3-L1 cells. Sci. Total Environ. 666, 431–444.

Kitamura, S., Kato, T., Iida, M., Jinno, N., Suzuki, T., Ohta, S., et al., 2005. Anti-thyroid hormonal activity of tetrabromobisphenol A, a flame retardant, and related compounds: affinity to the mammalian thyroid hormone receptor, and effect on tadpole metamorphosis. Life Sci. 76, 1589–1601.

Kleensang, A., Vantangoli, M.M., Odwin-DaCosta, S., Andersen, M.E., Boekelheide, K., Bouhifd, M., et al., 2016. Genetic variability in a frozen batch of MCF-7 cells invisible in routine authentication affecting cell function. Sci. Rep. 6, 28994.

le Maire, A., Grimaldi, M., Roecklin, D., Dagnino, S., Vivat-Hannah, V., Balaguer, P., et al., 2009. Activation of RXR-PPAR heterodimers by organotin environmental endocrine disruptors. EMBO Rep. 10, 367–373.

Legler, J., Zalko, D., Jourdan, F., Jacobs, M., Fromenty, B., Balaguer, P., et al., 2020. The GOLIATH project: towards an internationally harmonised approach for testing metabolism disrupting compounds. Int. J. Mol. Sci. 21.

Lehmann, J.M., Moore, L.B., Smith-Oliver, T.A., Wilkison, W.O., Willson, T.M., Kliewer, S.A., 1995. An antidiabetic thiazolidinedione is a high affinity ligand for peroxisome proliferator-activated receptor y (PPARy). J. Biol. Chem. 270, 12953–12956.

Li, X., Ycaza, J., Blumberg, B., 2011. The environmental obesogen tributyltin chloride acts via peroxisome proliferator activated receptor gamma to induce adipogenesis in murine 3T3-L1 preadipocytes. J. Steroid Biochem. Mol. Biol. 127, 9–15.

Luz, A.L., Kassotis, C.D., Stapleton, H.M., Meyer, J.N., 2018. The high-production volume fungicide pyraclostrobin induces triglyceride accumulation associated with mitochondrial dysfunction, and promotes adipocyte differentiation independent of ppargamma activation, in 3T3-L1 cells. Toxicology 393, 150–159.

M.Weiss, J., Ivd, Veen, Boer, J., SPJv, Leeuwen, Cofino, W., Crum, S., 2013. Analytical improvements shown over four interlaboratory studies of perfluoroalkyl substances in environmental and food samples. Trac Trends Anal. Chem. 43, 204–216.

Masuno, H., Kidani, T., Sekiya, K., Sakayama, K., Shiosaka, T., Yamamoto, T., et al., 2002. Bisphenol A in combination with insulin can accelerate the conversion of 3T3-L1 fibroblasts to adipocytes. J. Lipid Res. 43, 676–684.

Masuno, H., Iwanami, J., Kidani, T., Sakayama, K., Honda, K., 2005. Bisphenol A accelerates terminal differentiation of 3T3-L1 cells into adipocytes through the phosphatidylinositol 3-kinase pathway. Toxicol. Sci. 84, 319–327.

Meerts, I.A., van Zanden, J.J., Luijks, E.A., van Leeuwen-Bol, I., Marsh, G., Jakobsson, E., et al., 2000. Potent competitive interactions of some brominated flame retardants and related compounds with human transthyretin in vitro. Toxicol. Sci. 56, 95–104.

Mehinto, A.C., Jia, A., Snyder, S.A., Jayasinghe, B.S., Denslow, N.D., Crago, J., et al., 2015. Interlaboratory comparison of in vitro bioassays for screening of endocrine active chemicals in recycled water. Water Res. 83, 303–309.

Mehra, A., Macdonald, I., Pillay, T.S., 2007. Variability in 3T3-L1 adipocyte differentiation depending on cell culture dish. Anal. Biochem. 362, 281–283.

Melymuk, L., Goosey, E., Riddell, N., Diamond, M.L., 2015. Interlaboratory study of novel halogenated flame retardants: INTERFLAB. Anal. Bioanal. Chem. 407, 6759–6769.

Melymuk, L., Diamond, M.L., Riddell, N., Wan, Y., Vojta, S., Chittim, B., 2018. Challenges in the analysis of novel flame retardants in indoor dust: results of the INTERFLAB 2 interlaboratory evaluation. Environ. Sci. Technol. 52, 9295–9303.

Niemelä, S., Miettinen, S., Sarkanen, J.R., Ashammakhi, N., 2008. Adipose tissue and adipocyte differentiation: molecular and cellular aspects and tissue engineering applications. In: Topics in tissue engineering, Vol. 4, 1–26.

Orton, F., Rosivatz, E., Scholze, M., Kortenkamp, A., 2011. Widely used pesticides with previously unknown endocrine activity revealed as in vitro anti-androgens. Environ. Health Perspect. 119, 794–800.

Penza, M., Jeremic, M., Marrazzo, E., Maggi, A., Ciana, P., Rando, G., et al., 2011. The environmental chemical tributyltin chloride (TBT) shows both estrogenic and adipogenic activities in mice which might depend on the exposure dose. Toxicol. Appl. Pharmacol. 255, 65–75.

Pereira-Fernandes, A., Vanparys, C., Hectors, T.L., Vergauwen, L., Knapen, D., Jorens, P. G., et al., 2013. Unraveling the mode of action of an obesogen: mechanistic analysis of the model obesogen tributyltin in the 3T3-L1 cell line. Mol. Cell. Endocrinol. 370, 52–64.

Rochester, J.R., 2013. Bisphenol a and human health: a review of the literature. Reprod. Toxicol. 42, 132–155. C.

Rosen, E.D., Sarraf, P., Troy, A.E., Bradwin, G., Moore, K., Milstone, D.S., et al., 1999. PPAR gamma is required for the differentiation of adipose tissue in vivo and in vitro. Mol. Cell 4, 611–617.

Ruiz, D., Becerra, M., Jagai, J.S., Ard, K., Sargis, R.M., 2018. Disparities in environmental exposures to endocrine-disrupting chemicals and diabetes risk in vulnerable populations. Diabetes Care 41, 193–205.

Sargis, R.M., Johnson, D.N., Choudhury, R.A., Brady, M.J., 2010. Environmental endocrine disruptors promote adipogenesis in the 3T3-L1 cell line through glucocorticoid receptor activation. Obesity Silver Spring (Silver Spring) 18, 1283–1288.

Seimandi, M., Lemaire, G., Pillon, A., Perrin, A., Carlavan, I., Voegel, J.J., et al., 2005. Differential responses of PPARalpha, PPARdelta, and PPARgamma reporter cell lines to selective PPAR synthetic ligands. Anal. Biochem. 344, 8–15.

Shen, O., Du, G., Sun, H., Wu, W., Jiang, Y., Song, L., et al., 2009. Comparison of in vitro hormone activities of selected phthalates using reporter gene assays. Toxicol. Lett. 191, 9–14.

Somm, E., Schwitzgebel, V.M., Toulotte, A., Cederroth, C.R., Combescure, C., Nef, S., et al., 2009. Perinatal exposure to bisphenol A alters early adipogenesis in the rat. Environ. Health Perspect. 117, 1549–1555.
Spiegelman, B.M., 1998. Ppar-gamma: adipogenic regulator and thiazolidinedione receptor. Diabetes 47, 507–514.
Stapleton, H.M., Klosterhaus, S., Eagle, S., Fuh, J., Meeker, J.D., Blum, A., et al., 2009. Detection of organophosphate flame retardants in furniture foam and U.S. House dust. Environ. Sci. Technol. 43, 7490–7495.
Stapleton, H.M., Klosterhaus, S., Keller, A., Ferguson, P.L., van Bergen, S., Cooper, E., et al., 2011. Identification of flame retardants in polyurethane foam collected from baby products. Environ. Sci. Technol. 45, 5323–5331.
Takeuchi, S., Iida, M., Kobayashi, S., Jin, K., Matsuda, T., Kojima, H., 2005. Differential effects of phthalate esters on transcriptional activities via human estrogen receptors alpha and beta, and androgen receptor. Toxicology 210, 223–233.
Taxvig, C., Dreisig, K., Boberg, J., Nellemann, C., Schelde, A.B., Pedersen, D., et al., 2012. Differential effects of environmental chemicals and food contaminants on adipogenesis, biomarker release and PPARgamma activation. Mol. Cell. Endocrinol. 361, 106–115.
Temkin, A.M., Bowers, R.R., Magaletta, M.E., Holshouser, S., Maggi, A., Ciana, P., et al., 2016. Effects of crude oil/dispersant mixture and dispersant components on PPARgamma activity and : identification of dioctyl sodium sulfosuccinate (DOSS; CAS #577-11-7) as a probable obesogen. Environ. Health Perspect. 124, 112–119.
Trasande, L., Attina, T.M., Blustein, J., 2012. Association between urinary bisphenol A concentration and obesity prevalence in children and adolescents. JAMA 308, 9.
Voet, Hd, JAHv, Rhijn, HJvd, Wiel, 1999. Inter-laboratory, time, and fitness-for-purpose aspects of effective validation. Anal. Chim. Acta 391, 159–171.
vom Saal, F.S., Akingbemi, B.T., Belcher, S.M., Birnbaum, L.S., Crain, D.A., Eriksen, M., et al., 2007. Chapel Hill bisphenol A expert panel consensus statement: integration of mechanisms, effects in animals and potential to impact human health at current levels of exposure. Reprod. Toxicol. 24, 131–138.
Vom Saal, F.S., Nagel, S.C., Coe, B.L., Angle, B.M., Taylor, J.A., 2012. The estrogenic endocrine disrupting chemical bisphenol A (BPA) and obesity. Mol. Cell. Endocrinol. 354, 74–84.
Welshons, W.V., Nagel, S.C., vom Saal, F.S., 2006. Large effects from small exposures. III. Endocrine mechanisms mediating effects of bisphenol A at levels of human exposure. Endocrinology 147, S56–69.
Wong, J., Hao, C., Zhang, K., Yang, P., Banerjee, K., Hayward, D., et al., 2010. Development and interlaboratory validation of a QuEChERS-based liquid chromatography-tandem mass spectrometry method for multiresidue pesticide analysis. J. Agric. Food Chem. 58, 5897–5903.
Zava, D.T., Wyler-von Ballmoos, A., Goldhirsch, A., Roos, W., Takahashi, A., Eppenberger, U., et al., 1982. A quality control study to assess the inter-laboratory variability of routine estrogen and progesterone receptor assays. Eur. J. Cancer Clin. Oncol. 18, 713–721.
Zebisch, K., Voigt, V., Wabitsch, M., Brandsch, M., 2012. Protocol for effective differentiation of 3T3-L1 cells to adipocytes. Anal. Biochem. 425, 88–90.
Zenbio Inc, 2015. 3T3-L1 Cell Care Manual - Maintenance and Differentiation of Preadipocytes to Adipocytes. Available: http://www.zen-bio.com/pdf/ZBM0009.013T3L1CareprotocolRV08.08.pdf [accessed 30 September 2015.
Zhao, Y., Zhang, K., Giesy, J.P., Hu, J., 2015. Families of nuclear receptors in vertebrate models: characteristic and comparative toxicological perspective. Sci. Rep. 5, 8554.